Open access • Journal Article • DOI:10.1109/TDEI.2010.5448107

A comparative study of insulator materials exposed to high voltage AC and DC surface discharges — Source link

Heger G, Hendrik J. Vermeulen, Holtzhausen Jp, W.L. Vosloo

Institutions: Stellenbosch University, Eskom

Published on: 19 Apr 2010 - IEEE Transactions on Dielectrics and Electrical Insulation (IEEE)

Topics: Silicone rubber, EPDM rubber, High voltage, Silicone and Insulator (electricity)

A Comparative Study of Insulator Materials Exposed to High Voltage AC and DC Surface Discharges

by

Gernot Heger

Thesis presented in partial fulfilment of the requirements for the degree of Master of Science in Enginnering

at

Stellenbosch University

Department of Electrical and Electronic Engineering

Faculty of Engineering

Supervisor: Prof HJ Vermeulen
Co-supervisor: Dr WL Vosloo

March 2009

Declaration

By submitting this thesis electronically, I declare that the entirety of the work contained therein is my own, original work, that I am the owner of the copyright thereof (unless to the extent explicitly otherwise stated) and that I have not previously in its entirety or in part submitted it for obtaining any qualification.

Date:

Abstract

The rising worldwide popularity of HVDC applications for power transmission purposes increases the need to study the performance of commonly used insulation materials when exposed to this voltage type. The aim of this study is thus to compare several insulation materials according to their resistance to erosion and tracking when exposed to surface discharges of HVAC and HVDC voltages of both polarities. The materials are tested according to the Incline Plane Test method described in the IEC 60587 standard, using a test voltage of 4.0 kV (rms).

An important aspect of this project is the development of a bipolar DC source capable of delivering the required test voltage and current for both positive and negative polarities, while performing in accordance with the specifications set down in the standard. The design is intentionally kept modular in order to make it adaptable for future installations.

Since the standard describes two different test methods, i.e. the constant tracking voltage method and the stepwise tracking voltage method, a comparison is done between the two methods in order to determine which one delivers best results for the test samples. The comparison shows that the methods deliver comparable results, but the constant tracking voltage method is preferred due to its superior test procedure.

Finally, four different polymer insulator materials are tested and successfully compared under the effects of HVAC and HVDC of both polarities. The test materials include a RTV silicone rubber coated ceramic, two different HTV silicone rubbers and an EPDM rubber. The comparison is done according to the results obtained for a number of evaluation criteria. The results show that the RTV silicone rubber coating exhibits the least erosion for an AC voltage, but shows extensive erosion for a negative DC voltage. The HTV silicone rubbers exhibit only minimal erosion when exposed to an AC test voltage, but develop strong erosion under a positive DC voltage which can result in sample failure. The EPDM experiences its least erosion for a negative DC voltage, but shows maximum erosion severity for the AC voltage.

Opsomming

Die stygende wêreldwye gewildheid van die gebruik van HSGS toepassings vir krag transmissie doeleindes lei tot ‘n groter behoefte vir die studie van die gedrag van algemeen gebruiklike isolatormateriale indien hulle bloot gestel is aan hierdie soort spanning. Die doel van hierdie studie is dus om verskillende isolatormateriale met mekaar te vergelyk ten opsigte van hulle bestandheid teen spoorvorming en erosie indien hulle blootgestel word aan HSWS en bi-polêre HSGS spannings. Die materiale is getoets volgens die Skuinsvlak Toets metode, wat uiteengesit word in die IEC 60587 standaard. Die toetspanning is vasgepen op 4.0 kV (wgk).

‘n Belangrike aspek van die projek is die ontwikkeling van ‘n bi-polêre GS bron wat in staat is om die nodige toetspanning en stroom vir albei positiewe en negatiewe polariteit te lewer en wat aan die voorskrifte van die standaard voldoen. ‘n Modulêre ontwerp is gekies sodat dit aangepas kan word vir toekomstige installasies.

Omdat die standaard twee verskillende toetsmetodes beskryf, i.e. die konstante spoorvormingspanning metode en die stapwyse spoorvormingspanning metode, word hulle met mekaar vergelyk om vas te stel watter metode die beste resultate lewer. Die vergelyking wys uit dat hulle soortgelyke resultate lewer, maar die konstante spoorvormingspanning metode word verkies as gevolg van sy meer effektiewe toets prosedure.

Vier verskillende polimeriese isolatormateriale word getoets onder die invloed van HSWS en bi-polere HSGS en is suksesvol met mekaar vergelyk. Die materiale sluit in ‘n keramiek, bedek met RTV silikoon rubber, twee verskillende HTV silikoon rubbers en ‘n EPDM rubber. Die materiale word vergelyk volgens die resultate van ‘n reeks evalueringskriteria. Die resultate wys dat die RTV silikoon rubber bedeking die minste erosie toon vir ‘n WS spanning, maar sterk erosie toon vir ‘n negatiewe GS spanning. Die HTV silikoon rubbers toon minimale erosie onder ‘n WS toets spanning, maar ontwikkel uitgebreide erosie vir die positiewe GS spanning wat selfs kan lei tot ‘n faling van die toetsmonster. Die EPDM toon die minste erosie vir die negatiewe GS spanning, maar maksimale erosie by WS spanning.

Table of Contents

List of Figures

List of Tables

Nomenclature

AC	alternating current
ASTM	American Society for Testing and Materials
ATR	Attenuated Total Reflection
CMM	contour measuring machine
DC	direct current
EPDM	ethylene propylene diene monomer
EVA	ethylene vinyl acetate
FTIR	Fourier transform infrared
HTV	high temperature vulcanized
HV	high voltage
HVAC	high voltage alternating current
HVDC	high voltage direct current
IEC	International Electrotechnical Commission
IGBT	insulated gate bipolar transistor
IPT	Incline Plane Test
IR	infra-red
KIPTS	Koeberg Insulator Pollution Test Station
LMW	low molecular weight
LTV	low temperature vulcanized
NCI	Non-Ceramic Insulators
OLCA	Online Leakage Current Analyser
PCB	printed circuit board
PDMS	polydimethylsiloxane
rms	root mean square
RTV	room temperature vulcanized
SADC	Southern African Development Community
SAPP	Southern African Power Poll
SR	silicone rubber
TGA	Thermal Gravimetric Analysis
UV	ultra-violet
WC	wettability class

C	capacitance [F]
E	electrical field strength [kV/cm]
f	frequency [Hz]
h	hours
I	current [A]
min	minutes
P	power [W]
p	pressure [Pa]
Q	flow rate [ml/min]
R	resistance [Ω]
ρ	density [kg/m^3]
s	seconds
σ	volume conductivity [mS/cm]
V	voltage [V]
Z	impedance [Ω]

Acknowledgements

I wish to record my sincere appreciation and thanks to:

- My supervisors, Prof HJ Vermeulen and Dr WL Vosloo, for their support, guidance and continuous encouragements during the entire duration of the project.
- Dr JP Holtzhausen for providing valuable insights and observations at critical moments during the project.
- Petrus Pieterse for his continuous assistance in the construction of the test apparatus and during the tests.
- Dr K Schreve for his help during the erosion measurements.
- Dr P Mallon for assisting with the chemical tests and the analysis of the results.
- All the suppliers of the insulator samples for their generous support.
- NamPower for supporting and financing the project.
- My family, for providing all the love and emotional support which kept me going whenever the road became tough.

Chapter 1: Project Description

1.1 Project background & motivation

In light of the current power crisis affecting the entire Southern African region, NamPower, the Namibian power utility, has embarked on a number of projects to either locally generate or import additional power from neighbouring countries of the Southern African Development Community (SADC). One such project is the Caprivi Link Interconnector Project.

This project entails the importing of power from utilities in the eastern part of the Southern African Power Poll (SAPP) into Namibia via a High Voltage Direct Current (HVDC) overhead transmission line. Voltage conversion will be accomplished via Voltage Source Converters, i.e. insulated gate bipolar transistors (IGBT) valves where switching control is independent of the current flow, instead of the more common used Thyristor valve. The line will connect the HVDC converter stations at Zambezi Transmission Station, near Katima Mulilo, with Gerus Transmission Station situated between the towns of Otjiwarongo and Outjo, covering a distance of 970 km. Transmission will initially be in mono-polar mode with metallic or earth return at negative 350 kV direct current (DC). Phase 2 of the project will consist of the installation of the second pole for bipolar operation at ± 350 kV DC. Fig. 1 shows the intended routes of the planned lines.

The project will result in the transmission of 300 MW of electrical power, with a possible upgrading to 600 MW in the future. Connected to this project is the construction of a 285 km long conventional 400 kV AC transmission line from Gerus to Auas Transmission Station, situated near the capital of Windhoek.

As is the case for every power utility across the globe, reliable power transmission is one of the key concerns of NamPower. And since insulators play an important role in transmission networks, their correct selection, implementation and maintenance play a critical role in the successful operation of such networks.

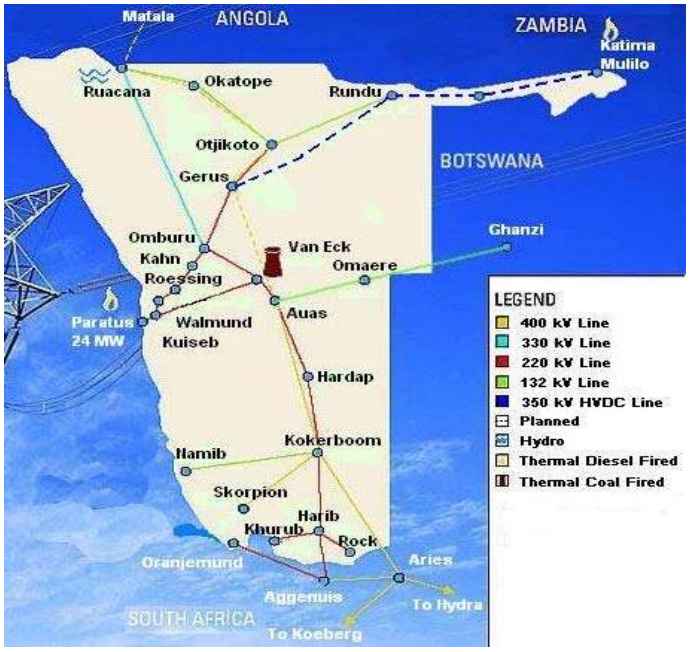

Fig. 1: Map of existing transmission lines in Namibia, also showing the planned 350 kV HVDC line (dashed blue line) [1].

During their lifetime, insulators are subjected to a number of factors which can cause the material to degrade, decreasing the mechanical and electrical strength of the insulator. This can ultimately lead to insulator failure, causing a line-to-earth fault on the line. Many studies have been performed on commonly used insulator materials in order to investigate their behaviour under a variety of conditions, both in laboratories and in the field, so as to gain a better understanding of their expected performance in actual applications. Most of these studies involved the use of alternating current (AC) voltages, as this represents the most common case in high voltage applications and since HVDC lines are a relatively recent development, although with an increasing trend in popularity. Consequently, there is not much information available on the performance of common insulator materials when used in HVDC applications.

NamPower's choice of using a HVDC line is in line with an international trend that has emerged over the past years. The reason for this lies in a number of advantages that HVDC lines have over HVAC lines. The following sections contain a brief outline of the history of the development of HVDC lines, as well as a comparison between HVAC and DC lines.

1.2 History of HVDC transmission

The first true HVDC transmission line was a 50 km long 2 kV DC line established between the two German towns of Miesbach and Munich [2]. Conversion between transmission and user-friendly voltages was achieved by rotating DC machines. Rene Thury, a Swiss engineer, designed a similar transmission system, which used pairs of DC machines (one acting as motor, the other as generator) connected in series to achieve voltages high enough for transmission purposes. One of the earliest installations of this system was in 1889 in Italy, transmitting 630 kW at 14 kV DC over a distance of 120 km [3]. However, these earlier methods of HVDC transmission proved uneconomical due to the high maintenance required by the DC machines and their inherent high energy loss.

The development of the mercury arc valve by Dr. Uno Lamm in 1939 [4] provided the means for a more economical way of transmitting HVDC. The first contract for a system using this technology was issued in Germany in 1941 (Elbe-Project), where a 400 kV underground line was to supply Berlin with 60 MW of electrical power over a distance of ± 110 km. Although ready for energizing in 1945, the collapse of the German government at the end of World War 2 resulted in this system never becoming operational [4]. The energizing of the 200 kV, 20 MW DC line connecting the island of Gotland to the Swedish mainland in 1954 is thus considered as the beginning of the modern HVDC transmission era [3].

Although HVDC were still designed and implemented after 1954, the bulk of worldwide power transmission was accomplished via AC systems. The reason for this development was due to the advantages of AC systems over DC systems at that time [2]:

- Voltage conversion in AC systems uses relatively simple devices, i.e. transformers.
- AC transformers allow for high power and insulation levels, have low losses and are easy to maintain.
- Three phase generators are superior to DC machines.

For these reasons, AC transmission systems became popular at a very early stage in the history of electrical power systems and were soon accepted as the only feasible technology for the generation, transmission and distribution of electrical power [2].

However, when compared to HVDC systems, high voltage alternating current (HVAC) transmission systems have inherent drawbacks [2]:

- Transmission capacities and distances are limited due to inductive and capacitive characteristics of overhead lines and cables.
- The achievable transmission distance of an AC cable lies between 40 and 100 km, depending on transmission capacity, system frequency and permissible power losses.
- Two AC systems with different frequencies cannot be directly connected.
- It may be impossible to directly connect two AC systems having the same frequency or establishing a new connection within a meshed grid due to system instability, unacceptable short-circuit levels or undesirable power flow scenarios.

HVDC transmission systems also have a number of other advantages when compared to HVAC, which are outlined in the following section.

1.3 Advantages and Disadvantages of HVDC versus HVAC

In this section a comparison is made between HVDC and traditional HVAC transmission systems, highlighting the advantages and disadvantages of HVDC systems.

1.3.1 Advantages

Due to its independence of frequency, HVDC lines can be used to transmit power between unsynchronised AC networks or AC systems with different frequencies [4]. Regulation of DC transmission power via electronic control can also be used to dampen power oscillations on AC grids, which improves the stability of such systems [4]. DC systems can also prevent cascading failures within AC networks, while still enabling power transfer if smaller failures occur [2]. Cascading failures occur on

either fully loaded or slightly overloaded systems, when one element fails and its load is shifted to other, nearby elements. Those elements are then pushed beyond their operating limit, thus shutting down and transferring their loads to yet other elements. This causes a chain reaction of failures which leads to a total system shut-down in a very short time [5]. Using digital control in HVDC transmission systems facilitates fast and accurate power regulation, allowing for quick compensation in the event of an element failure and so preventing the occurrence of cascading failures [2].

Stability problems may also occur in generators situated in remote areas and connected to long AC transmission lines. Such generators may loose synchronisation with the distant AC power system. A connection via a HVDC line would stabilize such a connection, since synchronization is of no concern when using DC transmission. This would make remote generating areas (e.g. off-shore wind farms) more feasible [3].

HVDC lines can carry more power per conductor than AC systems for a given power rating. The reason for this is that the peak voltages of an AC line are higher than the constant DC voltage [3]. Also, skin effects on conductors do not occur in DC systems, and so the whole conductor cross section can be utilized for power transmission [2]. In addition, digital control systems used in HVDC systems allow accurate and fast control of power flow. A newly patented scheme, called the Tripole current-modulating control, allows the conversion of existing HVAC lines to HVDC systems [3]. By controlling the loading of the conductors, such a system can then transmit up to 80% more power using the existing infrastructure. HVDC systems also do not require intermediate reactive power compensation [2].

In HVDC lines, inductive and capacitive parameters do not limit transmission capacities, which means the conductors are only subject to their thermal loading constraints [6]. Not only does this mean that the power transmission capabilities are greater in HVDC systems, but they also have smaller line losses due to the absence of high charging currents and additional I^2R losses brought about by capacitive and inductive elements on AC lines [2].

Both HVAC and HVDC lines exhibit corona discharges, since the electric fields surrounding the conductors and insulators of the lines cause the creation of ions in the surrounding air. Corona discharges result in power losses (termed 'corona losses'), radio-frequency interference, in the release of toxic gaseous compounds and in arcing damage to line equipment [3]. Corona losses on power lines are depended on weather conditions and can increase by a large margin in the event of rain or frost. However, HVDC lines show less sensitivity to weather changes than HVAC lines, reducing the corona power losses [6]. Space charges forming around the conductors in HVDC lines also help to reduce corona losses by up to half the loss per unit length of that found in HVAC lines with equal power ratings [3].

HVDC systems also carry economical advantages when compared to AC systems. When conducting feasibility studies on different possibilities for transmission systems, the following three factors are important [2]:

- Station terminal costs.
- Line costs.
- Capitalized value of losses.

HVDC systems require more sophisticated station equipment (e.g. rectifiers), resulting in higher station terminal costs for such systems. However, the cost per km for HVDC lines is less than that of HVAC lines, since HVDC lines require fewer conductors for a given power rating [3]. The reduced power losses on HVDC lines result in a reduction in the capitalized cost of line losses. In effect, this means that there exists a break-even point where the initial high station costs for DC lines are compensated by the lower line costs. After this break-even point, HVDC systems are a cheaper solution than HVAC systems [2]. This relationship is displayed in Fig. 2. Typical values for the break-even distance range from 500 to 800 km, depending on factors like country-specific cost elements, interest rates and cost of right of way [2].

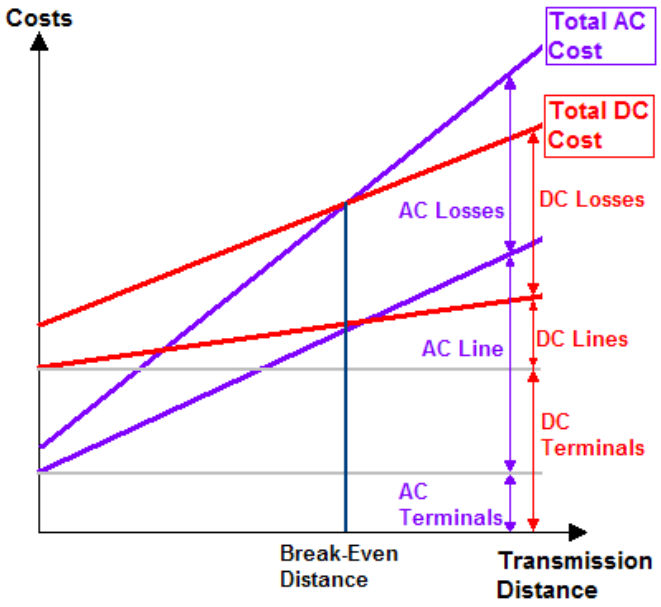

Fig. 2: Relationship between total cost of transmission lines vs. transmission distance for AC and DC voltages [2].

Finally, HVDC technology is also advantageous from an environmental point of view. Since it requires smaller structures and fewer conductors than HVAC systems of equal power rating, its visual impact is lower and it requires less land compensation when considered for a new project [4]. It is also possible to increase the power capacity of existing transmission systems by changing them from AC to DC, which can be done without building additional structures [4].

1.3.2 Disadvantages

Station equipment for HVDC lines (e.g. static inverters, rectifiers) are expensive as well as sensitive, and usually cannot be overloaded by a large extend [4]. Power regulation must thus be carefully observed to prevent damage to the equipment. Also, power losses in the inverters may exceed those on HVAC lines for short transmission systems. The high cost of the station equipment is thus not sufficiently countered by the low line cost of the HVDC line, making an AC system the more feasible solution [3].

The power flow in HVDC systems must be regulated by a control system in order to function efficiently. In a multi-terminal system, this means that good communication is required between individual terminals to achieve a fast and accurate control [3]. Realizing multi-terminal systems or expanding existing schemes is thus complicated

and requires careful design and planning to be implemented successfully [3].

A variation in altitude has similar effects for both AC and DC systems: the insulation requirements increase with an increase in altitude above sea level [6]. The required insulator dimensions are influenced by various factors, such as lightning, switching and pollution performance. However, AC and DC systems are not affected equally strong by these various factors. Insulation requirements for AC systems are dominated by the switching performance of the air gaps, while the dominant factor for HVDC systems is lightning performance [6]. The influence of lightning, switching and pollution on insulation requirements with increasing altitude is shown in Fig. 3.

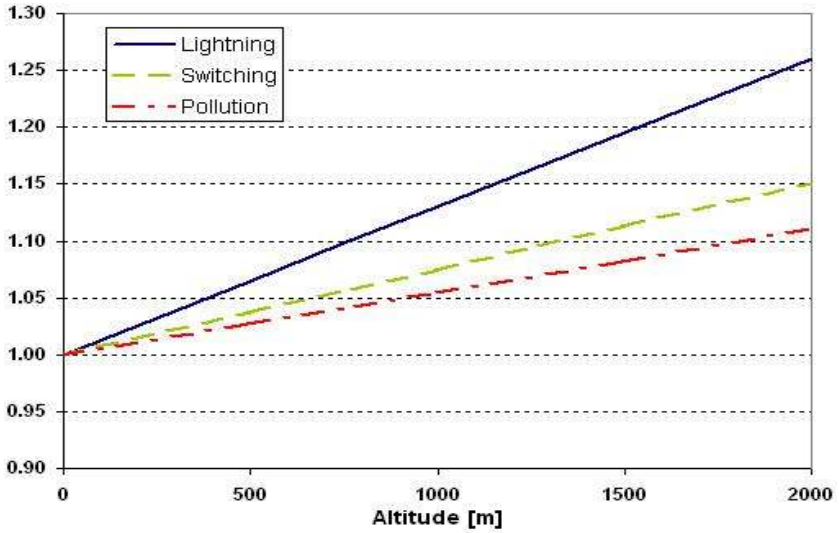

Fig. 3: Relative increase in insulation requirements at different altitudes [6].

As seen from Fig. 3, systems dependant on lightning performance needed a larger increase in insulation requirement with increasing altitude than systems dependant on either switching or pollution performance. It thus follows that HVDC systems require a larger increase in insulation requirement than HVAC systems with an increase in altitude [6].

Overall, HVDC systems present a superior alternative to HVAC systems for long distance transmission systems. Their capability for stabilizing existing systems is also a large advantage. It is thus to be expected that HVDC transmission systems will in future become more widely used by power utilities the world over.

1.4 Project description

As noted in section 1.1, the behaviour of insulator materials under HVDC conditions is not well documented to date. The aim of this project is thus to study the performance of several common insulator materials when exposed to HVDC voltages of both positive and negative polarity as well as to HVAC conditions. Although insulator materials can be affected by a large number of different factors, this study specifically focuses on the tracking and erosion resistance of the chosen materials when subjected to severe surface discharges caused by the application of surface pollution and the three different voltage types.

Considerable time has been spent on the development of a DC power source that can be configured for either polarity with a minimum of changes. The design of these sources is done in such a way that the final source can be implemented not only in a laboratory apparatus but also in field equipment for tests on actual insulators, again with only minimal changes to the design of the source.

The method of choice for these tests is the Incline Plane Test (IPT) method. Since this internationally standardized test method entails several different procedures for the testing of insulator material, the first part of this project thus focuses on the comparison of these different test procedures in order to determine the method that will deliver the most severe results in terms of tracking and erosion.

The second part of the project consists of a comparison of several common polymeric insulator materials exposed to AC as well as positive and negative DC voltages. The materials are compared according to a number of different evaluation criteria. Additionally, this study does not only focus on an inter-material comparison for each separate voltage type, but also on possible changes in the performance of different samples of each individual material when subjected to each of the three different voltages.

The results of this study will form the foundation work of further studies, which will include tests under field conditions. These studies will the aid NamPower in choosing the optimal insulator materials for the Caprivi Link project as well as in drawing up an

informed maintenance plan based on the expected insulator lifetimes on the HVDC lines.

1.5 Thesis overview

This thesis is structured as follows:

Chapter 2 provides a literature study covering the most common groups of insulators materials, their known failure modes and different factors responsible for the ageing of insulator materials. Special topics like the hydrophobic properties of silicone rubbers and typical chemical changes occurring in polymeric materials during electrical discharges are also described.

Chapter 3 covers the international test standard to be used during this project, the apparatus description and the design of diverse test equipment. The development of the DC sources is discussed in detail, as is the development of a mathematical model to refer the pollution conductivity measured at different temperatures back to a specific base temperature.

In **Chapter 4** the different test procedures for the IPT method are outlined, followed by the description of the analysis methodology and evaluation criteria used to compare the methods to one another. The results for each criterion are presented and discussed, and a choice for the preferred test method is made based on these results.

Chapter 5 consists of the comparison between the performances of the different insulator materials tested under the three different voltage types. The individual materials are described, as are the test procedure and evaluation criteria used to compare the materials to one another. The results for each of the criteria are discussed and explanations for certain observed trends and occurrences are given where applicable.

Finally, **Chapter 6** contains the final conclusions and recommendations.

Chapter 2: Literature Study

This chapter highlights some of the major topics in the field of insulator theory, with the emphasis on areas such as various insulator materials and their characteristics, as well as common causes for insulator degradation and failure.

2.1 Main groups of insulator materials

This section highlights the most commonly used insulator materials and their relative strengths and weaknesses. Insulator materials can be grouped together in two main groups:

- Inorganic materials.
- Polymeric materials (e.g. organic, Non-Ceramic Insulators or NCI's).

Inorganic materials consist of two major subgroups, glass and ceramics, while the polymeric materials can be further divided into composite insulators and resin insulators. Each of the four subgroups will be described in detail in the following sections.

2.1.1 Glass insulators

Glass insulators mostly consist of a mixture of silica, limestone, dolomite, feldspar and soda ash [7]. They are either made from annealed glass or, if high mechanical loads require it, from toughened glass. A good inspection method for identifying defective insulators is the use of thermal shocks, which shatter insulators that have not been properly toughened when manufactured.

The use of glass insulators for DC systems can lead to thermal runaway on the insulator [7], a process which will be described in later sections. Ionic migration caused by the application of a DC voltage can also lead to mechanical stresses developing in voids and inclusions in the insulator material. These stresses, under the right conditions and combined with stresses caused by other processes, can lead to shattering of the insulator shell [7].

Insulator types manufactured from glass usually include cap-and-pin and post insulators [61].

2.1.2 Porcelain insulators

Porcelain is a very stable material, and thus very immune to degradation through electrical discharge activities, ultra-violet (UV) radiation and other environmental factors [7]. Porcelain materials are often glazed to increase their mechanical strength as well as their resistance against pollution and contamination.

Porcelain is susceptible to thermal shocks similar to glass. Such shocks, often caused by arcing, may cause glaze damage and eventually lead to cracking of the porcelain [7]. The quality of porcelain insulators depends on material quality as well as the manufacturing process. The external shells are bonded to the core using cement, which is often aluminium or sulphur based. The consistency of the cement determines the mechanical characteristics of the insulator as well as its resistance to corrosion [7].

Porcelain materials are commonly used for insulator types such as cap-and pin, long rod, line and station post and hollow insulators [61].

2.1.3 Polymeric insulators

Polymeric insulators are usually classified into two groups [9]:

- Composite insulators, which are composed from more than one insulator material.
- Resin insulators, which are made using only one insulator material, such as a filled polymer.

These two subgroups will be discussed separately.

2.1.3.1 Composite insulators

Composite insulators can be divided into three major parts, namely the core, the housing and the end fitting.

The core is responsible for the structural integrity of the insulator. Conventionally, cores are manufactured by embedding glass fibres into a resin matrix [61]. The

volume of glass fibres used has a direct bearing on the mechanical properties of the insulator. An increase in the volume results in an improvement of some mechanical characteristics [7]. Additionally, the orientation of these fibres plays an important role in determining the electrical and mechanical properties of the insulator. Currently, a volume percentage of glass fibres of about 70% is utilized by most manufacturers [7].

The main purpose of the housing is to protect the core from UV radiation, moisture and electrical discharges [7]. Materials commonly used for housings include: silicone rubbers (SR), ethylene propylene diene monomer (EPDM), ethylene vinyl acetate (EVA), epoxy resins (e.g. cycloaliphatics) and various other polymer materials [61]. Silicone rubbers are usually preferred due to their ability to transmit their hydrophobic properties to pollutant layers on the insulator surface, preventing flashovers [19]. This will be explained in detail in later sections. The electrical performance of the housing depends on its shape and the characteristics of the housing material. SR and EPDM are preferred for transmission lines ($\geq$ 220 kV), while EVA is also commonly used for distribution levels ($<$ 220 kV) in addition to SR and EPDM [7].

Finally, the third part of composite insulators is the end fitting. Although this is also a critical part of a resin insulator, it is described at this point for the sake of consistency. End fittings are made from metal, as their mechanical strength must be sufficient to support the weight of the insulators and the attached cables or structures. Due to their importance, a high quality must be ensured in their manufacture. End fittings can take the form of pins, caps, flanges and a lot of other shapes. Metals commonly used include malleable cast iron, ductile iron, stainless steels and others [7]. Corrosion is a major problem on the fittings, and materials must thus be chosen so as to reduce that risk to a minimum. On HVDC lines, zinc rings can be added as sacrificial electrodes to prevent erosion [7]. Aluminium alloys are sometimes used due to their resistance to corrosion. However, their lower melting points make them more susceptible to damage by power arcs. Arcing horns thus have to be added when this material is used [7].

2.1.3.2 Resin insulators

Resin insulators are made from various types of heavily filled polymeric resins, including polyester, polyurethane and cycloaliphatic/bisphenol epoxies [7]. The fillers are added in order to improve the tracking and erosion resistance of the polymers, since their formulations include a fair amount of carbon [7]. However, high amounts of fillers make it more difficult to cast the final insulator shape. Formulations with filler contents above 90% are sometimes referred to polymer concrete [7].

Cycloaliphatic materials have the inherent weakness of being very susceptible to UV radiation [7].

2.2 Common failure modes

Insulators these days are very reliable items, with a failure rate of less than one in a thousand per annum [7]. The failure rate depends not only on the quality of the design and manufacturing process, but also if the correct insulator (in material and design) has been chosen for a specific service condition or application. Failure modes are specific to each type of insulator, being related to material and design [7]. The most common modes affecting the four major insulator materials outlined in the previous section are described here.

2.2.1 Mechanical failure and shattering

Mechanical failure is one of the most common modes encountered on insulators in the field. It is found on all insulator materials, although the reasons for such a failure are often connected to the specific design and material of the insulator [7].

A common mechanical failure mode found in glass and porcelain insulators is shattering. Shattering is caused by impurities gathered up during the manufacturing process. These impurities cause stress concentrations which can result in the insulator shattering spontaneously, although the rate for such occurrences lies at one per 10 000 annually [7].

Glass insulators are also prone to incur internal mechanical stresses produced by ionic migration within inclusions under the application of HVDC. These stresses can be high enough shatter the insulator [7].

Breaking or shattering due to thermal stresses is another common form of mechanical failure in porcelain insulators. Porcelain as a material is known to be damaged easily by abrupt temperature changes and/or uneven heating [7], such as experienced during power arcs. The damage usually takes the form of cracking of the glaze or shed breakage. Porcelain insulators thus need to be provided with arc protectors. High temperatures can also reduce the dielectric strength of porcelain. The material composition must thus be chosen according to the expected service conditions [7].

A special sort of mechanical failure found on the cores of composite insulators can take place at load levels well below the critical level. It occurs when both an acid and tensile stresses are present and is called brittle or stress corrosion fracture [7]. As the name suggests, the insulator fails due to a brittle fracture. The fracture area appears smooth over most of the cross section and is perpendicular to the core axis. A small area will be irregular, this being the area that was no longer able to withstand the load and thus failed in conventional tensile mode [14]. The sources of the acid can be due to several factors, including acid rain [15], the formation of nitric acid after electrical discharges in moist air [15] or the moisture reaching an improperly cured core, where hydrolysis of the core matrix produces the acid (this theory is yet to be proven) [16]. It is clear that brittle fracture can only occur when moisture is present in the core. Water-proof sealing of the core is thus critical [7]. Brittle fracture can be prevented by constructing the core from E-CR (corrosion resistant) glass fibres, which are less susceptible to acid erosion. This technique has been in use for 20 years with no failures by brittle fracture to date [7].

Further reasons for mechanical failure include vandalism and damages caused during transport, shipping and handling of insulators [61].

2.2.2. Thermal runaway

This failure mode is specifically found on glass insulators on HVDC lines. Electrical conduction through glass is mainly accomplished by ionic conduction. Ionic migration within the material can be aggravated by applying a DC voltage, depending on resistivity and temperature of the material. The flowing of an electrical current raises the temperature of the material, which decreases the resistivity. This increases the electrical current, which in turn increases the temperature. This process can repeat itself until the thermal capacity of the material is reached, leading to failure of the insulator. This process is called thermal runaway [7].

2.2.3. Material erosion due to electrical discharges

This failure mode is probably the most commonly found mode on any insulator in the field. It is mostly caused by pollution particles settling on the insulator surface. In the presence of water, this pollution layer becomes conductive and causes a small leakage current to flow through the layer along the length of the insulator. Through uneven drying of the surface, dry bands are formed. These dry bands are exposed to the system voltage [61]. Due to their small width (usually millimetres), the electrical fields exceed the breakdown strength of the surrounding air. The resulting electrical discharges cause local erosion and material deterioration due to the formation of large amounts of heat energy. The process also depends on the relative affinity for water of the insulator material.

In glass and porcelain insulator, severe erosion is usually found in the vicinity of the metal pin, as this is the area of the highest leakage currents [7]. Severe erosion at this critical point of the insulator can lead to mechanical of the insulator. Sacrificial zinc rings can be added to reduce the risk of such failures.

In composite and resin insulators, the combination of electrical stresses and environmental factors can not only cause erosion but also tracking, depending on the chemical composition of the insulator material [7]. Tracks are permanently conducting pathways and usually carbonaceous in nature [34]. They permanently decrease the creepage distance of the insulator, which increases the risk of flashover and insulator failure.

Sealing of the housing-to-core interface in composite insulators is particularly important. If pollutants are allowed to enter the core, they can produce internal electrical discharge that lead to erosion and tracking of the core [7]. This internal erosion is difficult to spot until the process has proceeded far enough along the length of the insulator so that flashover can occur, or if enough glass fibres have deteriorated along the cross sectional area of the core so that mechanical failure can occur [7]. Exposure of the core to the environment due to large erosion of the housing material can have the same effect [7].

Finally, electrical discharges occurring at the end fittings can develop into power arcs. Although usually not hot enough to damage the housing, power arcs might reach sufficient temperature to melt/evaporate enough of the metal so that the end fittings can no longer support the insulator. Depending on the severity of the arc, fracture can occur directly after or even during the arcing process. Aluminium fittings are especially susceptible to this failure due to the relative low melting point of aluminium metals [7].

2.2.4. Electrical punctures

This failure mode is similar to that of erosion through electrical discharges, but there are some marked differences in the processes.

Electrical punctures are mostly caused by steep fronted electrical pulses, which are caused by external processes like switching or lightning strikes rather than the normal operating system voltage. The dielectric strength of the insulating material is exceeded before the air can become ionized enough to flash over. The resulting breakdown of the material can create a channel in the insulating material, which can lead to intermittent line faults which are difficult to locate. Such faults are referred to as ‘nuisance tripping’ [7]. Resin and porcelain insulators are especially susceptible to this type of failure.

2.2.5. Ultra violet (UV) ageing

Although not directly a cause of insulator failure, UV radiation can further aggravate erosion and tracking, which can then in turn lead to insulator flashover and failure.

Some materials (like silicone) contain UV stabilizers to prevent this [7]. If not, UV radiation can cause chalking, crazing or cracking of the insulator surface, which speeds up the erosion process and ultimately insulator failure [12].

Splitting of sheds has been known to occur in some materials used for composite insulators (such as EPDM) due to a combination of mechanical hoop stresses, UV radiation and electrical stresses. This weakens the electrical characteristics of the housing and so insulator performance [7].

Resin materials are especially prone to damage through UV radiation [7], causing visual degradation of the insulator surface, such as chalking. Surface degradation is highly detrimental to the electrical performance of the insulator, especially in heavily polluted areas. For example, surface degradation can reduce the value of the power frequency wet flashover voltage of the insulator by up to 20% [10].

2.2.6. Failure of bonding materials

Cements, resin and other substances are frequently used as bonding materials at various interfaces in insulators. Failure of these bonds can either decrease the structural integrity of the insulator to a point where mechanical failure is inevitable, or it can yield possible sites of increased erosion and tracking, which can lead to flashover and electrical failure [7].

A common example of such a failure of the cement used to bind the metal fittings to the insulator body occurs in porcelain insulators. This cement must be carefully chosen according to the expected service conditions. Otherwise, separation could occur at the interface between the two substances, thereby weakening the connection and possibly leading to mechanical failure of the insulator [7].

Due to their large number of parts and resulting interfaces, composite insulators are especially vulnerable to this kind of failure. Problems commonly arise when the sheds are not bonded to the core. Filler materials like silicone grease can start to leak out and pollution can accumulate in the resulting gap. Finally, the sheds may start to

move along the core axis, exposing the core material and thus weakening the mechanical strength of the insulator [61].

Finally, exceeding the torsion or cantilever load limits can cause delamination (severing of bond between fibres and resin matrix) in the core of composite insulators, which can lead to mechanical failure. A specific location for such a failure is usually at the end fittings, since this area is subjected to extra stresses due to design and method of attachment of the fittings [7].

2.3. Factors affecting insulator material ageing

'Ageing' in connection with insulators is usually used to describe the deterioration of the insulator material over time. This slow breakdown of the material is induced by external factors, starting at the insulator surface and then proceeding deeper into the material or along the length of the insulator. Ageing of insulators decreases their electrical and mechanical performance, often to a point where failure of the insulator occurs and replacement is necessary.

This section illustrates some of the major factors responsible for insulator ageing. Although some of these factors do not actively cause material disintegration, they can be conducive to effects such as electrical discharges, which due to their high energy dissipation and temperatures can cause severe damage to the insulator material.

2.3.1. Pollution

Pollution is a broad term used for any particles that may accumulate on the surface of the insulator surface. Pollution is usually classified into two groups [7]:

- Pre-deposited pollution.
- Instantaneous pollution.

Pre-deposited pollution accumulates over a long period of time. It can either be active, which means that it can form a conducting electrolyte when wetted, or inert (non-soluble) pollution. Inert pollution cannot form an electrolyte, but it can act as binding material for active pollution and can so increase the area available for leakage current flow [7].

Instantaneous pollution occurs when the insulator surface becomes covered in a highly conductive pollutant. The status of the insulator changes from a clean, low conductive state to critical state/flashover in a very short time (< 1 hour). The contaminant then washes off, returning the insulator to a clean state [7].

Sources for pollution can be found in many different forms, ranging from marine and agricultural to industrial sources. Examples for pre-deposited pollution include salt, chemical waste products, bird droppings and many more [61]. Instantaneous pollution usually takes the form of already wetted contaminants, such as salt fog, acid fog or bird streamers [7].

2.3.2. Humidity and rain

A certain degree of humidity is usually needed in order for the pollution layer on the insulator surface to convert into a conducting electrolyte. Once this occurs, leakage currents can flow along the length of the insulator, leading to dry band formation and electrical discharges, which can damage the insulator material [26]. This humidity can be drawn from the surrounding air or can stem from fog and rain. Fog can also contain conductive particles (salts or acid) mixed in the water, which can lead to cases of instantaneous pollution and rapid flashover [7].

Rain is not only a source of humidity. Acid rain can also increase the conductivity of the pollution layer or react with the insulator material, causing degradation and erosion [7]. However, excessive rain (> 10 mm/h) can also wash off existing pollution on an insulator, thus preventing electrical discharges and ageing.

2.3.3. Solar radiation

Solar radiation consists of several radiation types of different wavelength and energy levels. Some types, such as high-energy UV-B photons, can cause deterioration in some insulator materials such as polymers and silicone rubbers [8].

2.3.4. Bird droppings and streamers

Bird droppings are rich in nitrogen. In the presence of water, this may lead to the formation of nitric acids which can damage the insulator material. Their highly

conductive nature also increases the leakage current, which can lead to increased electrical discharges. Special cases are bird streamers, which are long strings of bird excrement with a very high conductivity (20 - 40 kΩ/m) that can lead to immediate flashover [11]. The large energy levels set free in such processes can cause extensive damage to the insulator material.

2.3.5. Damage through animals & vandalism

Although these factors do not actively cause ageing, the damage caused by animals and/or vandalism can create areas on the surface of the insulator which deteriorate at a faster rate than the undamaged material and thus promote ageing of the insulator. Birds, rodents and termites are usually responsible for animal damage to insulators, especially in the case of polymeric insulators [7].

Vandalism is especially a problem with glass and porcelain insulators, since these types of materials are known to shatter under impact and thus present enticing targets [61]. Damage to the protective glazes of glass and porcelain insulators as well as the housings of composite insulators can present pollutants and acids with the opportunity to reach the core materials, promoting material deterioration and thus ageing [7].

2.4. Common pollution mitigation techniques

In the general case of insulator failure, the faulty unit is replaced with a new one which has improved mechanical and/or electrical capabilities to prevent a reoccurring of the failure. The improvement capabilities could consist of [7]:

- Increasing the creepage distance.
- Changing the profile.
- Choosing a different material.

However, sometimes limitations due to existing hardware and conditions prevent the replacement of the old type of insulator with a new, improved one. If this is the case, maintenance is needed in order to keep the insulator in a functional condition [7]. Since pollution is the single greatest factor in insulator failure, most of these methods deal with removing the pollution from the insulator or to prevent a large pollution build-up. Some of the most common methods are illustrated in the following sections.

2.4.1. Cleaning

Cleaning involves the removal of contaminant accumulations from insulators using either a liquid or solid cleaning agent. The procedure can be undertaken on live or dead lines, depending on the cleaning method employed [7]. Common methods include:

- Hand washing.
- Spray washing.
- Dry cleaning.

Hand washing, as the name indicates, is undertaken by human personnel who manually clean the insulators. Although this is a very effective method and requires no specialized equipment, it does have a number of serious drawbacks [7]. It can only be undertaken on non-active units to reduce the risk of electrocution for the workers. This means that long outage times must be expected when employing this method. The solvents used for cleaning must be tested prior to use to ensure that they do damage the insulator material. Most of them are also highly conductive, so the insulators have to be thoroughly rinsed after cleaning [7]. Abrasive cleaning utensils must be used with caution since they might cause damage to the insulator surface.

Spray washing involves spraying the insulators with high pressured water or other cleaning agents to wash pollution off. Specially designed nozzles break the water jets down into small droplets to increase the electrical resistance between operator and equipment [7]. It can be done on live, energized equipment, and can even be undertaken in difficult terrain using helicopters (although at high costs). However, this method is only effective for pollution which is easily soluble. The water used must be of low conductivity, and specialized equipment should be used [7]. Care must also be taken not to wet adjacent equipment under live conditions, which could otherwise cause flashovers in those units.

This method can also be implemented as a fixed, computerized washing system for live lines. This reduces the setup time for the process and poses no danger to the operator. However, it is a very capital-intensive option, and the equipment requires a high level of maintenance. Even the slightest malfunction can cause artificial wetting of the insulators rather then washing, inducing flashover faults [7].

Finally, dry cleaning employs small, solid particles which are blasted over the insulator surface in order to remove contaminants and pollutants. Due to their non-conducting nature, organic substances (e.g. ground corn cobs, walnut shells) are used [61]. This method has proven to be the most effective when dealing with compact, insoluble deposits. However, an accumulation of cleaning materials on the ground can present a serious fire hazard, as dried organic material is usually very flammable [7].

Overall, the biggest problem with cleaning of insulators as pollution mitigation is establishing an optimum time schedule. As insulator performance depends on several factors, it is difficult to determine the best time for cleaning based only on pollution level [7]. Leakage current levels have been suggested as a measure of the pollution level of the insulator, but can be misleading since they do not allow for the accumulation of dry contaminants which are non-conducting in the absence of water. Potential high leakage current levels are thus not discovered until it is too late [7]. Cleaning of insulators is also useless in areas where instantaneous pollution occurs, since even fully cleaned insulators can flash over in a matter of minutes [7]. Different kinds of preventative measures are thus needed.

2.4.2. Silicone greasing

This method entails coating the insulator surface in silicone-based grease. The grease is applied uniformly and at least 2 mm thick. Special care is taken that no bridging between adjacent sheds by grease clumps occurs. The grease creates a hydrophobic surface, which means that wetting and the formation of a continuous conducting layer is greatly inhibited [61]. It also encapsulates pollution particles, isolating them from one another and preventing them from forming a conducting electrolyte by rendering them insoluble. Combined, these two effects produce a pollution protection far more efficient than mere cleaning. The water-repellent property of the grease is also useful in combating instantaneous pollution [7].

Care must be given to choosing the correct type and quality of silicone grease for the desired application, since not all greases are applicable for HV applications. Newly introduced greases should be field tested on their applicability before being put into

service. Dielectric strength, water repellence and encapsulating ability are some of the most important properties according to which the grease is graded [7].

Over time, the grease becomes saturated with pollutants and loses its effectiveness. This causes leakage current levels to increase, causing localized heating which further accelerates material degradation [7]. If the grease is not replaced, leakage currents can cause damage to the insulator material itself. The service life of the grease depends on factors such as the conductivity of the pollution, or the amount of non-soluble contaminants adhering to the grease layer, cancelling its encapsulating effects [7]. The use of silicone grease is unsuited for areas where a large amount of non-soluble contaminants is present (e.g. cement dust, fly ash), as this could result in rapid clogging of the grease layer [7].

Replacing of silicone grease layers is a costly and often unpleasant task. The old layer must be completely removed before a new layer can be applied, which is a time-consuming process and can result in long power outages [61]. The waste materials must also be disposed of properly, since they can prove a safety hazard to operating personnel. The cost, frequency and nature of the re-greasing process have lead to the preference for utilizing silicone rubber coatings [7].

2.4.3. Silicone rubber coating

Rather than using grease, this method utilizes a layer of silicone rubber that is sprayed onto the insulator surface in layers of 0.3 – 0.5 mm thick in order to improve the pollution resistance. The coating of insulators with silicone rubber makes them highly hydrophobic, even under polluted conditions [61]. This is due to the capability of the silicone rubber to impart its hydrophobic nature on any contamination layer covering its surface, thereby providing protection even under adverse conditions [7]. And since the surface is not as sticky as grease, non-soluble contaminants are less likely to accumulate. Such insulators can even be washed in the same manner as uncoated insulators [7].

Prior to the coating process, the insulator surface has to be carefully prepared by cleaning it meticulously of any grease and other pollutants. Although often time

consuming, this process is necessary to ensure permanent adhesion of the layer, and the improved protection more than justifies the effort [7]. The coating life is determined by a combination of factors such as ambient pollution severity, creepage distance and insulator quality. However, it is considerably longer than that of silicone grease, lasting up to 10 years. The condition of the coating can be visually checked by spraying the surface with water and observing the degree of hydrophobicity [7].

Re-coating of existing layers can be achieved by rubbing the surface with a mildly abrasive cloth to remove all lose contaminants. The insulator is then rinsed off and the new layer can then be sprayed directly onto the old layer [7].

The advantages of silicone rubber coatings lie in its beneficial surface characteristics and resistance to degradation by electrical and climatic stresses. It also provides protection against both pre-deposited and instantaneous pollution and is suitable for all types of environment, even those with a high level of non-soluble pollutants [7].

2.5 Hydrophobicity properties of silicone rubbers

In a chemical context, hydrophobicity refers to the physical property of a molecule having a low affinity for water or a surface that resists the formation of a continuous water layer [17]. Hydrophobic molecules are usually non-polar, whereas water molecules are polarized. Hydrophobic molecules are also unable to form hydrogen bonds. Water molecules, on the other hand, are capable of forming hydrogen bonds internally [17]. Due to these chemical differences, water repels non-polar (hydrophobic) molecules in favour of bonding internally. This process is the reason for the minimal contact surfaces observed between water and hydrophobic substances.

Hydrophilic molecules, on the other hand, are molecules that exhibit the physical property of bonding with water through hydrogen bonding. Since these molecules are usually polar, they also readily dissolve in other polar solvents [17]. A hydrophilic surface will form a continuous water layer or film along its surface. Some materials have such a high affinity for water that they attract water molecules from the surrounding environment. The water molecules may even penetrate the surface and are stored within the material itself. Such materials are called hygroscopic [18].

Hydrophobic materials are extremely suitable and desirable for use as insulator materials. Hydrophobic materials prevent water films from bridging the gap between the insulator ends, thus inhibiting the formation of a conducting layer and a resulting line-to-earth fault [27]. This prevents electrical discharges which could damage the insulator surface. Leakage current levels and thus power losses are also greatly reduced [19].

Hydrophobicity is not a static property, but can rather be lost or gained depending on surface and environmental conditions [19]. The excellent recovery of its hydrophobic properties is one of the reasons why silicone rubbers have become one of the primary materials used for insulators.

2.5.1 Structure of silicone rubbers

Silicone rubber (SR) consists of a polymer fused together with a filler material by a process called vulcanisation [24]. The polymer usually consists of a backbone of silicone and oxygen, which bond in an alternating pattern to form either long molecular chains or, if the end molecules are bonded to each other, cyclic molecules [19]. Organic, carbon-based groups are attached to the silicone molecules, with the type of organic groups used determining the physical and chemical properties of the product [31]. Fig. 4 shows the structure of a typical silicone rubber molecule, where R stands for the organic groups attached to the silicone.

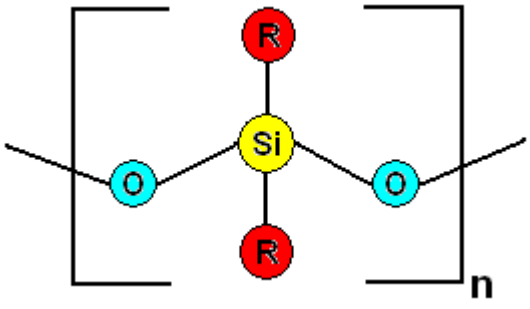

Fig. 4: Typical silicone rubber molecule, with silicone-oxide backbone and two functional groups [31].

The use of silicone as a base molecule (in conjunction with oxygen) offers many advantages. For one, the silicone-oxygen bond is very strong, which offers thermal stability for the final molecule over a wide range of temperatures [24]. Other advantages include the resistance to chemical or natural attack, good dielectric properties, fire resistance and it being a relatively harmless substance. Compared with

other polymers, silicone rubbers can offer good spreading capabilities (advantageous when used as a coating material), outstanding tolerance of high temperatures, UV and infra-red (IR) radiation and a strong resistance to a large number of external factors [31].

Several different forms of the common silicone-oxygen structure can be found within silicone rubber molecules. Each of these performs a different function within the molecule, according to the number of bonds not occupied by organic molecule groups. Table 1 lists the four different structural groups as well as their individual functions [31].

Table 1: Functional groups of silicone-rubber [31].

Name of Group	Structure	Number of Oxygen Links	Function
Monofunctional unit (M-group)	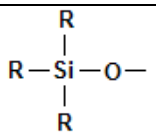	1	→ Serve as chain terminators → Found at end of long chain molecules
Difunctional unit (D-group)	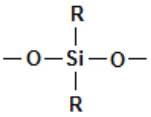	2	→ Most common backbone molecule → Found in both chain and cyclic molecules → Cyclic if low molecular weight & short-chained → Linear if high molecular weight & long-chained
Trifunctional unit (T-group)	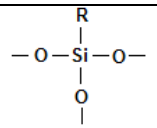	3	→ Used for cross linking between chains → Form three dimensional molecules
Quadrifunctional unit (Q-group)	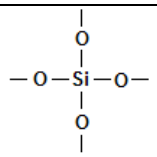	4	→ Used for cross linking → Strengthens molecule structure after curing

The intermolecular bonds cross-linking the individual chain molecules to each other are typically low in strength, resulting in excellent flexibility of the elastomers but also yielding a low mechanical strength [19]. Fillers are thus added to improve the mechanical properties (e.g. tensile strength, shear strength etc.) of the silicone rubber. Typical filler materials used are alumina trihydrate (ATH), silica, quartz, mica or

kaolin [20]. The filler material and quantity used have a significant influence on the properties of the final silicone rubber product, affecting such things as thermal conductivity, water absorption, hydrophobicity, leakage current development and erosion and tracking resistance [26, 31]. Laboratory and field tests have revealed that an ATH filler content of 40 – 60% by mass is satisfactory for silicone rubber materials used in outdoor applications [62].

As mentioned previously, cross-linking between the polymer molecules is done by the process of vulcanization. Performed at different temperatures, this process yields a number of different silicone rubber types. Curing at a temperature of 200 °C produces High Temperature Vulcanized (HTV) silicone rubber, whose good mechanical strength, resistance to ageing and dielectric properties make it an efficient material for manufacturing insulators [24]. Vulcanization at room temperatures results in a product aptly named Room Temperature Vulcanized (RTV) silicone rubber. The curing of this polymer either occurs on contact with atmospheric humidity (one-component RTV) or upon combination of two separately manufactured components of the same polymer (two-component RTV, or RTV-2) [31]. The dielectric properties and ageing resistance of RTV silicone rubber are similar to that of the HTV products. However, its lower viscosity and good adhesion allow it to be used for the coating of insulators and other high voltage equipment [31]. Other products include Low Temperature Vulcanized (LTV) silicone rubber and liquid silicone rubbers. However, these products are not commonly used for high voltage insulation purposes.

2.5.2 Mechanism of hydrophobicity

Since the 1970's, silicone rubbers have become very popular for use as insulator materials due to their strong hydrophobic capabilities. This hydrophobic property is mainly due to two factors, namely the diffusion of Low Molecular Weight (LMW) molecules and the orientation of the methyl groups attached to the polymer molecules [19].

2.5.2.1 Diffusion of LMW molecules

LMW molecules are pieces of polymer sections with a molecular weight < 1000, compared to the normal weight of HTV silicone rubber molecules of $5x10^5$ [20]. Due

to their low weight and small size, they can move freely throughout polymer and filler material and accumulate at the surface.

If a pollution layer forms on the surface of the silicon rubber, the LMW molecules diffuse into the pollution layer and encapsulate the pollution particles [19]. Since the molecules are hydrophobic themselves, the pollution layer turns hydrophobic as well, severely decreasing leakage current levels. This ability to turn a surface pollution layer hydrophobic is one of the greatest advantages of silicone rubber. An exception to this phenomenon occurs when the pollution layer consists of a homogeneous salt layer. However, such a type of pollution is very rare under natural conditions [19].

LMW molecules are lost when the pollution layer is washed off by rain or other causes, which is termed an indirect loss of LMW molecules [27]. Accordingly, the hydrophobicity of the surface is lost to some degree. LMW molecules diffuse from deeper levels of the rubber to the surface, and the surface hydrophobicity recovers. There are two major sources of LMW molecules within the silicone rubber:

- A large reservoir of LMW already existing within the material, formed during the process of vulcanization [22].
- LMW is produced by the breaking (scission) of long chain molecules, which is known as LMW regeneration. This process happens naturally, although surface discharges and concentrated radiation (ionizing radiation, high energy electrons, X-rays etc.) do speed up the process. In general, the quantity of LMW generated by regeneration is far less than that already present within the material [29].

The gradual loss of LMW molecules from the silicone rubber is one of the main factors in the ageing of such materials. Reasons for losses of LMW molecules are electrical surface discharges, evaporation, leaching through interaction with water and through chemical reactions [19]. These losses are termed direct losses of LMW molecules.

2.5.2.2 Orientation of methyl groups

As mentioned previously, different organic, carbon based groups can be attached to the silicon-oxygen backbone by various chemical processes. The most common group

used is methyl (CH_3). Silicone rubbers are thus often referred to as polydimethylsiloxanes (PDMS) materials. The methyl groups are free to rotate around the silicone-oxide backbone [31]. At the surface of the material, the molecules arrange themselves in such a way that the silicone oxide molecules face inwards and the methyl molecules point outwards. Since methyl is non-polar and water molecules are polar, the two different molecules repel each other. The layer of methyl molecules thus creates a hydrophobic surface, as shown in Fig. 5.

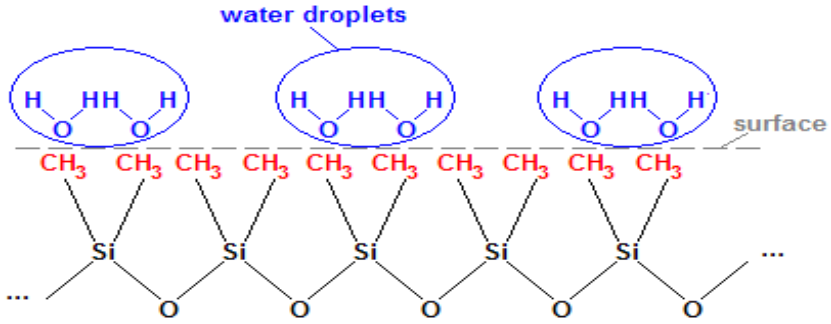

Fig. 5: Hydrophobicity mechanism in surface of silicone rubber [31].

Sometimes, however, the polymer molecules rotate around the axis, with the result that the methyl now point inwards and the silicone oxide now forms the surface layer [29]. The polar water molecules are now attracted to the polar oxygen atoms in the backbone. The rubber surface changes from hydrophobic to hydrophilic. A water film forms on the surface which, if pollutants are present, can form an electrolytic solution, causing an increase in leakage current levels. Surface hydrophobicity can be recovered by further reorientation of the molecule chains in such a way that the methyl groups once again face outwards.

Research has shown that the recovery of hydrophobicity in silicone rubber surfaces is two thirds due to LMW diffusion and one thirds due to reorientation of the polymer chains [23].

2.5.3 Causes for loss of hydrophobicity

Loss of hydrophobicity in silicone rubbers and other polymers depends on a number of external factors. One of the major causes is electrical discharge activity, such as dry band arcing or corona [19]. The energy liberated in the discharges causes fragmentation of the polymer chains, especially in smaller molecules such as the LMW molecules. These fragments can either evaporate directly or bond with water

and leach from the material [20]. In a secondary process, discharge activity can cause the formation of acids from air and water, which lead to surface degradation. This erosion causes a decrease in the hydrophobicity, which in turn aggravates the surface discharges [25, 28].

Water is another primary cause for the loss of hydrophobicity. Aside from causing a loss of LMW molecules by leaching them from the material, water can also cause a reorientation of the methyl groups in the polymer chains, causing an increase in hydrophillicty [19]. In the presence of a soluble pollution layer on the insulator surface, excess water can form a conductive film across the insulator. Local drying of this film leads to the formation of dry bands and an increase in surface discharges. Water droplets can also distort the electric field along the insulator, leading to an increase in field strength that can be up to six times higher along the edges of the droplets. The results can be the formation of water drop corona, increasing the discharge activity along the surface and promoting loss of hydrophobicity [30].

Temperature has a dual affect on hydrophobicity of polymer surfaces. Elevated temperatures (> 400 °C) caused by arcing lead to an increase in surface erosion. The relation between erosion mass and temperature is exponential [32] and causes a decrease in surface hydrophobicity. LMW diffusion and chain scission are also increased with elevated temperatures, further decreasing hydrophobicity [19]. However, an increase in LMW mobility means that these molecules diffuse to the surface faster, which aids in the recovery of hydrophobicity [21].

Material choice can also have an effect on hydrophobicity. Different vulcanisation processes can lead to different amounts of LMW molecules present in the polymer. For example, HTV silicone rubbers contain 3% LMW by mass, while RTV silicone rubbers contain 5% [27]. Higher amounts of LMW can result in higher hydrophobicity in the material. Since transfer of hydrophobicity is a property of bulk material rather than a surface phenomena, thin layers of polymer material are found to recover slower than thick ones [19].

Filler contents in the polymer may also influence its hydrophobic properties. Higher filler contents may result in decreased hydrophobicity levels. However, they also

seem to suppress leakage current development and thus, by extension, surface degradation [25]. Some studies have also shown that high filler levels decrease the rate of LMW diffusion, slowing the recovery of surface hydrophobicity [27]. However, some studies have shown the opposite to be true [25].

Finally, it should be stated although hydrophobicity can be lost temporarily, it is seldom completely lost in silicone rubber polymers. The LMW reservoirs within the materials have been found to be large and are also replenished due to scission of the molecule chains by electrical discharges. Since LMW diffuses into and encapsulates the pollution layers only in minimal amounts, these reservoirs are almost impossible to deplete. Studies have show that, even after eight to twelve years, depletion of the LMW reservoir has not reached significant levels [21].

2.6 Chemical reactions of PDMS materials during dry band arcing

It was already mentioned in previous sections that insulator materials are susceptible to erosion and tracking due to electrical discharges and dry band arcing occurring on the material surface in wet conditions. NCI materials such as PDMS (silicone rubber) are especially susceptible to this process. Apart of the visible erosion, these discharges also induce changes in the insulation material through chemical reactions occurring at the locations of the electrical discharges. This section gives an overview of the most common chemical changes occurring in PDMS type insulation materials.

The dissociation or breaking of the chemical bonds between the molecules requires sufficient amounts of energy. Accordingly, such processes usually occur in the insulation material at the location of the dry band arcing, due to the high temperatures frequently observed at these areas. However, heat can also be transmitted along the surface and through the bulk of the material to regions adjacent to the locations of electrical discharge activity. This results in a gradual heating of these areas until the accumulated heat energy is large enough to cause gradual chemical changes in these regions as well [47].

The type of chemical reaction taking place depends on the relative bond strengths of the molecules present in the material. Bond strength is measured in terms of bond-

dissociation energy, which is the energy required to break the bonds for one mole of a given molecule in its gaseous form [54]. When heat energy is being supplied to a material, those molecules showing the lowest bond strength are separated first. In the previous section, the general structure of PDMS was given as a silicone-oxygen (Si-O) backbone with two methyl groups (CH_3) attached to each silicone atom. The Si-O bond has a high bond energy of 444 kJ/mol, which explains the high thermal resistance of PDMS materials [49]. The Si-C and H-C bonds show weaker bond strengths of 327 kJ/mol and 414 kJ/mol, respectively. The chemical changes in PDMS thus usually occur preferably in the methyl groups (or other types of functional groups) rather than in the siloxane backbone. The type of chemical reaction occurring also depends on the types of elements present in the material and the surroundings at the time the reaction takes place.

The chemical change in a PDMS material is usually caused by the following three processes [48]:

- Scission (breaking) and interchange of either bonds or chains.
- Hydrolysis of siloxane bonds and hydrocarbon groups.
- Oxidation of hydrocarbon groups and crosslinking of siloxane bonds.

In the scission process, the heat energy liberated by the arcing process causes scissions in either the methyl groups or even the siloxane backbone, creating free radicals of form ·O, ·CH_3 or ·Si, with the dot designating the atom as a free radical [51]. Free radicals are molecular fragments with a highly reactive nature, due to them having one or more unpaired electrons in the outer electron shell [54]. Due to their reactive nature, they usually exist only in a transitional state before combining with other molecules to form new substances. Fig. 6 shows the formation of these free radicals from the PDMS structure.

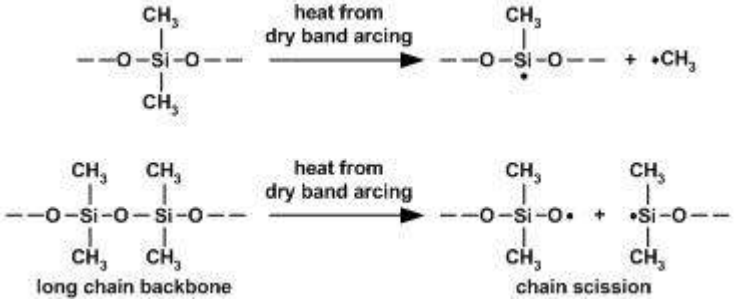

Fig. 6: Scission of PDMS chain and formation of free radicals [47].

After the formation of the free radicals, interchange reactions can occur. This means that two neighboured chains combine after having been broken into smaller chains, with the shorter chains fusing with their counterparts in the neighbouring chain according to the type of radicals formed [47]. This process is shown in Fig. 7.

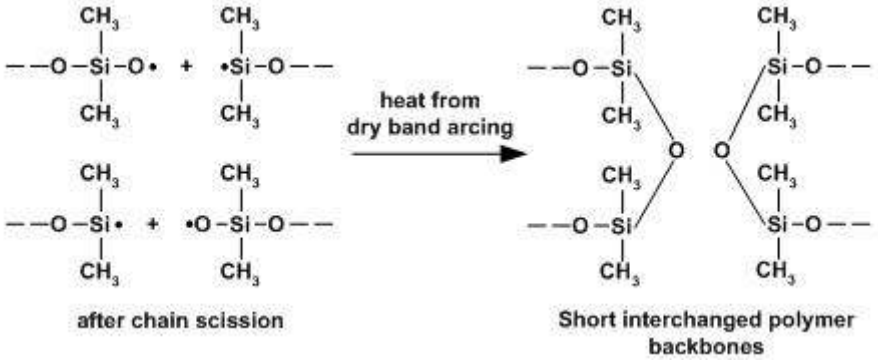

Fig. 7: Interchanging reaction between two split polymer chains [47].

In some cases, however, no free radicals are formed. Rather, one polymer chain combines with a hydrogen atom from another polymer chain after scission to form an –OH group through a hydrolysis reaction. Crosslinking occurs in the remaining polymer chains as indicated in Fig. 8 [47].

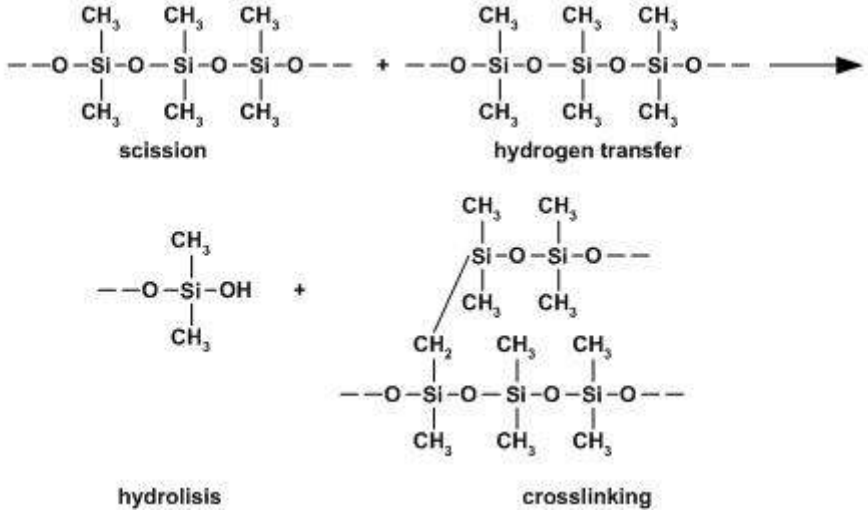

Fig. 8: Polymer chain scission without free radical formation through hydrolysis and crosslinking [47].

The hydrolysis process usually takes place in the presence of water (H_2O), deposited on the material surfaces by processes like rain or fog. If such a condition exists, hydrolysis of the PDMS structure will occur due to water being split into –OH and –H groups through electrical discharge processes. Hydrolysis reaction can be responsible for a large mass loss due to random scission occurring in the polymer chains [52].

The –OH and –H groups formed during the disassociation of water combine with the free radicals formed in the scission process to form chains with silanol (SiOH) as side and end groups, with a possible liberation of methane gas (CH_4) depending on the free radicals present [47]. Fig. 9 shows typical hydrolysis reactions in the presence of water, with the (g) indicating the formation of a gaseous compound.

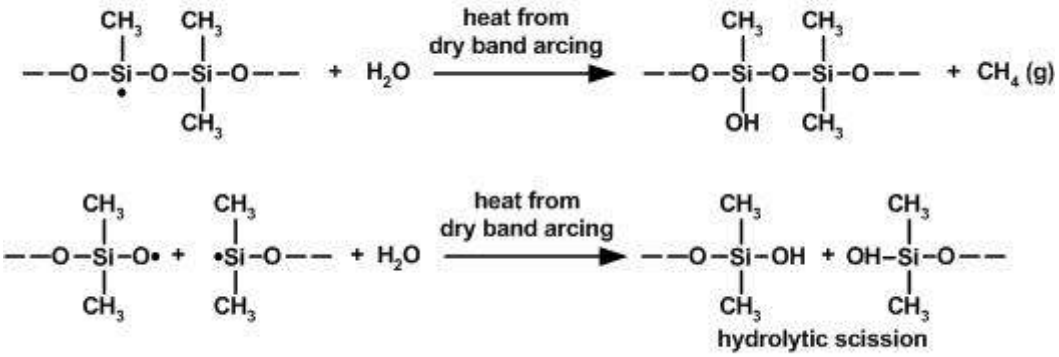

Fig. 9: Hydrolytic reactions in the presence of water [47].

The rate of scission in the PDMS chains is directly proportional to the amount of water present on the material and in the surrounding atmosphere, reaching a maximum when the water vapour content in the environment reaches its saturation point [47].

Finally, the oxidation process follows the hydrolysis of the siloxane bonds and hydrocarbon groups. The crosslinking process can link two parallel polymer chains, create a branching from one polymer chain to several others or form several shorter polymer chains [47]. All these different processes are presented in Fig. 10.

However, the hydrolysis reactions do not occur on materials in well ventilated surroundings due to the low water vapour content in the atmosphere at the material surface. Instead, further crosslinking reactions occur between the PDMS chains through oxidation of the methyl groups, which causes the material to become brittle if exposed to extended periods of high temperatures [48].

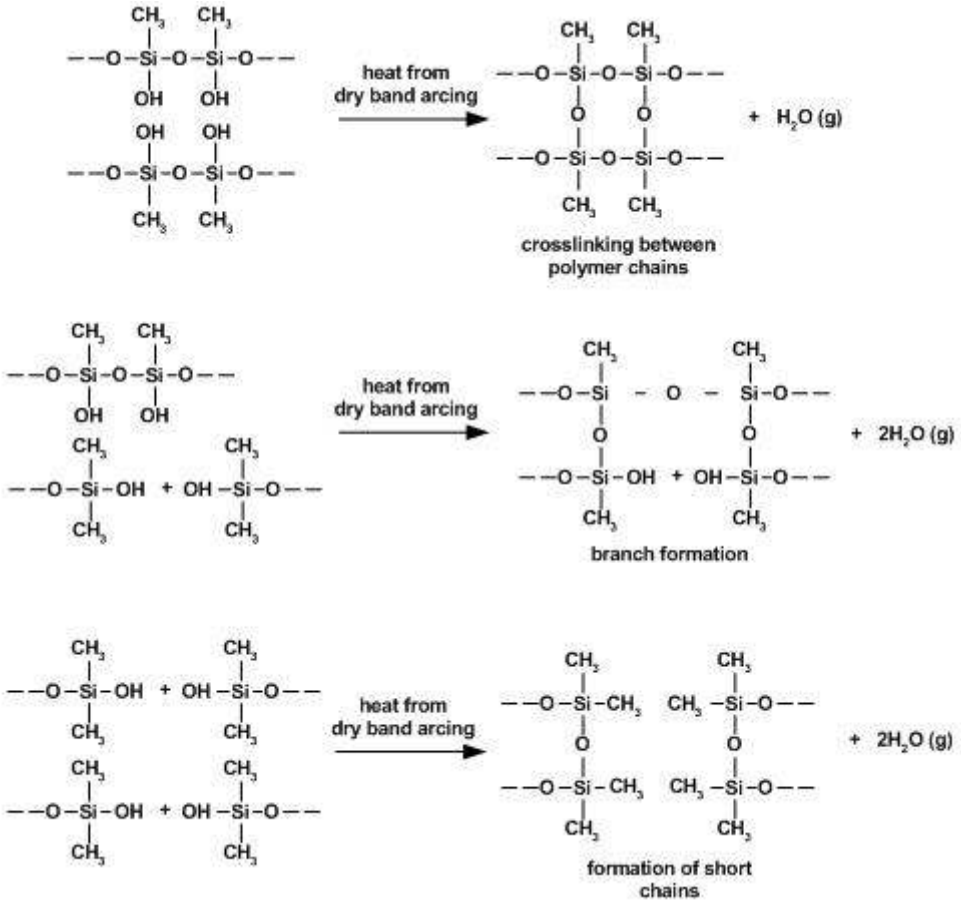

Fig. 10: Possible forms of crosslinking between polymer chains [47].

The chemical changes observed in PDMS materials are not necessarily due to the chemical reactions of the three processes described in this section. If the temperature of the dry band arcs becomes high enough, methyl groups can be split off directly and even the bonds of the siloxane backbone can be broken, resulting in the formation of gaseous methane and deposits of silicone dioxide (SiO_2) [47]. The reactions are shown in Fig. 11.

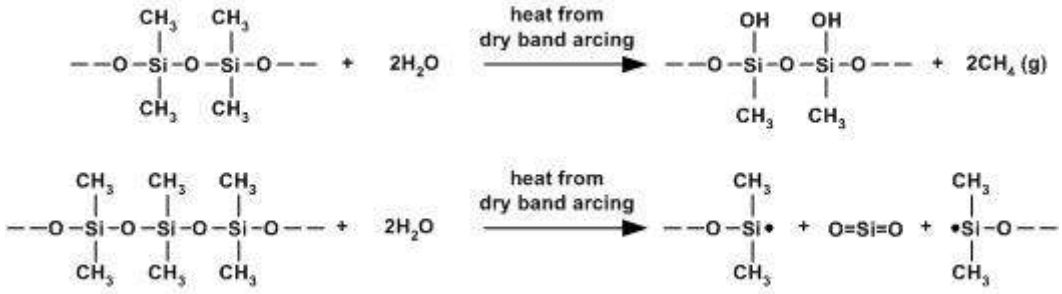

Fig. 11: Formation of methane and silicone dioxide through intense arcing [47].

The silicone dioxide deposits can be removed from the material surface by excess water, resulting in a mass loss from the material. The temperature of the arcing process has to rise to a level higher than 400 °C, since tracking and erosion in PDMS materials have only been observed to occur if hotspots of a temperature of > 400 °C were formed [33, 62]. However, chemical changes have been observed to occur at temperatures of ± 200 °C, especially if sufficient oxygen is present [50].

Chapter 3: Test Apparatus & Methodology

As outlined in the project description, the main objective of this project is to compare different insulator materials under the effects of high voltage AC and DC. Insulator performance, however, depends not only on the material, but also on form and design factors, such as specific creepage distance, number of sheds and shed spacing. A test is thus needed in which every factor except that of material influence is kept constant or even eliminated. Accordingly, the test-of-choice for this project is the Incline Plane Test (IPT), which is detailed in the IEC 60587 [34] and the ASTM D2303 standard [35].

3.1 General test procedure

The Inclined Plane Test method is specifically designed to evaluate insulation materials according to their resistance to electrical erosion and tracking [34, 35]. Material degradation is induced allowing dry band arcing to take place on the surface of the material sample, thus causing the material to erode.

The material samples to be tested are clamped onto a stand which orientates them at an angle of 45° to the horizontal, with the test surface facing downwards. Two electrodes are then fastened to the top and bottom of the sample. The respective shapes of these electrodes are shown in Fig. 12.

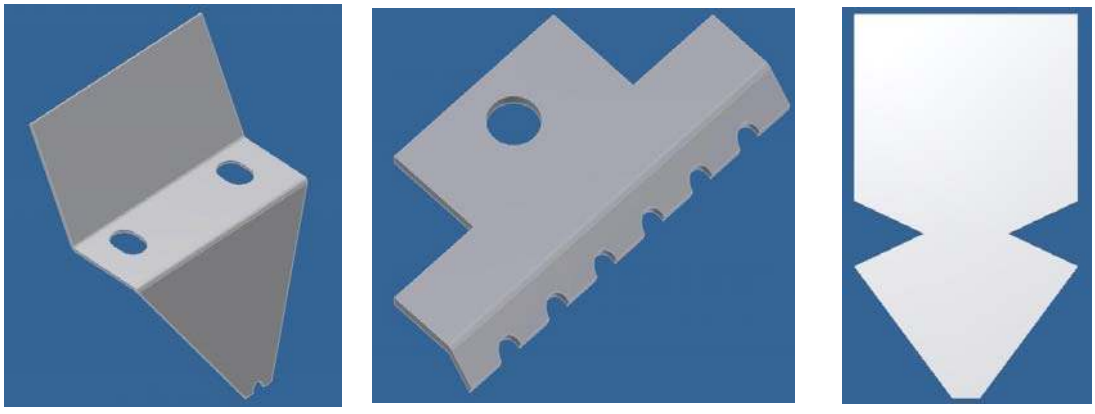

(a) **(b)** **(c)**

Fig. 12: General shapes of (a) High voltage electrode, (b) Ground potential electrode and (c) Filter paper.

In order to induce dry band arcing, the sample surface is polluted using a liquid contaminant. The contaminant is pumped from an external container into a small reservoir consisting of eight layers of filter paper clamped between the top electrode and the sample. Fig. 12 shows the form and dimensions of the filter paper. The contaminant then flows from the semi-circular hole in the top electrode along the sample surface between to the bottom electrode. The filter paper serves to make the contaminant stream more continuous. Fig. 13 shows the arrangement of the test sample.

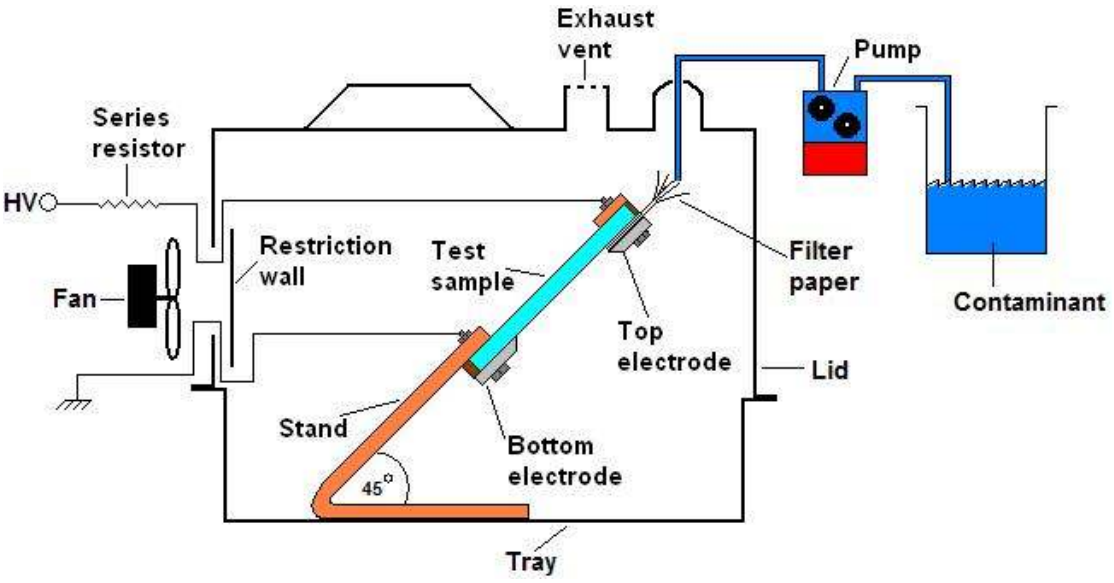

Fig. 13: General arrangement for insulator sample for Incline Plane Test.

The selected test voltage is then applied to the electrodes. Since the bottom electrode is connected to the ground potential, it is often referred to as the ground potential electrode and the top electrode is called the high voltage (HV) electrode. This causes a leakage current to flow along the contaminant path over the sample surface. A resistor is connected in series with the sample on the high voltage side to reduce the leakage current to a safe magnitude. The leakage current causes the liquid to heat up and evaporate. A dry band starts forming at the bottom electrode, and dry band arcing is induced at this point, causing the sample to erode. If the material is prone to the formation of tracks, the erosion/tracking will proceed to move along the sample towards the top electrode.

Although not specifically stated in any of the international standards, the mounted samples are placed within a Perspex tray and covered by a Perspex lid during all experiments for the purpose of this study (see Fig. 13). This was done to protect the

operator and any person coming into close proximity of the test, as well as to prevent any interference with the test proceedings.

The contaminant used in this type of test consists of distilled water mixed with 0.1% by mass of ammonium chloride (NH_4Cl) and 0.02% by mass of a non-ionic wetting agent [34]. The ammonium chloride makes the contaminant conducting. The volume conductivity of the solution should be σ_S = 2.53 mS/cm at a temperature of 23 °C, with a tolerance of ± 0.03 mS/cm. The wetting agent lowers the surface tension of the liquid, allowing it to wet the sample surface more thoroughly. This is especially important when testing material with highly hydrophobic surfaces to ensure a continuous stream of contaminant between the two electrodes in order to keep the arcing process as constant as possible. The wetting agent used in this project was Triton X-100, a non-ionic surfactant which has been recommended by several studies [33, 36]. Some studies also state that the reason for using NH_4Cl is that it supports the development of heat and leaves no surface residue [36]. However, this is not supported in either of the two international standards [34, 35].

The contaminant evaporating due to the heating effect of the leakage current results in the formation of steam and other gaseous by-products. These may condensate on the sample surface, forming a liquid film at locations other than the normal contaminant path. This can result in unwanted electrical discharge activity all over the test sample, interfering with the normal test procedure [34]. In order to prevent this, ventilation is provided by a small fan at the back of the Perspex enclosure (see Fig. 13). Exhaust vents allow the gaseous to escape the enclosure before condensation can take place. However, since direct airflow over the sample is also undesirable (as this increases the rate of evaporation of the contaminant fluid) the airflow is directed against a restricting wall (see Fig. 13) [34]. This disperses the airflow around inside of the enclosure before it exits through the exhaust vents, carrying the gaseous products with it.

Since the samples used for the IPT method have similar geometries for the energized area, the erosion and tracking resistance of the tested materials are not influenced by differences in shape of the sample specimen, which otherwise can have a significant effect on evaluation criteria such as leakage current magnitude [55]. Pollution and

environmental factors are also kept constant at a chosen level. The only major factor affecting the performance of the sample is thus the type of insulation material used, and the samples can be compared based on this specific aspect alone.

Each one of the two international standards mentioned previously describes two alternate test methods which can be employed, namely the constant voltage method and the stepwise voltage method [34, 35]. Both test duration and failure criteria for a sample are determined by the choice of test method and standard. Since the choice of test method depended on the outcome of a series of tests conducted during the course of this project (see Chapter 4), a decision had to be made only regarding to which international standard should be employed for all experiments done in this project.

3.2 Choice of international standard

As mentioned previously, two standards exist for the IPT method, namely the IEC 60587 and the ASTM D2303 standard. These standards agree on most points concerning test arrangement and apparatus, sample preparation and test procedure. Even the two test methods available for this kind of experiment are similarly described in both standards.

However, the two standards differ quite clearly on the critical issue of failure criteria for a given test sample. Each standard lists two major failure criteria. In the case of the IEC 60587 standard, the two criteria are the same for each test method [34]:

- *Criterion A*: A sample is deemed failed if the magnitude of the leakage current exceeds the value of 60 mA for more than 2 seconds, the sample shows a hole due to excessive erosion or the sample catches fire.
- *Criterion B*: A sample is deemed failed if the sample displays a track longer than 25 mm (as measured from the lower electrode), the sample shows a hole due to excessive erosion or the sample catches fire.

These criteria can be used for either one of the two test methods.

In the ASTM D2303 standard, the failure criteria are directly linked to the employed test method [35]:

- *Stepwise voltage method*: A sample is deemed failed if progressive tracking due to formation of hotspots has occurred between the 2nd and 3rd full hour of the test. The hotspot should develop a track of a minimum length of 13 mm measured from the bottom electrode.
- *Constant voltage method*: A sample is deemed failed if the sample develops a track longer than 25 mm measured from the bottom electrode. Samples are compared according to the time needed to reach that track length.

After careful consideration, it was decided to utilize the IEC 60587 standard for all tests conducted during the course of this project. Sample failure was to be determined using failure criterion A. This decision was based upon the fact that it is difficult to positively distinguish between simple erosion and tracks merely by visible observation. Conductivity tests can only be conducted once the test has been completed, and even then often remain inconclusive.

On the other hand, leakage current magnitude can be measured with relative ease and accuracy. Leakage current is also widely regarded as a main parameter for measuring insulator performance [7]. Analysis of leakage current data also facilitates the comparison between different insulator materials, which is one of the main objectives of this project. Moreover, use of this failure criterion allows the use of a safety relay which monitors the leakage current and interrupts the circuit if the current exceeds 60 mA for more than 2 seconds. The process of classifying a sample as failed or not can thus be automated, increasing its accuracy. Examples of such an overcurrent relay can be found in the standard [34].

Although the test will be run according to the IEC 60587 standard, the author has introduced some minor changes based on information given in the ASTM D2303 standard. These changes will be mentioned at a later stage. A more detailed description of the two different test methods described in the standard is given in Chapter 4.

3.3 Test apparatus & arrangement

3.3.1 General apparatus & control circuit

According to the IEC 60587 standard, the IPT apparatus requires a power supply with a frequency of 45 – 65 Hz and variable up to a minimum voltage of 6 kV. The source should be able to deliver a current of 100 mA for every test specimen connected to the supply. It should be noted at this point that it is possible to test up to five samples simultaneously when using the IPT method. The output voltage of the supply should be stabilized to 5% [34]. Fig. 14 shows the circuit diagram of the Incline Plane Test apparatus used for the AC tests.

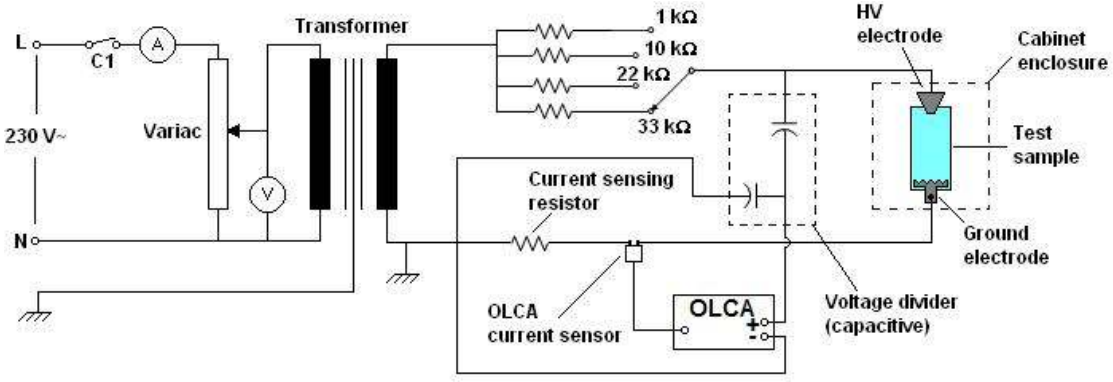

Fig. 14: Circuit diagram for Incline Plane Test apparatus - AC arrangement.

The machine is powered by a 3.75 kVA, 230 V / 7.5 kV step-up transformer, which in turn is powered from a wall socket. The transformer is capable of supplying a maximum current of 500 mA on the secondary side [37]. This allows the simultaneous testing of five samples. The output is variable up to 7.5 kV by means of a variac, which is situated on the primary side of the transformer. The frequency of the test voltage is 50 Hz.

The test apparatus is operated via a control circuit shown in Fig. 15 [37]. It is activated by pushing the start button, which is a normally open switch. This closes the control circuit (provided that the stop and the emergency stop button are in their normally-closed states) and activates relay C1, which in turn closes contactor C1 in Fig. 15 and activates the machine. Additionally, the relay also closes auxiliary switch $C1_X$ in the control circuit, which allows the relay to remain energized even if the start button is released. A test indicator lamp is lit upon activation to give visual confirmation that the apparatus is live, and a digital timer is also activated. The timer

allows the user to keep track of the experiment duration, and can be manually deactivated via the timing input switch.

The test can be interrupted either by pressing the stop button or the emergency stop button, both of which are normally closed switches [37]. Both open the control circuit, de-energizing relay C1 and subsequently opening contactor C1 in the primary circuit, which interrupts the supply voltage. The emergency stop was introduced as a safety feature, since it locks into place once activated, permanently disabling the apparatus until it is reset by the user.

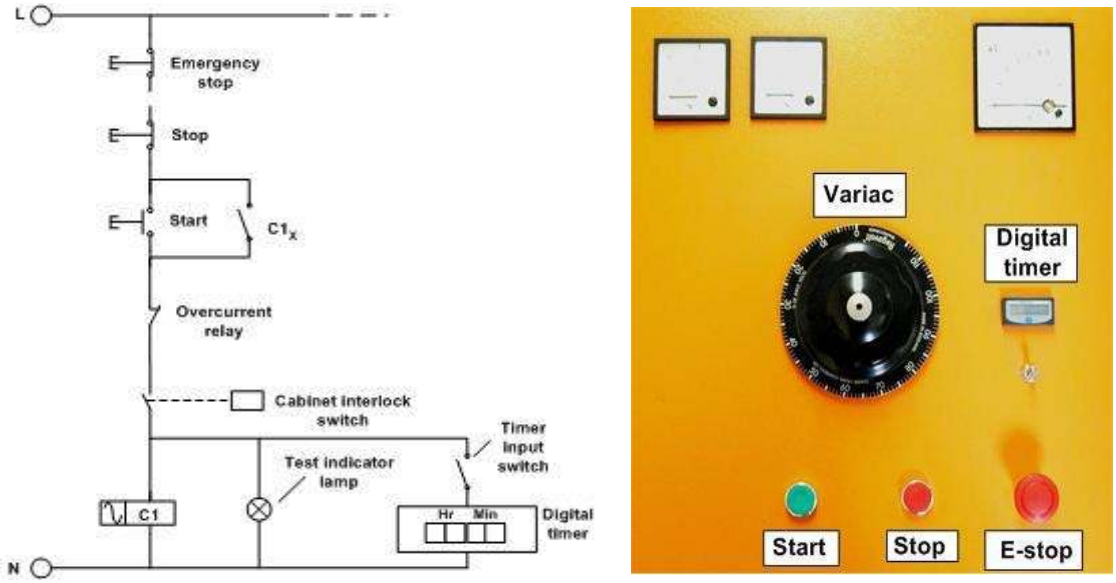

(a) (b)

Fig. 15: (a) Circuit diagram and (b) Actual photograph of control circuit of IPT.

The Perspex cabinet is also fitted with a normally open cabinet interlock switch as an additional safety precaution [37]. This switch is connected in series with relay C1 in the control circuit and is only closed if the Perspex lid is correctly placed onto the tray. If the cabinet is opened under live conditions, the interlock switch opens and interrupts the control circuit. This prevents the user from interfering with a live sample and reduces the risk of electrocution.

As mentioned previously, the IEC 60587 standard specifies that a test specimen has failed if the rms current exceeds 60 mA for a time period longer than two seconds [34]. The standard also states that an overcurrent relay can be used to deactivate the machine in the occurrence of such an event. Such a device also provides additional safety against damage to the apparatus due to high currents. Fig. 16 shows a block

diagram outlining the operation of the ovecurrent relay employed in the IPT apparatus, which was designed as part of an undergraduate thesis. Detailed circuit information can be found in the original source [38].

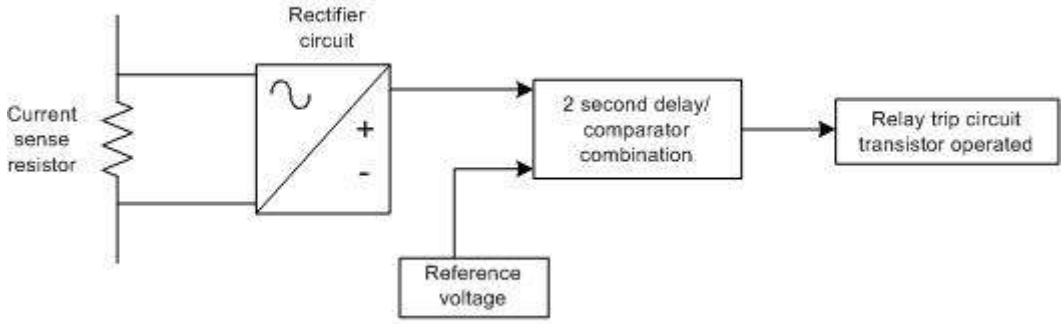

Fig. 16: Schematic diagram of overcurrent relay circuit [38].

The current flowing in the test circuit is converted into a voltage measurement by means of a 10 Ω resistor placed in series with the test samples, on the ground potential side. The measured voltage is then rectified and compared to a reference voltage. Once the measured voltage exceeds the reference voltage, the comparator circuit enables a two second delay timing circuit while still continuously monitoring the voltage over the current sensing resistor. If the measured voltage exceeds the reference voltage for a duration longer than two seconds, a transistor-operated relay is activated. This relay is situated in the control circuit (see Fig. 15). Upon activation, the relay opens the control circuit, cutting off the power supply to the apparatus and stopping the test. The relay resets itself to its normally closed position after a short time period. However, since an opening of the control circuit also deactivates contactor C1 (see Fig. 15), the test needs to be manually restarted before a voltage is applied to the test sample again.

3.3.2 Current limiting resistors

As described in section 3.1, a resistor must be placed in series with the test sample in order to limit the leakage current flowing through the circuit. The value of the resistor as well as the flow rate of the liquid contaminant depends on the magnitude of the test voltage applied to the sample. Table 2 shows resistor values and contaminant flow rates for different voltage ranges as given in the IEC 60587 standard [34].

Table 2: Resistor values and contaminant flow rates for chosen test voltage ranges [34].

Test voltage [kV]	Contaminant flow rate [ml/min]	Series resistance [kΩ]
1.0 to 1.75	0.075	1
2.0 to 2.75	0.15	10
3.0 to 3.75	0.30	22
4.0 to 4.75	0.60	33
5.0 to 6.0	0.9	33

According to the IEC standard, the resistors should have a power rating of 200 W each. However, due to problems with availability of resistors with that power rating, the 22 kΩ and the 33 kΩ had to be made up from series and parallel combinations of smaller resistors. No such problem was experienced with the 1 kΩ and 10 kΩ resistors, and single wirewound resistors were used for these two values. Fig. 17 shows the set of current limiting resistors used in the apparatus.

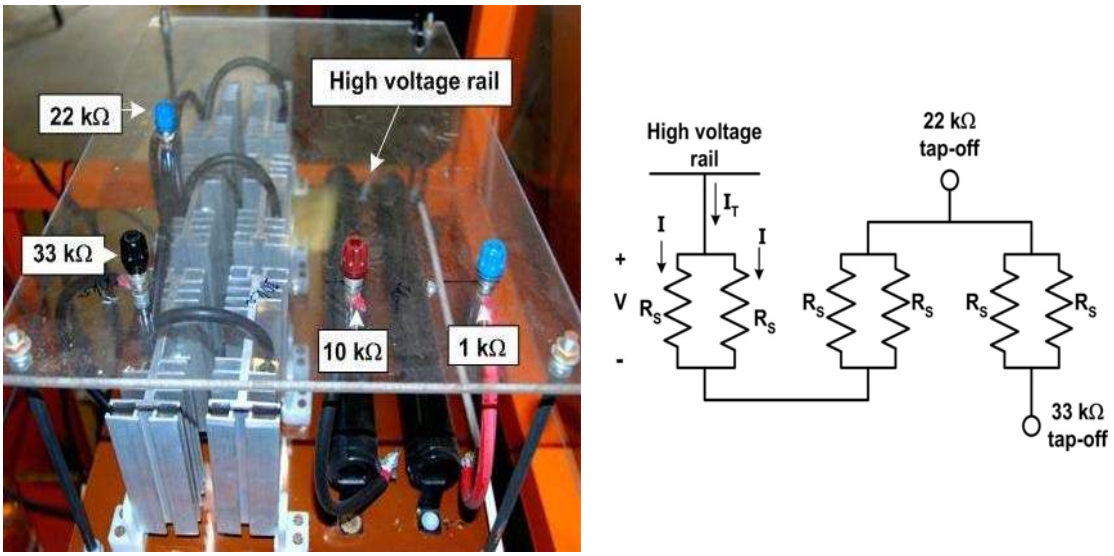

(a) **(b)**

Fig. 17: (a) Actual resistor configuration and (b) Ladder network design for 22 kΩ and 33 kΩ resistors.

A single ladder network of three parallel resistor pairs connected in series was used to for both the 22 kΩ and the 33 kΩ resistors, as shown in Fig. 17. For the individual resistors R_S, wirewound resistors of 22 kΩ each were used. Each parallel combination of two R_S has the total resistance of

$$R_{2S} = \frac{R_S^2}{2 \times R_S} = \frac{(22\,\text{k}\Omega)^2}{44\,\text{k}\Omega} = 11\,\text{k}\Omega\,. \qquad (3.1)$$

Since resistances in series are added together, the 22 kΩ tap-off is situated after the second parallel combination and the 33 kΩ tap-off after the third parallel combination.

The resistors were mounted on heatsinks, which increased the power rating of each resistor to 50 W. In each parallel combination, the total current can be expressed with reference to Fig. 17 as

$$I_T = I + I. \tag{3.2}$$

The voltage drop over each resistor in the combination is V and the resistors are of equal magnitude R_S. The currents flowing through each resistor of the combination are thus equal to each other and can be expressed as

$$I = \frac{V^2}{R_S}. \tag{3.3}$$

The magnitude of the individual currents is thus half the magnitude of the total current flowing through the parallel combination, $I_T = 2*I$. Since the power dissipated in each resistor R_S is $P_S = I^{2*}R_S$, it follows that the power rating of each parallel combination is double the power rating of R_S, i.e.

$$P_{Parallel} = I^2 \times R_S + I^2 \times R_S = 2 \times I^2 \times R_S = 2 \times P_S. \tag{3.4}$$

Since the power dissipated over resistors in series is the sum of the power dissipated in each resistor, it follows that the power rating of the 22 kΩ tap-off is 200 W and that of the 33 kΩ tap-off is 300 W. Although the increased power rating of the 33 kΩ tap-off is not in accordance with the standard, it ensures that the resistors are capable of handling the leakage currents without running the risk of burning out, which would disrupt test proceedings.

3.3.3 Measuring of leakage current

The leakage current data is measured and logged by use of an Online Leakage Current Analyzer (OLCA). This device was designed by CT Lab (Pty) Ltd for measuring leakage current data on live insulators in the field, as well as corresponding weather data of the site. The device has twelve channels available for measurements, nine of which used for current and three for voltage measurements. Four additional channels can be used for logging weather data. The logged data is stored on an internal database and can be downloaded via a RS232 connection or remote modem to a designated workstation. Plots of various parameters can then be generated using the supplied software. Fig. 18 shows the OLCA device.

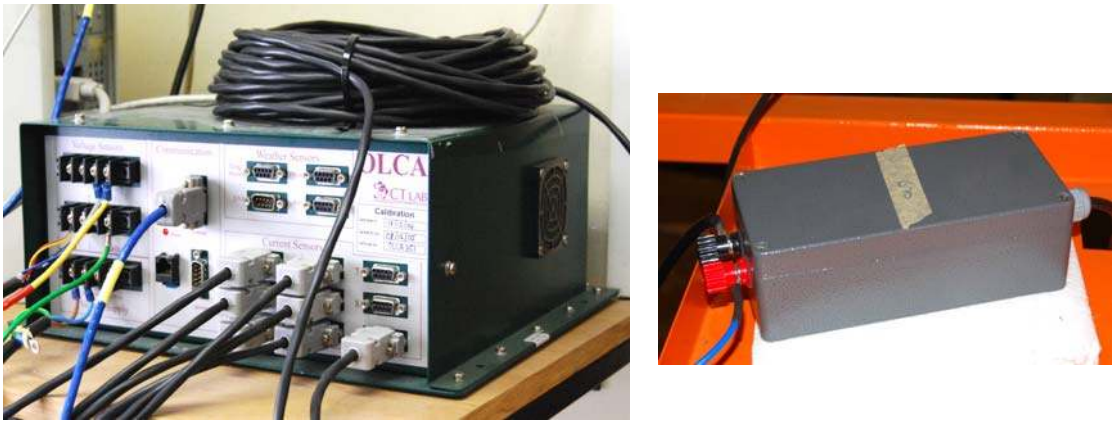

(a) **(b)**

Fig. 18: (a) OLCA apparatus and (b) OLCA current sensor

Fig. 18 also shows the current sensor used to measure leakage current data. Although the OLCA can operate 9 sensors simultaneously, only one current sensor and channel is utilized for this experiment, since only one sample is tested at any given time. The current sensor is installed in series with the test samples on the ground potential side (see Fig. 14). The sampling rate of the device is 2 kHz, and the sensor is capable of measuring peak currents up to ± 500 mA.

The measured data is used to compute several parameters over a user-defined interval. This interval was set to the lowest possible value of one minute for all experiments conducted during this project. Computed parameters that can be downloaded from the device include rms current, electrical charge conveyed (both positive and negative) and maximum peak current (both positive and negative) for each interval. The OLCA further counts all occurrences of peak currents that fall within certain user-defined categories or bins. These bin counts can then be displayed on a daily basis or over a certain period (greater than one day).

For voltage measurements, the measurement points are connected to one of the three differential voltage channels. For all experiments conducted during this project, the voltage measured is the voltage drop over the test sample, since this is the actual voltage applied to the sample. Again, only one voltage channel was utilized, since only one sample was tested at a time. By linking the voltage channel with the corresponding current channel, the OLCA is able to compute the average power dissipated over the test sample during each interval.

The input measuring range of the OLCA's voltage channels is ± 400 V (rms). Since the voltage drop over the test sample is in the kilo-volt range, a voltage divider is needed in order to reduce the voltage magnitude so that it can be safely measured by the OLCA. The reduction ratio is entered in the device software, which then multiplies the measured voltage with this ratio to obtain the true voltage drop between the measuring points.

3.3.3.1 Design of capacitive voltage divider

It was decided to construct a capacitive voltage divider for the AC test arrangement. As a design starting point, the dividing ratio was chosen to be such that for the full transformer output voltage of 7.5 kV, the input voltage to the OLCA should not exceed 250 V. This voltage was chosen so as to protect the OLCA voltage channels. The minimum divider ration is thus

$$N = \frac{7500\ \text{V}}{250\ \text{V}} = 30. \tag{3.5}$$

The choice of the capacitor magnitude and arrangement is largely left to the designer's discretion. The final design consisted of a number of 2.2 nF capacitors connected in series for the high voltage side and a 4.7 nF capacitor for the low voltage side of the divider. Fig. 19 shows a schematic of the divider circuit.

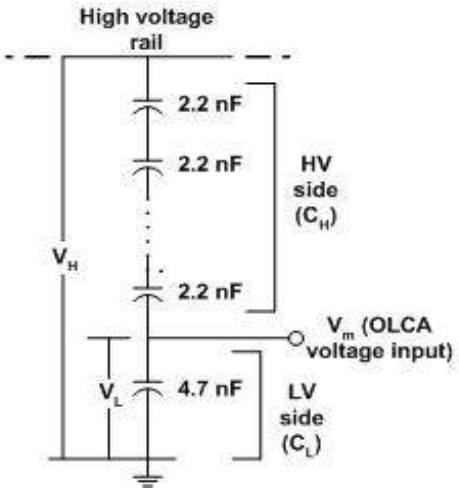

Fig. 19: Capacitive voltage divider circuit.

The maximum voltage rating for both types of capacitors is 1000 V (DC) and 400 V (AC). The minimum number of capacitors needed on the high voltage side of the divider to withstand this voltage can be obtained by dividing the expected peak voltage by the AC rating of the capacitor. This number was calculated to be

$$N = \frac{7500\ \text{V}}{400\ \text{V}} = 18.75 \approx 19. \tag{3.6}$$

In order to prevent damage to the divider, the total number of capacitors for the high voltage part of the divider was chosen as 25 capacitors of 2.2 nF each, connected in series. The total capacitance of the high voltage part is

$$C_H = \frac{2.2\ \text{nF}}{25} = 88\ \text{pF}. \tag{3.7}$$

The capacitance of the low voltage part is $C_L = 4.7$ nF.

Since the frequency of the input voltage is f = 50 Hz, the impedances of the two parts of the divider can be calculated as

$$Z_H = \frac{-i}{2\pi f C_H} = -i36.172\ \text{M}\Omega \tag{3.8}$$

and

$$Z_L = \frac{-i}{2\pi f C_L} = -i677.255\ \text{k}\Omega\,. \tag{3.9}$$

The ratio of the divider can now be calculated by solving the circuit of Fig. 19 for the ratio of V_H/V_L, which is

$$\frac{V_H}{V_L} = \frac{(Z_H + Z_L)}{Z_L} = 54.41 \approx 54. \tag{3.10}$$

The voltage measured by the OLCA at the divider tap-off must thus be corrected by multiplying it with a ratio of 54 in order to obtain the true measured voltage.

However, initial testing of the divider revealed the ratio of 54 to be inaccurate. The reason for this is that the previous calculations make no provisions for the input impedance of the OLCA voltage channel. Fig. 20 shows the circuit diagram of the divider with the input impedance.

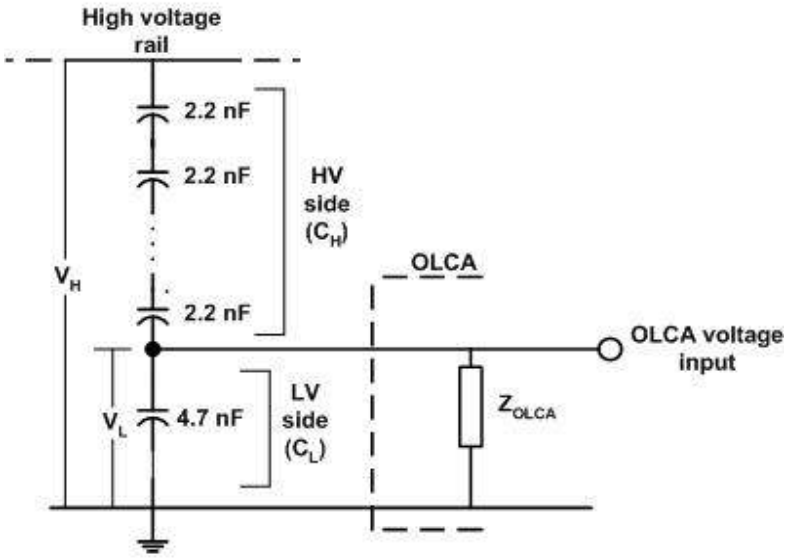

Fig. 20: Capacitive voltage divider circuit including OLCA input impedance (Z_{OLCA}).

Datasheets state the input impedance of the OLCA voltage channels to be larger than 1 MΩ. Actual measurements using a TBM811 digital multimeter showed an input impedance of Z_{OLCA} = 4.03 MΩ. Since the multimeter showed a measurement under resistive settings, it can be safely assumed that the impedance is resistive in nature and will thus be referred to as R_{OLCA} in future. The voltage channel of the OLCA uses the same earthing point as the IPT apparatus and the voltage divider. R_{OLCA} is thus situated in parallel with C_L, forming an RC-circuit. The impedance of the low voltage part of the divider calculated in equation 3.9 is now changed to

$$Z_L^* = \frac{(Z_L * R_{OLCA})}{(Z_L + R_{OLCA})} = 110.689 - i658.652 \ \text{k}\Omega . \tag{3.11}$$

The new divider ratio is now

$$\frac{V_H}{V_L} = \frac{(Z_H + Z_L^*)}{Z_L^*} = 54.41 - i8.976 = 55.145\angle -9.37°. \tag{3.12}$$

Although equation 3.12 suggests that the new divider ratio is approximately 55, actual tests showed that a ratio of 63 delivered more accurate results. These tests consisted of an open circuit test arrangement as displayed in Fig. 14, with no load connected to the secondary side of the transformer. While slowly raising the voltage, the OLCA measurements are compared to the measurements obtained using an oscilloscope connected between the high voltage point of the divider and ground. Table 3 shows the results of the test for a divider ratio of 63, as well as the error of the OLCA measurement compared to the oscilloscope.

Table 3: Open circuit measurements for capacitive voltage divider.

Oscilloscope measurement, V_{OS} [kV]	OLCA Measurement, V_{OLCA} [kV]	Absolute error, $\|e\| = ((V_{OLCA} - V_{OS})/V_{OS})*100\%$ [%]
0.611	0.615	0.655
1.22	1.23	0.820
1.59	1.60	0.629
2.13	2.15	0.939
3.07	3.08	0.325
4.01	4.02	0.249

The errors displayed in Table 3 are all less than 1%, which shows that the voltage divider functions with sufficient accuracy for a ratio of 63. The large difference between this ratio and the calculated ratio of equation 3.12 leads to the assumption that the measured value of 4.03 MΩ for the OLCA input impedance Z_{OLCA} (or R_{OLCA}) is incorrect and that the true input impedance is in fact much higher.

As mentioned previously, the introduction of R_{OLCA} into the circuit also creates a RC-circuit. The V_L-part of the divider now has the form of a high-pass filter. The magnitude and phase of the measured voltage can experience significant distortion if the frequency of the voltage is below the cut-off point of the RC-circuit. A frequency analysis was thus performed to see if the test frequency of 50 Hz falls below the cut-off point. The cut-off point is generally referred to as the frequency which induces a change of -3 dB in the magnitude of the input-output ratio of the circuit. In order to obtain the transfer function of the circuit, a nodal analysis was performed at node N, as shown in Fig. 21.

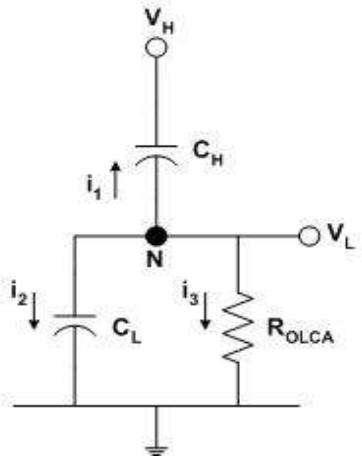

Fig. 21: Nodal analysis of capacitive voltage divider.

With their direction chosen as indicated in Fig. 21, the sum of the currents at node N is

$$i_1 + i_2 + i_3 = 0. \tag{3.13}$$

Replacing each current with the corresponding voltage drops across the circuit elements and transforming the equation from the time domain to the complex-frequency domain by replacing the term $2\pi f$ with s, equation 3.14 can be written as

$$s * C_H (V_L - V_H) + s * C_L * V_L + \frac{V_L}{R_{OLCA}} = 0. \tag{3.14}$$

After solving equation 3.15, the transfer function of the circuit is found to be

$$H(s) = \frac{V_L}{V_H} = \frac{R_{OLCA} * C_H * s}{[s * R_{OLCA}(C_H + C_L) + 1]}. \tag{3.15}$$

The frequency response of the circuit was simulated using Matlab. Fig. 22 shows the bode diagram of the transfer function in equation 3.16, displaying both its frequency response and phase shift as a function of frequency in rad/s.

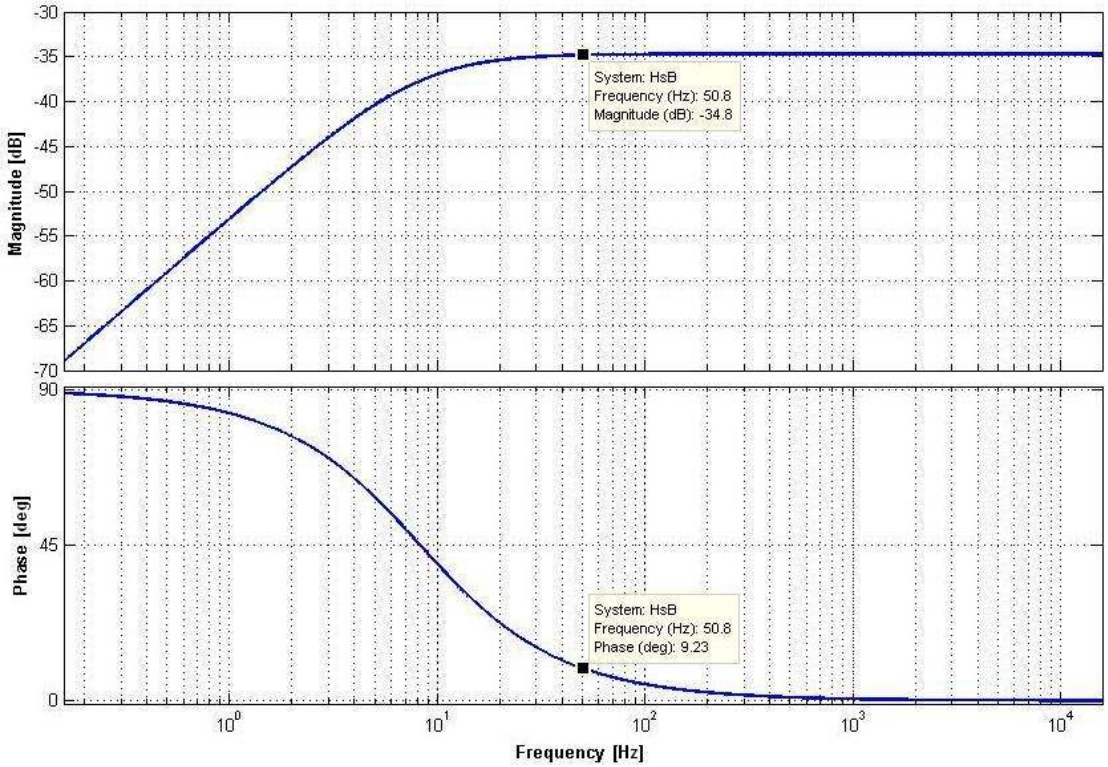

Fig. 22: Bode diagram for capacitive voltage divider, showing frequency response (top) and phase shift (bottom).

By inspection of Fig. 22, the -3 dB cut-off point was found to be at $f_{cut\text{-}off} = 8.37$ Hz. The test frequency of 50 Hz is thus far enough from the cut-off frequency so that the

voltage measurement incurs negligible magnitude distortion of ± 0.1 dB. A small phase shift of ± 9.23 ° occurs (see Fig. 22 and equation 3.12), but was deemed acceptable.

This section has described the test arrangement for the AC tests. For the DC tests, the apparatus had to be modified. These modifications are outlined in the following section.

3.4 Adaptation of apparatus for DC test arrangement

In order to obtain the DC voltage necessary for the comparison of insulator materials under different voltage types, it was decided to use a simple single phase, half-wave rectification topology in combination with a smoothing capacitor. Several other topologies were considered, but could not be implemented due to an unavailability of power sources.

3.4.1 Rectifier topology

In this project, voltage rectification was achieved by means of rectifying diodes connected in series. The total number of diodes depends on the maximum voltage applied to the circuit. At this point it should be mentioned that the rectifier circuits utilized in this project were designed for final implementation in a mobile HVDC test rig at Koeberg Insulator Pollution Test Station (KIPTS). This rig will utilise a 50 kVA, 400 V/ 22 kV three phase step-up transformer to produce a DC output voltage of 18 kV, with a nominal output current of 1 A and a voltage ripple of less than 3 %. A half-wave rectification arrangement will be used for this rig as well, with each phase receiving its own rectifier. The rectifier components were chosen to accommodate the KIPTS test rig design, and thus might seem somewhat excessive for use in this project.

The chosen diode is the 40EPS16 rectifying diode, with forward biased current limit I_F = 40 A (rms) and a reverse biased voltage limit of V_{rrm} = 1.6 kV (rms). The diodes will be connected in series. Additionally, each diode will have a 900 kΩ resistor and a

10 nF capacitor connected to it in parallel. Each diode will thus be part of small circuit as shown in Fig. 23.

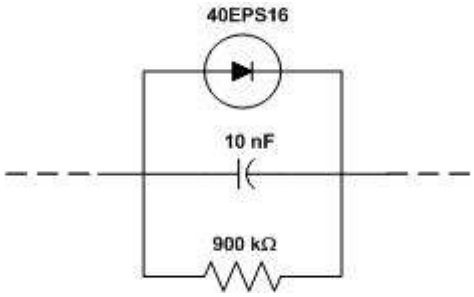

Fig. 23: Circuit for each individual rectifying diode.

Each diode might have a different resistance when reverse biased (i.e. in the 'off' state). Diodes with higher resistances will experience a higher voltage drop across them. The inclusion of a parallel resistor ensures that the reverse biased resistance of each diode is of similar magnitude, resulting in an even distribution of the voltage across the rectifier during steady-state conditions. The magnitude of the resistors is chosen according to the reverse-biased voltage rating of the diode, with the generally accepted rule being 500 Ω/V_{rrm}.

The parallel capacitor serves a similar purpose in the transient state of the rectifier. When the diodes switch from forward to reverse biased state (i.e. from 'on' to 'off' state), they do not react simultaneously. Some diodes may switch faster than others, resulting in a large portion of the voltage being applied over such this specific diode, possibly exceeding the voltage rating and causing damage to the diode. The capacitors ensure an even voltage division across all the diodes during the transient state.

The actual configuration of the rectifier diode stacks was aimed to be as modular as possible, for easy assembly and disassembly of the stacks as well as to facilitate replacement of damaged units. The final design consisted of the small rectifier circuits being mounted on rectangular printed circuit boards (PCB's) specifically designed for this purpose. Two diode-resistor-capacitor circuits are mounted on each PCB, as shown in Fig. 24. The diodes are additionally mounted on rectangular aluminium sheets, which act as heatsinks.

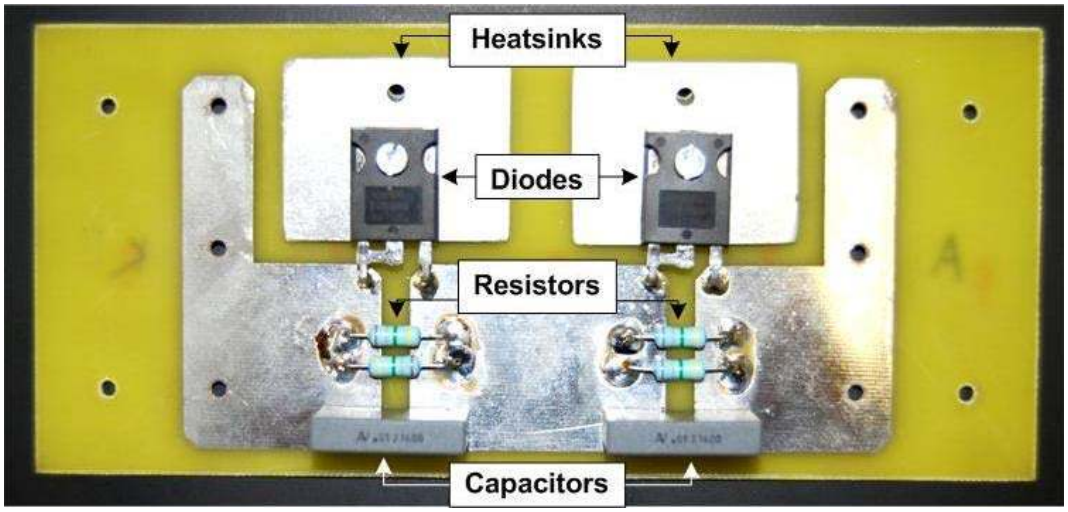

Fig. 24: PCB mounting two rectifier diode circuits.

The PCB's can be connected to one another by means of plastic spacers at each of the corners. The spacers also ensure that the PCB's maintain a safe distance to each other, eliminating the risk of flashover between the boards. Conduction between the boards is achieved by means of a single metal spacer connecting printed tracks on the two individual boards. The boards can then be stacked horizontally as well as vertically, creating a stack of varying height and thickness to suit the individual user's needs. The stack is kept rigid by Teflon rails (or any other non-conducting material) mounted along the sides of the first and last board in each horizontal stack. A model of such a stack is shown in Fig. 25.

Fig. 25: Stack of rectifier PCB's with elongated end-plates for better mounting of stack.

These rails can also be used to mount the rectifier stacks within a tank or enclosure if the rectifiers are to be oil-cooled (as intended for the KIPTS mobile rig). Transformer oil and similar liquids can be used to improve heat conduction away from the circuit elements as well as to reduce the risk of flashovers. However, initial tests on prototype rectifier stacks show that for test voltages below 10 kV and currents below 1A, the rectifiers can be used in an air-cooled environment without significant heat development or risk of flashover.

3.4.2 Modelling the DC power source

The IEC 60587 standard stipulates that any power source used must have an output voltage stabilized to ± 5 %. It was thus necessary to check if the single phase transformer used for the AC tests is capable of maintaining this voltage regulation while supplying a load current of 0.1 mA. The DC test arrangement was thus simulated using HSpice. A circuit diagram of the test model is shown in Fig. 26.

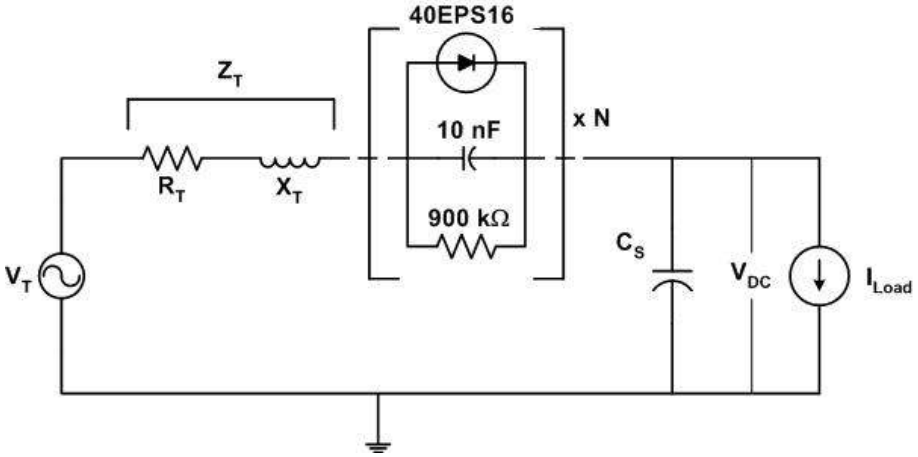

Fig. 26: Circuit diagram for Spice model of DC source.

In the model, Z_T represents the equivalent transformer impedance consisting of a resistive part R_T (representing the copper losses) and a reactive part X_T. N represents the number of rectifying diodes used in the simulation. The resistive per unit value of Z_T, R_{pu}, was calculated during the original construction of the IPT apparatus by means of a short circuit test [37] as

$$R_{pu} = \left(\frac{\text{copper losses}}{\text{kVA rating}} \right) * 100\,\% = 2.24\,\%. \qquad (3.16)$$

The base value of the transformer impedance, Z_B, can be determined by [39]

$$Z_B = \frac{V_{rated}}{I_{rated}} = \frac{7.5\,kV}{0.5\,A} = 15\,k\Omega. \tag{3.17}$$

The per unit transformer impedance, Z_{pu}, can then be determined as

$$Z_{pu} = \left(\frac{V_{SC} / I_{rated}}{Z_B} \right) * 100\,\% = 3.26\,\% \tag{3.18}$$

using the results from the short circuit test, where V_{SC} is the voltage measured during the short circuit test [39]. Since Z_{pu} is in reality a complex number consisting of R_{pu} and the per unit transformer reactance, X_{pu}, it follows that [37]

$$X_{pu} = \sqrt{\left(Z_{pu}^2 - R_{pu}^2\right)} = 2.37\,\%. \tag{3.19}$$

Since the magnitude of the base impedance is the same as that of the base resistance or reactance of the transformer, $Z_B = R_B = X_B$ [39], the equivalent values of R_T and X_T can now be calculated as

$$R_T = Z_B * R_{pu} = 15\,k\Omega * 2.24\,\% = 336\,\Omega \tag{3.20}$$

and

$$X_T = Z_B * X_{pu} = 15\,k\Omega * 2.37\,\% = 356\,\Omega. \tag{3.21}$$

In order to simulate X_T, the actual inductance L_T of the transformer winding must be calculated as

$$L_T = \frac{X_T}{2\pi f} = \frac{356\,\Omega}{2\pi * 50\,Hz} = 1.13\,H. \tag{3.22}$$

This is the value entered into the simulation model for the transformer inductance.

The objective of smoothing capacitor C_S is to smooth the DC output voltage during two conducting cycles of the rectifier diodes. The capacitor supplies the load with electrical charge (and thus current) while voltage measured across it is larger than the supply voltage. Once the supply voltage becomes larger than the capacitor voltage, the depleted electrical charge is restored to the capacitor. This effect is depicted in Fig. 27.

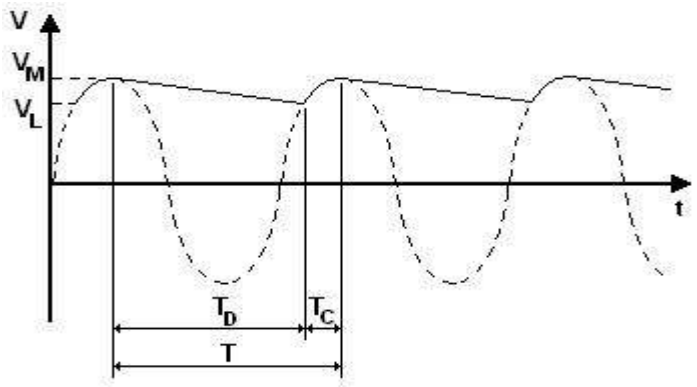

Fig. 27: Sinusoidal source voltage (dotted line) with capacitor voltage (full line) during charging (T_C) and discharging phase (T_D).

T_D is the time period in which the smoothing capacitor supplies electrical charge to the circuit, becoming discharged in the process. T_C is the time period in which the supply voltage V_T is larger than the voltage across the capacitor and its lost electrical charge is replaced. For a very small voltage ripple, $T_D >> T_C$ and can thus be approximated to be equal to the time period T of supply voltage V_T, with a magnitude of

$$T_D \approx T = \frac{1}{f} = \frac{1}{50\,\text{Hz}} = 0.02\,\text{s}. \tag{3.23}$$

The voltage ripple factor r_V can be defined as

$$r_V = \frac{\delta V}{V_D}, \tag{3.24}$$

where

$$\delta V = \frac{V_M - V_L}{2} \tag{3.25}$$

and

$$V_D = \frac{V_M + V_L}{2}. \tag{3.26}$$

V_M is the highest and V_L the lowest voltage values measured during the voltage ripple (see Fig. 27). V_D is approximately equal to the average voltage value. As will be described in Chapter 5, the test voltage for the comparison of different materials was chosen as 4.0 kV. Setting V_D = 4.0 kV and r_V = 0.05 (5 %), δV can then be calculated from equation 3.25 as

$$\delta V = r_V * V_D = 0.05 * 4.0\,\text{kV} = 200\,\text{V}. \tag{3.27}$$

The maximum voltage drop experienced by the capacitor during the discharging phase is equal to 2* δV. The electrical charge supplied by the smoothing capacitor during this phase can be calculated by using either of the following two equations:

$$Q = I * T_D \tag{3.28}$$

and

$$Q = 2 * \delta V * C_S. \tag{3.29}$$

Since only one insulator sample will be tested at a time, the current in equation 3.28 can be taken as I = 0.1 A, which is the current the test apparatus must be able to supply per test sample [34]. By combining equations 3.28 and 3.29, the value for C_S can be calculated as

$$C_S = \frac{I * T_D}{2 * \delta V} = \frac{0.1\,A * 0.02\,s}{2 * 200\,V} = 5\,\mu F. \tag{3.30}$$

The capacitors available for this project had a magnitude of 8.7 μF each. The simulation model shown in Fig. 26 was run with two different values for C_S, once with a single capacitor (i.e. C_S = 8.7 μF) and once with two capacitors in parallel, doubling the total capacitance (i.e. C_S = 17.4 μF).

The minimum number of rectifier diodes needed for the DC test arrangement depends on the maximum voltage experienced in the system and on the maximum voltage rating V_{rrm} of the diodes. The maximum voltage is the peak value of the rated voltage V_R of the transformer. Since the input voltage has a sinusoidal waveform, the peak value can be calculated by multiplying V_R with a factor of √2.

However, the actual maximum voltage experienced by the rectifier is twice this peak value, since capacitor C_S is charged to V_R*√2 during the conducting phase of the rectifier. In the non-conductive phase, the rectifier thus experienced the sum of the peak voltage of the transformer and the voltage across capacitor C_S. It is also common practice to introduce a safety factor to reduce the risk of failure in the rectifier. A safety factor of SF = 2 was judged sufficient for this particular application. The minimum number of diodes required can now be calculated as

$$N = \frac{2\sqrt{2} * V_R * SF}{V_{rrm}} = \frac{2\sqrt{2} * 7.5\,kV * 2}{1.6\,kV} = 26.5 \approx 27. \tag{3.31}$$

The final number of diodes was further increased to 30 in order to form a diode stack of three vertically arranged packages of five PCB's connected to one another, with two diodes per PCB (see Fig. 25 for typical stacking arrangement).

Since an insulator sample being tested on the IPT apparatus does not have a fixed resistance, the load for simulation purposes was modelled as a perfect independent current source. The load current was set at 0.1 mA, as this is the current the source should be able to supply for one test sample. Fig. 28 shows V_{DC} (output voltage measured across load) as well as the diode current for a smoothing capacitance of C_S = 8.7 µF.

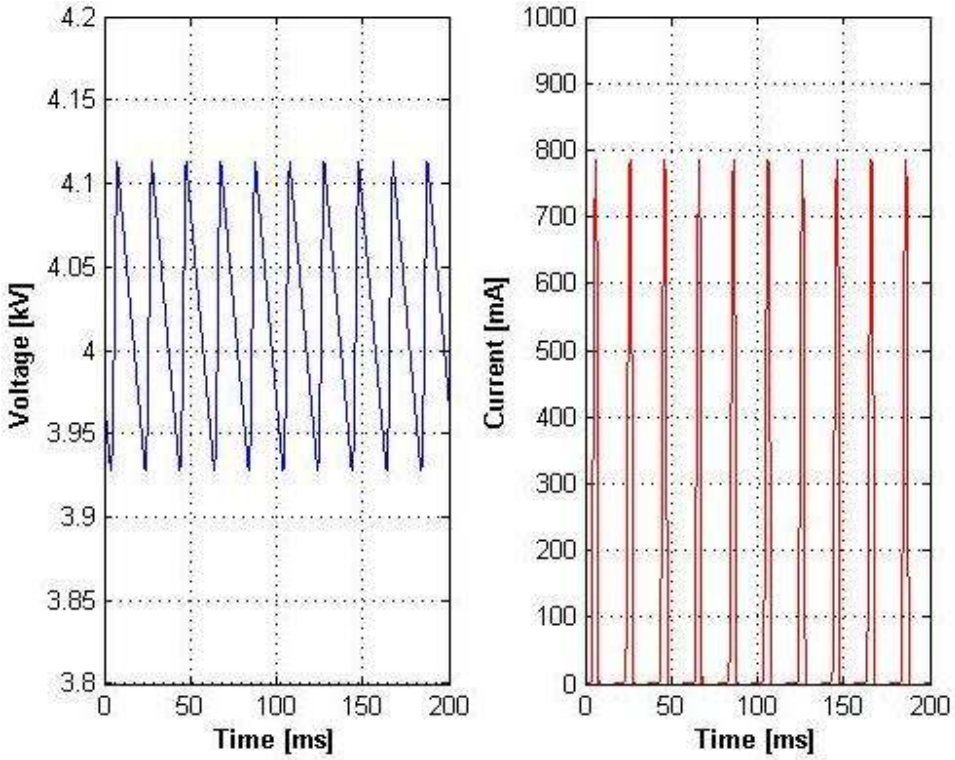

Fig. 28: DC voltage across load and diode current for C_S = 8.7 µF.

Fig. 29 shows V_{DC} and the diode current for C_s = 17.4 µF.

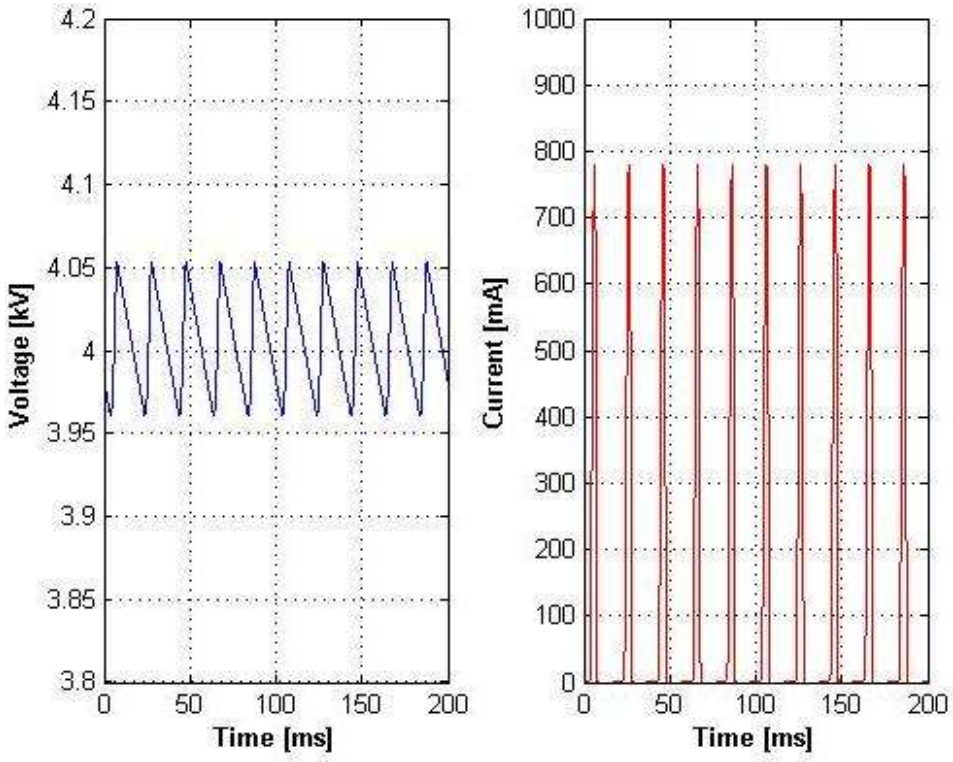

Fig. 29: DC voltage across load and diode current for C_S = 17.4 µF.

For both simulation models, the input voltage was adjusted until the average DC output voltage measured ± 4.0 kV. Table 4 summarizes the simulation results for both models, with the values obtained from generated figures. Note that the input voltage displayed is the rms value.

Table 4: Simulation results of DC source at V_{DC} = 4.0 kV and I_{load} = 0.1 mA.

Smoothing Capacitance C_S [µF]	Input voltage V_T [kV]	Maximum output voltage V_M [kV]	Minimum output voltage V_L [kV]	Peak diode voltage V_{diode} [V]	Peak diode current I_{diode} [mA]	Voltage ripple factor r_V [%]
8.7	3.25	4.11	3.93	288	786	2.24
17.4	3.26	4.05	3.96	287	780	1.12

The model of C_S = 17.4 µF shows slightly lower values for both peak diode voltage and current as well as a lower voltage ripple factor than the model for C_S = 8.7 µF. The DC test arrangement was thus constructed using two capacitors of 8.7 µF connected in parallel.

3.4.3 Design of resistive voltage divider

Since a capacitive voltage divider cannot be used to measure DC voltages, the divider designed in section 3.3.3.1 had to be redesigned as a resistive voltage divider in order to allow the OLCA to measure the voltage across the test sample. Fig. 30 shows the divider circuit, incorporating the OLCA input resistance of 4.03 MΩ.

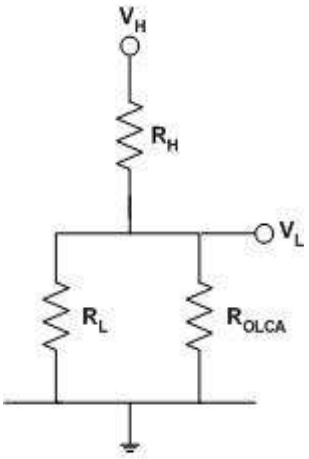

Fig. 30: Resistive voltage divider circuit.

As the voltage drop over resistor R_H is large compared to R_L, a resistor type has to be chosen that is capable of handling voltages in the kV-range. A limited availability of components set the value of the high voltage part of the divider at R_H = 3 MΩ. It was further decided to keep the divider ratio at V_H/V_L = 54 so as not to exceed the OLCA's voltage input limits of ±400 V rms.

Since the low voltage part of the divider is a parallel combination of R_L and R_{OLCA}, its new value can be written as

$$R_P = \frac{R_L * R_{OLCA}}{R_L + R_{OLCA}}. \tag{3.32}$$

Using voltage division across series elements, voltage V_L in Fig. 30 can be expressed as

$$V_L = \frac{R_P}{R_H + R_L} * V_H. \tag{3.33}$$

Solving this equation for R_P yields

$$R_P = \frac{R_H}{V_H / V_L - 1} = \frac{3\,\text{M}\Omega}{53} = 56.6\,\text{k}\Omega. \tag{3.34}$$

The true value for R_L can then be found by solving equation 3.32, obtaining a value of

$$R_L = \frac{R_P * R_{OLCA}}{R_{OLCA} - R_P} = 57.4\,k\Omega. \quad (3.35)$$

Choosing the closest matching resistor value to that calculated in equation 3.35, the value of R_L was taken as 56 kΩ.

Although recalculation using the values above brings the voltage divider ratio closer to V_H/V_L = 55, measurements showed that a ratio of 54 yielded the most accurate results for the OLCA. Table 5 shows voltage measurements obtained during an open circuit test on the DC arrangement, where the voltage was raised in steps of 1000 V. The OLCA measurements are compared to measurements taken with an oscilloscope with rms and peak measuring functions.

Table 5: Accuracy test of resistive voltage divider.

Voltage step [kV]	OLCA voltage measurement V_{OLCA} [kV]	Oscilloscope voltage measurement V_{Osc} [kV]	Absolute error $e = \lvert V_{OLCA} - V_{Osc}\rvert / V_{Osc} * 100\%$ [%]
1.0	0.997	0.96	3.7
2.0	1.95	1.94	0.515
3.0	2.95	2.93	0.685
4.0	3.92	3.93	0.254
5.0	4.89	4.91	0.407

With the exception of the measurement at 1.0 kV, the voltage divider functions with an accuracy error of less than 1%. Since the test voltage will be 4.0 kV (see Chapter 5), the divider was deemed accurate enough to be implemented.

3.4.4 Final DC test arrangement

Fig. 31 shows the IPT apparatus modified for the DC tests, including the rectifier circuit, the smoothing capacitor C_S and the resistive voltage divider.

As a final test of the DC source stability, the entire load circuit (including the current limiting resistors, the OLCA measuring circuit and the current sensing resistor) was replaced by a resistor consisting of two electrodes placed into a solution of distilled water and ammonium chloride salt. This type of resistor represents impedance that is

purely resistive in nature. The resistance can be altered by adding more salt (decreasing the resistance) or more distilled water (increasing the resistance).

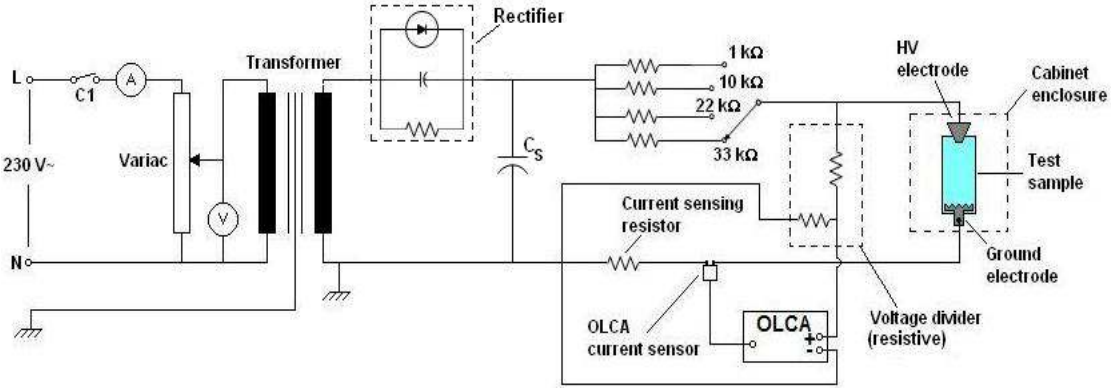

Fig. 31: Full IPT apparatus with implemented DC source.

While keeping the voltage fixed, the resistance was then varied in order to draw a load current of ± 60 mA, which is the leakage current value at which a sample is deemed failed if it persists for longer than 2 s [34]. An oscilloscope was used to measure the maximum and minimum value of the DC voltage over the resistor in order to determine the voltage ripple of the DC source. Table 6 shows the results for measurements taken at several voltage and current levels. The voltage ripple was calculated according to equation 3.24.

The results show that for the chosen test voltage of 4.00 kV (see Chapter 5), the voltage ripple of the source lies well below the standard-specified value of 5 %, even if the current exceeds the failure limit of 60 mA. The source was thus judged stable enough for the purpose of this project.

Table 6: Voltage ripple of DC source for different voltage levels at load current.

DC voltage step [kV]	Load current I_{Load} [mA]	Maximum DC voltage V_M [kV]	Minimum DC voltage V_L [kV]	Voltage ripple r_V [%]
2.0	59.8	2.18	1.98	4.81
3.0	61.2	3.12	2.90	3.65
4.0	54	4.14	3.94	2.48
4.0	58.2	4.14	3.96	2.22
4.0	75.2	4.14	3.92	2.73

3.5 Improvement of contaminant flow

As described in section 3.1, a liquid contaminant is allowed to run along the surface of an energized IPT test sample in order to induce dry band arcing at the ground potential electrode. The contaminant is usually stored in an external container from which it is pumped into the reservoir of eight layers of filter paper clamped between the HV electrode and the sample surface. Such an external container is necessary since the test duration can cover a time span of several hours, which means that a significant amount of liquid is needed to guarantee an unbroken supply of contaminant to the sample. The contaminant flow should be as constant and unvarying as possible so as to ensure uninterrupted arcing at the ground potential electrode, which is essential for the test to yield accurate results [34].

Previous tests performed on the IPT apparatus utilized a peristaltic pump to convey the liquid contaminant from its container to the sample. During these tests, difficulties were experienced in maintaining constant dry band arcing at the ground potential electrode. Observations documented by previous operators revealed this to be a common problem for this particular apparatus and test arrangement, and further suggested that careful adjustments to the contaminant flow rate might provide a solution [40]. In order to improve the control of the flow rate, a flow meter was installed between pump and outlet nozzle so as to obtain a true measurement of the flow rate at any given moment in time. The flow meter is shown in Fig. 32.

Fig. 32: Flow meter as installed in apparatus.

Measurements using the flow meter revealed the contaminant flow rate to vary in a pulse-like fashion. This is due to the pumping mechanism of the peristaltic pump, which uses a set of rollers to compress the fluid hose between the rollers and a fixed length of barrier, increasing the pressure on the fluid column inside the hose. This effectively 'pushes' a fixed volume of fluid along the hose. Since the pump only has a fixed number of rollers available, there are delays between the pressure increases, resulting in an oscillating flow rate. This can result in a situation where the flow rate becomes too low to supply sufficient contaminant to the sample. The fluid path dries up along the sample surface, causing the dry band to grow in width until the electrical field strength E_a across the dry band gap becomes too small to sustain a constant arc (typically $E_a < 30$ kV/cm if the medium in the gap is air), resulting in a disruption of the arcing process.

In order to improve the flow rate, a reservoir was constructed and installed in the fluid path between the pump and the discharge nozzle. The reservoir consists of a cylindrical container with one inlet and two outlets, as shown in Fig. 33. The inlet is situated at the top of the reservoir and is directly connected to the pump. The outlets consist of a main outlet at the bottom of the reservoir, which delivers the contaminant to the sample via the flow meter, and an overflow in the middle of the reservoir.

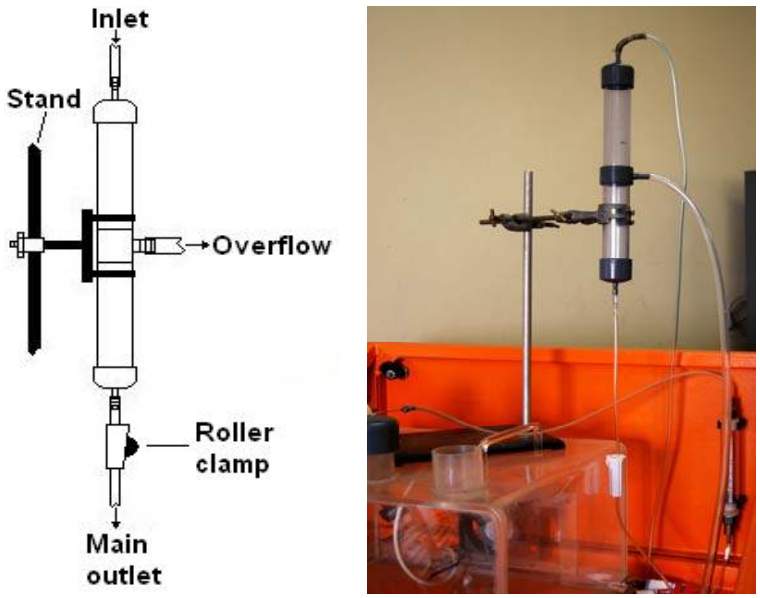

(a) **(b)**

Fig. 33: (a) Diagram of flow reservoir and (b) Actual implementation of reservoir in apparatus.

The contaminant is then pumped into the reservoir. By selecting a high speed setting on the pump, the inlet flow rate of the contaminant is kept higher than the outlet flow

rate, causing the reservoir to fill until the fluid level reaches the overflow. The overflow keeps the fluid level in the reservoir constant. Connecting the overflow to the original liquid container ensures that no contaminant is wasted.

The reservoir is mounted on a vertical stand using adjustable clamps. The pressure p at a given point within column of liquid is depended on the liquid density ρ and the distance h of the point to the surface of the liquid (also termed the 'head' of the fluid) [41], i.e.

$$p = g \times \rho \times h, \tag{3.36}$$

where g represents the gravitational acceleration constant, usually taken at a value of 9.81 m/s^2. Since the discharge nozzle stays at a fixed location at the top of the sample, shifting the reservoir upwards on the stand causes an increase in the vertical distance h between the nozzle and the liquid surface inside the reservoir, as shown in Fig. 34. This results in an increase in the pressure at the discharge nozzle according to equation 3.36, which results in an increased flow rate Q. A lowering of the reservoir similarly leads to a decrease in the flow rate.

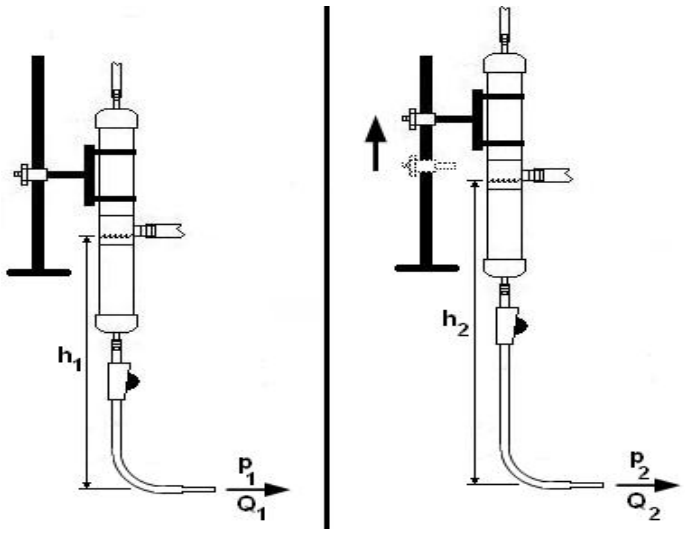

Fig. 34: Regulation of flow rate by shifting reservoir upwards, with $h_2 > h_1$, $p_2 > p_1$ and $Q_2 > Q_1$.

The flow rate can further be regulated by either adjusting the roller clamp on the tube beneath the reservoir (see Fig. 33). Tightening the clamp constricts the fluid path and reduces the flow rate, while a loosening of clamp increases the cross-sectional area of the fluid path, thus also increasing the flow rate.

Test runs conducted with the reservoir implemented in the fluid path showed a definite reduction in the flow oscillations, resulting in a smoother and more

continuous contaminant flow. Dry band arcing on energized samples also remained constant for longer periods, which according to standard is essential for the accuracy of the test results.

3.6 Development of conductivity model

As mentioned in section 3.1, the IEC standard states that the liquid contaminant has to have a volume conductivity σ of 2.53 mS/cm at a temperature of 23 °C, with a tolerance of 0.03 mS/cm. The conductivity of a given solution depends on the type of conductive substances present in the solution, their relative quantities and the temperature of the solution. This dependency on temperature is the reason the solution conductivity is stated for a specific temperature in the IEC standard.

In order to determine the required volume conductivity σ_t of a solution for any measured temperature T_t, the following equation can be used:

$$\sigma_t = \sigma_S \times [1 + \alpha(T_t - T_S)] \tag{3.37}$$

where the variables are defined as follows:

- σ_t: measured volume conductivity of solution [µS/cm] at temperature T_t [°C]
- σ_S: calibration volume conductivity [µS/cm]
- T_S: calibration temperature [°C]
- α: temperature coefficient of solution

The value of α depends on the substance present in the solution as well as the solution concentration and can range from 0.0156 to 0.31. For common salt solutions like NaCl or NH_4Cl in water, a value of 0.019 to 0.02 is judged accurate enough.

Another formula used for temperature correction of conductivities of salt solutions is given in the International Standard IEC 60507 for artificial pollution tests on insulators [43] as

$$\sigma_{20} = \sigma_t \times [1 - k_t(t_S - 20)], \tag{3.38}$$

where σ_t denotes the measured volume conductivity and σ_{20} the volume conductivity corrected to a temperature of 20 °C, both measured in S/m. The variables t_s and k_t represent the solution temperature [°C] and the temperature coefficient, respectively.

The value of k_t depends on the temperature of the solution and can be found by interpolation from a table of values for a set of known temperatures. Plotting these values allows the generation of a best-fit trend line through the data points. Using a polynomial fit, the resulting equation for k_t based on this trend line is [7]

$$k_t = -3.2\times10^{-8}\times t_s^3 + 1.032\times10^{-5}\times t_s^2 - 8.272\times10^{-4}\times t_s + 3.544\times10^{-2}. \quad (3.39)$$

However, since these equations are based on a NaCl solution rather than a NH_4Cl solution as used in the IPT method, it was decided not to utilize this method.

In order to find an accurate model for temperature correction of the solution conductivity, a test contaminant solution was prepared strictly according to the guidelines laid out in the standard [34]. The solution was then heated to the specified temperature of 23 °C and its conductivity was measured. Adjustments were made as needed (either by adding NH_4Cl or de-ionized water) until the conductivity fell within the specified range. The solution was then further heated to a temperature of ± 40 °C and was then left to cool. The solution conductivity was continuously monitored and values were recorded at every change of 1 °C in temperature. The results are shown in Table 7.

Table 7: Measured conductivities of contaminant solution and trend line models.

Measured values		Linear trend line		Logarithmic trend line	
Solution Temperature [°C]	Volume Conductivity [mS/cm]	Volume Conductivity [mS/cm]	Error [%]	Volume Conductivity [mS/cm]	Error [%]
19	2.28	2.29	0.50	2.24	1.79
20	2.33	2.34	0.43	2.31	0.94
21	2.38	2.39	0.37	2.37	0.27
22	2.45	2.44	0.51	2.44	0.57
23	2.5	2.49	0.56	2.50	0.17
24	2.55	2.53	0.60	2.55	0.11
25	2.6	2.58	0.63	2.61	0.30
26	2.64	2.63	0.30	2.66	0.77
27	2.67	2.68	0.41	2.71	1.54
28	2.73	2.73	0.01	2.76	1.10
29	2.78	2.78	0.06	2.81	0.97
30	2.83	2.83	0.11	2.85	0.80
31	2.87	2.88	0.20	2.90	0.93
32	2.92	2.92	0.15	2.94	0.66
33	2.97	2.97	0.10	2.98	0.36
34	3.01	3.02	0.39	3.02	0.36
35	3.07	3.07	0.02	3.06	0.34
36	3.12	3.12	0.03	3.10	0.72
37	3.16	3.17	0.25	3.13	0.81
38	3.24	3.22	0.72	3.17	2.16

The measured data points were then plotted in Microsoft Excel. Two different trend line models, a straight line and a logarithmic model, were then fitted to the data. This yielded the trend line equations

$$\sigma = 0.0487 \times T + 1.366 \tag{3.40}$$

and

$$\sigma = 1.343 \times \ln(T) - 1.7152 \tag{3.41}$$

for the straight line and the logarithmic model, respectively. The expected conductivity for each measured temperature was then calculated using both models. The resulting values are also displayed in Table 7, as well as the corresponding error of each value when compared to the measured conductivity. The results show that the straight line model yields smaller errors for most of the temperature points and is thus the preferred model. This corresponds with the common conductivity model shown in equation 3.37.

The conductivity model in equation 3.37 can also be written as

$$\sigma_t = \sigma_S + \alpha\sigma_S(T - T_S). \tag{3.42}$$

This represents a straight line equation with a gradient of:

$$m = \frac{\sigma_t - \sigma_S}{T - T_S} = \alpha\sigma_S. \tag{3.43}$$

By substituting the gradient from the straight line model derived from the measurements, i.e. m = 0.0487 mS/(cm x °C), one can rewrite equation 3.42 as

$$\sigma_{23} = \sigma_t - 0.0487(T - 23), \tag{3.44}$$

where σ_t denotes the measured solution volume conductivity and σ_{23} denotes the solution volume conductivity corrected to a temperature of 23 °C, both measured in mS/cm. The variable T represents the measured solution temperature in °C. This model was used to correct the measured conductivities of all measured contaminant solutions to a temperature of 23 °C for the duration of this project.

By solving equation 3.43 for α and then substituting the values m = 0.0487 mS/(cm * °C) and σ_S = 2.53 mS/cm, the value of the temperature coefficient α for this model becomes

$$\alpha = \frac{m}{\sigma_S} = \frac{0.0487 \dfrac{mS}{cm \times °C}}{2.53 \dfrac{mS}{cm}} = 0.0192\,°C^{-1}. \tag{3.45}$$

This result corresponds well with the common value range of α (0.019 to 0.02) for solution containing salts like NaCl or NH_4Cl.

Chapter 4: Comparison of Test Methods

As outlined in Chapter 3, the IEC 60587 standard was chosen as the guideline for this project. Two different test methods are described in this standard. Uncertainty existed in regards as to which test method would yield better results or if there is in fact any difference between the methods in terms of ageing of the insulator samples. An experiment was thus conducted in which both test methods were applied to identical samples and the results were compared according to several evaluation criteria. The two test methods are described in detail in the next section.

4.1 Test methods of IEC 60587

The test methods described in the IEC 60587 standard are called the constant tracking voltage method and the stepwise tracking voltage method [34].

4.1.1 Constant tracking voltage method

The test voltage applied to the insulator sample is raised to a specific value and is then kept constant for the full test duration of six hours. The contaminant flow rate and the value of the current limiting resistor are selected according to Table 2 displayed in section 3.3.2 and are also kept constant for the entire test duration. Preferred test voltages for this method are 2.5, 3.5 and 4.5 kV. The selected test voltage should be reached in a time not exceeding 10 s after starting the test.

It is customary to classify a test material according to the maximum test voltage withstood by all samples within a test series, i.e. without the occurrence of failure in any of the samples. According to the standard, a test series should consist of five samples. Classification of the material is done according to the following method [34]:

- *Class 1A 0 or 1B 0:* One or more samples fail in less than six hours at a test voltage of 2.5 kV, where failure is judged according to failure criterion A or B (see section 3.2).
- *Class 1A 2.5 or 1B 2.5:* All samples of the test series survive for six hours at 2.5 kV and one or more samples fail in less than six hours at 3.5 kV.

- *Class 1A 3.5 or 1B 3.5:* All samples of the test series survive for six hours at 3.5 kV and one or more samples fail in less than six hours at 4.5 kV.
- *Class 1A 4.5 or 1B 4.5:* All samples of the test series survive for six hours at 4.5 kV.

In order to use this classification correctly, one full test series should be tested per voltage class until failure is recorded. The highest voltage withstood by all samples within a test series for the full test duration of six hours without the occurrence of failure is sometimes called the constant tracking voltage for that specific insulating material [34].

4.1.2 Stepwise tracking voltage method

In this method, the test voltage is initially raised to a pre-selected starting voltage. Both the contaminant flow rate and current limiting resistance are adjusted according to Table 2 (see section 3.3.2). After each full hour, the test voltage is then raised by 250 V. The starting voltage must be selected so that failure in a sample does not occur until the third voltage step (i.e. the start of the fourth test hour). Preliminary trials may be necessary to find the correct starting voltage. The voltage is raised in hourly steps of 250 V until failure is recorded in a sample.

Again, a test series usually consist of five samples. Tested materials are labelled Class 2A x or 2B x (according to which failure criterion was used), where x is replaced by the highest voltage withstood by all samples without the occurrence of failure. This voltage is also called the stepwise tracking voltage of the material.

For this particular method, achieving and maintaining effective scintillation throughout the duration of each test is essential. Effective scintillation is defined by the standard as the formation of continuous arcs just above the teeth of the ground potential electrode. The arcs should be of a white, yellow or blue colour and should remain continuous throughout the test. Jumps between teeth along the ground potential electrode are allowed. If effective scintillation is not achieved, the electrical circuit, contaminant flow rate and contaminant conductivity should be checked and adjusted if necessary [34].

As stated in section 3.2, failure criterion A was chosen as the preferential criterion and was employed in both test methods. Therefore, a test sample is deemed failed if the leakage current exceeds a value of 60 mA rms for a time longer than 2 seconds, a hole develops due to extensive erosion or if the sample ignites [34].

4.2 Comparison methodology

4.2.1 Sample material & preparation

In order to compare the test methods with one another, one full test series consisting of five samples each was conducted using each method. All samples consisted of the same material, namely an industrial grade High Temperature Vulcanized (HTV) silicone rubber. The samples were pre-cut by the manufacturer to a size of 115 x 47 x 6 mm. Fig. 35 shows a test sample prior to testing.

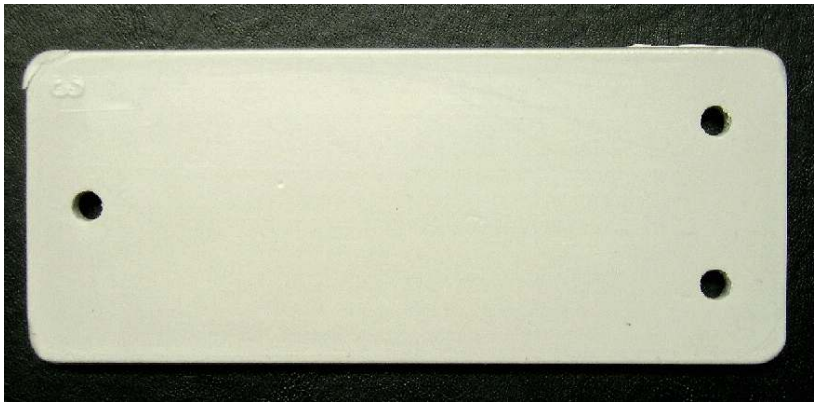

Fig. 35: HTV silicone rubber sample used in comparison of test methods.

Prior to testing, each sample was cleaned first with propanol alcohol and then with deionised water. Furthermore, HTV silicone rubber surfaces have a high degree of hydrophobicity. This can hinder the contaminant flow along the sample surface, possibly disrupting the arcing process at the ground potential electrode. In order to reduce this effect, the surfaces of all samples were lightly abraded using P800 grade sandpaper until the surface is evenly wetted, as described in the standard [34]. Fig. 36 shows the difference in surface hydrophobicity of the samples before and after abrasion.

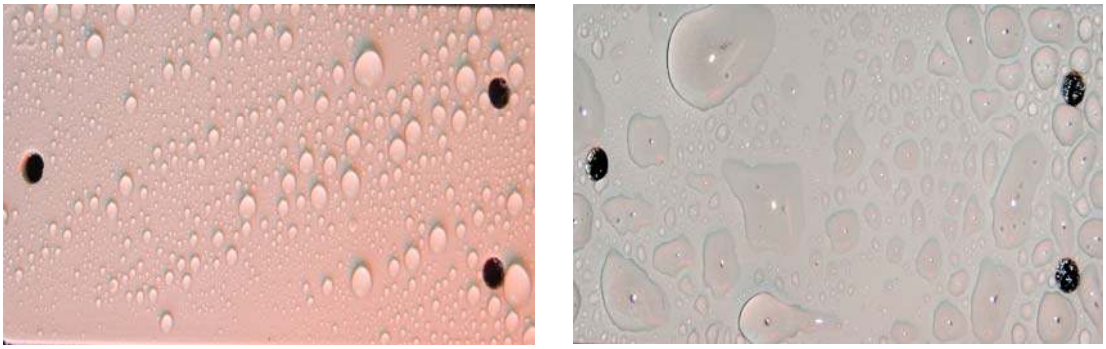

(a) (b)

Fig. 36: Change in surface hydrophobicity through abrasion: (a) Unabraded sample and (b) Abraded sample

Before the samples are installed in the apparatus, a layer of silver conductive paste (Conductrox 3347 Ag Conductive Paste) was applied between sample surface and ground potential electrode. This ensures an even contact between electrode and sample, allowing for better conduction of the leakage current. This procedure is an adjustment from the ASTM D2303 standard [35]. Although such a procedure is not mentioned in the IEC standard, it is a useful adjustment which could aid in keeping the arcing process as stable as possible.

4.2.2 Test voltages & evaluation criteria

As stated before, one test series was conducted using each test method. Since no prior data existed for this specific test material regarding the IPT method, a voltage of 3.5 kV was chosen for the constant tracking voltage method. This voltage is the midrange value of the voltages suggested by the standard.

Since the voltage for the stepwise tracking voltage method is raised by 250 V every hour, a suitable starting voltage had to be selected so that failure of a sample would not occur before the third voltage step. It was further decided to limit the test duration of this method to a period of six hours, which is the same test duration prescribed for the constant tracking voltage method. Choosing the same test duration for both methods will facilitate comparison between them.

The voltage values chosen for the stepwise tracking voltage method ranged from 2.5 to 3.75 kV in steps of 250 V over the test duration of six hours. Reasons for this specific choice depended on two concerns. First, the standard states that the

contaminant flow rate and the current limiting resistance have to be adjusted according to Table 2 (see section 3.3.2). Whereas adjusting the flow rate is easily done, changing the resistance in the current test apparatus means that the test has to be temporarily interrupted to ensure the safety of the operator while changing the resistance. Interrupting the test in this manner might interfere with the results. With the chosen voltage range, the test has to be interrupted only once when changing from a voltage of 2.75 kV to 3.0 kV (see Table 2 in section 3.3.2). Interruptions to the test procedure are thus kept at a minimum, ensuring that the test runs are as continuous as possible.

Secondly, the choice of this specific voltage range ensures that a voltage of 3.5 kV, i.e. the voltage chosen for the constant tracking voltage method, is reached in the fifth test hour. Since failure of a sample may not occur before the third voltage step (i.e. the fourth test hour), this means that both test series are exposed to similar conditions in a time period where failure is permitted for both methods. This facilitates comparison between the two different test methods.

As stated in Chapter 3, the leakage current flowing along the sample surface was measured using the OLCA. Additionally, each test run was monitored, with visual observations recorded in form of a test report every 15 minutes. A digital camera was used to take photographs at 15 minutes time intervals, corresponding with the records in the test report. The photographs were used to monitor the progress of ageing on each sample. At the half hour mark of each full test hour, a one minute video was recorded in order to monitor the arcing process. Fig. 37 shows a diagram of the arrangement of the measurement and observation equipment.

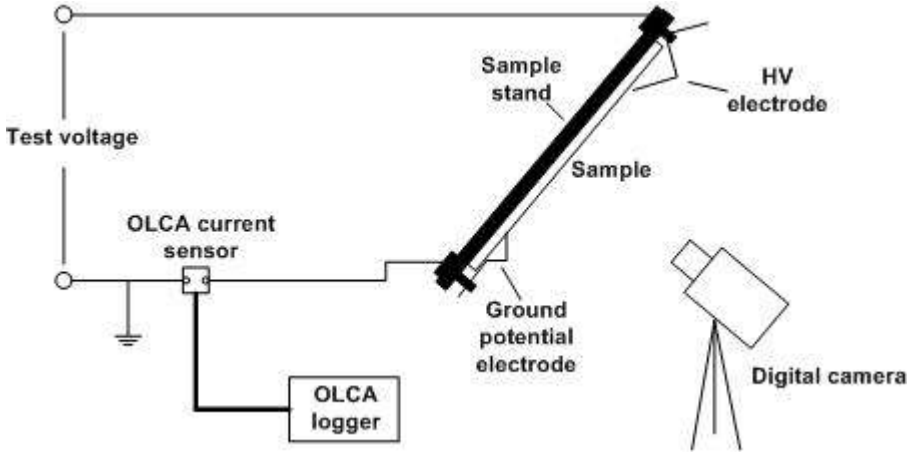

Fig. 37: Measuring & monitoring equipment used during test runs of method comparison.

After all the samples were tested, the two methods were compared by evaluating each test series according to several criteria. These criteria were:

- *Visual observations & sample appearance:* The methods were compared according to the arcing behaviour observed during the test runs, as well as general sample appearance during and after the experiments.
- *Sample mass loss:* A comparison between the methods was made according to the amount of mass lost by the tested samples due to electrical erosion.
- *Sample erosion depth:* A comparison of the methods was made according to the maximum erosion depth measured on the samples.
- *Average hourly rms leakage current:* The methods are compared according to the average rms leakage current values obtained from OLCA measurements for each test hour.
- *Peak current bin counts:* A comparison was done between the test methods according to the number of peak currents measured over the entire test period which fall into certain pre-defined categories, or 'bins'.
- *Chemical analysis:* The methods were compared according to the chemical changes occurring in the samples. These changes were investigated using Attenuated Total Reflection Fourier Transform Infrared (ATR FTIR) spectroscopy.

A more detailed description of each individual criterion is given in the following section. The chemical analysis was performed only on one sample of each test series. These samples are not included in the comparisons of mass loss and erosion depth, to

avoid any effects on the sample surface which might influence possible chemical changes in the samples.

4.3 Results of method comparison

This section presents the results obtained for each individual evaluation criterion. Names were assigned to the two test series in order to distinguish between them without having to refer to the full name of the individual methods. The test series conducted using the constant tracking voltage method was labelled series A, while the series performed using the stepwise tracking voltage method was denoted as series B. Individual samples within each series were numbered from 1 to 5 according to the chronological sequence they were tested in.

4.3.1 Visual observation & sample appearance

A summary of the visual observations made during the test runs is given for each test series, based on the test reports, photos and videos recorded as described in section 4.2.3. The main focus is on the continuity and intensity of the arcing behaviour displayed by the samples, as well the appearance of the samples during and after the test runs.

4.3.1.1 Series A

During the first hour, the samples showed mostly weak dry band discharges and scintillations over most of the sample surface. This caused mild discolouration of the samples surface in the regions were these discharges took place. Arcing behaviour close to the ground potential electrode was slightly more stable, but still very interrupted. The discolouration in this area was thus more pronounced. Fig. 38 shows a photo of a sample during this particular stage.

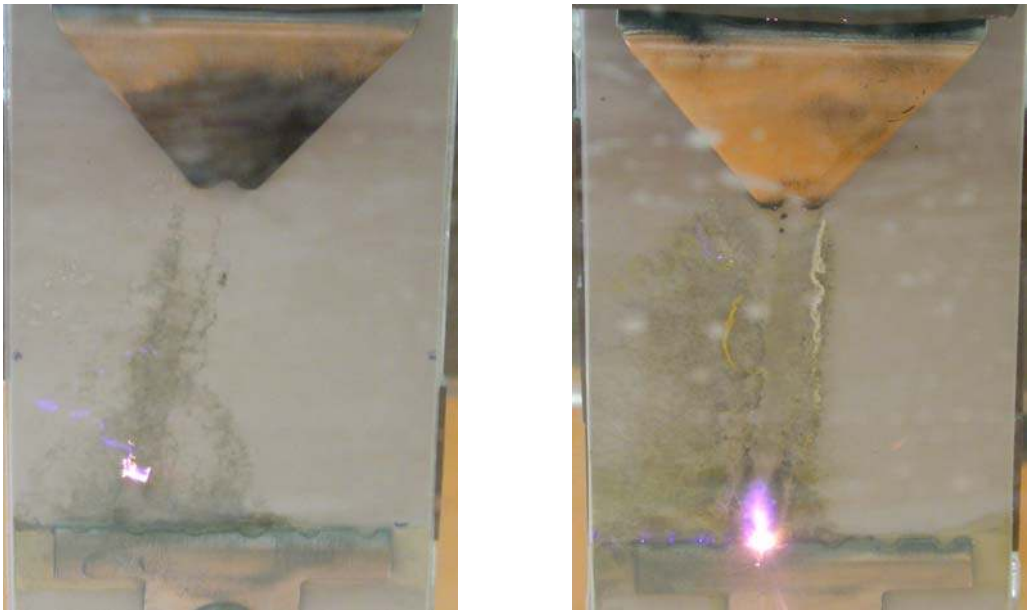

(a) (b)

Fig. 38: Test sample of series A: (a) During weak arcing phase in test hour 1 and (b) During effective scintillation phase from test hour 3 onwards, showing hotspot at ground potential electrode.

Arcing behaviour tended to stabilize during the second test hour, with stable arcs starting to occur at the ground potential electrode. Periods of good effective scintillation were observed, but interruptions to the arcing process or periods of weak scintillation across the entire sample face still occurred regularly. The surface discolouration started to intensify along the ground potential electrode. Hotspots (small areas of high temperature and intensive glow, usually localized at arc ends) were observed to occur sporadically. Discolouration also increased at other regions on the samples due to isolated dry band discharges, but to a lesser degree than what was observed at the ground potential electrode.

By the third test hour, effective scintillation had been established at the ground potential electrode, with continuous periods of stable arcs of blue-yellowish colour being observed. Interruptions due to dead times (periods of no arcing on sample) did occur, but continuous arcing re-established quickly. Small hotspots occurred frequently in the vicinity of the ground potential electrode. A typical photograph of such a continuous arcing process as well as hotspot formation is shown in Fig. 38 (b).

Sample discolouration was now very vivid at the ground potential electrode, with the surfaces being increasingly burnt black by the continuous arcs as the tests progressed.

A yellowish deposit was also observed to form alongside the fluid path, which increased in volume during the tests. The deposit was presumed to be NH_4Cl crystals being deposited as contaminant fluid evaporates due to the heating action of the leakage current. However, no further tests were performed to ascertain the nature of this deposit. Some discolouration was also evident along the fluid path, which was again presumed to occur due to the heating effect of the leakage current flowing through the contaminant. Minor dry band discharges at other regions of the samples also caused the formation of lightly discoloured branches spreading outwards from the contaminant path. These effects can be observed in Fig. 39 (a).

For reasons that will be outlined in following sections, the samples underwent a cleaning procedure after testing had been completed. Erosion damage to the samples surface was observed to be minimal and only located in the vicinity of the ground potential electrode, where the arcing process was strongest throughout the tests. The surface discolouration was found to be superficial only, as most of the discolouration was removed during the cleaning of the samples. Fig. 39 shows a typical sample of series A before and after being cleaned. Note that most the discoloured area was restored to the original surface colour after cleaning.

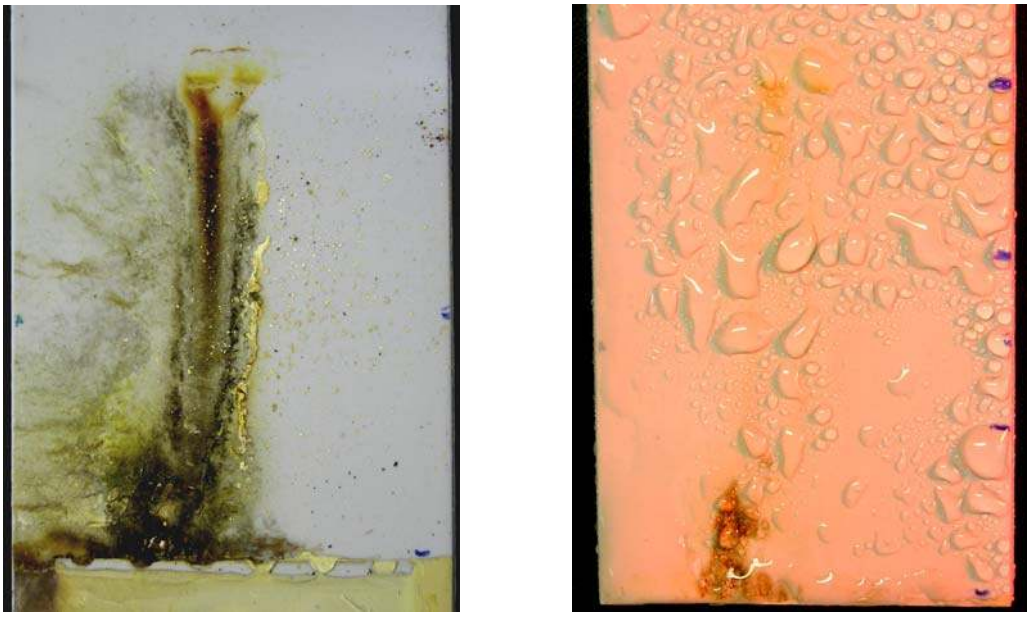

(a) **(b)**

Fig. 39: Test sample of series A: (a) Before and (b) After cleaning procedure, with lower region covered by conductive paste moved.

4.3.1.2 Series B

Weak scintillations and dry band discharges across the sample face occurred in the first minutes during test runs in this series, causing only minimal discolouration of the sample surfaces. However, between 30 minutes and one hour into the tests (usually before the first voltage step of 250 V) this developed into continuous effective scintillation at the ground potential electrode, accelerating the rate and intensity of surface discolouration in this region. The arcing remained fairly constant throughout the duration of the experiment and only weakened slightly towards the end of the test runs. The only major change in the arcing process was a lengthening of the arcs at the ground potential electrode when increasing the test voltage from 2.75 to 3.0 kV, which also entailed an increase in both contaminant flow rate and current limiting resistance. This increase in arc length is shown in Fig. 40. Hotspots were also observed more frequently along the ground potential electrode once this changeover was made.

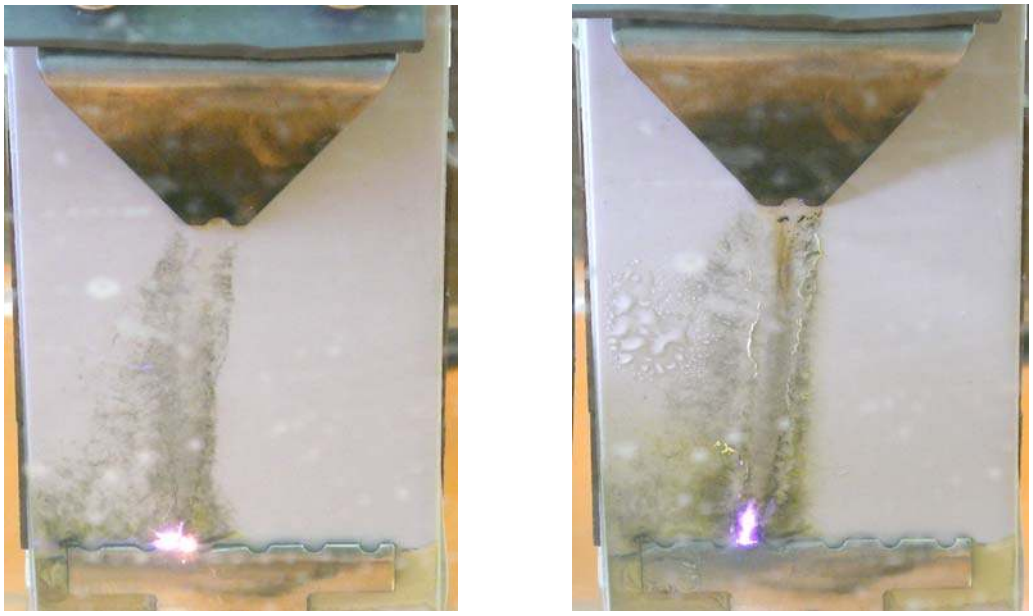

(a) **(b)**

Fig. 40: Change of arc length during voltage step from (a) 2.75 to (b) 3.0 kV.

The discolouration of the sample surface started within the first half hour of the tests and then increased steadily over the entire test duration. The same yellow deposits observed in series A also occurred in this test series, usually appearing between the end of the second and the middle of the third test hour. The deposits increased over time, although a decrease could sometimes be observed due to the contaminant washing away part of the deposits.

As in series A, the discolouration was severest along the ground potential electrode, where continuous arcing burned the sample surface to a deep black colour. A discolouration along the fluid path similar to that observed in series A also occurred in this series, as did the discolouration of other surface areas due to sporadic discharges at those locations. However, the discolouration once again proved to be superficial, since most of it was removed once the samples underwent the washing procedure. Erosion damage to the samples was observed to be minimal and located along the ground potential electrode, similar to series A. Fig. 41 shows a typical sample of series B before and after the washing procedure.

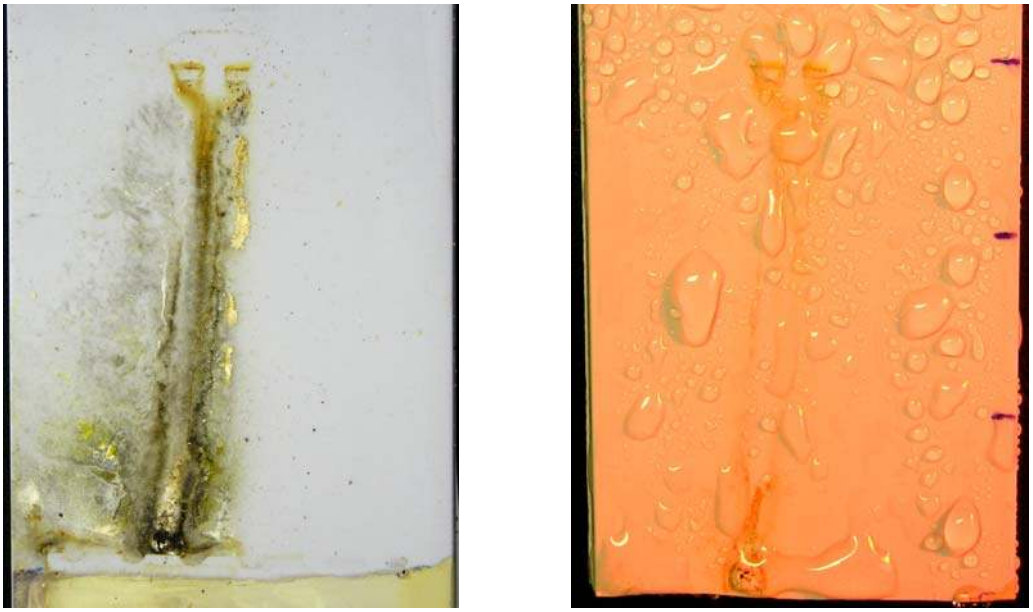

(a) **(b)**

Fig. 41: Test sample of series B: (a) Before and (b) After cleaning procedure, with lower region covered by conductive paste removed.

An exception in terms of erosion damage was observed in sample B5. During the test run on this sample, a hotspot of high intensity developed at the ground potential electrode at the begin of test hour 3, causing heavy erosion in a small area at the centre of the electrode. This eroded area slowly increased in depth and severity until the end of hour 3, after which no discernable growth was observed. However, hotspots of reduced intensity continued to form at this location until the end of the test. Fig. 42 shows the occurrence of a hotspot on this sample during test hour 3, as well as the appearance of the sample after the completion of the test.

Comparison of the visual observations during both test series showed that the samples exhibit similar behaviour for the two different test methods. Both test series showed

the same discolouration of the sample surfaces, and the formation of yellow deposits was also observed during both series. Visual appearance of erosion damage to the samples was revealed to be equally minimal for both methods, with the sole exception of sample B5. And although the arcing at the ground potential electrode stabilized faster in series B than in series A, both test series showed continuous effective scintillation during those test hours where contaminant flow rate and current limiting resistance were the same for both test series.

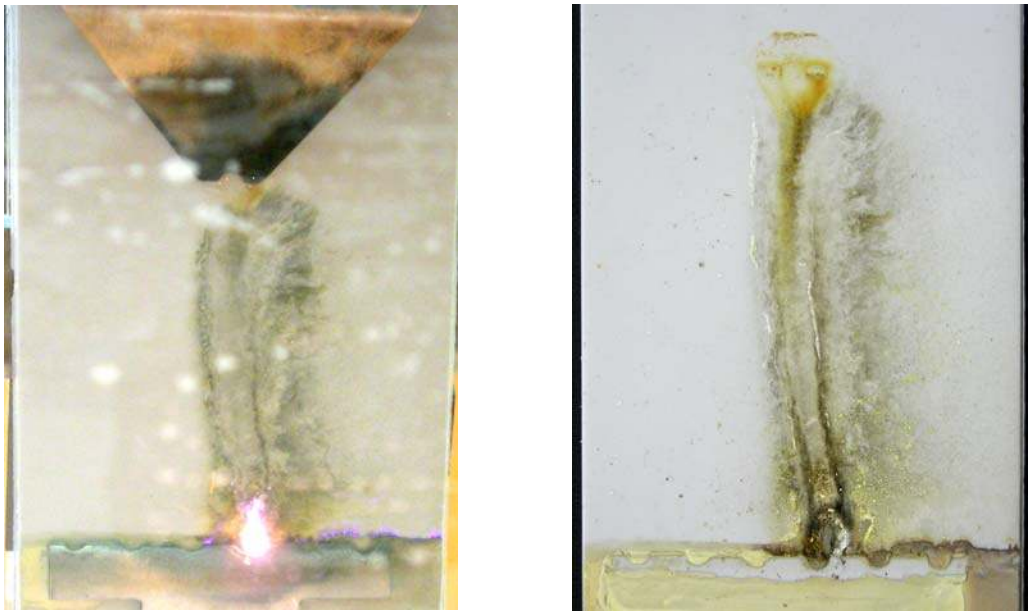

(a) **(b)**

Fig. 42: Sample B5: (a) During development of intense hotspot and (b) Appearance after completion of test run.

It should be noted at this point that the author refrained from labelling any dark or black areas on the samples as tracks. This resulted from the observation that continuous arcing always took place at the interface of sample surface and ground potential electrode. A track is defined as a permanently conducting path, often of carbonaceous nature [34]. If the dark areas were indeed tracks, one would expect the majority of the arcing process to take place at the edges of these areas rather than the electrode-sample interface. The arcing process should thus have moved upwards along the sample surface during test proceedings. However, although some arcing did take place some distance above the ground potential electrode, it always eventually returned to the electrode-sample interface rather than moving up the sample. This led to the conclusion that the dark areas are not or only minimally conducting, and thus do not qualify as tracks.

4.3.2 Sample mass loss

The samples experienced a loss of material due to electrical erosion induced by continuous arcing at the ground potential electrode. In order to determine the mass loss, the samples were weighed prior and after the test runs. The difference in the two measurements (if any) was taken as the mass lost due to electrical erosion. The prior weighing was done after the initial cleaning and abrasion of the samples, to prevent an error to be introduced into the measurement due to weight loss by abrasion. After testing, the samples were washed using distilled (deionised) water and a soft toothbrush in order to remove any surface deposits and waste materials. This is the washing procedure mentioned in section 4.3.1. The samples where then dried and weighed again to determine the mass loss of the sample.

In order to achieve a better comparison between the series, the series average $\bar{x}$ for each test method was calculated using the relationship [44]

$$\bar{x} = \frac{1}{N}\sum_{i=1}^{N} x_i, \tag{4.1}$$

where x_i denotes the individual measurements and N the total number of measurements made. In addition, the standard deviation of the measured data in each series was also calculated by [44]

$$S_x = \sqrt{\frac{1}{N-1}\sum_{i=1}^{N}(x_i - \bar{x})^2} \tag{4.2}$$

so as to better observe the distribution of the data around the series average. These relations are based on finite statistics theory due to the small number of data points available. Table 8 summarizes the mass loss measurements for each sample as well as the series average and standard deviation for each test series.

Table 8: Mass loss results during method comparison.

Series A		Series B	
Sample name	**Mass loss [mg]**	**Sample name**	**Mass loss [mg]**
A1	67	B2	31
A2	59	B3	25
A4	31	B4	25
A5	17	B5	67
Series average	44	Series average	37
Standard deviation	24	Standard deviation	20

The results reveal that the samples of series A have a higher mass loss than those of series B, although with a wider distribution around the mean value. However, both test series contain either very high or very low values that do not correspond with the other measurements in the respective test series. The decision was thus taken to repeat the calculations for the series mean and standard deviation using equations 4.1 and 4.2, while excluding those samples in each series whose measurements show the largest deviation from the series averages shown in Table 8. The samples omitted were samples A5 and B5. Both the previous values (based on four samples) and the newly calculated values for the series means and standard deviations are shown in Table 9.

Table 9: Series mean and standard deviation for mass loss.

Test Series	Series average [mg]		Standard deviation [mg]	
	4 Samples	3 Samples	4 Samples	3 Samples
A	44	53	24	19
B	37	27	20	3

A visual comparison of the measurements is given in Fig. 43. Vertical coloured bars represent the mass loss for each sample indicated. The horizontal dashed lines indicate the series mean based on three samples for each series, while the vertical lines indicate a spread of one standard deviation around the mean.

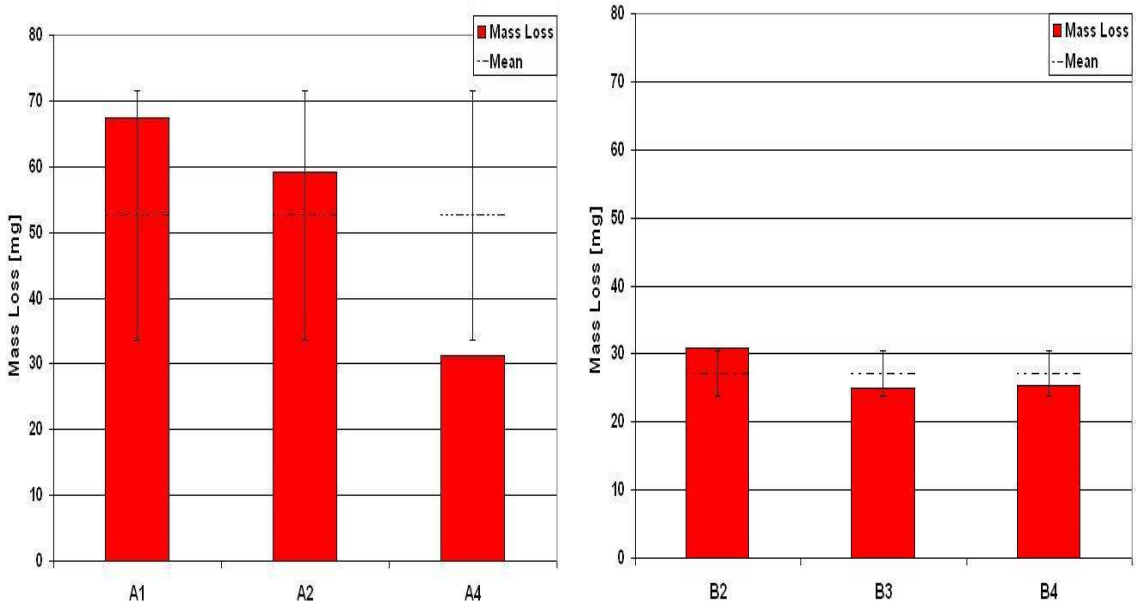

(a) **(b)**

Fig. 43: Mass loss for three considered samples: (a) Series A and (b) Series B.

Inspection of Fig. 43 as well the results displayed in Table 9 confirms the initial observations. Test series A shows a higher mass loss in its samples, with its three sample average more than double in magnitude than that of test series B. The constant tracking voltage method thus seems to be the more severe method in terms of electrical erosion. However, the samples of series B exhibit a much smaller variation around the series average, with the three sample standard deviation being 9 times smaller in magnitude than that of series A. This indicates that the stepwise tracking voltage method might have a higher repeatability, thus producing more constant results than the constant tracking voltage method.

4.3.3 Sample erosion depth

The measuring of the maximum erosion depth on sample is stated as a requirement in the IEC 60587 standard and is to be included in all test reports. Depth measurements should be taken using a gauge with ± 0.01 mm accuracy with a hemispherical probe of 0.5 mm in diameter [34]. In order to comply with these strict guidelines, a Mitutoyo Bright Apex 710 contour measuring machine (CMM) with a volumetric accuracy of up to 6 µm was used for the erosion depth measurements. The dimensions of the probe were according to standard specifications. Measurements were taken along contour lines spaced 0.5 mm apart in steps of 0.25 mm along the longitudinal axis of the samples, starting at the position of the ground potential electrode. Since only the maximum erosion depth is of importance, measurements were taken only in areas where erosion was visible to the naked eye. Erosion measurements were undertaken after the samples were cleaned so as to prevent interference in the measurements by surface deposits.

Equations 4.1 and 4.2 were again utilized to calculate the series mean and standard deviations for each test series for comparison purposes. Table 10 shows the maximum erosion depth measured for each tested sample, as well as the series means and standard deviations.

Table 10: Erosion depth measurements during method comparison.

Series A		Series B	
Sample name	**Erosion depth [mm]**	**Sample name**	**Erosion depth [mm]**
A1	0.28	B2	0.22
A2	0.18	B3	0.27
A4	0.24	B4	0.33
A5	0.38	B5	1.58
Series average	0.27	Series average	0.60
Standard deviation	0.08	Standard deviation	0.66

Upon initial inspection, test series B is revealed to have a higher average erosion depth, while series A shows a smaller variation in the measurements. However, the unusually high erosion in sample B5 has a large influence on the mean and the standard deviation of that test series. The calculations for the mean and standard deviation were thus repeated after eliminating the sample of each series that shows the largest deviation from the series mean. The samples eliminated for this criterion are the same as for the mass loss criterion, samples A5 and B5. Table 11 shows the change in series mean and standard deviation resulting from the elimination of the respective samples.

Table 11: Series mean and standard deviation for erosion depth.

Test Series	Series average [mg]		Standard deviation [mm]	
	4 Samples	**3 Samples**	**4 Samples**	**3 Samples**
A	0.27	0.24	0.08	0.05
B	0.60	0.27	0.66	0.06

Fig. 44 shows the individual measurements of the three samples considered per series, plotted as vertical coloured bars. The three sample series average is indicated once again by horizontal dashed lines, while the vertical lines show a variation around the mean value of one standard deviation based on the three considered samples.

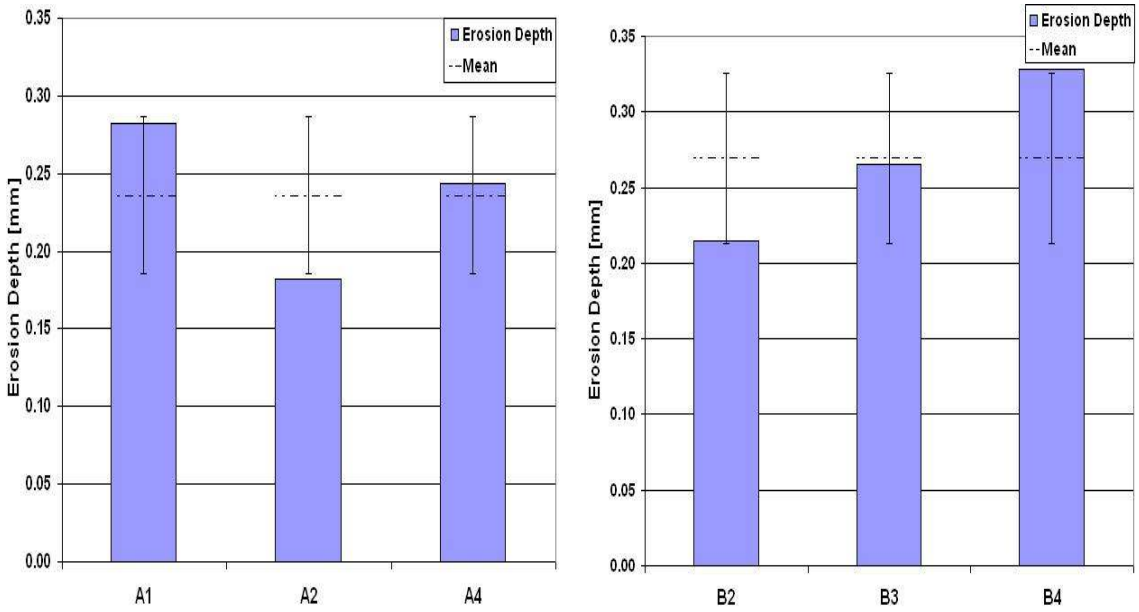

(a) **(b)**

Fig. 44: Erosion depth for three considered samples: (a) Series A and (b) Series B.

Inspection of Table 11 and Fig. 44 shows the mean values of the two test series to be very similar to one another in magnitude, only differing by ± 0.03 mm. The standard deviation is virtually identical for both methods, which is also confirmed by the similar distribution of measurements around the series means as displayed in Fig. 44. The maximum erosion depth experienced in the test samples is thus similar for both test methods.

When comparing the measured erosion depths in Table 10 with the measured mass losses in Table 8, it becomes apparent that the two criteria are not always equally severe in a given sample. The reason for this is that the mass loss in a sample depends on the volume of material removed. This volume depends on the eroded area as well as the relative erosion depth, according to the equation

$$\text{Volume} = \text{Area} \times \text{Depth}. \tag{4.3}$$

A large mass loss can thus occur if the area covered by the erosion is large, even if the sample shows a relatively small erosion depth. Erosion depth is an important criterion nonetheless, since deep erosion on insulator coatings or compound insulators can expose the core material to the environment. This allows environmental ageing factors to attack the core material directly, thus facilitating mechanical failure in the insulators [7].

Sample B5 shows the highest erosion depth of both test series, as well as an unusually high mass loss for a sample of series B (see Table 8). This extensive erosion occurred on a relatively small area on the sample (see Fig. 42). Since no such abnormal behaviour was observed in any other sample of either test series, it is suspected that a fault existed in the material of the sample at that specific location.

4.3.4 Average hourly rms leakage current

As described in section 3.3.3, the rms leakage current measured by the OLCA is computed over an interval of one minute and then logged in the memory of the device. A test duration of six hours thus equals a total of 360 data points for the rms leakage current parameter for every sample tested. To improve the comparison between the two test series, the hourly mean as well as the standard deviation was calculated for each test series using equations 4.1 and 4.2. The results are displayed in Table 12.

Table 12: Hourly average rms leakage current for both test series.

Test series	Sample name	Average rms leakage current [mA]					
		Hour 1	Hour 2	Hour 3	Hour 4	Hour 5	Hour 6
A	A1	4.92	7.16	7.31	6.95	6.44	6.38
	A2	6.44	6.92	6.81	6.79	6.67	6.76
	A3	6.91	6.96	6.13	6.32	6.14	6.57
	A4	6.78	7.03	6.46	6.04	5.88	5.56
	A5	6.77	6.95	6.61	6.47	6.29	6.31
	Series mean	6.36	7.00	6.66	6.51	6.28	6.32
	Standard deviation	0.83	0.10	0.44	0.37	0.30	0.46
B	B1	4.06	4.71	7.32	7.26	7.29	7.08
	B2	4.07	4.53	6.47	6.83	6.85	6.89
	B3	3.91	4.15	6.54	6.54	6.81	6.90
	B4	4.24	4.79	7.57	7.48	7.38	7.16
	B5	4.16	4.58	6.67	5.97	5.77	5.34
	Series mean	4.09	4.55	6.91	6.82	6.82	6.67
	Standard deviation	0.12	0.25	0.50	0.60	0.64	0.75

In order to be able to observe possible underlying trends in the samples of each test series, the hourly averages for each test sample displayed in Table 12 were plotted on a single common plot displayed in Fig. 45. The vertical bars are labelled to indicate which sample they represent.

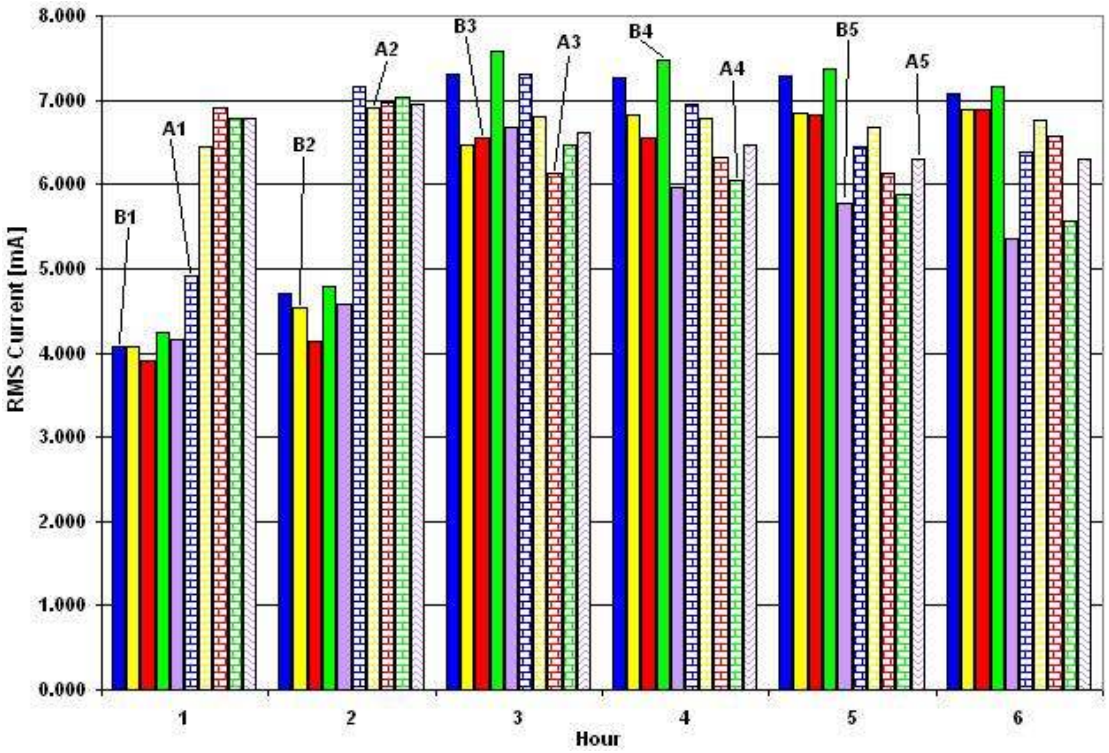

Fig. 45: Hourly average rms leakage currents for test series A and B.

Both Fig. 45 and Table 12 reveal the samples of test series B to have lower average currents in the first two test hours than those of series A. During this specific time period, both the contaminant flow rate and the current limiting resistance were different for each test series, both being lower in test series B than in A. Since these important test parameters differed for both test series, a comparison between the two methods will yield no useful information for this specific time period. The leakage current data for test hour 1 and 2 will thus not be considered for this evaluation criteria.

The series means for each test hour displayed in Table 12 are similar in magnitude for both test series during hours 3 to 6. However, the relatively high values for the standard deviations during some test hours (especially during hours 5 and 6 for series B) reveal the presence of extreme data points, which have a tendency to distort statistical analysis. As with the other evaluation criteria, the mean and standard deviation calculations were thus repeated while excluding those samples whose hourly averages show the greatest deviation from the series mean.

Inspection of Fig. 45 shows that samples A4 and B5 have lower average rms currents than the other samples for test hours four to six. A closer inspection of the data in

Table 12 confirms that these are the samples with the highest deviation from the mean values of each test series for the relevant test period of hour three to six. Table 13 shows the difference between the original and recalculated series means and standard deviations for the time period of hour three to six.

Table 13: Original & recalculated hourly series means & standard deviations for rms leakage current.

Test series	No. of samples per series	Data type	Test hour			
			3	4	5	6
A	5	Series mean	6.66	6.51	6.28	6.32
		Standard deviation	0.44	0.37	0.30	0.46
	4	Series mean	6.71	6.63	6.38	6.50
		Standard deviation	0.49	0.29	0.22	0.20
B	5	Series mean	6.91	6.82	6.82	6.67
		Standard deviation	0.50	0.60	0.64	0.75
	4	Series mean	6.97	7.03	7.08	7.01
		Standard deviation	0.55	0.42	0.29	0.14

The hourly average rms current for the considered samples are plotted in Fig. 46. Additionally, the hourly series means together with a positive and a negative standard deviation around the mean are displayed as horizontal dashed lines, forming an envelope in which the individual data points should lie if the variation in the data is acceptable.

The hourly means are similar for both test series, the maximum difference between them reaching a value of ± 0.7 mA. The magnitude of the standard deviations is also similar, as is the distribution of the individual data points around the mean value (see Fig. 46). The two test methods thus also deliver similar results for this evaluation criterion.

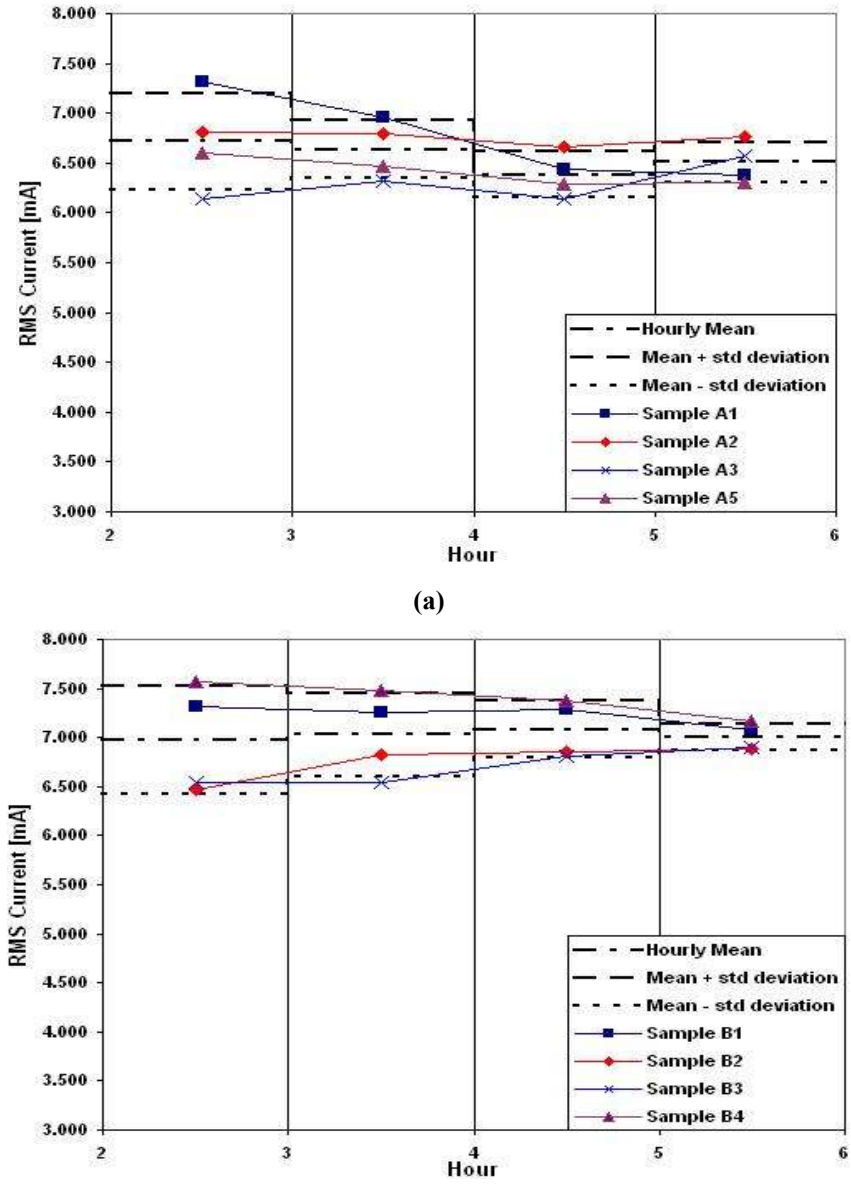

Fig. 46: Hourly average rms leakage currents with 4 sample mean and standard deviation shown: (a) Series A and (b) Series B.

Upon inspection of Table 12 and Fig. 45, it was noticed that sample A1 shows a lower average leakage current during test hour one than any other sample of series A. The test report and recorded visual observation were consulted in order to discover the reason for this behaviour. It was discovered that sample A1 showed weaker arcing and electrical discharges at the ground potential electrode during this period, which accounts for a low rms leakage current. A possible explanation for this is that some surface areas of the sample still retained a higher degree of hydrophobicity, even though the sample was abraded in order to counter this effect. A high degree of surface hydrophobicity hinders the flow of contaminant fluid along the sample

surface, thus preventing the establishing of a constant arc at the ground potential electrode. Proper arcing was established after the first test hour and the sample showed leakage current levels comparable with the other samples of the series during all following test hours.

4.3.5 Peak current bin counts

The OLCA also measures and logs the positive and negative peak currents occurring during each one minute interval. The peak currents are then sorted into bins, where each bin represents a range of values which are predefined by the user. Six bins each are available for positive and negative peak currents. The ranges selected for the bins for this experiment are as follows: 1 to 5 mA, 5 to 20 mA, 20 to 60 mA, 60 to 100 mA, 100 to 250 mA and 250 to 500 mA. The bin ranges are identical for both positive and negative peak current counts.

The first bin (1 to 5 mA) will contain noise measurements and was thus not considered in the comparison. Since the overcurrent relay will cut the power supply to the apparatus as soon as the rms leakage current exceed a value of 60 mA, the maximum expected peak currents will fall into the 60 to 100 mA range. The three bins thus considered during this comparison were: 5 to 20 mA, 20 to 60 mA and 60 to 100 mA. Table 14 shows the total occurrences for each peak current bin for each individual sample, as well as the series mean and standard deviation of each test series for each of the bins. Again, since current limiting resistance and contaminant flow rate are different for the test methods during the first two test hours, only test hours three to six were considered for this comparison.

The test series show comparable results for both positive and negative counts in the first bin. Test series B, however, shows more occurrences of medium (20 to 60 mA) and high peak currents (60 to 100 mA), indicating that the use of the stepwise tracking voltage method results in higher peak currents across the samples. Test series A showed smaller standard deviations than series B for each of the bins, indicating more stable results for the constant tracking voltage method.

Table 14: Bin counts for positive & negative peak currents for test hours 3 to 6.

Test series	Data name	Negative peak currents			Positive peak currents		
		5 - 20 mA	20 - 60 mA	60 - 100 mA	5 - 20 mA	20 - 60 mA	60 - 100 mA
A	Sample A1	236005	14116	0	252359	21203	1
	Sample A2	253598	26726	2	237345	26395	2
	Sample A3	255915	2475	12	261010	3808	12
	Sample A4	214410	2539	0	192568	3827	0
	Sample A5	212623	6433	0	208017	7239	0
	Series mean	234510	10458	3	230260	12494	3
	Standard deviation	20663	10255	5	29153	10574	5
B	Sample B1	199079	22110	45	194320	30607	44
	Sample B2	283818	4558	38	289116	7037	42
	Sample B3	243228	14047	1	247092	16236	0
	Sample B4	150694	43148	11	144955	49073	11
	Sample B5	301029	5361	34	239945	6818	34
	Series mean	235570	17845	26	223086	21954	26
	Standard deviation	61658	15853	19	55119	17990	20

These results correspond well with the results of the rms leakage current criterion, where test series A showed lower series means but also smaller standard deviations than test series B for the hourly average rms currents.

4.3.6 Chemical analysis of selected samples

In order to gain more information about possible differences in chemical changes in the test samples of the two methods, one sample of each test series was selected to undergo a chemical analysis using Fourier transform infrared (FTIR) spectroscopy. This is a commonly used method to investigate polymeric materials by determining the chemical composition of the analyzed material, both quantitative and qualitative. It can be used to investigate different parameters (e.g. types of polymer end groups present, chain branching etc.) or to identify and determine the concentration of impurities, filler materials, residual monomers and other substances within the material. It also allows for the study of the effects of external conditions on polymer substances, such as changes with temperature and pressure or the effects of irradiation, deformation, fatiguing and weathering [45].

The method entails the bombardment of the material sample with infrared rays of varying frequency. Some of these rays are transmitted through the surface before being reflected back to a detector, which measures the intensity of the reflected rays. Other rays are absorbed by different functional groups within the material at certain

frequency bands and transformed into vibration energy, thus diminishing the intensity of the reflected rays. By applying the Fourier transform method, an intensity spectrum of the relative transmitted (or absorbed) rays can be generated for the entire applied frequency band. Different components can then be identified by comparing the spectra of a tested sample against reference spectra. Since different functional groups have characteristic vibration energies, their presence can be easily determined [46]

This analysis method is used primarily for the analysis of surface changes in a material, the effective infrared spectral region usually lying in range from 2 to 50 μm [46]. It thus usually works best for thin, specially prepared samples. However, several method exist which can be used to enhance the FTIR method, making it possible to also analyze untreated material specimens. One such method is the attenuated total reflection (ATR) FTIR method. A special crystal lens, usually made from zinc selenide (ZnSe) or KRS5 (thallium bromoiodide), is mounted onto the FTIR machine. This lens acts as a prism, reflecting the incoming infrared beam several times onto the sample, where it enters the surface each time it is reflected. This multiple re-entry increases the absorption of the infrared rays by the functional groups in the material, thus increasing the signal-to-noise ratio [46]. This makes it possible to analyze samples with increased thicknesses. The ATR FTIR method was used for all chemical analyses in this project.

The previous paragraphs were intended to give some background information on the ATR FTIR spectroscopy method. The following sections will summarize the analysis method and the obtained results, respectively.

4.3.6.1 Sample selection & analysis methodology

As mentioned previously, the chemical analysis was performed on one sample per test series. This small number of samples reserved for chemical testing was chosen since such samples could not be included in the mass loss or the erosion depth comparison. The cleaning procedure utilized for these criteria could have otherwise possibly interfered with the results of the chemical analysis. For similar reasoning, the samples selected for this criterion were not treated in any way. It thus follows that these samples had to be representative of each individual test series.

These samples were selected based on the following criteria:

- *Visual appearance:* The surface erosion/discolouration of the selected sample should be comparable to the other samples of the series, i.e. no unusually excessive damage/discolouration or lack of it.
- *RMS leakage current:* The rms current of the sample measured by the OLCA over the test period of six hours should be comparable to other samples in the series, both in magnitude and trend.
- *Maximum leakage current:* The maximum peak currents (measured per one minute interval) of the sample should be comparable to those of the other samples within the series over the test period of six hours, both in magnitude and trend.

In order to compare the rms and peak currents of the samples, plots were generated using the OLCA DataManager software, which is specifically developed for displaying the data measured by the OLCA device. To qualify for chemical testing, the selected sample had to be comparable to at least two other samples of the series. The selected samples were sample A3 for test series A and sample B1 for test series B. As a result, these samples are not represented in the comparisons of mass loss and erosion depth between the series.

Each selected sample was then divided into three separate regions by dividing the fixed distance of 50 mm between the electrodes into three areas of equal length and a width identical to the sample width. These three regions are called the lower 17 mm, the middle 17 mm and the upper 16 mm region as measured from the ground potential electrode upwards. The ground potential electrode was chosen as a reference since this is the region where most of the dry band arcing should take place. A small circular sample of 10 mm diameter and a thickness of ± 1 mm was cut from each of these three regions and analyzed. The spectra of these samples were then compared to spectra obtained from samples of untested virgin material. The samples were not treated in any other way so as not to influence the results of the chemical analysis, although other studies exist were similar samples were washed using acetic acid and distilled water before the analysis [47].

The spectra were obtained using a Smart Golden Gate ATR lens (made from ZnSe). The pressure exerted by the lens on the samples can be manually regulated by turning a knob at the top of the lens and monitoring a built-in scale on the lens. This pressure was kept constant for all samples. The spectra were done in a wavenumber band ranging from 4000 to 650 cm^{-1}. It should be noted at this point that FTIR spectra are usually plotted as transmittance versus wavenumber. The wavenumber is the number of wave maxima per unit length and are related to the wavelength of the emitted infrared ray by the relationship [53]

$$\text{wavenumber} = \frac{10^7}{\lambda}, \tag{4.4}$$

where λ is the wavelength of the beam in nm and wavenumber is measured in cm^{-1}. Transmittance on the other hand is defined by the relationship [53]

$$T = \frac{I}{I_O}, \tag{4.5}$$

where T denotes the transmittance ratio, I the transmitted light intensity and I_O the original light intensity incident on the sample surface.

It is also possible to express the spectra in absorbance versus wavenumber, where absorbance is defined as [53]

$$A = -\log_{10}\left(\frac{I}{I_O}\right) = -\log_{10} T, \tag{4.6}$$

where A is the absorbance of the beam by the sample expressed as a percentage. Although transmittance is more commonly used, it was decided to analyze the samples in absorbance mode. This was done since the conversion of transmittance to absorbance induces a smoothing effect in the displayed spectra, reducing the data scatter introduced by background noise.

For each scanned sample, the background spectrum was obtained first by running the scan without the sample. The sample was then placed into the machine and the scan was repeated to obtain the final spectra. The number of scan repetitions for both the background and actual sample was kept at 16. The following section presents the results obtained for the scanned samples of the two test series.

4.3.6.2 Results of chemical analysis

Fig. 47 shows the spectra obtained for the lower 17 mm regions of samples A3 and B1. Each sample spectra is shown in comparison with the spectrum obtained for the virgin sample. No further spectra will be shown in this text however, since the large number of spectra generated would require an excessive amount of space. Instead, all of the remaining spectra, including enlarged spectra for different wavenumber ranges, can be found on a DVD appended to this thesis.

An analytical analysis of the spectra was performed on the spectra using the specific software provided with the FTIR apparatus. The analysis focused on three different areas:

- Loss of alumina trihydrate filler (ATH, or Al_2O_3-$3H_2O$) shown by a reduction in the peak height at 3522 cm^{-1}.
- Loss of methyl (CH_3) groups from the polydimethylsiloxane (PDMS) structure, which can be detected by a decrease in the spectra peak height as well as in the area under the peak at 2963 cm^{-1}.
- Oxidation of the PDMS and formation of carbonyl (C=O) groups, revealed as an increase of the area under the curve in the range of 1550 to 1800 cm^{-1}.

These focus areas were adopted from an analysis report for tests on polymer insulator materials frequently performed at the Department of Chemistry and Polymer Science of Stellenbosch University.

For a comparison of peak heights between tested and virgin samples, the ratio of tested to virgin peak height is commonly used. This peak height is measured from a baseline drawn between two chosen base wavenumbers on either side of the peak rather than from the x-axis of the spectra and is known as the corrected peak height. A comparison for the area under a certain peak also utilizes the ratio of tested to virgin sample. Again, the area considered is taken as the area between the spectrum curve and a baseline drawn between two base wave numbers. For the area, these base wavenumbers often coincide with the limit wavenumbers between which the area is calculated. This area is called the corrected peak area.

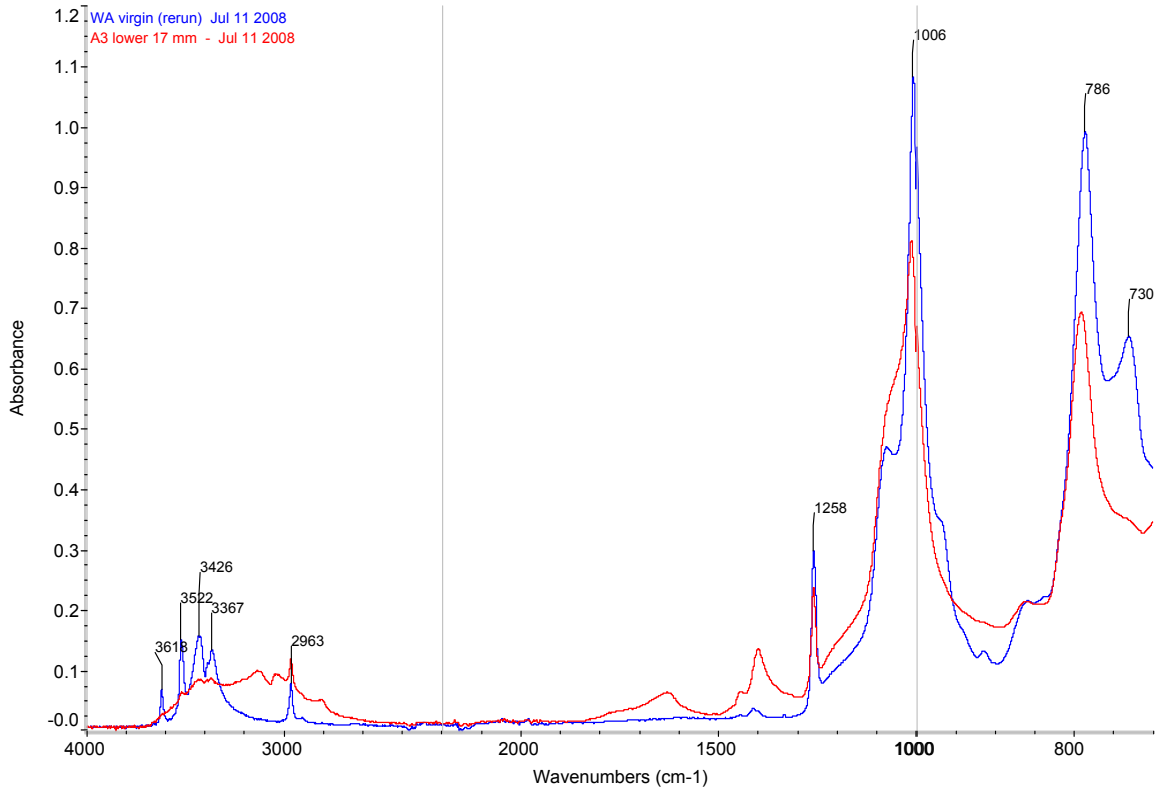

(a)

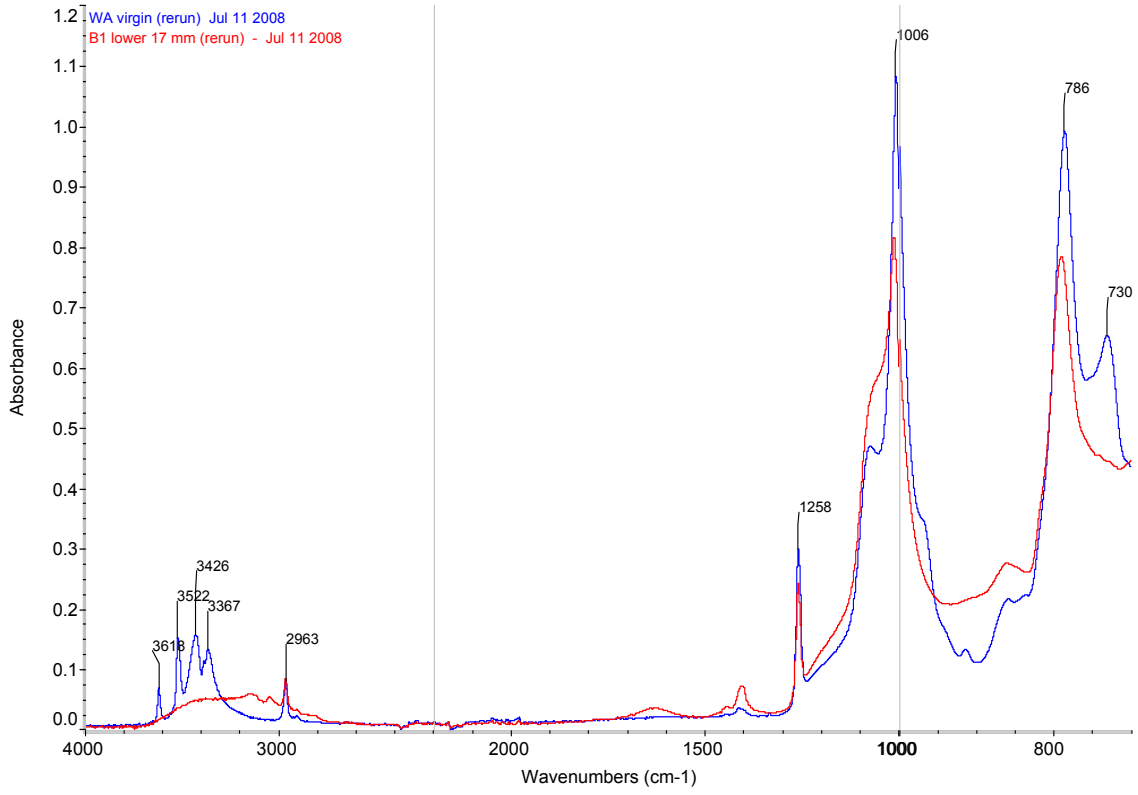

(b)

Fig. 47: Spectra of lower 17 mm region of (a) Sample A3 and (b) Sample B1, showing tested (red line) and virgin sample (blue line).

For the criterion of loss of methyl groups, the change in area is displayed using the relation

$$\beta = \frac{(H_0 - H)}{H_0}, \tag{4.7}$$

where H_0 and H are the areas underneath the peaks of the virgin and tested samples, respectively and β is referred to as the degree of conversion.

The locations of the peaks, area limits and base values for the baselines for each analysis criterion are as follows:

- *Loss of ATH filler:* Peak location: 3522 cm^{-1}; baseline values: Base 1 = 3690 cm^{-1}, Base 2 = 3036 cm^{-1}.
- *Loss of methyl groups:* Peak location: 2963 cm^{-1}; peak area limits: Limit 1 = 3010 cm^{-1}, Limit 2 = 2930 cm^{-1}; baseline values: Base 1 = 3010 cm^{-1}, Base 2 = 2930 cm^{-1}.
- *Oxidation by carbonyl formation:* Peak area limits: Limit 1 = 1800 cm^{-1}, Limit 2 = 1550 cm^{-1}; baseline values: Base 1 = 1800 cm^{-1}, Base 2 = 1550 cm^{-1}.

The results for each criterion for all the tested specimens are shown in Table 15.

The data obtained from the chemical analysis, as displayed in Table 15, suggests that the two different test methods yield similar chemical changes in the test samples. However, differences between some regions of the sample are observed and have to be investigated closer. Bar plots of the results were also generated in order to obtain a visual comparison between the different regions of the two tested samples.

Table 15: Results of chemical analysis for test series A and B.

Test Series	Analysis		Sample region		
			Lower 17 mm	Middle 17 mm	Upper 16 mm
A	Loss of ATH filler – peak height ratio		0.241	0.610	0.716
	Loss of methyl groups	Peak height ratio	0.720	0.917	0.900
		Degree of conversion β	0.314	0.127	0.144
	Oxidation by carbonyl formation – peak area ratio		19.038	3.211	3.930
B	Loss of ATH filler – peak height ratio		0.131	0.652	0.390
	Loss of methyl groups	Peak height ratio	0.786	0.900	0.884
		Degree of conversion β	0.292	0.162	0.153
	Oxidation by carbonyl formation – peak area ratio		7.285	3.381	5.450

Fig. 48 shows the peak height ratios for the loss of ATH filler for all three regions of the two samples. A low value for the peak height ratio indicates a high loss of ATH filler.

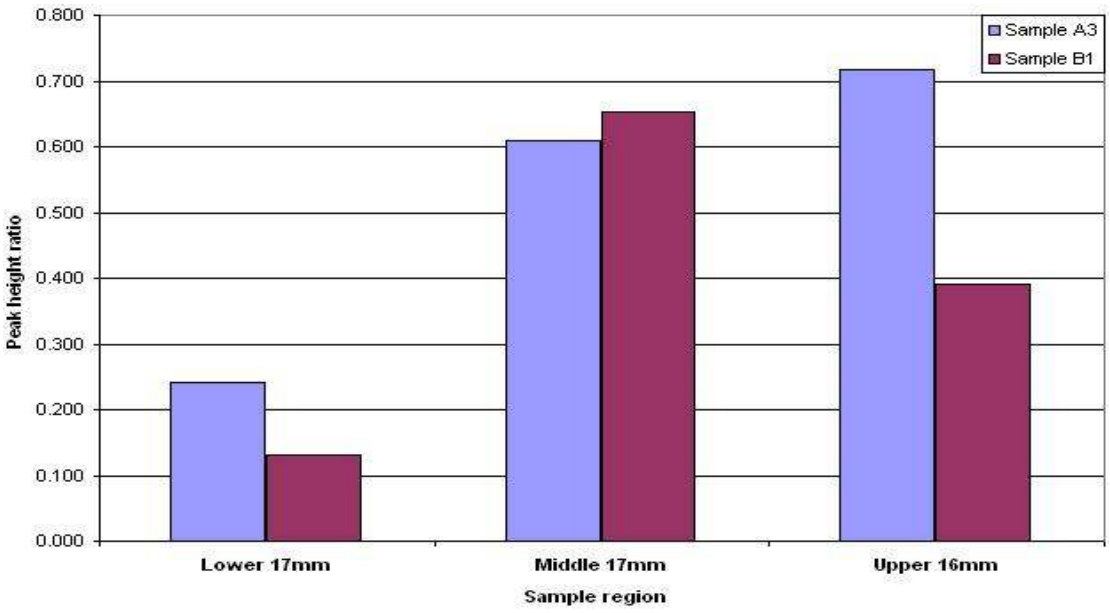

Fig. 48: Peak height ratios for loss of ATH filler for samples A3 and B1.

Both samples show similar ratios in the lower and middle regions of the sample. The loss of ATH filler is greatest in the lower region for both samples. This is to be expected, since this is the area where the majority of the dry band arcing occurs during the test. Any chemical changes are thus expected to the most severe in this region of the sample. The middle regions show high ratios for both samples, indicating little loss of filler in this region due to little arcing behaviour being observed in this region.

However, a difference between the samples is observed in the upper 16 mm region. Sample B1 shows a significantly lower ratio in this area compared to sample A3, indicating a higher loss of ATH filler. Sample A3 shows the least loss of ATH filler in this particular region for all three of its specimens. A possible explanation for this can be found in the fact sample B1 showed a higher hourly rms leakage current than sample A3 for the four final test hours, the difference in current ranging from 0.5 to 1 mA. This increased current over such a long time period could have lead to an increased heating effect of the steel electrodes. Sources state that heat can be conducted along insulation materials into adjacent surfaces and into the bulk material, causing gradual chemical changes [47]. Since the upper 16 mm region is close to the

top electrode, the increased heating effect in sample B1 due to a higher hourly rms current could have resulted in a larger loss of ATH filler near the top electrode. This effect is largely masked at the ground potential electrode due to the constant dry band arcing taking place in this area, producing a significant chemical change in both samples. However, the slightly lower ratio for sample B1 in the lower region suggests that the increased heating effect of the electrode might add to the large chemical change induced by dry band discharges.

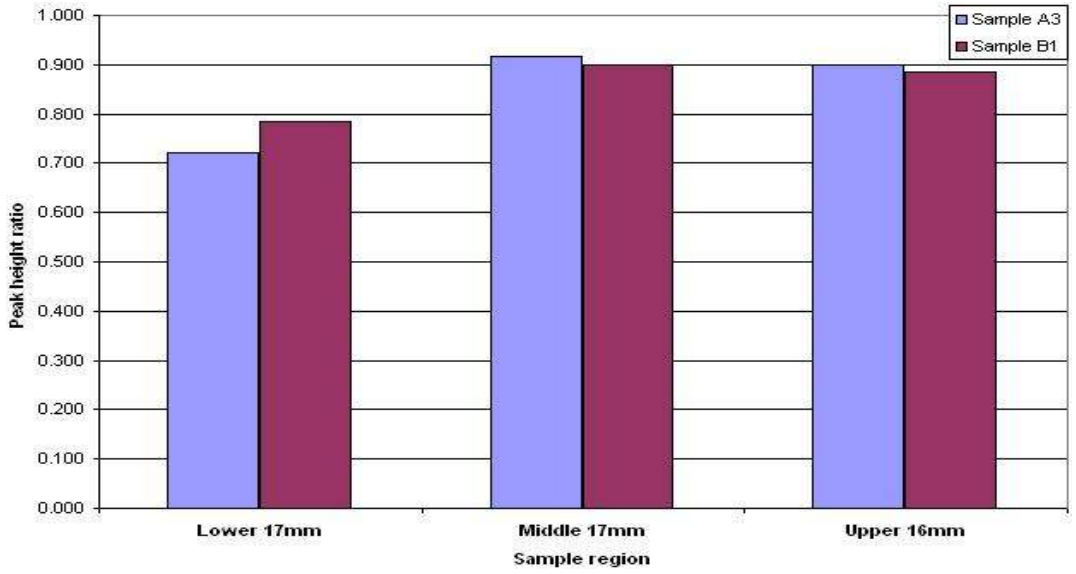

(a)

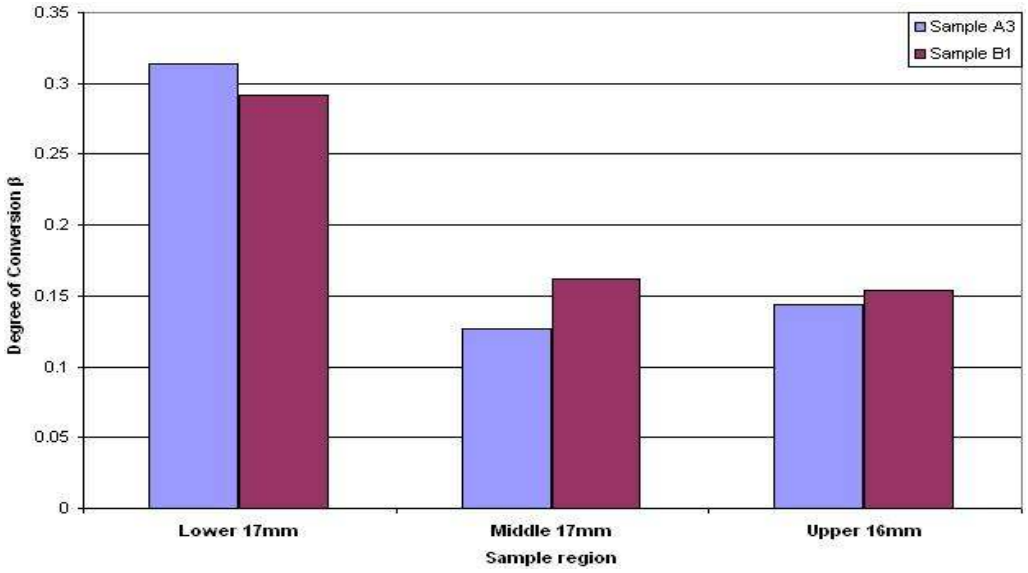

(b)

Fig. 49: Loss of methyl groups in samples, measured by (a) Peak height ratios and (b) Degree of conversion.

Fig. 49 shows the plots for the loss of methyl groups in the samples, displaying both the peak height ratios and the degrees of conversion. Both samples show very similar

results for all three regions, indicating that both test methods are comparable in regards to this criterion. Again the severest chemical change is shown to occur at the lower 17 mm region of the samples due to the high occurrence of dry band discharges in this region.

There seems to be a slight change in trend for sample B1 between the peak height ratio and the degree of conversion analysis. The middle region shows a higher ratio than the upper region for this sample, indicating a smaller loss of methyl groups in the former region. The reverse is true for the degree of conversion analysis, where a higher value for β in the middle region suggests a higher loss than in the top region. However, these differences are relatively small.

Finally, Fig. 50 shows a plot of the oxidation of the polymer through formation of carbonyl groups. An increase in the peak area ratio shows as increase in the oxidation of the sample. Both samples show almost identical results for this criterion in the middle 17 mm region. At the top region, sample B1 shows a slightly higher ratio than sample A3, but not by a large degree. However, a significant difference between the samples can be observed at the lower 17 mm region. Sample A3 shows a peak area ratio of more than double the magnitude of the ratio of sample B1, indicating that this sample underwent strong oxidation in this particular region.

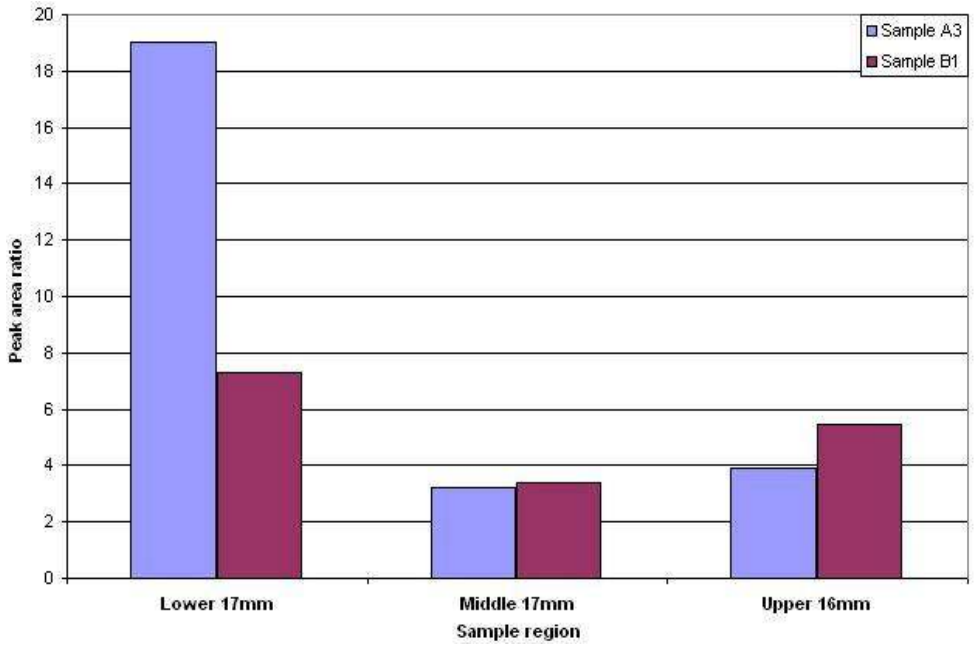

Fig. 50: Oxidation by formation of carbonyl groups in samples A3 and B1.

A possible explanation for this marked difference at the lower 17 mm region was found by examining the visual observations. Sample A3 developed a hotspot at the ground potential electrode at the beginning of the fifth test hour. This hotspot reappeared frequently during the last two test hours, often reaching a high intensity and thus also high temperatures. In order to form carbonyl groups by forming a double bond with an oxygen atom, the carbon in the methyl groups of the silicone rubber first has to break the hydro-carbon bonds. Since the hydro-carbon bond has a relatively high bond energy of 414 kJ/mol, a lot of energy is needed to break this bond [54]. A high intensity hotspot might deliver enough thermal energy to sever the bonds. No such hotspot was observed in sample B1, and the oxidation is thus lower than in sample A3. The increased heating of the electrodes due to increased leakage currents in sample B1 can again be used to explain the difference in ratios at the top region. The difference in magnitude between the ratios is small, since such a gradual heating will not supply enough thermal energy to break a large number of hydro-carbon bonds, thus only resulting in a small chemical change such as observed in Fig. 50.

It should be noted that the C=O bond of carbonyl groups typically has a strong infrared absorption [46]. A small increase in oxidation thus will result in a large increase in peak height and area in the spectrum. Large differences in the results for this particular criterion should thus not be overplayed in their importance for the overall analysis, since they might represent only a small increase in oxidation in the samples.

Overall, the chemical analysis revealed no major differences between the samples of the two test series. The two test methods are thus comparable in regards to the chemical analysis criterion.

4.4 Conclusions for method comparison

After careful evaluation of the results obtained for each of the six evaluation criteria, it can be concluded that the two methods yield similar results for most of the criteria and are thus comparable. Almost identical results were yielded for the erosion depth and the visual observation and sample appearance criterion by both test methods.

Some differences were observed for the mass loss criterion, the hourly rms leakage currents and the chemical analysis. Series A shows a slightly higher average mass loss, while the samples of series B has shown higher hourly average rms currents for those test hours where the contaminant flow rate and current limiting resistance where the same for both test methods. The chemical analysis revealed isolated differences in some analysis criteria for some regions on the test samples, but these differences were generally negligible.

The only evaluation criterion which revealed marked differences between the two test methods was the peak current criterion. Test series B shows higher counts for both the medium (20 to 60 mA) and the high peak currents (60 to 100 mA) than test series A. However, the relevance of this criterion in terms of erosion severity must be called into question, since test series A showed a slightly higher average mass loss in its samples. These results support the theory that it is the rms current levels rather than the peak currents which determine the severity of erosion on insulator samples, since the rms value of the leakage current determines the electrical energy dissipated over the sample. And even though series B showed slightly higher rms currents for test hours 4 to 6, its rms currents for test hours one and two were significantly lower (by ± 2.5 mA) than those of the samples of test series A. The samples of series A might have undergone significantly more erosion damage during these two hours than the samples of series B, with test series B making up the difference by having slightly larger rms currents during hours three to six.

In order to support this theory, the peak current counts shown in Table 14 for test hours three to six was redone to include all six test hours, to check if this would change the peak current count in any significant manner. The results are shown in Table 16.

The counts are still comparable for the low level peak currents (5 to 20 mA). Series A does show a higher count for the medium current levels of 20 to 60 mA. However, series B still shows higher counts for the high peak current levels of 60 to 100 mA, supporting the theory that it is the rms current levels rather than large peak current values that cause electrical erosion. The peak current level criterion should thus be

regarded as a minor criterion for judging the severity of electrical erosion in insulator samples when using the IPT method.

Table 16: Peak current counts of test series A and B for 6 hour duration.

Test series	Data name	Negative peak currents			Positive peak currents		
		5 - 20 mA	20 - 60 mA	60 - 100 mA	5 - 20 mA	20 - 60 mA	60 - 100 mA
A	Sample A1	363141	22419	0	378910	30291	1
	Sample A2	334237	41753	22	316325	41363	24
	Sample A3	341654	20205	12	346974	21920	12
	Sample A4	310230	17174	0	290040	19130	0
	Sample A5	314898	19785	0	309202	20750	0
	Series mean	332832	24267	7	328290	26691	7
	Standard deviation	21395	9951	10	34936	9266	11
B	Sample B1	339748	24127	45	341924	32588	44
	Sample B2	424384	6238	38	438261	8795	42
	Sample B3	372198	15633	1	391857	17771	0
	Sample B4	269806	44121	11	264769	50203	11
	Sample B5	413325	6947	51	356257	8487	50
	Series mean	363892	19413	29	358614	23569	29
	Standard deviation	62464	15620	22	64303	17819	22

Overall, the test results lead to the conclusion that neither test method is preferable to the other. However, several operational problems were experienced during the tests using the stepwise tracking voltage method. Determining the correct starting voltage for this method so that failure in the samples does not occur before the third voltage step can require several trial runs every time a new material is tested. These trial runs can consume an unreasonably large amount of time until true testing of the samples can commence. The IEC standard also states that when using this method, effective scintillation must be maintained at the ground potential electrode at all times during the testing period [34]. In practice, this was difficult to achieve without significantly varying the contaminant flow rate or other test parameters. A lot of experience is needed to perform the stepwise tracking voltage method correctly, making it an unsuitable method for inexperienced users.

Concerns might also be raised that an hourly increase of 250 V in the test voltage might not be representative of the field conditions that insulator materials might be exposed to. The voltage in transmission lines and other high voltage applications remains fairly constant over long periods of time. Difficulties might thus arise upon

trying to relate the test results of the IPT to data gathered from insulators under field conditions when using the stepwise tracking voltage method.

Finally, the next big phase in this project involved the comparison of several insulator materials under the application AC and DC voltages. The stepwise tracking voltage method requires the changing of the contaminant flow rate and the current limiting resistance during the active test period. This can have significant influence on the test measurements, as could be seen in the results for the rms leakage current criterion. Such changing test parameters can make the comparison of results between different materials difficult, since it can be impossible to tell if an observed change is due to a difference in test material or due to a variation in the test parameters.

It was thus decided to utilize the constant tracking voltage method for all further tests during this project. Correspondence with the manufacturers of the test samples for the AC/DC comparison also revealed a general preference in the insulator industry for the constant tracking voltage method. Consequently, this method was utilized in the comparison of several different insulator materials in terms of their resistance to electrical erosion when exposed to AC and DC voltages of both polarities.

Chapter 5: Material Comparison under AC & DC Conditions

This chapter focuses on the main work done for this project. It describes the comparison of samples made from several different insulator materials exposed to both AC and bipolar DC voltages using the IPT method. The materials are compared according to the results obtained for several evaluation criteria, which are described in detail in this chapter.

5.1 Choice of test materials & sample preparation

A total of four insulator materials were tested during this project. The suppliers of the various materials will be kept anonymous and letters will be used to distinguish between them throughout this entire thesis. Letters were also used to label the different materials for easier reference, without having to refer to the full material name. The chosen materials were:

- *Material A*: Ceramic tiles coated with room-temperature vulcanized (RTV) silicone rubber, with 14% alumina tryhydrate (ATH) filler content; pre-cut by supplier to size 86 x 50 x 8 mm, with coating thickness of 0.3 mm; source: supplier W.
- *Material B*: High Temperature Vulcanized (HTV) silicone rubber with 54% ATH filler content; pre-cut by supplier to size 122 x 52 x 10 mm; source: supplier X.
- *Material C*: Ethylene propylene diene monomer (EPDM) rubber, containing 84% ATH filler; supplied in large slabs of 6 mm thickness; source: supplier Y.
- *Material D*: HTV silicone rubber, with 58% ATH filler content; supplied in large slabs of 6 mm thickness; source: supplier Z.

The filler contents of each material were determined by means of a Thermal Gravimetric Analysis (TGA) performed on virgin material samples.

For materials C and D, the author cut samples of size 125 x 50 x 6 mm from the existing slabs delivered by the suppliers. This size was chosen for the samples to fit

the existing sample supports in the IPT, while keeping in accordance with IEC standard specifications of a minimum sample size of 120 x 50 mm [34]. Typical sample specimens for each of the four materials are shown in Fig. 51.

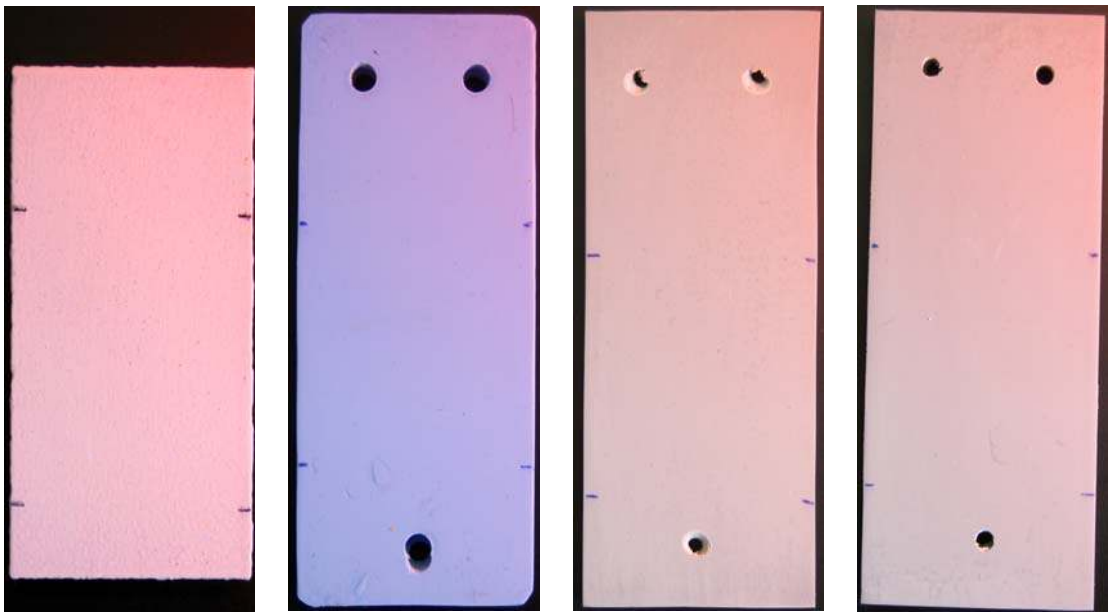

(a) (b) (c) (d)

Fig. 51: Sample specimen: (a) Material A, (b) Material B, (c) Material C and (d) Material D.

These materials were chosen since they represent four insulation materials commonly used in HV applications. Information about their behaviour under extreme electrical discharge conditions is important in order to select the most suitable insulation material for a given environment. Materials B, C and D are regarded as insulation materials of above-average quality and their behaviour during the IPT test can thus be safely related to other similar material products in the insulator market. Material A was included in the comparison to observe the behaviour of a commonly used coating material under different voltage types, since silicone rubber coatings are often used in HV applications. Although materials B and D are both HTV silicone rubbers, they differ in their manufacturing methods and specimen thickness. Insulators made from material B are made from extruded sheaths with pre-moulded vulcanized sheds. The sample thickness for these specimens was 10 mm. Material D, on the other hand, is produced by injection moulding, with the sample thickness being 6 mm.

As with the samples in Chapter 4, all samples were cleaned using deionised water and propanol alcohol in accordance with the IEC standard [34]. Since all four materials displayed a high initial level of hydrophobicity, the surfaces of the samples were

afterwards abraded using sandpaper of grade P800 and then rinsed with deionised water again. Upon installation in the IPT apparatus, a layer of conductive paste was again applied underneath the ground potential electrode in order to improve leakage current conduction.

The names used to designate the results for each individual test series are based on the applied voltage type, voltage magnitude and test material used for that specific test series. A typical example is shown in Fig. 52, along with the meaning of each part of the name.

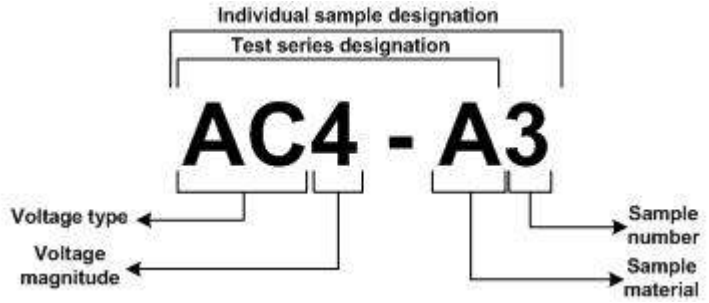

Fig. 52: Test sample designation methodology.

The voltage types are indicated using two letters, with AC standing for AC voltage, DP for positive DC voltage and DN for negative DC voltage. For reasons described in the following section, the test voltage magnitude was kept at 4.0 kV, and this field in the sample designation will thus contain a '4' for all samples. The material names have been given at the beginning of this section. Finally, the sample number indicates the order in which the samples in each individual test series were tested, increasing from one to six for a total of six samples per test series.

5.2 Material comparison methodology

One test series per test material was conducted for each of the three voltage types, namely AC, positive and negative DC. The number of samples per test series was increased from five to six. The reason for this will be explained later in this section. All tests were performed using the constant tracking voltage method, as per the findings of the method comparison described in Chapter 4.

Due to the large number of samples tested, it was decided to test the materials for one voltage magnitude only during this project. The choice of the test voltage magnitude

was based on studies done on HTV silicone rubber samples using the IPT method with varying contaminant conductivity and test voltages [56]. The erosion depth on the samples was measured for varying applied test voltages for a given contaminant conductivity. This erosion depth depends on the energy of the electrical surface discharges, which are proportional to the leakage current magnitude and the arcing duration. For a given contaminant conductivity, the current magnitude increases while the arcing duration decreases when the applied test voltage is increased. A maximum energy impact thus exists at a certain test voltage for a specific contaminant conductivity, which results in a maximum erosion depth on the sample. For a contaminant conductivity of ± 2.5 mS/cm, the HTV silicone samples showed a maximum erosion depth at a test voltage of 4.0 kV rms [56]. The test voltage for this project was thus chosen as 4.0 kV rms for both AC and positive and negative DC. This ensured that the samples are tested to their full capabilities, since this test voltage represents the worst condition scenario at a contaminant conductivity of ± 2.5 mS/cm. This also increases the chance of observing differences in the electrical erosion resistances of the different materials. Both the contaminant flow rate and the current limiting resistance were chosen according to Table 2 for this specific test voltage and were kept constant for every test series.

Both the AC and DC test arrangements have been described in detail in Chapter 3. The OLCA was again used to measure the leakage current flowing across the sample. Visual observations were also taken using a camera arrangement similar to that described in Chapter 4. However, a VCR camera was used instead of digital camera for this part of the project. A short 30 seconds video was taken every 30 minutes during the test procedure. Visual observations were also recorded in writing within a test report every 15 minutes. Additionally, an oscilloscope was used to measure the waveforms of the leakage current, the voltage applied across the test sample and the source voltage. Short instants of the waveforms of observed electrical discharges were stored during each video recording so as to gain additional information about the arcing behaviour of the tested sample. Fig. 53 shows the arrangement of the measuring equipment employed during this part of the project.

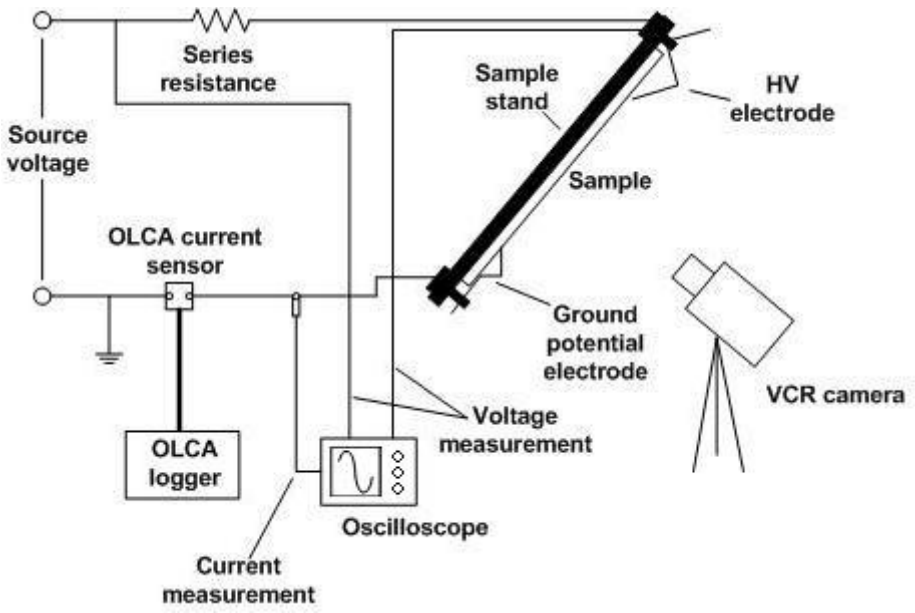

Fig. 53: Measuring & monitoring equipment used during material comparison tests.

Once the tests were completed, the different materials were compared using the following evaluation criteria:

- *Visual observations, sample appearance & oscilloscope waveforms*: The materials are compared according to their observed arcing behaviour as well as general sample appearance. The visual observations are augmented by studying the recorded waveforms of the arcing behaviour.
- *Sample mass loss*: The materials are compared according to the mass loss recorded in the samples due to electrical erosion.
- *Sample erosion depth*: The materials are compared according to the maximum erosion depth caused by electrical erosion measured in their respective samples.
- *Sample erosion area*: The samples of the different materials are also compared according to the approximate area of their surfaces taken up by erosion.
- *Rms leakage currents*: The materials are compared according to the average hourly rms leakage currents measured during the testing of their respective samples. Furthermore, the rms currents are also investigated on possible trends.
- *Average dissipated power*: A comparison between the materials is also done based on the average electrical power dissipated in the samples.

- *Sample hydrophobicity*: The samples of the different materials are investigated on their surface hydrophobicity both with a polluted surface and once the samples have been cleaned.
- *Chemical analysis*: A sample of each test series of the different materials tested under different voltage types is investigated on possible chemical changes within the sample materials using the ATR FTIR spectroscopy method.

After testing was completed, the surfaces of the material samples were cleaned using deionised water and a soft toothbrush in order to remove pollution particles and other waste deposits. However, the samples selected for the chemical analysis were not included in this cleaning procedure, as was the case during the method comparison in Chapter 4. This was done to allow the selected samples to remain untreated after testing was completed so as not to interfere with the results of the chemical analysis. Since the cleaning procedure was a pre-requisite for several of the evaluation criteria, these selected samples are not included in the comparisons of the materials for the mass loss, erosion depth and area and the hydrophobicity criteria. In order to maintain a minimum number of five samples per test series for the different evaluation criteria, the total number of samples per test series was increased to six samples. The tests for the hydrophobicity of the sample surfaces were done directly before and after the aforementioned cleaning procedure.

It should be noted at this point that the analysis of the materials was done in two ways:

- Firstly, the four different test materials are compared to one another for each of the three voltage types (AC, positive and negative DC). The differences in behaviour of each material are then evaluated for each voltage type.
- Secondly, each material is individually evaluated on changes of behaviour and the severity thereof when exposed to the three different voltage types.

This gives rise to a 2D matrix structure of results along which the materials are evaluated, as is shown in Fig. 54.

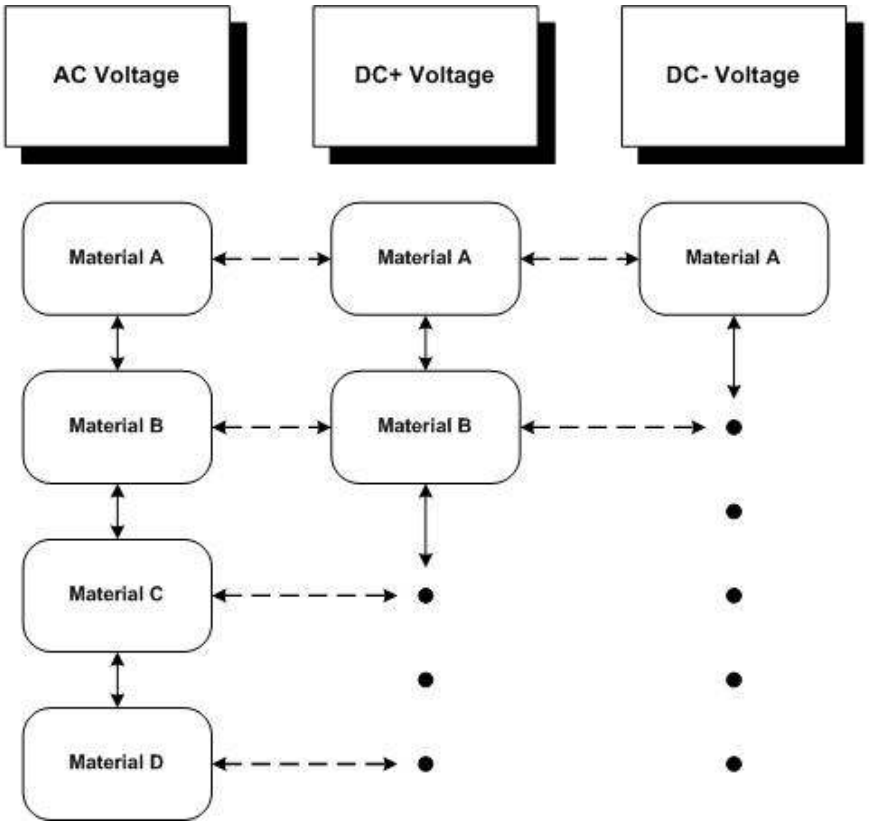

Fig. 54: Analysis hierarchy for the material comparison.

The solid line arrows in Fig. 54 indicate a comparison between the different test materials for one specific voltage type, while the dotted line arrows indicate a comparison of the effects of the three different voltage types on one material. By utilizing this general analysing procedure for the evaluation criteria, it is not only possible to gain an indication of the relative performance of the different test materials for a given voltage type, but also to observe the behaviour of the various materials with regards to a change in voltage type.

5.3 Test results

The following sections will describe the test results obtained for each evaluation criterion for the different materials exposed to the three voltage types. Conclusions and possible explanations for the observed results and trends will be offered throughout the sections for each individual evaluation criterion.

5.3.1 Visual observations, sample appearance & oscilloscope waveforms

This section summarizes the visual observations of sample appearance and arcing behaviour of the test materials when exposed to the different voltage types, based on the video recordings and written test reports composed during the tests. Each material is separately described with a further distinction being made between the test series of each individual material conducted using a different voltage type. The test series are also compared according to the leakage currents waveforms recorded during the sample test runs.

5.3.1.1 Material A, AC voltage

Samples of this test series initially displayed weak electrical discharges across their entire surfaces. However, stable arcing was usually established at the ground potential electrode within the first test hour and then remained fairly constant throughout the remainder of the test. Short, intermittent hotspots started developing at the ground potential electrode towards the beginning of test hour three and were observed at this location throughout the remainder of the test period.

Interruptions to the arcing process were observed to be caused by the contaminant being heated to boiling point by the leakage current flowing through it. This caused the contaminant to evaporate until the formed dry band at the ground potential electrode was wide enough to reduce the electric field strength sufficiently to interrupt the arcing process. Arcing was re-established once the contaminant stream reached the ground potential electrode again. This raises questions if the contaminant flow rates prescribed in the IEC standard are indeed high enough to allow for constant arcing at the ground potential electrode.

Fig. 55 shows a typical sample of this test series during three different instants of the test period, each time displaying good arcing behaviour at the ground potential electrode.

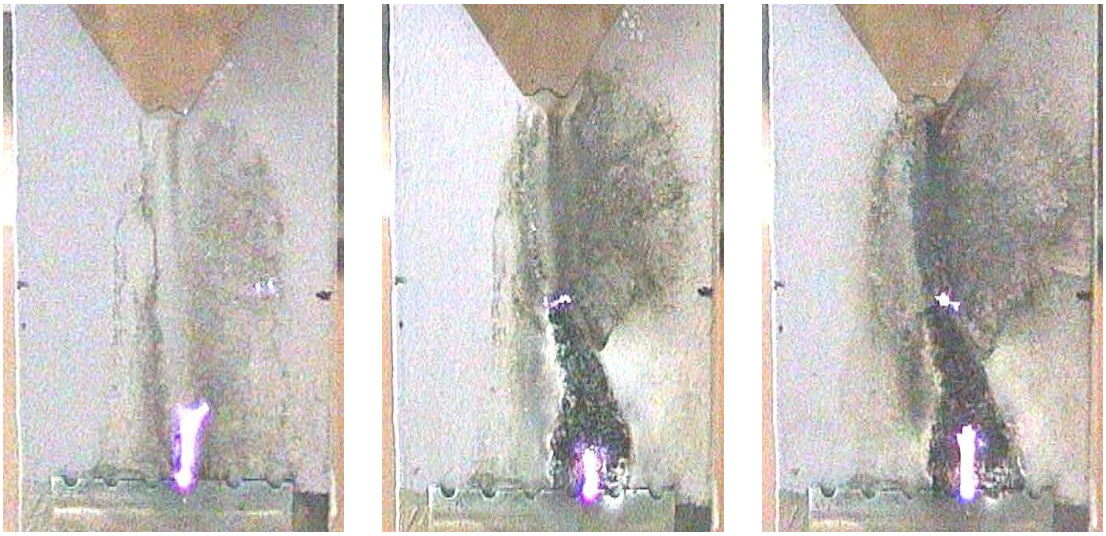

(a) **(b)** **(c)**

Fig. 55: Typical sample of test series AC4-A at time: (a) 1 h 00 min, (b) 3 h 30 min and (c) 5 h 30 min.

Visible surface erosion occurred early in this series, usually by the end of the first test hour, and was located close to the ground potential electrode. The extent of the erosion occurring over the full test period varied between the samples. Some specimens showed only small, localized erosion close to the ground potential electrode, which occurred early during the test period and which did not grow to any significant extent until the end of the test. Others developed a strong, intensely glowing path which burned away at the coating for several seconds, eroding a relatively large area before extinguishing. This behaviour was observed only once for each affected sample, after which the erosion area stabilized and showed no further significant growth. The glowing paths were observed between the middle of the second and the beginning of the fourth test hour.

Fig. 56 shows a sample displaying only localized erosion as well as a sample which developed a glowing path during its test run. Again, the eroded areas are not labelled as tracks, since it was observed that the contaminant filtered through the eroded areas until coming in close enough proximity to the ground potential electrode to induce arcing. As a result, the eroded areas were judged not to be permanently conducting, since the majority of the electrical discharges would then have been observed at the apex of the eroded areas.

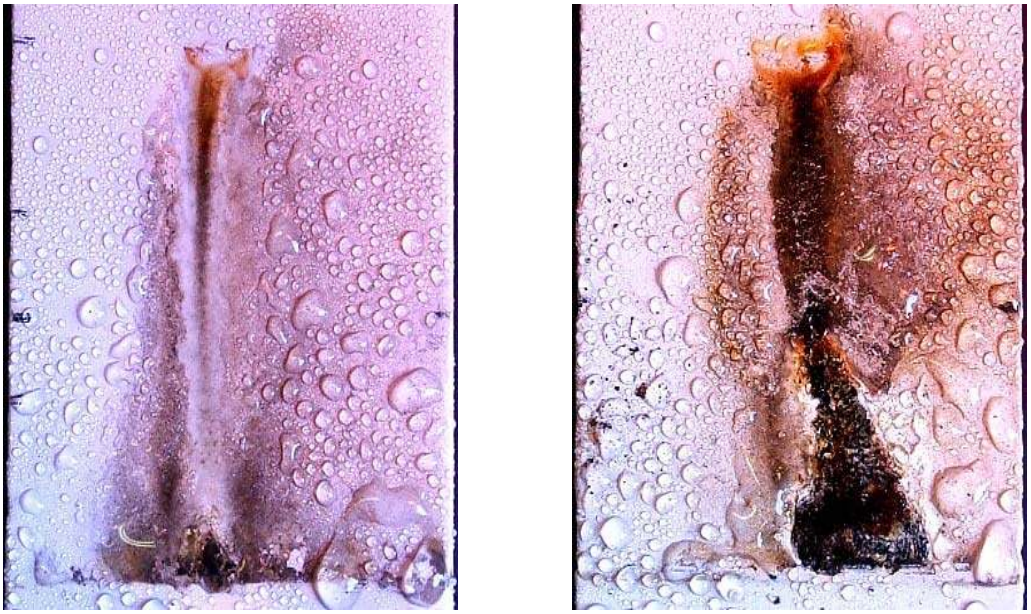

(a) (b)

Fig. 56: Samples of test series AC4-A with: (a) Localized erosion and (b) Heavy erosion after development of glowing path.

All samples showed extensive discolouration across their surfaces, with the most severe discolourations located at the ground potential electrode (area of constant arcing) and along the contaminant path. It was already surmised in section 4.3.1 that the discolouration along the contaminant path is due to the heating action of the leakage current flowing along the contaminant stream. The discolourations on other areas of the sample surfaces can be ascribed to weak, localized dry band discharges which occurred during every test run of this series.

The cleaning procedure revealed the discolourations to be mostly superficial and easy to clean off. The heavily eroded areas commonly formed rough, scab-like surfaces which were also easily removed during the cleaning procedure by brushing with a soft toothbrush. The RTV silicone rubber coating was often completely consumed in these areas, leaving the surface of the ceramic tiles exposed. Fig. 57 shows a sample of this test series before and after cleaning.

(a) (b)

Fig. 57: Appearance of a typical sample of test series AC4-A: (a) Before and (b) After washing.

A special mention must be made at this point of sample AC4-A6. This sample was not abraded during the cleaning procedure prior to testing like the other samples in the series in order to investigate the effect of the abrasion process on the samples. The visual observations revealed that there seems to be some improvement in the arcing stability at the ground potential electrode, but no major differences could be observed in the arcing behaviour. On the other hand, this sample also developed a glowing path towards the end of the second test hour, which resulted in this sample showing some of the largest erosion areas of this particular test series. Fig. 58 shows sample AC4-A6 after having been cleaned after testing. These observations call into question the validity of the abrading of hydrophobic test samples prior to testing to improve arcing behaviour, since no such improvements were observed. This sample will be closely observed during the other evaluation criteria in order to see if the absence of abrasion has resulted in other changes of sample performance.

Fig. 58: Appearance of test sample AC4-A6 (not abraded) after washing.

5.3.1.2 Material A, positive DC voltage

The arcing behaviour and erosion damage observed in this test series (DP4-A) was very different to that of the AC series. The arcing at the ground potential electrode stabilized within the first 15 minutes of the test, reaching greater length than those observed during series AC4-A. Within about 15 to 20 minutes, massive erosion damage to the sample surface occurred due to the development of glowing paths that burned away at the coating material. The erosion grew to a length exceeding 25 mm along the sample surface and then stopped growing. Sample discolouration was also more severe along the ground potential electrode and the contaminant path than in the AC series.

Once this initial erosion had occurred, the arcing at the ground potential electrode became interrupted by dead times. The arcing periods were still longer, more stable and of higher intensity than those observed in the AC series, but the dead times were also longer. After inspection of the video recordings, it is postulated that the interruptions were due to an impeding effect of the erosion area in the contaminant flow. The fluid first has to filter through the eroded area to get to the ground potential electrode in order to establish arcing. This impeding effect is directly proportional to the degree of erosion found on the sample. The interrupted periods grew longer as

erosion on the sample increased, which is why these periods tended to get longer at the later stages during the test runs.

However, the intensity of the arcs also steadily increased with increasing testing time. High intensity hotspots were observed as early as the beginning of the second test hour and kept growing in intensity. These hotspots sometimes developed into glowing paths within the eroded area at later stages of the test runs (after 4th test hour). The high temperature of these arcs and discharges was confirmed by the fact that the edges of the eroded area sometimes still glowed due to intense heat radiation even after arcing was extinguished. The severity of the erosion within the existing areas as well as the colour of the discolouration along the fluid path also increased during the test runs, both having reached a dark black colour once the tests were stopped. Fig. 59 shows a typical test sample of the series DP4-A at the beginning, the middle and close to the end of its test run.

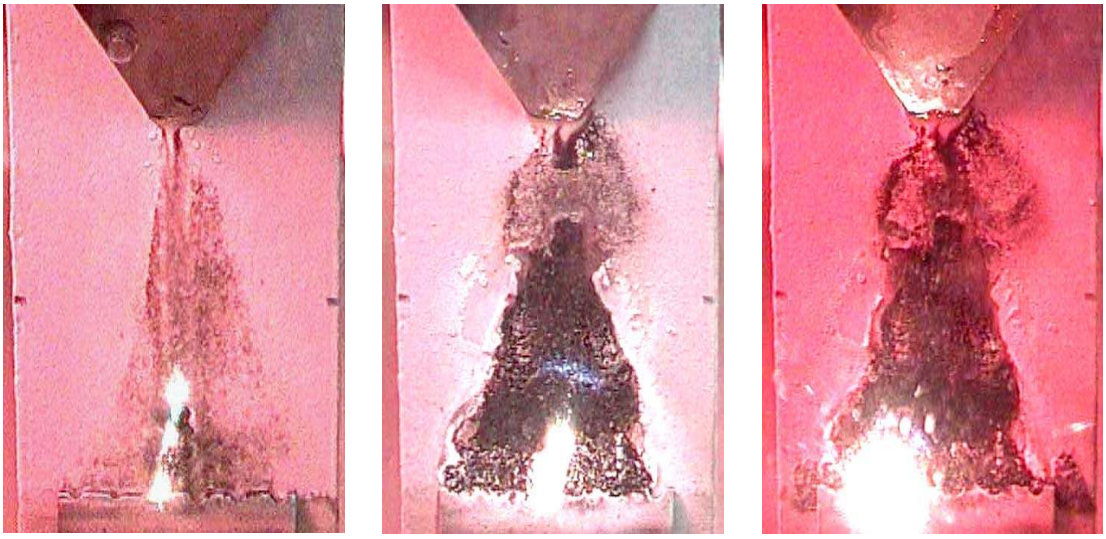

(a) **(b)** **(c)**

Fig. 59: Typical sample of series DP4-A at test time: (a) 0 h 19 min, (b) 3 h 00 min and (c) 5 h 30 min.

The samples of this series showed fewer discolourations towards the edges of the samples, since they lacked the frequent but weak dry band discharges all over the sample face which were observed in the AC series for material A. The discolouration rather concentrated along the fluid path and the ground potential electrode. However, these discolourations were no longer superficial and could not be completely removed during the cleaning procedure. Also, the coating material around the erosion area showed a lighter colour than the rest of the sample.

Within the eroded areas, the coating material was completely destroyed. Instead, the areas were covered in dark, rough deposits similar to those observed in series AC4-A. However, in this series the cleaning procedure failed to remove all of the deposits, due to them being melted into the surface of the ceramic tiles. This again attests to the high temperature and intensity of the arcs observed in this test series. Some small damage to the surface of the ceramic tiles was also observed. Fig. 60 shows a typical sample of the DP4-A series before and after the cleaning procedure.

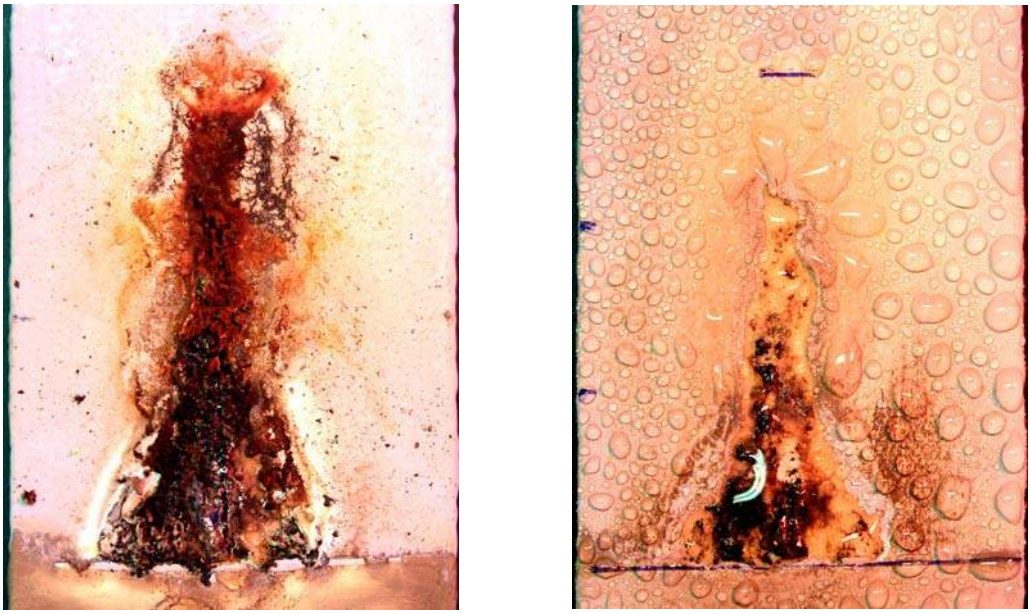

(a) **(b)**

Fig. 60: Typical sample of series DP4-A: (a) Before and (b) After washing.

A special mention must be made for sample DP4-A3. The arcs grew to such intensity at the ground potential electrode during the last 30 minutes of the final test hour that a puncturing of the ceramic tile occurred. From this point on, arcing also occurred sporadically on the backside of the sample. The arcing process was now observed to be very interrupted at the ground potential electrode, but high-intensity arcs still developed at irregular intervals. Although the test was allowed to run to completion, this sample can be seen as having failed the test procedure. Fig. 61 depicts the backside of sample DP4-A3 after testing was completed, showing the area burnt black by arcing occurring at that location.

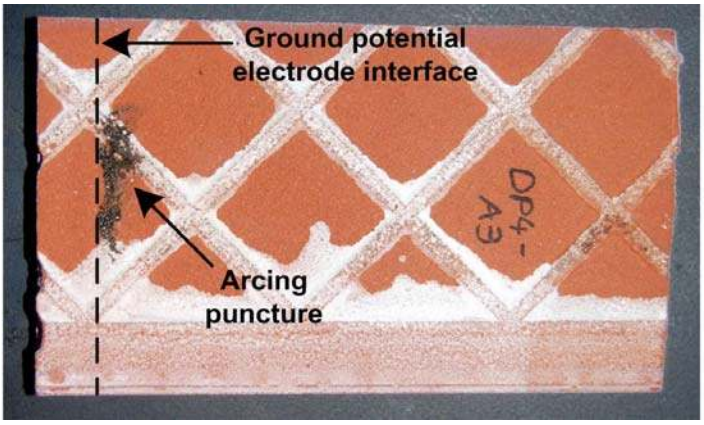

Fig. 61: Backside of sample DP4-A3, showing traces of arcing after puncture of ceramic tile occurred.

5.3.1.3 Material A, negative DC voltage

During this test series (DN4-A), stable arcing established at the ground potential electrode within minutes of starting the test. In fact, a glowing path developed in every sample between six and fifteen minutes into the test, burning an erosion path into the sample surface that quickly reached a length of 25 to 30 mm. Once this length was reached, the eroded area started to expand in width by means of glowing paths and hotspots burning away at the interface of eroded area and coating material. Since the erosion growth occurred more rapidly towards the ground potential electrode, the eroded area took on the form of an inverted V.

This process caused the formation of a large erosion area within a time period of 30 minutes. After this time, the samples developed stable arcing at the ground potential electrode within the eroded area. The arcs were of less intensity than those observed in test series DP4-A, but were still longer in length and of stronger intensity than those observed in series AC4-A. The arcing was interrupted by dead times. This was caused by the contaminant being spread over the entire erosion area, filtering through a network of fine channels covering the entire erosion area. Arcing was interrupted as soon as the contaminant burned away to such an extent that the electric field strength grew too weak to maintain constant arcing. The arcs were also observed to jump along the ground potential electrode, always occurring at the point where the contaminant came closest to the electrode. Hotspots of medium to strong intensity, but of only short duration were also frequently observed along the electrode after the first 30

minutes. Minor dry band discharges were observed above the eroded area, causing some discolouration in that area.

The eroded area on the samples kept growing towards the outer edges after the initial 30 minutes. This resulted in the erosion area covering the entire sample width along the ground potential electrode in most test specimens. Even if this did not occur, a stable point was reached between the second and third test hour after which no significant growth of erosion area was detected for the remainder of the tests. Fig. 62 shows pictures of the erosion progress and arcing behaviour of a typical sample of the series at the beginning, the middle and near to the end of the test duration.

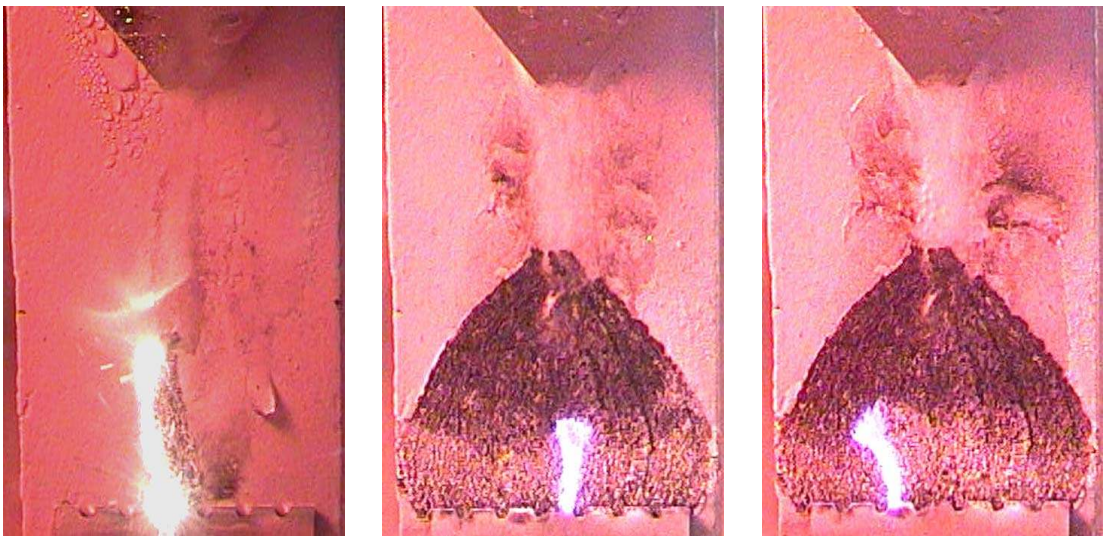

(a) **(b)** **(c)**

Fig. 62: Typical sample of series DN4-A at test time: (a) 0 h 12 min, (b) 2 h 30 min and (c) 5 h 30 min.

As described previously, the samples developed large erosion areas in which the coating material was completely consumed. These areas were instead covered in a rough deposit, criss-crossed by a network of small cracks and channels. Some surface discolouration developed along both sides of the contaminant path above the eroded areas, caused by the minor dry band discharges observed in those areas. These discolourations were found to be only superficial and were almost completely removed during the cleaning procedure. This was also true for the deposits in the eroded areas, exposing the surface of the ceramic tiles in those areas. However, some deposits were melted to the ceramic surface along the ground potential electrode due to the heating effect of intense hotspots occurring in those vicinities. Fig. 63 shows a typical sample of this series before and after the cleaning procedure.

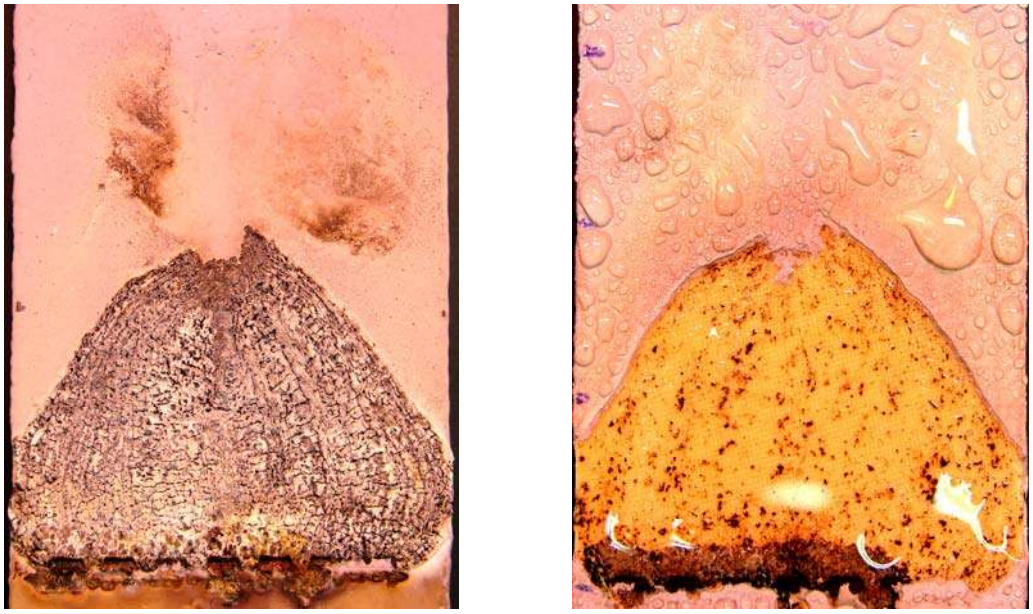

(a) (b)

Fig. 63: Typical sample of series DN4-A: (a) Before and (b) After washing.

An interesting fact to be noted is that, although series DP4-A showed the highest intensity in its arcing behaviour; it is series DN4-A that showed the largest erosion on the surfaces of its specimen. This hints at another process being involved in the erosion of the samples aside from that of electrical erosion.

5.3.1.4 Material B, AC voltage

The test specimens showed only weak scintillations and dry band discharges along the contaminant path for the first half hour during test runs of this series. This behaviour improved steadily until effective arcing at the ground potential electrode was established in a period of 60 to 90 minutes after the starting of the tests. Up to this point, any change in sample appearance consisted mainly of light surface discolourations along the electrode and the contaminant path, with the electrode areas showing slightly more intense discolourations.

Arcs observed at the ground potential electrode were of relatively short length and of weak to medium intensity, displaying a blue-whitish colouration. The arcing process was frequently interrupted by short dead times or by brief periods of weak electrical discharges along the fluid path, but always re-established at the electrode. This type of arcing behaviour continued from the 90th minute onwards for the remaining duration of the test runs without any major changes being observed. Almost no hotspots were

observed at the ground potential electrode throughout the test runs, which gives testimony to the relatively weak intensity of the arcing behaviour.

Accordingly, only minor surface erosion was observed during the tests, consisting only of the formation of a small, roughened and burnt area at the intersection of the contaminant path with the ground potential electrode (the primary arcing location). The discolouration continued to intensify along the electrode and along the sides of the contaminant path, becoming less severe towards the high voltage (top) electrode. Interestingly, the fluid path itself showed no discolouration. Fig. 64 shows pictures taken of a specimen of this test series at the beginning, middle and end of its test run.

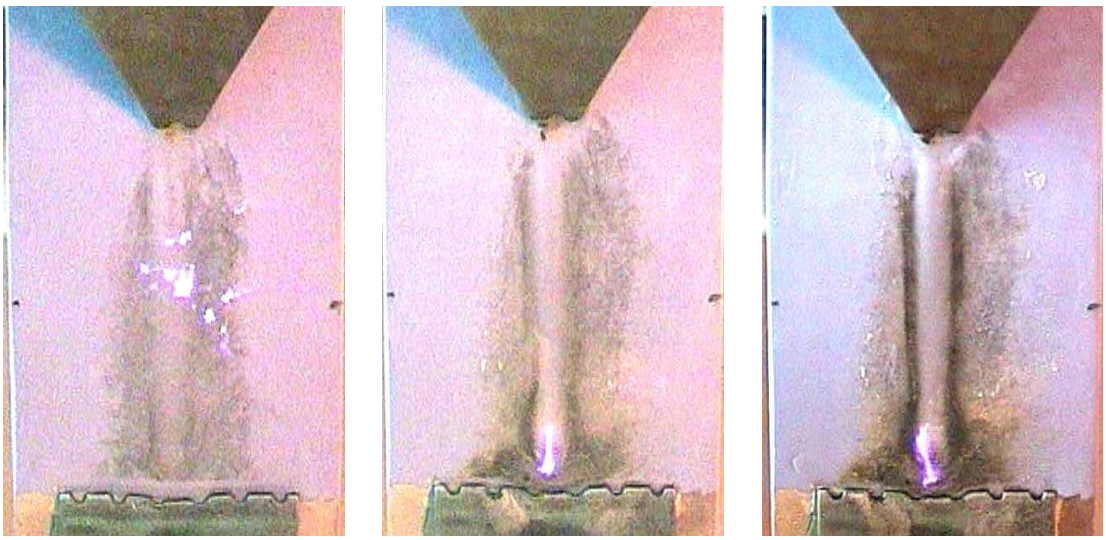

(a) **(b)** **(c)**

Fig. 64: Typical sample of test series AC4-B at time: (a) 0 h 30 min, (b) 3 h 00 min and (c) 5 h 30 min.

All samples also showed the formation of a small dry band at a location on their right lower regions. These dry bands showed continuous, but very weak discharges throughout the test runs and are believed to be caused by splattering of the contaminant fluid early on in the test runs.

After testing was completed, the samples showed dark brown to black discolourations along the ground potential electrodes and along both sides of the contaminant path. However, these discolourations were judged to be superficial since the fluid path itself showed no discolouration, indicating a removal of any discolourations by washing through the contaminant stream. This observation was confirmed by the cleaning procedure after testing, in which most of the discolourations were removed from the

sample surface, leaving only slight traces of light brownish discolourations. As described previously, no significant erosion was observed during the tests. This was also confirmed by the washing procedure, which showed the only signs of erosion to be slight surface indentations at the junction of ground potential electrode and contaminant path. Fig. 65 shows a typical sample of series AC4-B before and after the washing procedure after completion of the test runs.

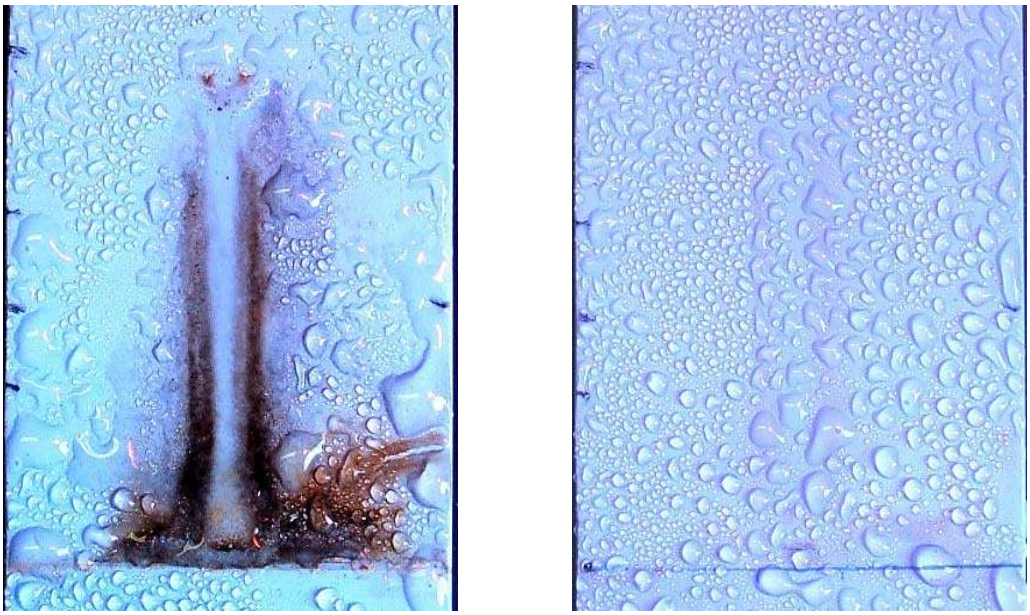

(a) **(b)**

Fig. 65: Typical sample of series AC4-B: (a) Before and (b) After washing.

5.3.1.5 Material B, positive DC voltage

The samples of this series displayed weak electrical discharges along the contaminant path for the first few minutes after the tests were started. During the first 30 minutes, stable arcing developed at the ground potential electrode, occasionally interrupted either by dead times or weak discharges along the fluid path. The samples already showed strong discolourations as well as first signs of erosion (displayed as a roughened area of sample surface) along the fluid path and the ground potential electrode.

After the first 30 minutes, arcing at the electrode grew more stable, with the arcs displaying a greater intensity and length than those observed in series AC4-A. Interruptions still occurred at this point. The first intense hotspots were observed at the ground potential electrode, which caused erosion to grow more severe at this

location. During the following minutes, the intensity and stability of the arcs and hotspots at the electrode continued to increase, as did the severity of the erosion and discolouration in that area.

Anywhere between the middle of the second and beginning of the third test hour, the samples began to develop hotspots or even glowing paths of severe intensity along the ground potential electrode, which caused the eroded areas to grow significantly both in area and depth. The intensity of these discharges was so great that tinted goggles had to be used for the visual observations in order to prevent damage to the eyes. Deposits of black/white waste material formed in the eroded area, sometimes even covering them completely. The glowing paths and hotspots continued to burn underneath the waste material. Some minor discharges could also be observed at top of the waste material.

However, sometimes glowing paths formed only at the lower corners of the waste materials, some distance away from the top point of the deposits. Fig. 66 shows the initial formation of a large erosion area by means of a glowing path, as well as a glowing path existing only beneath the lower corner of the waste material covering the eroded area.

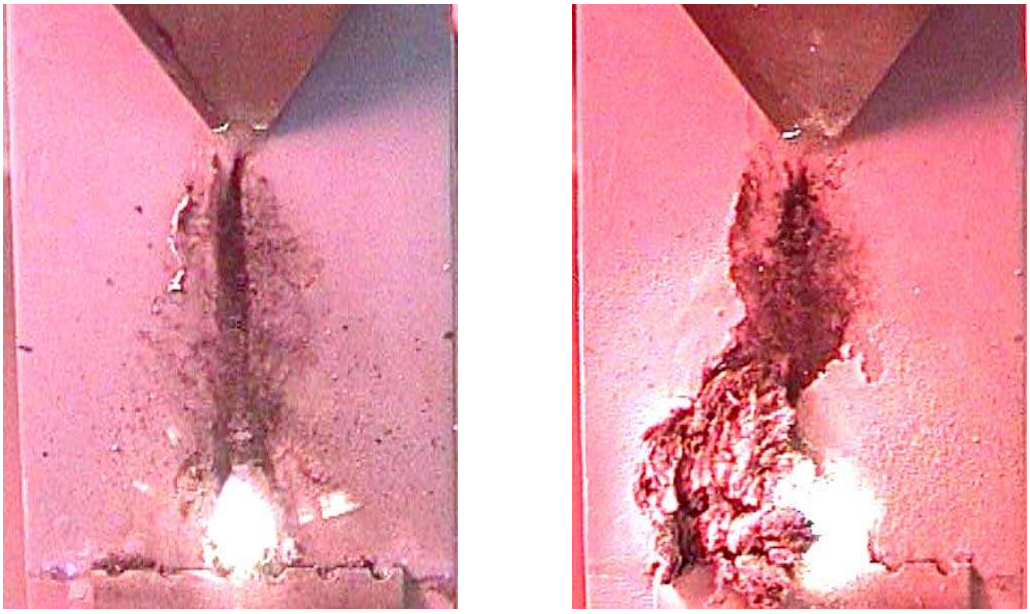

(a) **(b)**

Fig. 66: (a) Initial formation of intense erosion by glowing path and (b) Glowing path only occurring beneath lower corner of waste material.

It was thus concluded that rather than the waste material itself being conductive, it serves as a conduit for the contaminant fluid, channelling it to the ground potential electrode. In some cases the waste material was burned off by the intense discharges taking place underneath it. Arcing then either took place along the edges of the eroded area or within the area itself, depending on the path taken by the contaminant fluid. These arcs were of reduced intensity until a new glowing path or hotspot developed, which in most cases occurred along the edges of the erosion area.

Another development that could be observed with the onset of severe erosion was the appearance of white deposits on the sample surfaces surrounding the eroded areas. Since these deposits were of the same colour as the surfaces within the eroded areas, they were assumed to be deposits of filler material. This process can thus be called chalking, which is defined as the appearance of filler particles on the outer surface of an insulator material, resulting in a rough or powdery surface [57]. This created an extremely hydrophobic surface around the eroded area, presumably because of the presence of substances like LMW molecules and broken polymer chains bonded to the filler particles [19]. This caused an impediment for the contaminant flow which, combined with sample being angled forward at 45°, sometimes caused the contaminant to accumulate at a point above the eroded area until it started to drip directly downwards from that location, causing it to miss the ground potential electrode and so interrupting the arcing process. Sometimes the flow corrected itself and arcing resumed, but mostly the test was interrupted permanently.

Since these interruptions were not considered a valid termination of the tests, a cleaning procedure was developed in order to restore arcing in the samples. The apparatus was switched off and the fluid dispenser was removed from the Perspex enclosure. The contaminant was not switched off, however, so as not to tamper with the flow rate. The sample surfaces were then cleaned using distilled (deionised) water and a paper towel. The main objective was to clean away the hydrophobic deposits. Removal of the waste material covering the erosion areas was also deemed acceptable, since this was observed to occur naturally as well. After cleaning, the contaminant flow to the sample was then resumed and monitored for a couple of minutes to ensure its capability of reaching the ground potential electrode. Once this was confirmed, the apparatus was switched on again and the test was resumed. Care

was taken to synchronize the OLCA logging interval with the actual test time. The OLCA intervals covering the cleaning procedure were ignored in following analyses.

The cleaning procedure was observed to restore the arcing process at the ground potential electrode. Glowing paths and hotspots were also observed in the eroded areas after the cleaning procedure to the samples, which indicates that the cleaning procedure does not interfere with the test results. During the tests, the samples also showed small arcs around the perimeter of the eroded areas. These were attributed to dry bands forming at these locations due to the sudden level changes in surface elevation, which can cause the contaminant to dry up faster at these locations.

The common pattern for the remainder of the tests for all samples was that of arcs occurring regularly and with great stability at the edges of or within the eroded areas. Hotspots and/or glowing paths were frequently observed, mostly at the edges of the eroded areas. The contaminant stream mostly followed the outlines of the erosion areas, causing minor dry band discharges in these regions. The number of interruptions to the arcing process due to the contaminant dripping past the electrode varied from sample to sample. The total number of interruptions and, subsequently, cleaning procedures applied per sample are shown in Table 17.

Table 17: Number of interruptions to arcing process for test series DP4-B.

Data	Sample					
	DP4-B1	DP4-B2	DP4-B3	DP4-B4	DP4-B5	DP4-B6
No. of interruptions to arcing process	1	3	4	0	9	2

An increase in erosion area was observed to able to occur suddenly during the final three test hours, by means of glowing paths burning away at the sample material. New waste material deposits also frequently formed in the eroded areas where these glowing paths were located. Fig. 67 shows pictures of a typical test sample taken at the beginning, middle and at the end of the test duration.

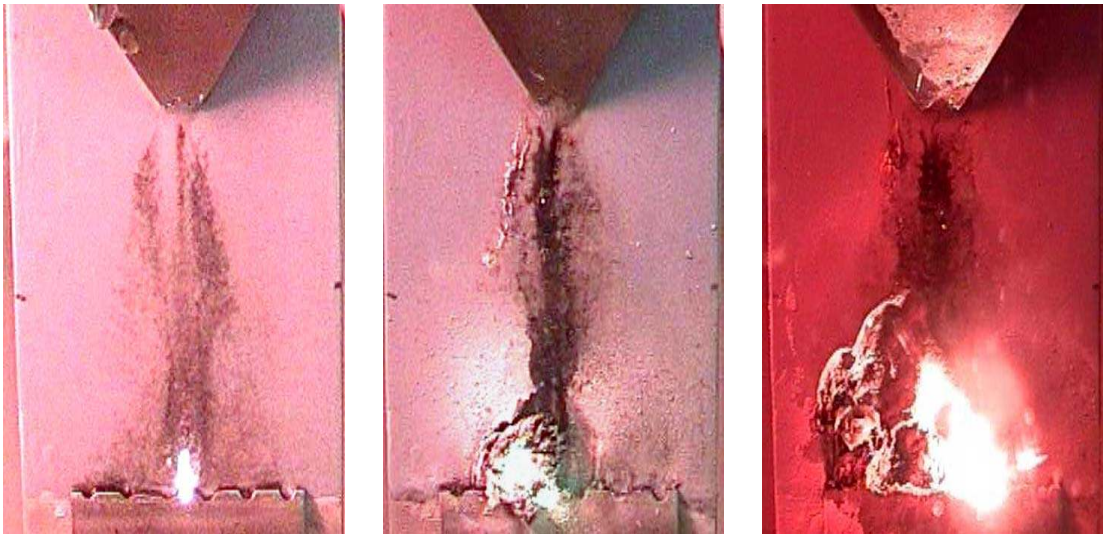

(a) (b) (c)

Fig. 67: Typical sample of test series DP4-B at time: (a) 0h 30 min, (b) 3 h 00 min and (c) 5 h 30 min.

As mentioned previously, the samples of this test series showed severe erosion after the completion of the tests, both in area and depth. The eroded areas were covered by the same whitish deposits observed on the sample surface, which lead to the conclusion of it being filler material. The areas of constant arcing within the eroded areas were either discoloured or were covered by a deposit of waste material, depending on the intensity of the arcs. The samples surfaces between the eroded area and the top (high voltage) electrode showed strong brown or black discolourations, with the rest of the surfaces showing significant amounts of chalking, especially around the eroded areas. However, the discolourations were observed to be superficial, since they were largely removed during the cleaning of the samples after testing was completed. Fig. 68 shows a typical sample of this test series before and after the final cleaning procedure.

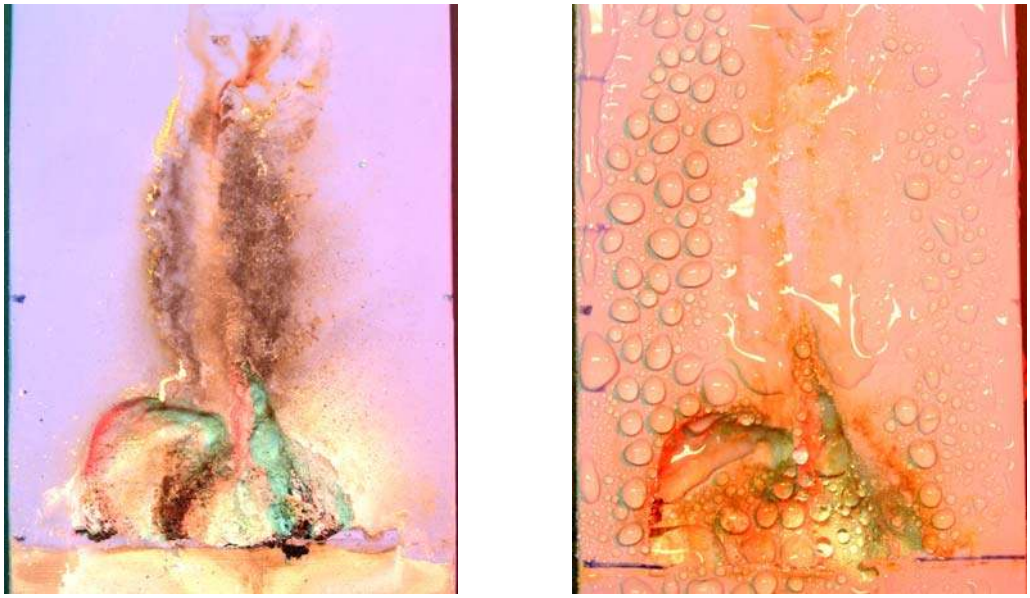

(a) **(b)**

Fig. 68: Typical sample of test series DP4-B: (a) Before and (b) After washing.

A special mention must be made of sample DP4-B3. The erosion depth on this sample spanned the entire sample thickness after five full test hours, creating a hole through the sample as seen in Fig. 69. The sample was thus judged as failed according to failure criteria A of the IEC 60587 standard, and the test was interrupted once the hole was observed. This was the only sample to fail during this test series, although the other samples also showed extensive erosion varying in area size and depth, especially when compared to the samples of test series AC4-B.

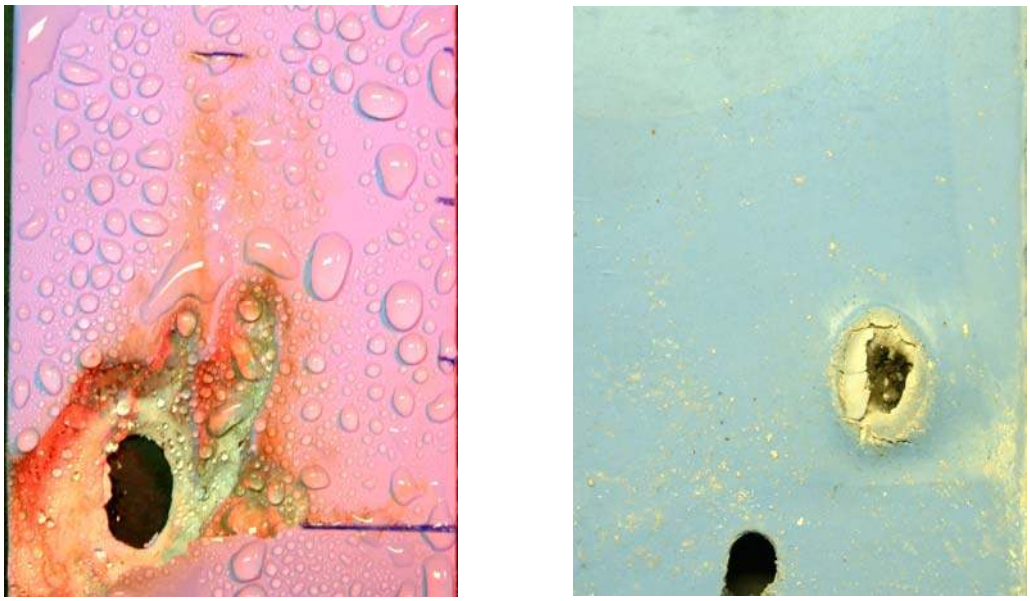

(a) **(b)**

Fig. 69: Failed sample DP4-B3: (a) Front and (b) Back view.

5.3.1.6 Material B, negative DC voltage

The samples of this series initially displayed weak discharges along the fluid path similar to those observed in the other series, but the majority of the arcing quickly focused at the ground potential electrode. Black discolourations along the electrode were observed as early as two minutes into the test. Strong arcing with frequent formation of hotspots was established at the electrode within 10 minutes, resulting in a significant erosion area and the occasional formation of waste material deposits. However, the erosion was not nearly as severe as observed in series DP4-B. Once this initial erosion was established, the arcing reduced in intensity but gained stability, with some minor hotspot formation at the ground potential electrode. Some amount of chalking was observed on the surface surrounding the erosion area, which increased somewhat during the test proceedings.

After a period of 45 minutes, arcing had become almost entirely constant at the ground potential electrode. Interruptions were only very brief and consisted usually of short dead times. The arcs themselves were of medium intensity and of a blue-whitish colouration. Hotspots now formed with reduced frequency, but were still observed to occur. Some yellowish deposits similar to those observed in the samples described in Chapter 4 were observed to form along the fluid path. Again, since no chemical tests were performed on these specific deposits, they were assumed to be salt deposits due to them always appearing in close proximity of the contaminant path.

Arcing at the ground potential electrode continued for the remainder of the tests with immense stability. Some samples showed a slight increase in interruptions to the arcing process after the third test hour, but the arc stability was still greater than in any other test series for this material. The erosion area showed no significant increase from its original inception in the first test hour onwards, except becoming increasingly discoloured by the continuous arcing occurring within its boundaries. This general behaviour continued unchanged until the completion of the tests. Pictures of a typical sample taken at the beginning, the middle and the end of its test run are shown in Fig. 70.

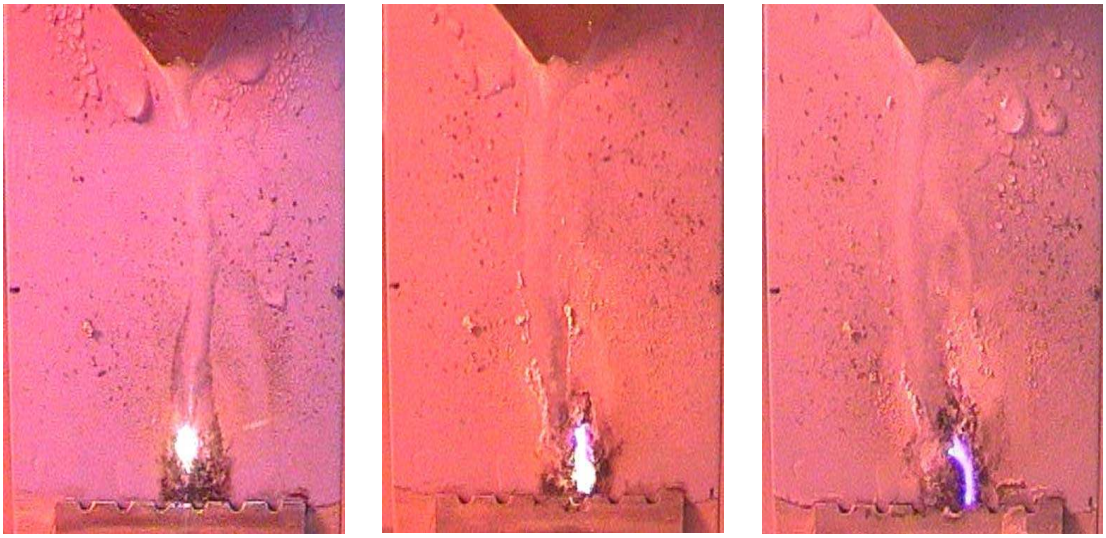

(a) (b) (c)

Fig. 70: Typical sample of test series DN4-B at time: (a) 0 h 30 min, (b) 3 h 00 min and (c) 5 h 30 min.

The formation of chalking during the first test hour caused the contaminant to drip past the electrode again in some samples. However, these samples re-established proper contaminant flow in a very short time without external interference, and the cleaning procedure used on the samples of series DP4-B was thus not applied in this series.

After completion of the tests, the samples showed very little or almost no discolouration along the fluid path or in their upper regions. The fluid path was only lined by the yellowish salt deposits mentioned previously. Some chalking could be observed on the lower regions of the samples, especially around the eroded area. These areas, however, were significantly smaller than those observed in series DP4-B. All samples showed significantly sized and strongly discoloured erosion areas along the ground potential electrode. However, these areas showed a far smaller area and depth than those of series DP4-B. The final cleaning procedure removed the majority of any discolourations observed on the samples, with slight residues only remaining in the eroded areas where continuous arcing was observed. Fig. 71 shows a typical sample of this series before and after the final washing procedure.

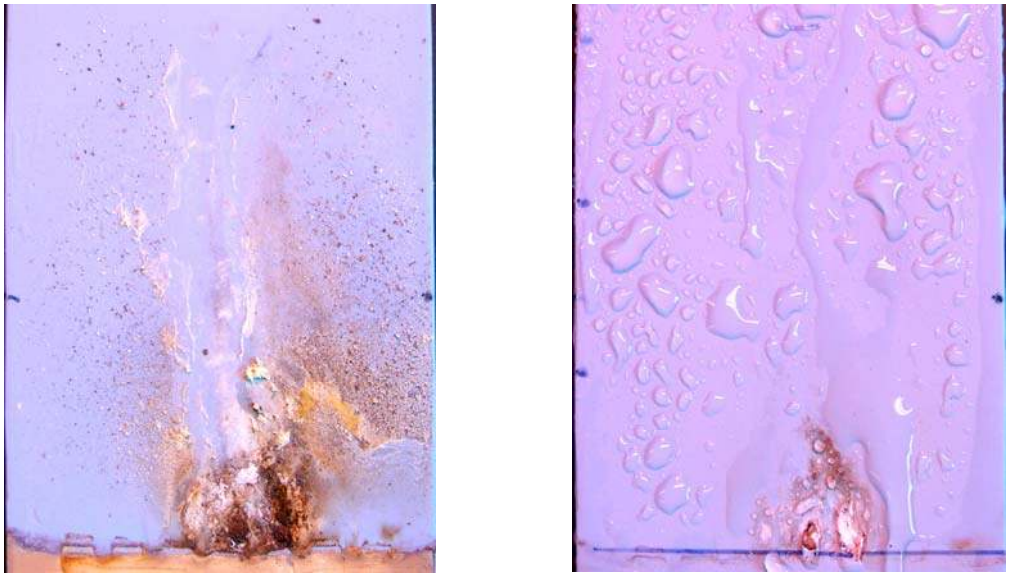

(a) (b)

Fig. 71: Typical sample of test series DN4-B: (a) Before and (b) After washing.

Sample DN4-B1 differed slightly in its appearance to the other samples, showing stronger erosion and more waste material deposits close to the ground potential electrode. This resulted from a reoccurrence of hotspots and even small glowing paths during the final test hour. However, even though these hotspots remained constant for nearly 30 minutes, the erosion area increases only slightly both in size and depth during this time. The overall erosion was more severe than in any other sample of this series, but still not comparable to the extensive material erosion observed in the samples of series DP4-B. Fig. 72 shows sample DN4-B1 before and after the final washing procedure.

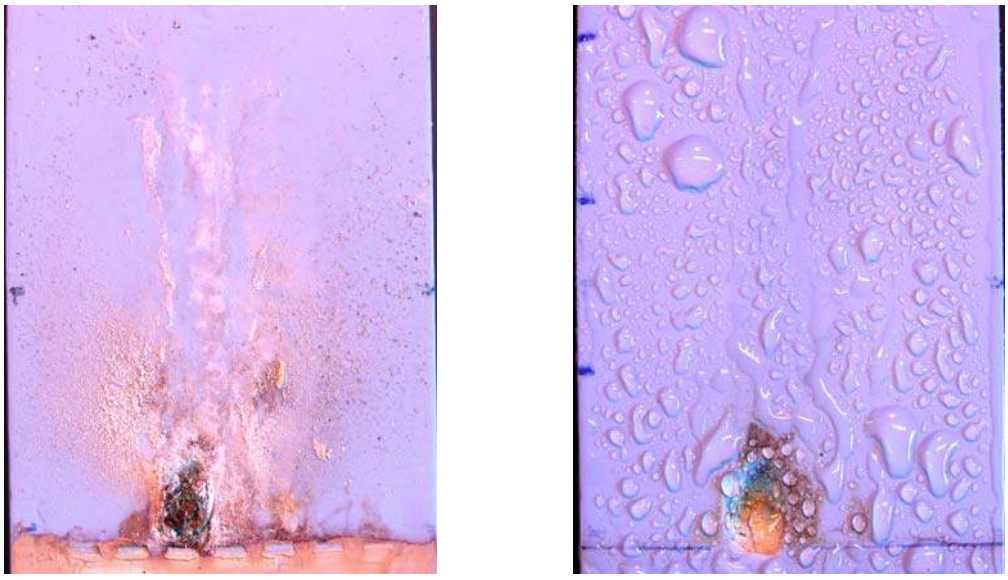

(a) (b)

Fig. 72: Sample DN4-B1 showing unusual erosion: (a) Before and (b) After washing.

5.3.1.7 Material C, AC voltage

Two major groups were observed in the samples of this test series in terms of both arcing behaviour and degree of electrical erosion. The first group of the samples showed an immediate broadening of the contaminant stream towards the ground potential electrode instead of continuing as a centralized path, hinting at a complete loss of surface hydrophobicity. This resulted in wild scintillations and discharges all over the sample surfaces, causing initial discolouration in the samples during the first few minutes. However, the majority of the discharges occurred at the ground potential electrode, initializing significant erosion at this location.

Within 30 minutes of the starting of the tests, these samples developed strong, continuous arcing at the ground potential electrode. Due to the large wetted area, the arcs occurred at different locations on the electrode, but the overall process remained very stable. Simultaneous discharges occurred all over the sample face, but did not interfere with the main arcing process. The strong arcs frequently developed into hotspots or short glowing paths, resulting in significant erosion and discolouration along the electrode. Both erosion and discolouration continued to increase, with the growth in erosion area being most severe.

Rapid growth in erosion area was achieved halfway through the second test hour due to the almost constant arcing at the ground potential electrode. High intensity hotspots developed frequently within the eroded areas, burning away at the sample material. The areas tended to grow in width rather than in length and showed significant depth. The arcing process remained constant within the areas, with simultaneous discharges frequently occurring all across the sample faces. As a result, the discolouration also continued to increase across the entire sample surfaces.

The growth in erosion area in these samples stabilized between the third and fourth test hour. After that, the areas only occasionally increased by small increments due to brief formation of hotspots at the edges of the erosion area. This coincided with a slight reduction in stability in the arcing process. However, arcing within the eroded area still continued with reasonable consistency. This condition remained unchanged until the tests were completed. Fig. 73 shows photographs of a typical sample of this group during the early, middle and end stages of the test runs.

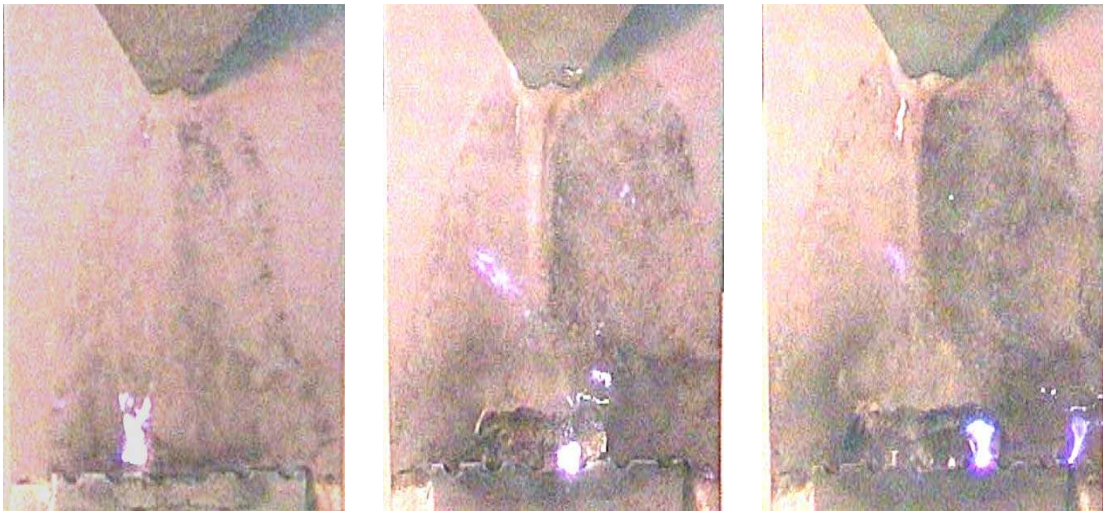

(a) (b) (c)

Fig. 73: Typical sample of first group of test series AC4-C at time: (a) 0 h 30 min, (b) 3 h 00 min and (c) 5 h 30 min.

The second group of samples (specifically consisting of samples AC4-C2 and AC4-C3) showed similar starting behaviour as those of the first group. However, these samples did not establish stable arcing behaviour or intense hotspots until the end of the fourth test hour. Though these samples also developed some erosion along the ground potential electrode during the first 30 minutes, they showed no further growth in erosion area due to absence of intense hotspots. Instead, the arcing in these samples was frequently interrupted by weak scintillations all along the sample surfaces or even short dead times. Accordingly, these samples showed far less material erosion and sample discolouration than the samples of the first group. Fig. 74 shows photographs of a sample of this group, arranged in chronological sequence.

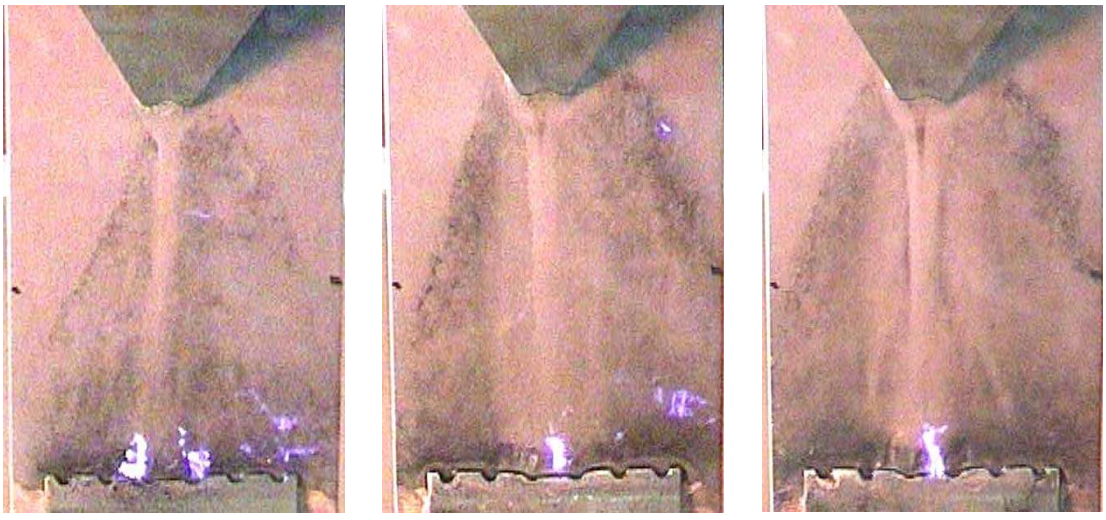

(a) (b) (c)

Fig. 74: Typical sample of second group of test series AC4-C at time: (a) 0 h 30 min, (b) 3 h 00 min and (c) 5 h 30 min.

The visual appearance of the two groups of samples differed, as was described in the previous paragraphs. The samples of the first group showed larger erosion areas as well as a higher intensity in sample discolouration than those of the second group. However, both groups of samples showed that the discolouration occurring in this test series was not entirely superficial, since the final cleaning procedure failed to remove large parts of the discolourations from either group. Fig. 75 shows typical samples of each group of this test series both before and after the final cleaning procedure.

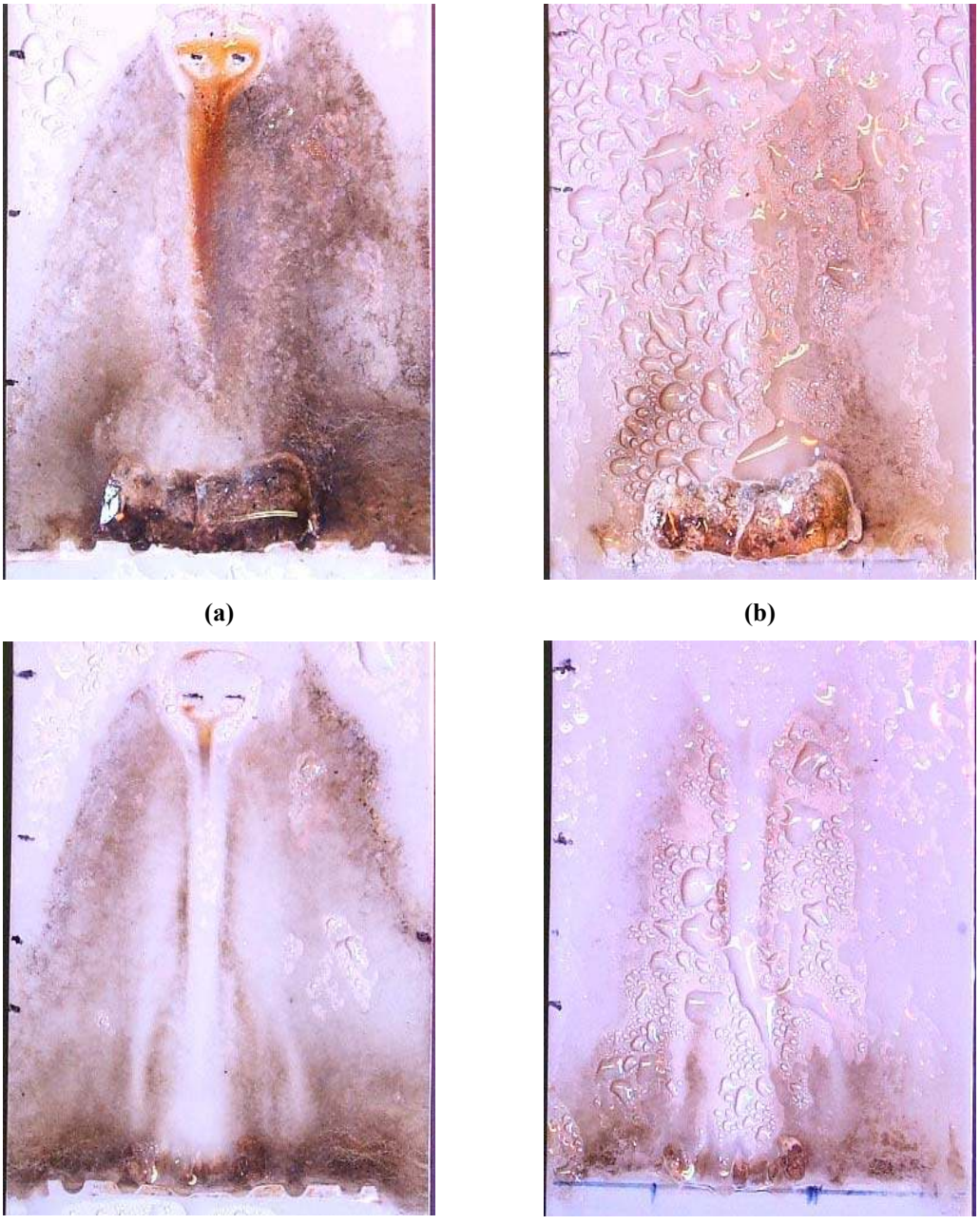

(a) **(b)**

(c) **(d)**

Fig. 75: Samples appearance after testing: (a) Group 1 before washing, (b) Group 1 after washing, (c) Group 2 before washing and (d) Group 2 after washing.

5.3.1.8 Material C, positive DC voltage

Similar to the previous test series, the fluid path on the samples of this series immediately broadened towards the ground potential electrode, covering a large area of the sample and thus indicating a complete loss of surface hydrophobicity. Weak electrical discharges occurred all over the sample face, while stronger arcs were observed along the ground potential electrode.

Within 30 minutes of starting the tests, continuous arcing was established at the ground potential electrode. Some interruptions in form of dead times and weak scintillations at other locations along the sample occurred regularly, with the weak scintillations often coinciding with arcing at the electrode. The observed arcs were of relatively strong intensity, as well as longer than those observed during test series AC4-C. Hotspots were also observed to form at the interface of sample surface and ground potential electrode. The surface of the samples already showed strong discolouration at this point, especially along the main fluid path and the electrode. Smaller areas of discolouration branched out from the main fluid path, which were caused by small dry band discharges at those locations. However, minimal erosion was observed at this point in time. Some electrical erosion developed up to the end of the first test hour, at which point all erosion growth stopped again.

Over the following hours, the intensity, stability and length of the arcs at the ground potential electrode as well as the severity of the surface discolouration started to increase slowly. The arcing process was still accompanied by weak discharges all across the sample surfaces, but hotspots developed more frequently and with increased intensity along the ground potential electrode. The discolouration intensified to a deep black colour at certain locations. However, the erosion at the ground potential electrode continued to remain unchanged or increased only in very small increments.

This condition continued up to the end of the test runs. Some samples did develop a slight increase in erosion area during the final test hour, but the areas still remained relatively small in all observed samples. Fig. 76 shows photograph of a typical sample of the series taken in chronological sequence throughout its test run.

(a) **(b)** **(c)**

Fig. 76: Typical sample of test series DP4-C at time: (a) 0 h 30 min, (b) 3 h 00min and (c) 5 h 30 min.

The samples showed massive discolourations of brown/black colour across their entire surfaces after the tests were completed, especially along the ground potential electrode and the main contaminant path located along the centreline of the samples. This made observation of the erosion progress difficult during the tests, especially since the samples only showed minimal erosion along the ground potential electrode. The discolourations were once again revealed not to be superficial but permanent, since they still remained to large degrees even after the application of the final cleaning procedure. This was especially the case in the areas where continuous arcing was observed. An interesting observation was that the erosion at the centre of the ground potential electrode showed no clearly visible edges, rather appearing smooth and shallow, giving the impression of a shallow depression in the sample surface. This erosion area was very hard to detect with the naked eye, but could be clearly felt when sliding a finger along the interface of sample material and ground potential electrode. Overall, no sample of this series displayed excessive erosion. Fig. 77 shows a typical sample of this series before and after undergoing the final washing procedure.

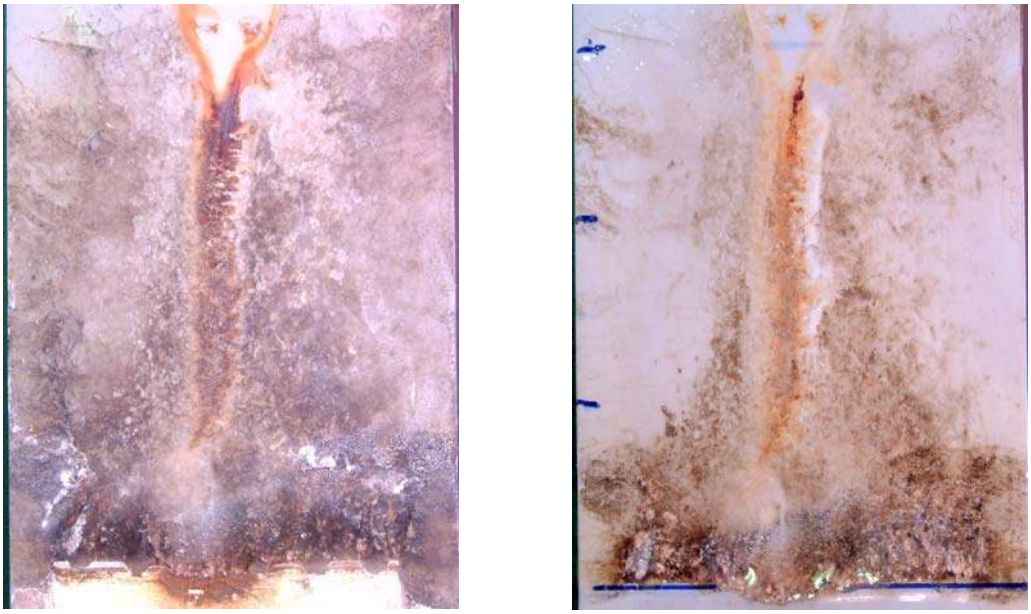

(a) (b)

Fig. 77: Typical sample of test series DP4-C: (a) Before and (b) After washing.

5.3.1.9 Material C, negative DC voltage

The initial behaviour of the samples in this series was identical to that of the other two series of this material. Immediately after starting the test, the contaminant flow broadened towards the ground potential electrode, creating a large wetted surface. Electrical discharges were again observed along the fluid path, with the majority occurring along the electrode. However, the arcing was observed to be more stable than that observed in the previous two series.

The arcing process stabilized at the ground potential electrode within 30 minutes. Interruptions were seldom observed, but did appear in form of short dead times or scintillations along the contaminant path. The arcs occurring at the electrode were thin and of blue-whitish colour similar to those observed during series DP4-C, but showed increased stability. Erosion was clearly visible along the ground potential electrode within the first 10 to 15 minutes and increased until the beginning of the second test hour, after which the eroded areas stabilized. Small hotspots were observed to form close to the ground potential electrode within the first 30 minutes, causing the initial erosion. Extensive sample discolouration was also visible after 30 minutes and continued to increase.

Once stabilized, the arcing process did not change significantly throughout the remainder of the tests. However, the discolouration developed two distinct areas by the beginning of the second test hour. The two areas were divided into an upper and a lower part by an imaginary line situated ± 10 mm above the ground potential electrode. The upper region contained strongly discoloured branches and paths which covered most of the sample surface. The lower region showed no such branches, displaying a more uniform surface discolouration. This distinction became more apparent as the tests continued.

The discolouration of the surfaces stabilized during the fourth test hour. After that, the arcing process, surface discolouration and erosion remained relatively unchanged for the remainder of the tests. Small increases in discolouration or erosion were sometimes observed, but not to any significant degree. Fig. 78 shows photos of a typical sample of this series during the three major stages of the test runs, i.e. at the beginning, middle and end of the test runs.

(a) **(b)** **(c)**

Fig. 78: Typical sample of test series DN4-C at time: (a) 0 h 30 min, (b) 3 h 00 min and (c) 5 h 30 min.

An inspection of the samples after testing confirmed the division of the surface discolouration into two separate areas. The upper regions showed a lighter colouration, with dark paths criss-crossing the surfaces. The lower regions revealed a darker and more uniform colouration. The final cleaning procedure revealed the discolouration of the upper regions to be superficial, with most of the discolouration removed during cleaning. Discolourations in the lower regions were more permanent

and could only be partially removed. Since the lower regions coincided with the area of constant arcing, it seems that constant electrical discharges result in a more permanent discolouration in this material.

The erosion in the samples was located along the ground potential electrode, taking the form of separate small, elliptic areas. The largest erosion areas were found at the centre of the samples, at the region of permanent arcing. These areas were more severe than those of series DP4-C, but less than those of AC4-C. Fig. 79 shows a typical sample of this test series before and after the cleaning procedure was applied.

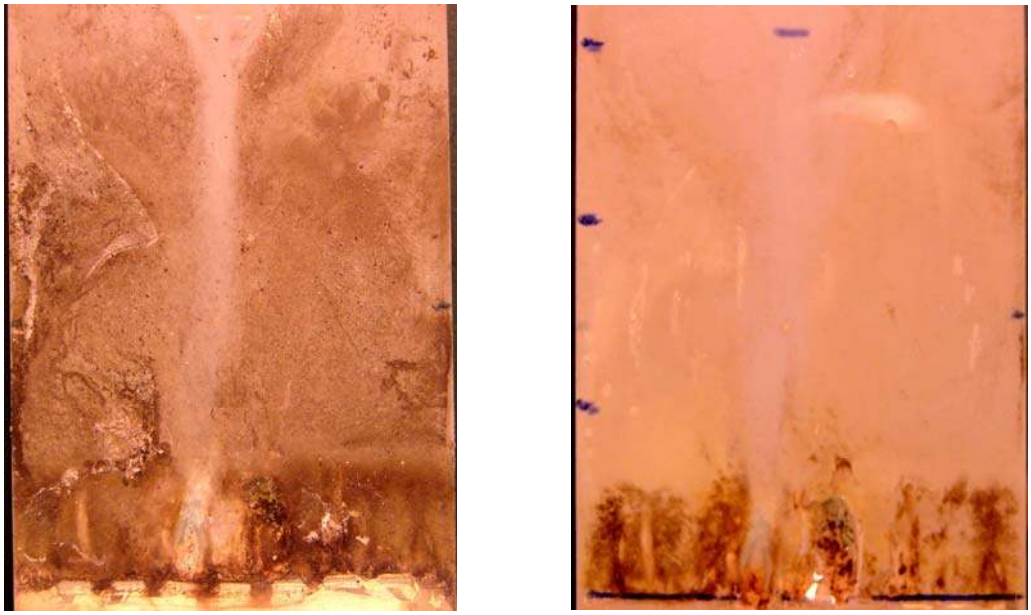

(a) **(b)**

Fig. 79: Typical sample of test series DN4-C: (a) Before and (b) After cleaning.

5.3.1.10 Material D, AC voltage

Some brief periods of strong arcing at the ground potential electrode was observed in the samples of this series immediately after test begin, which quickly deteriorated into weak discharges all along the fluid path. However, the majority of the discharges still focused around the ground potential electrode.

The arcing process regained moderate stability at the electrode after 30 minutes. The arcs were of medium intensity, thin and of a blue-whitish colouration. Interruptions to the arcing process still occurred frequently in form of either dead times (periods of no observed electrical discharges) of weak discharges along the fluid path. By this time,

some light discolouration along both sides of the fluid path as well as the ground potential electrode was observed in the samples.

This general arcing procedure continued largely unchanged throughout the remainder of the test runs. The stability of the arcs decreased or increased to some degree during the tests, as did the frequency and length of occurrence of the interruptions, but neither changed to any large degree. Some electrical discharges also occurred along the edges of the samples due to a presence of contaminant fluid in these regions. These resulted from a splatter in the contaminant flow observed early on in the tests. Small areas of shallow erosion developed at the junction of fluid path and ground potential electrode anytime between 30 minutes and the end of the second test hour. However, these areas showed no significant growth after their initial inception. Only the discolourations along fluid path and electrode continued to increase both in severity and area throughout the tests. No significant hotspot development was observed on any sample of this test series. Fig. 80 shows a chronological sequence of photographs taken during a typical test run of this series.

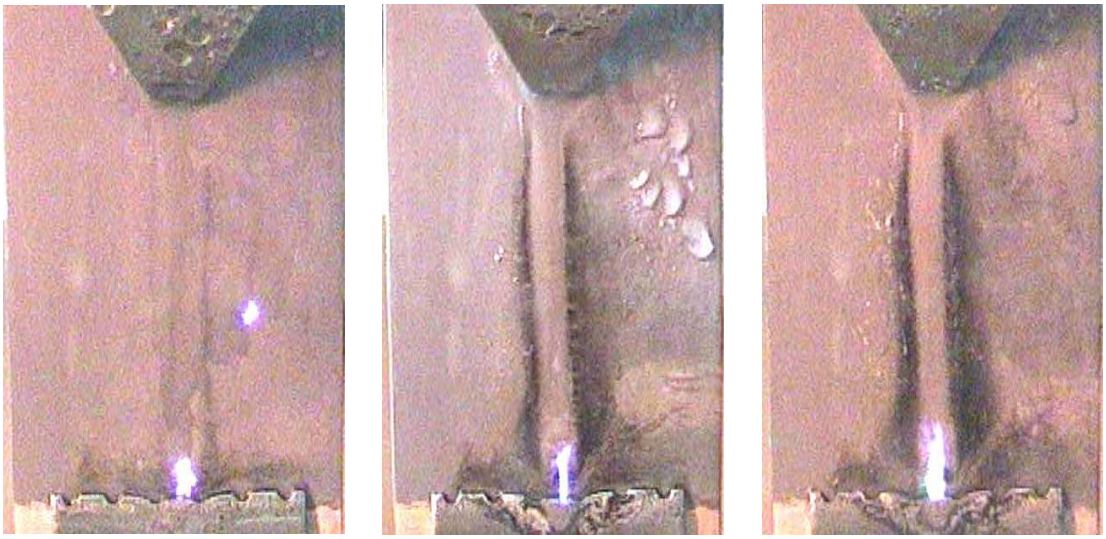

(a) **(b)** **(c)**

Fig. 80: Typical sample of test series AC4-D at time: (a) 0 h 30 min, (b) 3 h 00 min and (c) 5 h 30 min.

As described earlier, all samples of this series showed strong discolourations along both sides of the fluid path as well as the ground potential electrode, being especially severe along the fluid path. However, these surface discolourations were observed to be mainly superficial and were almost completely removed during the final cleaning procedure, with small residues only remaining along the fluid paths. The erosion areas

at the ground potential electrodes were very small and only of shallow depth in all samples of this series and were all located at the junction of electrode and fluid path, which was observed to be the region of strong arcing on the samples. Fig. 81 shows a typical sample of this test series before and after cleaning.

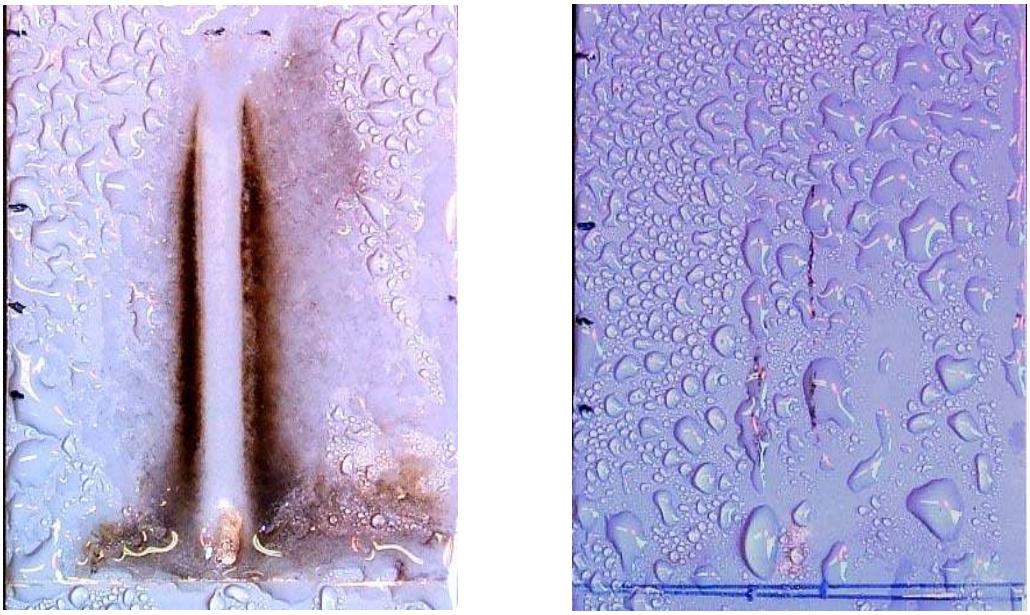

(a) **(b)**

Fig. 81: Typical sample of test series AC4-D: (a) Before and (b) After cleaning.

All samples of this material produced similar results for this test series, indicating a strong stability of this material when exposed to AC voltages. Furthermore, the results are quite similar to those test series AC4-B, which is to be expected since both materials are HTV silicone rubbers.

5.3.1.11 Material D, positive DC voltage

Immediate discharges were observed on the samples of this series upon starting the test runs. These discharges occurred all along the contaminant path, with the majority appearing close to the ground potential electrode. Frequent interruptions by dead times were observed during these early stages. All samples developed signs of slight surface erosion within 15 minutes of test begin, which appeared as roughened areas along the fluid path. Initial surface discolourations along the fluid path and the electrode were also observed by this time.

The arcing stabilized at the ground potential electrode by the end of the first test hour. These arcs were observed to be of greater intensity than those observed in the AC

series, with brief high-intensity hotspots occurring frequently along the electrode. Interruptions by short dead times still occurred frequently. Both surface erosion and discolouration continued to increase during this stage, although the erosion depth continued to be relatively shallow.

The samples then developed strong hotspots and even glowing paths at the area of constant arcing within the second test hour. As a result, the erosion started to increase both in area and depth, with some waste deposits similar to those observed in test series DP4-B forming in parts of the erosion areas. Small areas of chalking (deposits of filler material) formed around the regions of significant erosion, and the surface discolouration also started to increase. Arcing at the ground potential electrode was now observed to be very stable, with only very brief dead time interruptions.

From this point on, the arcing remained fairly constant with frequent formations of hotspots and glowing paths. Erosion areas and surface discolourations (especially above the eroded areas) also continued to increase slowly. However, at a certain point in time the samples developed very intense and stable glowing paths along their eroded areas, which continued to burn into the sample material and resulting in a sudden and large increase in both erosion area and depth. This behaviour was observed in every sample, but at various times throughout the test runs. The waste materials within the eroded areas also increased along with the areas. They were frequently burned off by the intense glowing paths, but always reformed within the eroded areas where intense hotspots or arcing occurred. Continuous arcing always resumed at the ground potential electrode, at which point the sudden increase in erosion area abated.

This arcing behaviour continued for the remainder of the test runs. The sudden increases in erosion area were sometimes observed to occur more than once within a sample. The contaminant paths were observed to adhere to the edges of the eroded areas, which resulted in strong arcs and subsequent erosion growth in these regions. Fig. 82 shows a chronological sequence of photographs taken during a typical test run of this series.

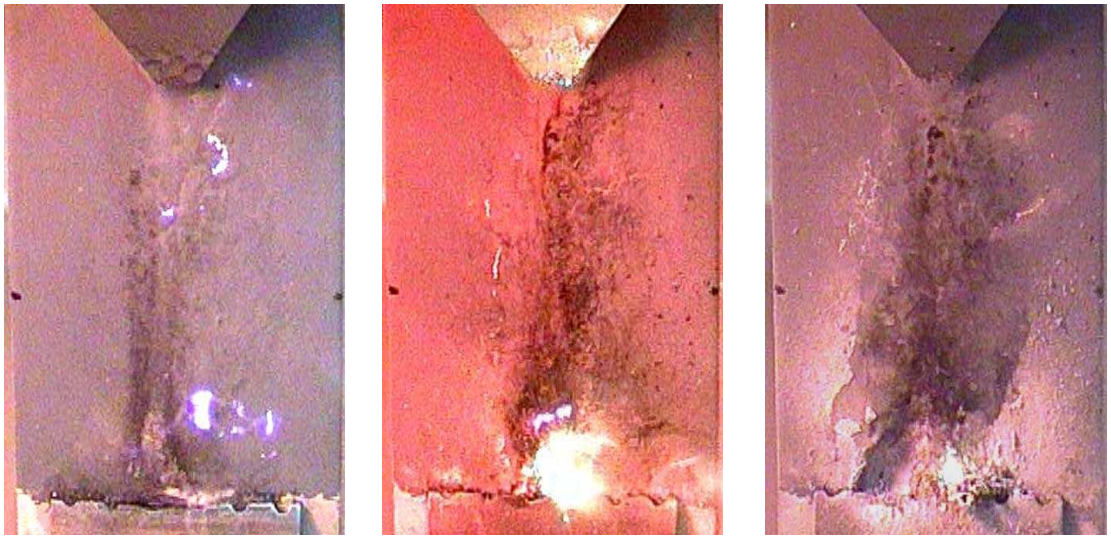

(a) (b) (c)

Fig. 82: Typical sample of test series DP4-D at time: (a) 0 h 30 min, (b) 3 h 00 min and (c) 5 h 30 min.

The sudden increase of erosion area also caused a large increase in surface areas covered by the chalking. These areas were again observed to be highly hydrophobic, similar to those observed in series DP4-B, and thus hindered the flow of contaminant flow. Accordingly, some samples developed interruptions to the arcing process caused by the contaminant flow dripping past the ground potential electrode. These samples were treated using the same cleaning procedure as for series DP4-B (see section 5.3.1.5), with the same positive results. Table 18 shows a summary of the observed interruptions for each sample tested in this series. As can be seen, the number of interruptions was significantly lower for this series than for series DP4-B.

All the samples of this series showed extensive material erosion in both area and depth located in the vicinity of the ground potential electrode. Severe surface discolourations were observed between these eroded areas and the high voltage (top) electrode, especially along the fluid path. Discolourations also occurred within the eroded areas where continuous arcing took place. Large areas of the samples showed signs of chalking, especially along the erosion areas. The degree of chalking seemed to increase with the degree of erosion observed on the samples. The deposits and discolourations were observed to be mainly superficial, since they were largely removed during the cleaning procedure. Only light traces of discolouration were observed along the fluid path and around the erosion area afterwards. Fig. 83 shows a typical sample of this series before and after the final washing procedure was applied.

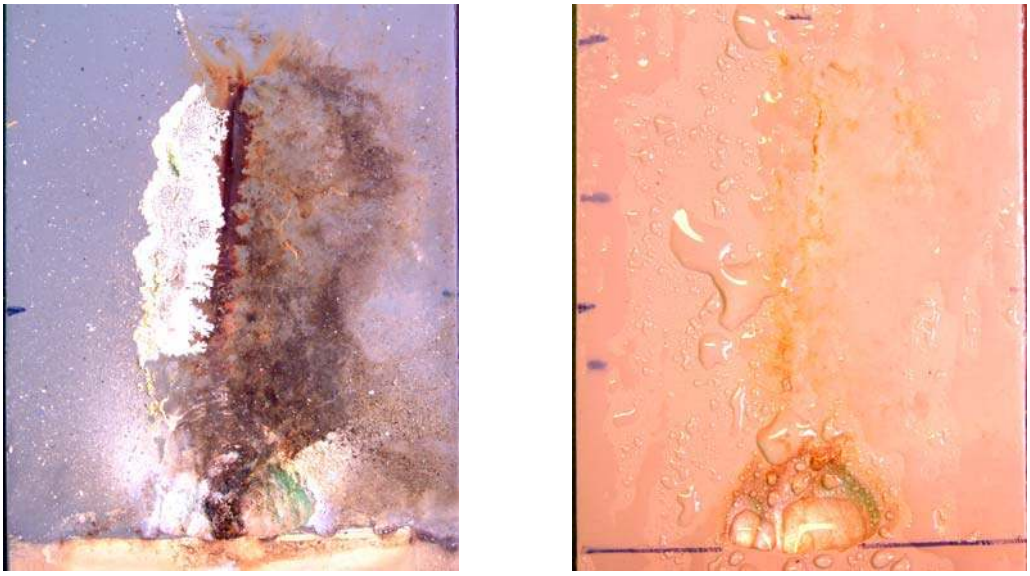

(a) (b)

Fig. 83: Typical sample of test series DP4-D: (a) Before and (b) After washing.

The erosion was indeed so extensive in samples DP4-D4, DP4-D5 and DP4-D6 that each one of them developed a hole running through the entire sample during their respective test runs. Fig. 84 shows each of these samples after the final washing procedure was applied.

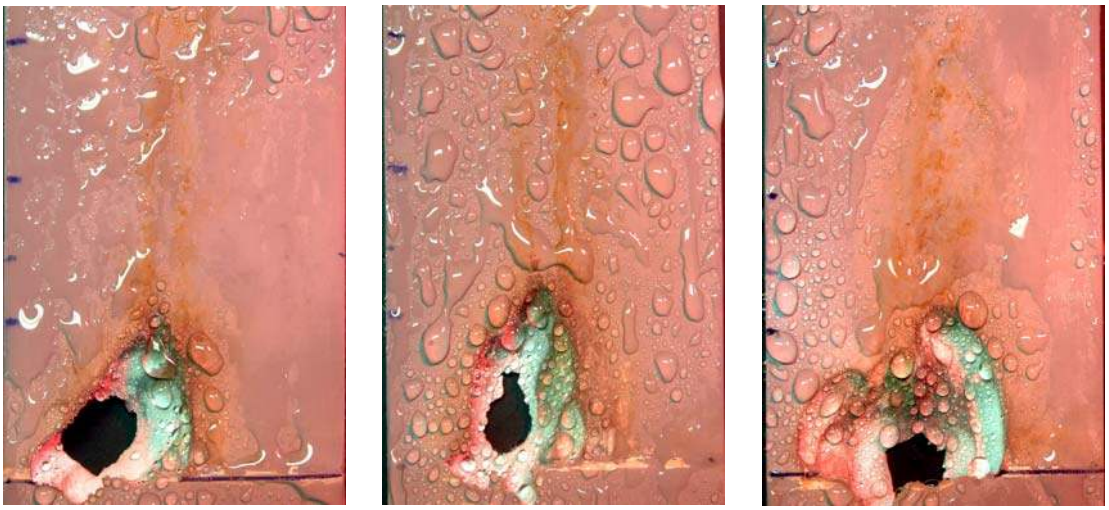

(a) (b) (c)

Fig. 84: Failed samples of series DP4-D: (a) DP4-D4, (b) DP4-D5 and (c) DP4-D6.

According to standard, each of these samples failed the test and the test runs were thus aborted once the holes were detected. The failure in sample DP4-D4 was especially severe, since the sample burst into flames during the final stages of excessive erosion. Table 18 also summarizes the results for this test series, stating for each sample if failure occurred as well as the total duration of the individual test runs. A test duration of six hours signifies a successful test run.

Table 18: Summary of test results for test series DP4-D.

Data	Sample					
	DP4-D1	DP4-D2	DP4-D3	DP4-D4	DP4-D5	DP4-D6
Failure occurred?	No	No	No	Yes	Yes	Yes
Test duration	6 h 00 min	6 h 00 min	6 h 00 min	3 h 44min	4 h 19 min	5 h 38 min
No. of interruptions	0	0	1	0	3	1

5.3.1.12 Material D, negative DC voltage

Weak discharges occurred at the ground potential electrode right after the start of the test runs in this series. This developed into constant arcing with great stability within 15 minutes of the start of the tests, with only very brief interruptions by weak discharges along the fluid path. Hotspots formed frequently at the electrode, resulting in initial erosion and surface discolouration at that location in as little time as eight minutes.

The stable arcing at the electrode continued for the entire test runs in every sample of this series. The observed arcs were mostly thin and of a blue-whitish colour, with the occasional formation of brief hotspots. Interruptions in form of weak discharges all over the sample surface or dead times did occasionally occur, but stable arcing always re-established at the ground potential electrode. Erosion in the vicinity of the electrode continued to increase for the first two test hours. Small areas of chalking also started to develop around the erosion areas. Surface discolouration was mostly observed to appear within the eroded areas, with almost none appearing along the fluid path.

Erosion growth started to stabilize towards the end of the second test hour. After this point, no significant increase in erosion area was observed in the samples, except for some samples which developed short but intense hotspots during later test hours. These hotspots caused some increase of the erosion areas, but not by any significant amount. In these cases, the areas of chalking around the erosion areas also increased by a small degree.

Some yellowish deposits similar to those observed on the samples in section 4.3.1 were observed to appear along the fluid path from the end of the first test hour onwards. The amount of these deposits varied during the test runs, increasing or decreasing randomly. As already explained in section 4.3.1, these deposits were

presumed to be salt deposits caused by an evaporation of the contaminant. Surface discolourations were observed to be only light in the samples of this series, occurring mainly in the areas along the ground potential electrode. Fig. 85 shows a typical sample of this test series photographed at the beginning, middle and end of its test run.

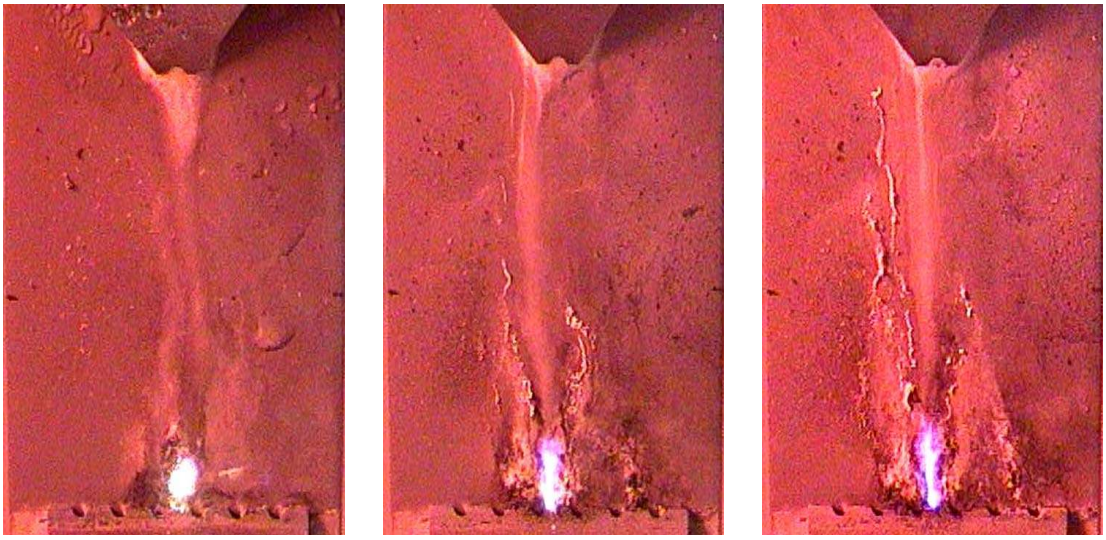

(a) **(b)** **(c)**

Fig. 85: Typical sample of test series DN4-D at time: (a) 0 h 30 min, (b) 3 h 00 min and (c) 5 h 00 min.

After completion of the tests, all the samples displayed significantly sized areas of surface erosion. However, these areas only showed a relatively shallow depth. The areas were of a whitish colour, but also displayed considerable discolouration. In fact, the surface discolouration in these samples appeared almost entirely in the eroded areas, with only light discolourations along the fluid path. The majority of these discolourations were removed during the cleaning procedure, revealing them to be largely superficial in nature. Only light residues remained in the eroded areas. Small areas of chalking were observed along the erosion areas, but not nearly as extensive as those observed in test series DP4-D.

Overall, the samples of this series displayed a greater degree of erosion than the samples of series AC4-D, but far less than those of series DP4-D. Fig. 86 shows a typical sample of series DN4-D before and after undergoing the cleaning procedure after completion of the tests.

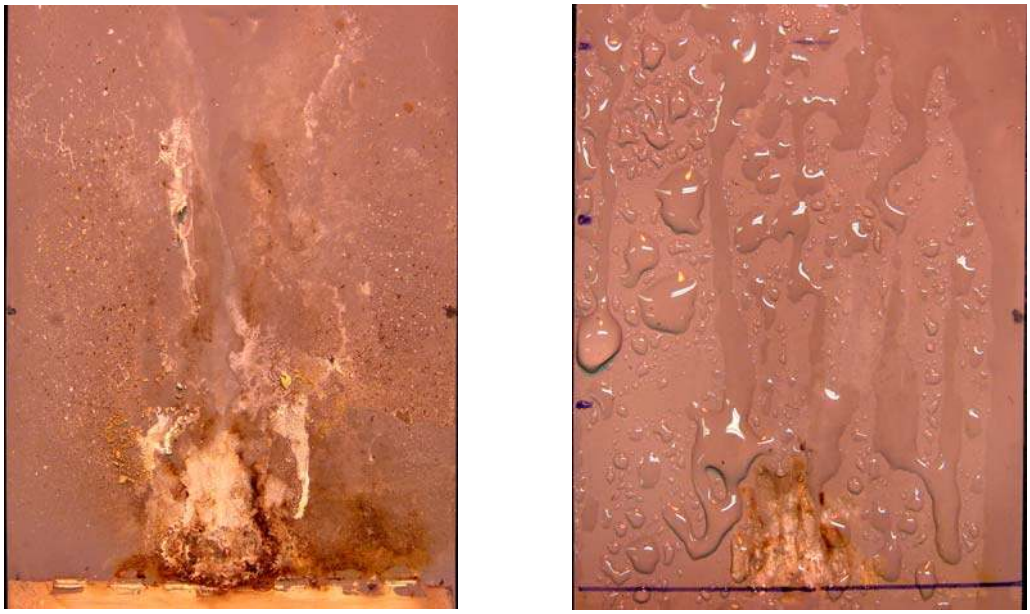

(a) (b)

Fig. 86: Typical sample of test series DN4-D: (a) Before and (b) After cleaning.

During all of the test runs for the DC voltage series of the four materials, it was observed that the dry band discharges for the positive DC voltage produced arcs of greater intensity and length than for the negative DC voltage. It is believed that this is due to the polarity effect and the influence of the space charge developing in the air between the end of the contaminant path and the ground potential electrode. Since the contaminant path usually has a small width compared to that of the ground potential electrode and is in direct contact with the high voltage electrode, the contaminant path can be modelled as a sharp extension of the high voltage electrode, forming a point-plane gap arrangement across the dry band forming at the ground potential electrode. Fig. 87 shows this model for the case when a positive DC voltage is applied to the high voltage electrode.

Ionisation of the air in the gap will take place due to the high field strength around the end of the contaminant path, i.e. the sharp point of the 'electrode'. The liberated electrons, due to their higher mobility, are swept towards the anode, while the positive ions are left behind, moving slowly towards the ground potential electrode [61]. In fact, the positive ions will form a sharp extension of the anode, resulting in an increase in the electric field strength at their location. The electrons, on the other hand, form a broad end for the space charge cloud close to the anode, resulting in a field strength reduction [61]. The resulting field distortion is also shown in Fig. 87,

with the dotted line representing the distribution of the original electric field and the solid line depicting the field distortion caused by the space charge.

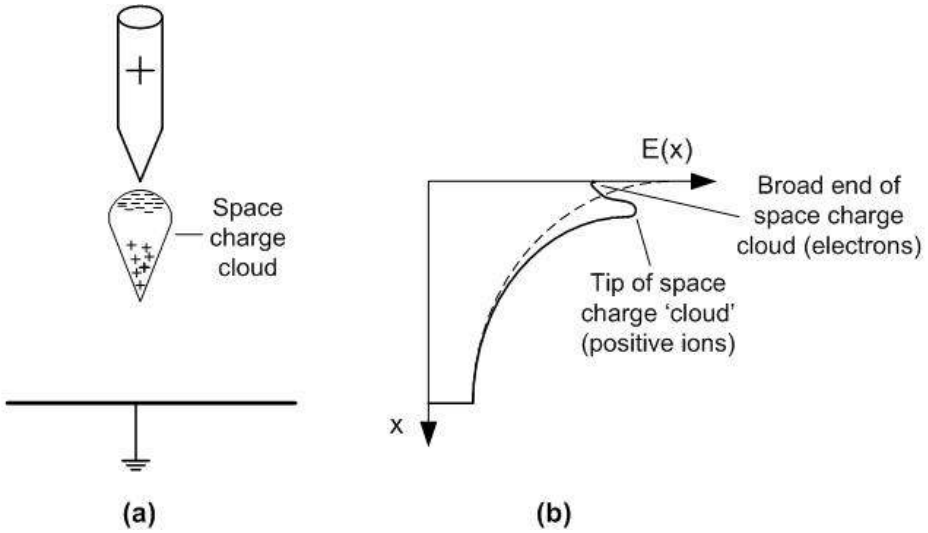

Fig. 87: Positive DC voltage applied to sample: (a) Space charge cloud forming in air gap and (b) Resulting field distortion [61].

In time, the field distortion moves along the gap towards the ground potential electrode. The sharp tip of the space charge cloud will result in an increased field strength, which can be high enough to result in the formation of streamers moving towards the cathode and which may finally lead to full arcing [61].

Fig. 88 shows the effect of a negative DC voltage on the point-plane gap that is the dry band forming at the ground potential electrode.

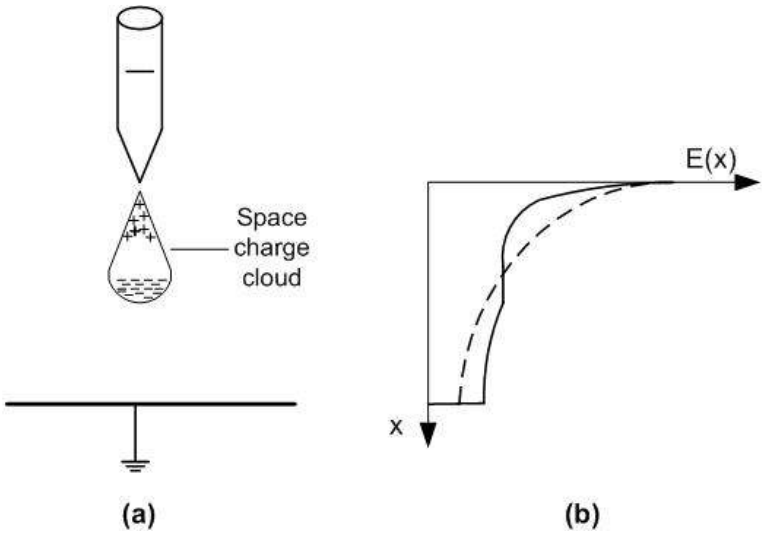

Fig. 88: Negative DC voltage applied to sample: (a) Space charge cloud forming in air gap and (b) Resulting field distortion [61].

In this case, the electrons are repelled by the cathode towards the ground potential electrode, while the positive ions now move towards the sharp point electrode (i.e. the contaminant path) [61]. The space charge cloud formed in the gap is thus the exact reverse to that formed for the positive DC arrangement. Since the broad end of the cloud formed by the electrons now faces the ground potential electrode, the field strength is reduced at the location of the electron cloud. This effect is shown in Fig. 88, with the dotted line representing the original field distribution and the solid line showing the field distortion caused by the resulting space charge cloud. The reduction in field strength prevents further ionisation, causing the existing space charges to be absorbed by the respective electrodes and allowing the cycle to restart. A higher applied voltage is thus necessary in order to overcome this retarding action caused by the space charge and allow arcing to occur within the air gap [61]. For similar gap lengths, the breakdown voltage V_b needed to produce arcing in the air gap between the electrodes is thus higher for a negative DC voltage than for a positive DC voltage [61].

While the processes outlined in the previous paragraphs do seem to explain the observation that a positive DC test voltage resulted in stronger dry band arcing than a negative DC test voltage, it should be noted that this theory was developed for an arrangement of metal electrodes with a fixed gap length. In the case of the IPT method, the use of a liquid contaminant results in a varying width for the dry band forming between the ground potential electrode and the contaminant stream, which serves as an extension of the high voltage electrode. Space charges forming in the dry band can also be neutralized if the conducting contaminant bridges the dry band. The point-plane gap discharge theory, while indicating that positive DC test voltages do result in increased electrical discharges due to the occurrence of field intensification in the electrode gap, might thus not be fully applicable to the discharge process observed in the IPT.

5.3.1.13 Recorded voltage & current waveforms

As described in section 5.2, the waveforms of the source and sample voltage as well as the leakage current were measured during each test run using an oscilloscope. Instants of the waveforms were stored during each half-hourly video recording. The

results of the inspection of these waveforms will now be described for each individual test voltage type.

The waveforms of the leakage current recorded during the AC test series revealed the current to follow the basic frequency of the test voltage of 50 Hz. A significant drop in the sample voltage (i.e. the voltage measured across the test specimen) compared to the source voltage was observed as soon as leakage current flow occurred. This effect is not due to the arcing process, but rather due to the voltage drop across the current limiting resistor situated in series with the test sample. Fig. 89 shows the leakage current waveform for a typical beginning of the arcing process on a test sample as well as the corresponding sample and source voltage.

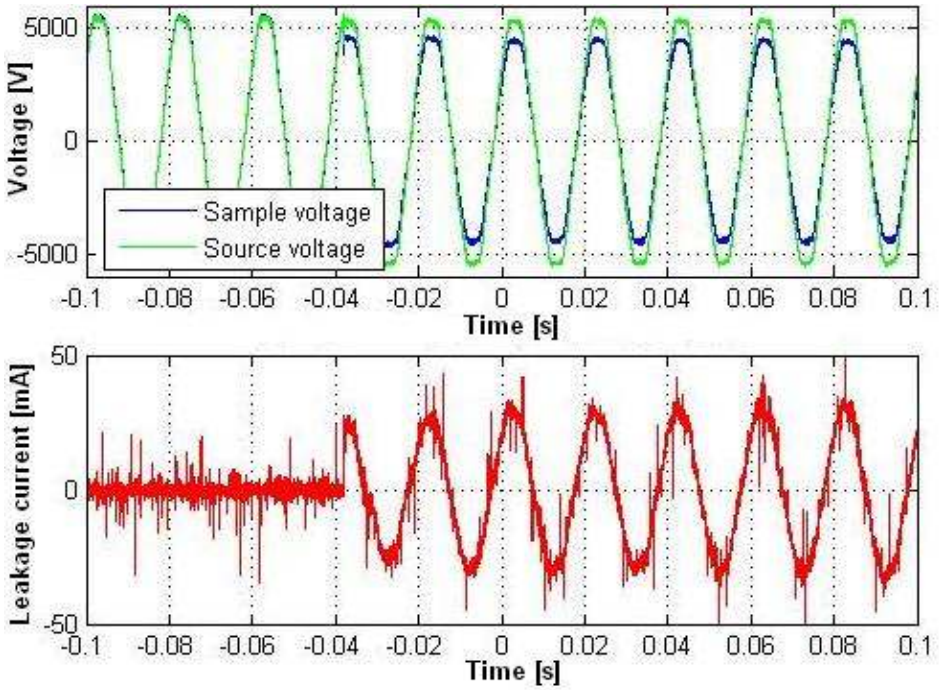

Fig. 89: Typical waveform of arcing inception during AC test series.

As can be seen, the leakage currents show sinusoidal waveforms, which were observed to grow more stable with an increase in current magnitude. On the other hand, lower currents showed increasing signs of irregularities and interruptions at the zero crossings, as can be observed in Fig. 90.

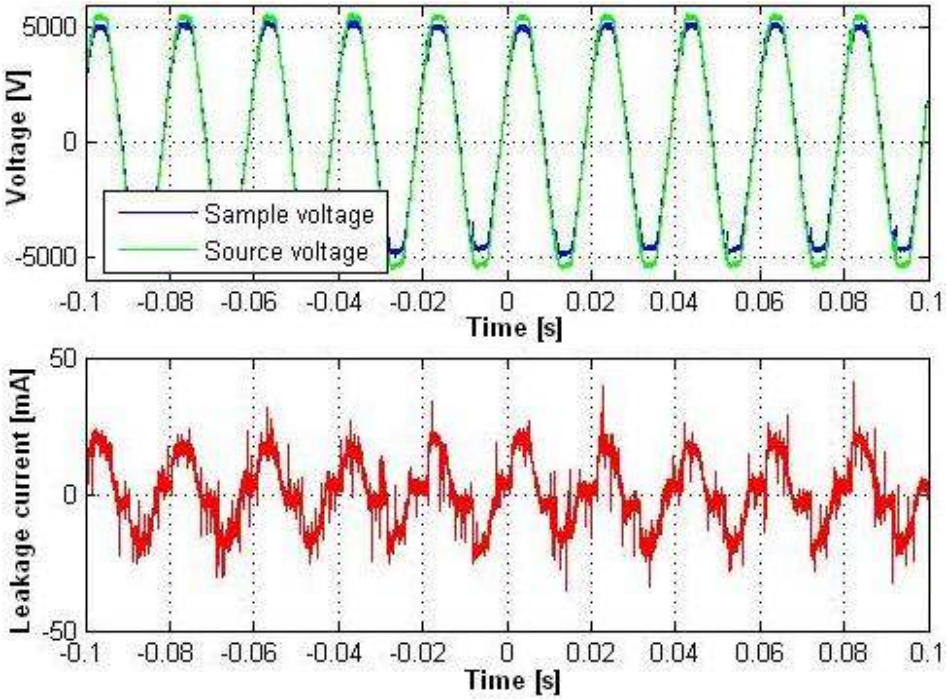

Fig. 90: Waveform of reduced current magnitude during AC test series.

A possible explanation for this could be a weakening in the electric field strength at the arcing location, which would require the voltage to increase to a greater degree before stable arcing can be established and the waveforms of current and voltage can coincide again. Before the actual arcing inception, i.e. during the interrupted periods, the current is close to zero in magnitude as observed in Fig. 89.

In order to better inspect the stability of the arcing processes observed, waveforms with an increased time scale were recorded halfway through the test runs (at time 3 h 00 min). Typical recordings of such waveforms are given in Appendix A. The time of 3 h 00 min was chosen in order to allow the arcing processes to stabilize fully, since most test series showed an initial period in which the arcing process greatly varied in intensity and stability. An inspection of these waveforms reveals the silicone rubber based materials to have similar stability in their arcing processes. Material A (RTV silicone rubber coating) shows slightly better stabilities than either material B or D, which can be seen in the longer periods of current flow and shorter dead times. Fig. 91 shows a recorded waveform of the leakage current of a sample of series AC4-A at time 3 h 00 min.

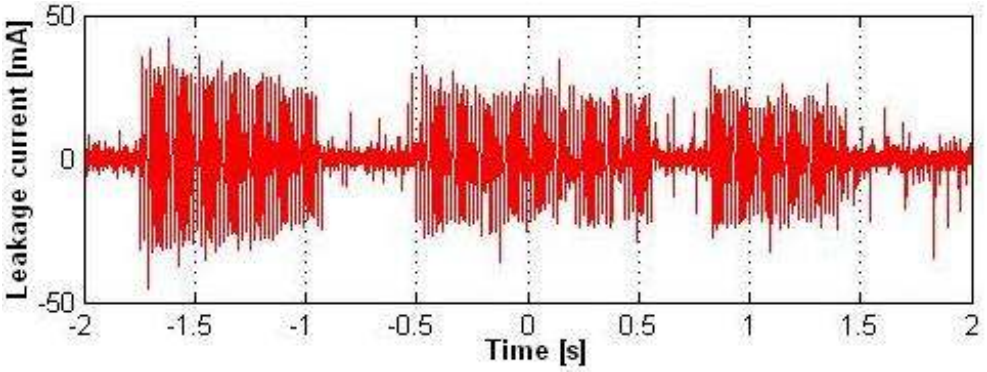

Fig. 91: Leakage current waveform showing amplitude envelope of test series AC4-A, taken at 3 h 00 min.

The most stable arcing processes were observed in Material C (EPDM), with only very short dead times interrupting the current flows. This is confirmed by the visual observations described in the previous sections, which describe the samples of test series AC4-C to have almost constant arcing occurring along the ground potential electrode. A typical waveform of series AC4-C taken at time 3 h 00 min is shown in Fig. 92.

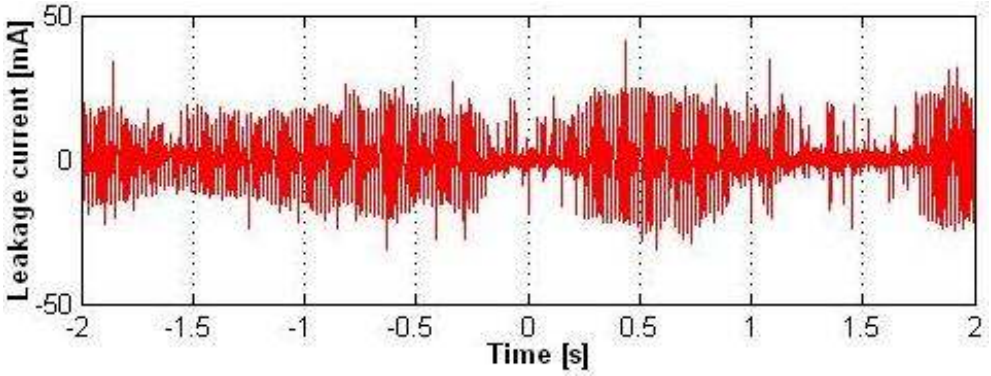

Fig. 92: Leakage current waveform showing amplitude envelope of test series AC4-C, taken at 3 h 00 min.

Marked differences can also be observed in the magnitudes of the leakage currents shown in the waveforms for the various materials. However, the analysis of the leakage current magnitude is reserved for another evaluation criterion and will thus be addressed in later sections.

A typical graph of the inception of arcing at the ground potential electrode for the tests performed under positive DC is shown in Fig. 93.

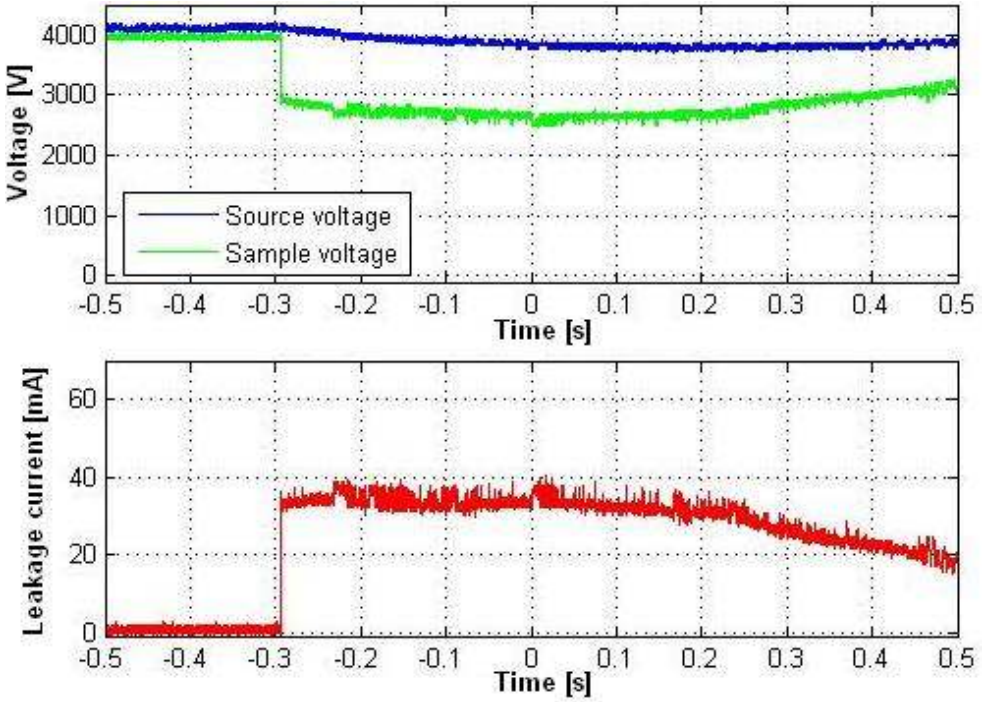

Fig. 93: Typical graph for arcing occurring under positive DC voltage conditions.

The arcs show very fast rise times upon inception up to a certain magnitude. Smaller increases in magnitude over longer periods of time are still possible after this, but the current then either remains constant for a time or immediately starts to continuously decrease over time. This process continues until arcing is interrupted, at which point the leakage current falls to zero in a relatively short time, as well.

Some interruptions or oscillations can occur at this point before the current stabilizes at zero magnitude, as is shown in Fig. 94. These displayed graphs were typical for the arcing processes observed in all the materials when tested under positive DC voltage conditions. Large drops in the sample voltage during arcing were once again caused by the voltage drop over the current limiting resistor in the test circuit.

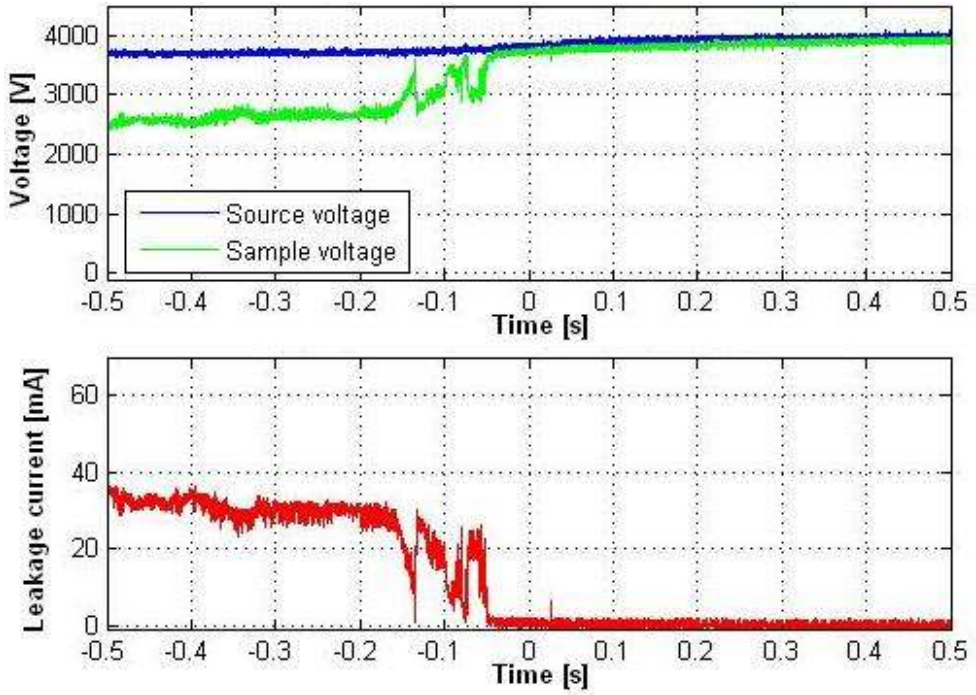

Fig. 94: End of arcing period for positive DC voltage, showing interruptions at final stage.

Graphs with increased time scales taken at a time of 3 h 00 min into the positive DC test runs for each material are shown in Appendix A. All materials show similar arcing behaviour under this test voltage type, with good long periods of stable arcing and only short interruptions. Material A showed the most stable arcing, with very long periods of almost constant leakage current flow, as shown in Fig. 95.

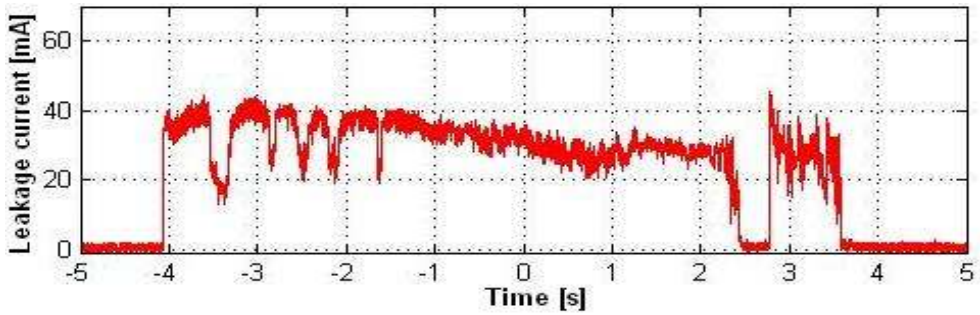

Fig. 95: Graph showing amplitude envelope of arcing process in series DP4-A at time 3 h 00min.

This once again corresponds well with the visual observations described in the previous sections, which revealed an increase in arcing intensity and stability for all test materials for this voltage type.

The general form of arcing observed during tests under negative DC was the same as those observed under positive DC voltage conditions. The leakage current again showed fast rise times upon arcing inception, constant current flows for extended

periods and then a rapid decline back to zero. As observed during the other test voltage types, a decrease in sample voltage occurred during actual current flow due to a voltage drop across the current limiting resistor. The only real difference between the arcing processes observed under positive and negative DC voltage conditions was the magnitude of the current levels, which will be discussed thoroughly in later sections. Fig. 96 shows a typical arcing process for negative DC voltage conditions.

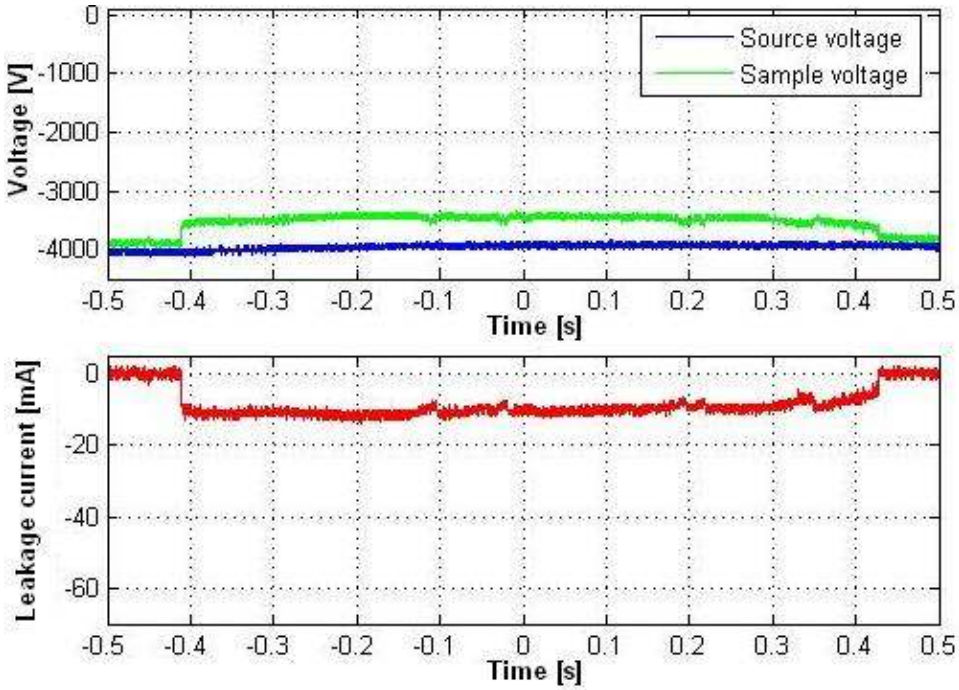

Fig. 96: Graph of typical arcing process for negative DC voltage conditions.

Graphs with extended times scales showing the stability of the arcing process for each test material under negative DC voltage conditions are again displayed in Appendix A. The graphs were recorded at a time of 3 h 00 min so as to allow the arcing behaviour of the samples to fully stabilize. An analysis of the graphs for the leakage current showed that this voltage type produced extremely stable arcing processes on the samples of every material, with very long and continuous current flows observed.

In fact, materials B and C showed long uninterrupted current flows at time 3 h 00 min, as can be seen in the figures displayed in Appendix A. In order to determine which test material experienced a greater stability in its arcing behaviour, the materials were compared according to their leakage current graphs recorded at a test time of 5 h 30 min, close to the end of the sample test runs. These graphs are shown in Fig. 97.

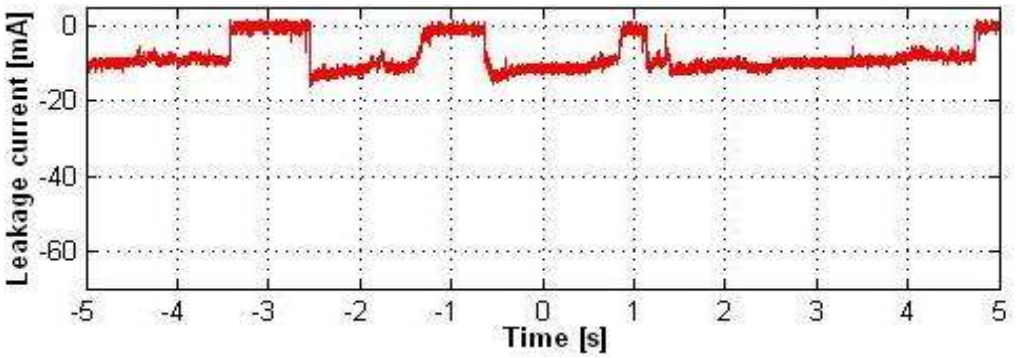

(a)

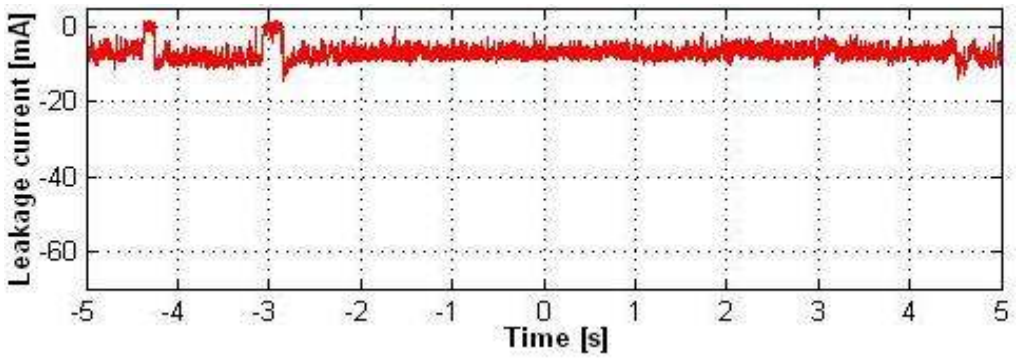

(b)

Fig. 97: Current graphs showing amplitude envelope captured at time of 5 h 30 min: (a) Material B and (b) Material C.

At this point during the test runs, material B showed the occurrence of some interruptions to the current flow, while material C still showed largely uninterrupted arcing at the ground potential electrode, making it the material displaying the most stable arcing behaviour for this type of test voltage. Overall, the negative DC test voltage resulted in the most stable arcing behaviours and leakage current flows in all tested materials.

A further analysis of the current and voltage waveforms was not deemed beneficial, since the waveforms were recorded randomly during the 30 second intervals of video recordings taken every 30 minutes in order to document the test runs. It was thus impossible to link a recorded waveform to a specific recorded arcing occurrence, which is critical for a more complete analysis of the arcing process by means of recorded waveforms. They were thus mainly used, as previously indicated, to confirm visual observations according to the stability of the arcing performance of the various test materials and to obtain a sense of the current waveforms commonly found during electrical discharges for each different test voltage.

5.3.2 Sample mass loss

As the name suggests, the tested samples were evaluated according to their material mass lost due to electrical erosion in this criterion. The mass loss was taken as the difference between the initial sample mass and the mass measured after testing was completed. In order to determine the initial sample mass, the samples were weighed prior to test begin after their surfaces had been cleaned and abraded, so as to compensate for the small mass loss occurring during the abrasion of the surfaces for hydrophobicity reduction. The final sample mass was measured after the samples had undergone the final cleaning procedure described in section 5.2. All deposits and waste materials were removed during this procedure so as to gain an accurate reading of the actual mass of insulation material remaining in each sample. As mentioned in section 5.2, the samples chosen from each test series to undergo a chemical analysis were not included in this criterion due to their selection preventing them of undergoing the cleaning procedure. A summary of the loss in material mass for each individual sample is given in Table B 1 in Appendix B.

For comparison purposes, the mean mass loss of each individual test series based on the remaining five samples per series was calculated using the same finite statistics relation as in section 4.3.2. The standard deviation was also calculated for each test series so as to gain an impression of the quality of data distribution within each series, which will give an indication of the relative stability of the results. The same equation used in section 4.3.2 was again utilized for the calculation of the standard deviation. Finite statistics theory was again utilized for these calculations due to the small number of samples available for each series.

The calculations for series mean and standard deviation based on five samples per series revealed large deviations in the results due to the presence of extreme points within several test series. In order to eliminate the effect of these data points and gain a better impression of possible underlying trends, the difference between the mass loss for each individual sample and the series mean was calculated and the sample showing the greatest difference was then eliminated from each series. The calculations for series mean and standard deviation were then redone based on the remaining four samples per series. Appendix B contains tables showing the mass loss for each individual sample as well as the series mean and standard deviation based on

five and four samples for each individual test series. The test series were grouped into tables according to voltage type. Table 19 is shown in this text as an example, displaying the data for the test series conducted for the AC test voltage.

Table 19: Mass loss summary for test series performed using AC voltage.

Material A		Material B		Material C		Material D	
Data	Mass loss [mg]	Data	Mass loss [mg]	Data	Mass loss [mg]	Data	Mass loss [mg]
AC4-A2	209	AC4-B1	119	AC4-C1	605	AC4-D1	137
AC4-A3	198	AC4-B2	126	AC4-C2	115	AC4-D2	134
AC4-A4	91	AC4-B3	120	AC4-C3	163	AC4-D4	152
AC4-A5	136	AC4-B4	116	AC4-C4	312	AC4-D5	140
AC4-A6	627	AC4-B6	124	AC4-C6	394	AC4-D6	148
5 sample series average	252	5 sample series average	121	5 sample series average	318	5 sample series average	142
5 sample standard deviation	215	5 sample standard deviation	4	5 sample standard deviation	196	5 sample standard deviation	8
4 sample series average	159	4 sample series average	120	4 sample series average	246	4 sample series average	139
4 sample standard deviation	55	4 sample standard deviation	3	4 sample standard deviation	130	4 sample standard deviation	6

During the mass loss measurements, it was observed that several samples of material A (RTV silicone rubber coated ceramic) showed a gain in sample mass rather than a loss. This was especially evident in the two test series of this material performed under both DC voltages. An inspection of the samples revealed large, wet spots on the back of the samples, which lead to the assumption that the ceramic tiles had absorbed water during testing and the final cleaning procedure. This condition was probably aggravated by the large erosion that developed on the sample specimens of this material, which was especially severe for the two DC voltage test series. Consequently, the samples of these two series showed an especially high mass gain.

In an attempt to decrease or even remove the water retention, all sample specimens of this material were placed into an oven preheated to a temperature of 40 °C. The samples were then heated for a period of 24 hours while keeping the temperature constant at 40 °C. This relatively low temperature was chosen to prevent any further damage to the sample coating through excessive heating, which would have influenced the mass loss measurements and thus created false results. A control sample was included in the tests to ensure that no damage to the sample material due

to heating occurred. The surface of this control sample was cleaned using distilled water and propanol alcohol, with no other treatment being applied. After being heated for 24 hours, the samples were removed from the oven and weighed. The new sample mass was then recorded. The change in sample mass caused by the heat treatment was calculated by subtracting the new sample mass from the one measured prior to the treatment. The heat treatment was repeated using the same period and temperature if a significant change in sample mass was still observed in the majority of the samples. Table 20 shows the measured values of the sample mass both before and after testing as well as the results of three rounds of heat treatment, each time giving the sample mass measured after heat treatment, the new mass loss compared to the virgin sample mass and the mass loss experienced during that specific round of heat treatment.

After the third round of heat treatment, the changes in sample mass were observed to be less than 10 mg for every sample of the test series, which was taken as a sign that the majority of the absorbed water had been extracted from the samples. The final mass loss for the samples of this material was thus taken as the difference between the initial sample mass and the mass measured after the third round of heat treatment.

The mass measurements of the untreated control sample revealed the mass to remain constant throughout all three rounds of heat treatment, only changing between 2 to 5 mg. This indicated that the chosen temperature of 40 °C was low enough so as not to cause damage to the sample material, and that all changes in mass can indeed be attributed to the evaporation of water from the samples. The small increase in sample mass during the third round of heat treatment is so small in magnitude that it could have been caused by small deposits occurring on the sample surface during the handling of the sample, and can thus be safely ignored. Since an increase in sample mass was not observed in any other test material, this heat treatment procedure was conducted only for the samples of test material A.

Table 20: Heat treatment of samples of material A.

Sample		Initial mass [g]	Mass after washing [g]	Mass loss [mg]	1st round of heat treatment			2nd round of heat treatment			3nd round of heat treatment		
					Mass after heating at 40°C for 24h [g]	New total mass loss [mg]	Mass loss due to treatment [mg]	Mass after heating at 40°C for 24h [g]	New total mass loss [mg]	Mass loss due to treatment [mg]	Mass after heating at 40°C for 24h [g]	New total mass loss [mg]	Mass loss due to treatment [mg]
AC Series	A2	70.148	70.079	68	69.945	203	134	69.943	204	2	69.939	209	5
	A3	68.019	67.831	188	67.825	194	6	67.824	195	1	67.822	198	3
	A4	73.476	73.389	87	73.387	89	2	73.387	89	0	73.385	91	2
	A5	71.956	71.829	127	71.822	134	7	71.821	135	0	71.820	136	2
	A6	71.872	71.172	700	71.166	706	6	71.165	707	1	71.163	709	2
	AST	71.654	71.038	617	71.030	624	8	71.029	625	1	71.027	627	2
DC+ Series	A1	70.977	72.465	-1488	71.090	-113	1375	70.859	118	231	70.852	126	8
	A2	69.446	71.849	-2403	70.067	-621	1782	69.302	144	765	69.295	151	7
	A3	71.062	73.784	-2722	71.589	-527	2195	70.824	238	765	70.815	247	9
	A4	70.223	73.261	-3038	71.152	-929	2109	70.046	177	1106	70.039	184	7
	A5	72.333	75.125	-2793	72.605	-272	2520	72.014	319	592	72.006	327	8
DC- Series	A1	70.159	71.189	-1030	69.832	327	1358	69.208	951	624	69.203	956	5
	A2	69.602	70.858	-1256	69.593	9	1265	69.089	513	504	69.084	519	5
	A3	69.935	70.699	-764	69.530	405	1169	69.101	834	429	69.097	838	4
	A5	71.352	73.403	-2051	71.737	-384	1667	70.899	454	838	70.894	458	4
	A6	70.156	71.510	-1354	69.792	365	1719	69.230	926	561	69.226	930	4
Control Sample		72.882			72.877	5	5	72.874	7	2	72.878	4	-4

As mentioned previously, the tables summarizing the individual sample mass loss as well as the mean and standard deviation based on both five and four samples for each test series are given in Appendix B. Fig. 98 shows the series means based on four samples for each test material for each of the three different test voltage types. A variation of one standard deviation around the mean value of each test series is indicated by vertical black lines centred on the series mean. All shown values are based on four samples so as to eliminate the effect of extreme data points.

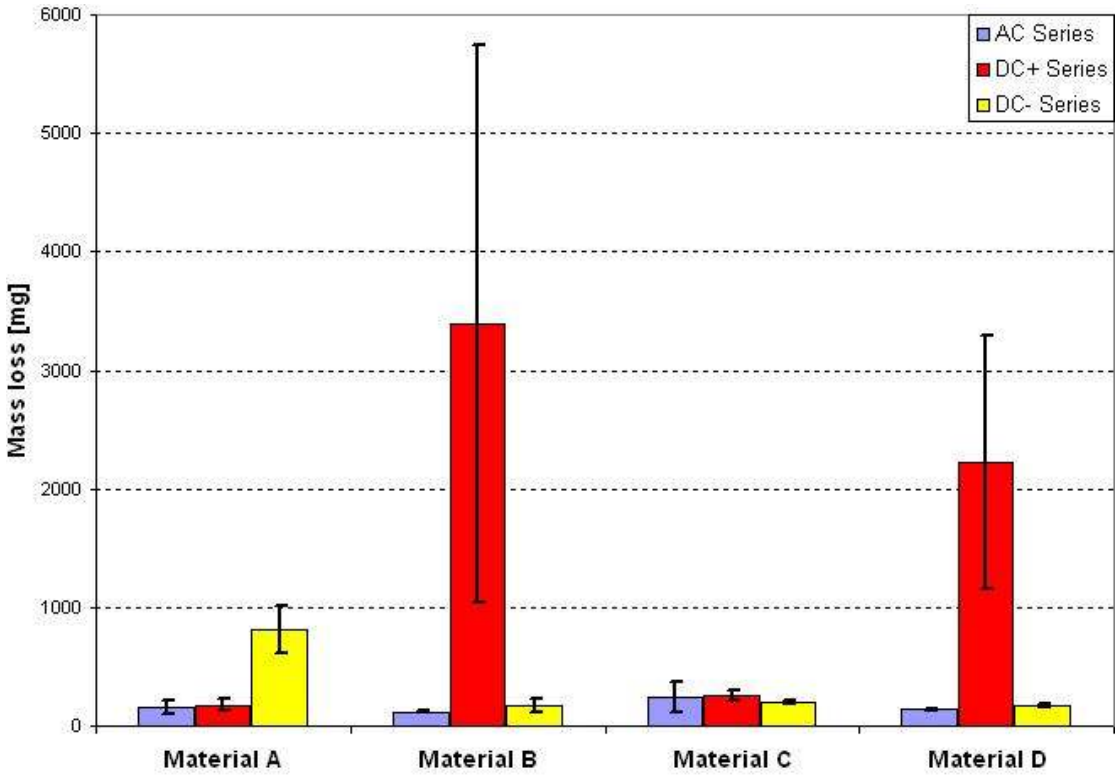

Fig. 98: Mass loss measurements for four different insulation materials and three different voltage types.

The results show that all three silicone rubber based materials, i.e. materials A, B and D, show an increase in mass loss for both the positive and negative DC test series compared to the results for the AC test series. However, material A (RTV silicone rubber coated ceramic) shows a much higher increase for the negative DC series than for the positive DC series. This was expected after the large surface erosion observed during the negative DC test series, as was described in section 5.3.1.3. This material only shows a slight increase in sample mass loss for positive DC series when compared to the results for its AC series. This does not entirely corroborate with the visual observations for these two test series, which showed the surface erosion in the samples of series DP4-A to be far more severe than that of the samples of AC4-A, more than is indicated by the results of the mass loss criterion. However, the

permanent deposits observed to form on the surfaces of the samples of series DP4-A could have influenced the results for this series, showing the mass loss to be less than it actually is.

Material B and D show similar results for each of their different test series, which is to be expected since both materials consist of HTV silicone rubber. Both materials show the smallest mass loss when exposed to an AC voltage, during which both materials also show very stable behaviour in terms of electrical erosion. This is revealed by the small standard deviations for the AC test series of both materials. However, both materials show extremely high mass loss for the positive DC series. The materials also show a relatively unstable behaviour during this series, which is depicted by the high standard variations observed for both materials. Material D does show a smaller average mass loss than material B. However, this can simply be due to the samples of material B having a larger sample thickness, resulting in a larger mass of sample material available for erosion. Also, it must be taken into account that more samples failed during the positive DC test for material D than for material B. The test runs for these samples were interrupted as soon as the failure was observed instead of being allowed to run for the full six hours. A lower number of failed samples thus resulted in a higher overall test time for material B, increasing the time during which electrical erosion can take place.

The mass loss for the negative DC series for both materials was significantly less than that for the positive DC series, but slightly higher than that of the AC series. The series means are almost identical for both materials, but material B does show a higher standard variation for this voltage type than material D, indicating a slightly lesser stability in its erosion performance.

The mass loss results for material C (EPDM), on the other hand, show marked differences to the results of the silicone rubber materials. The lowest average mass loss for this material was observed during the negative DC series, which also showed the lowest standard deviation. Fig. 98 also suggests that the highest mass loss was observed for the positive DC series. However, the AC series shows a large standard deviation that indicates the presence of samples with a mass loss higher than that of the samples of the positive DC series. An inspection of the results in the tables in

Appendix B shows that the lower average mass loss in the AC series was caused by the large variation in mass loss observed in the samples of this series. Taking into account the results for the visual observations, the mass loss due to electrical erosion is more severe for this material when exposed to an AC voltage than a positive DC voltage.

Table 21 displays the material showing the greatest average mass loss for each voltage type. Materials B and D show the greatest variation in mass loss for the different voltage types, while material C shows similar mass loss results for all three voltages. It can thus be concluded that the effect of voltage type on mass loss due to electrical erosion is of less importance for material C than for the other materials.

Table 21: Material showing largest average mass loss for different voltage types.

Test material	Voltage type		
	AC	DC +	DC -
	C	B (& D)	A

It was noted during the visual observations in section 5.3.1 that materials B and D (HTV silicone rubber) did show a higher occurrence of high temperature hotspots and glowing paths in the DC test series than in the AC series, with the highest number of occurrence observed in the positive DC series. The duration of these hotspots and glowing paths also increased along with the number of occurrences, with the most stable periods once again observed in the positive DC test series for these materials. Simultaneously, the average series mass loss increased for both materials when moving from the AC series through the negative DC series to the positive DC test series. A direct correlation thus seems to exist between the temperature of the dry band arcing and the mass loss caused by erosion of the samples. In fact, similar observations have been made in studies performed by Meyer et al., who further proposed an exponential relationship between the arcing temperature and the erosion mass loss in silicone rubber samples in the form of [32]

$$\text{Eroded\_Mass} = 7 \times 10^{-8} \times e^{0.02T}, \tag{5.1}$$

where T is the average arcing temperature rather than the maximum temperature recorded, since the arcing duration is also of critical importance to the erosion process [32]. The mass loss results of material B and D obtained during this project do seem to adhere to this relationship, judging by visual observation of the arcing process.

5.3.3 Sample erosion depth

The erosion depth measurements on the samples were undertaken after the samples were cleaned of any deposits and waste materials in order to measure the actual erosion depth up to the remaining sample material. The samples selected for chemical analysis are thus also not included in this analysis, which means that each test series contains a total of five valid samples for this evaluation criterion.

In order to meet the stringent guidelines given in the IEC 60587 standard, which state that the measurements should be taken using a gauge of ± 0.01 mm accuracy with a hemispherical probe of 0.5 mm diameter, the measurements were done using the same CMM machine (Mitutoyo Bright Apex 710) as described in section 4.3.3. Depth measurements were taken along contour lines along the longitudinal axis of the samples. The measurements points were spaced 0.5 mm apart, with the contour lines themselves spaced 1 mm apart across the width of the samples.

However, due to a limited time schedule available for these measurements, the measurements for all samples of the negative voltage test series were done on a Renishaw Cyclone Analogue Scanner. This machine is capable of much greater measuring speeds than the CMM machine, reducing the processing time for each sample. However, it is less accurate than the CMM machine, having a volumetric accuracy of ± 0.05 mm compared to a volumetric accuracy of ± 6 µm for the CMM machine. Although this accuracy is less than that prescribed by the IEC standard, it was judged sufficiently large to deliver adequate results for the erosion depth measurements. The scans using this machine were again conducted along contour lines along the longitudinal axis of the samples. The pitch for the measurement points was reduced to 0.25 mm, and the spacing of the contour lines was reduced to 0.5 mm.

Measurements using both machines were conducted over a rectangular area covering locations on the sample surface where erosion was visible to the naked eye. The position of the ground potential electrode was taken as the zero axes, with a positive measuring direction towards the position of the high voltage electrode. The measured data was then processed in a Matlab environment in order to find the maximum erosion depth for each measured sample. The results for each individual sample can be found in Table C 1 in Appendix C.

The average erosion depth and standard deviation were then calculated for each test series based on the five available data points, again using equations 4.1 and 4.2. For each series, the individual sample depths were then compared to their respective series means and the samples with the greatest difference were omitted. The series average and standard deviation were then recalculated for the remaining four samples, so as to reduce the distortion of the series average by the presence of extreme data points. Appendix C contains tables summarizing the individual erosion depths as well the series mean and standard deviation for both five and four samples for each test series. The test series are grouped together for each voltage type. For example, Table 22 shows the summarized erosion depth data for the positive DC voltage of all materials.

Table 22: Summary of erosion depth data for test series of positive DC voltage.

Material A		Material B		Material C		Material D	
Sample	**Erosion depth [mm]**	**Sample**	**Erosion depth [mm]**	**Sample**	**Erosion depth [mm]**	**Sample**	**Erosion depth [mm]**
DP4-A1	0.39	DP4-B1	6.71	DP4-C1	1.19	DP4-D2	2.60
DP4-A2	0.48	DP4-B3	10.37	DP4-C2	1.46	DP4-D3	5.14
DP4-A3	0.37	DP4-B4	6.88	DP4-C3	1.45	DP4-D4	6.68
DP4-A4	0.50	DP4-B5	8.00	DP4-C5	0.78	DP4-D5	6.65
DP4-A5	0.29	DP4-B6	7.66	DP4-C6	0.83	DP4-D6	6.55
5 sample series mean	0.41	5 sample series mean	7.93	5 sample series mean	1.14	5 sample series mean	5.52
5 sample standard deviation	0.09	5 sample standard deviation	1.47	5 sample standard deviation	0.33	5 sample standard deviation	1.76
4 sample series mean	0.44	4 sample series mean	7.31	4 sample series mean	1.23	4 sample series mean	6.25
4 sample standard deviation	0.07	4 sample standard deviation	0.62	4 sample standard deviation	0.30	4 sample standard deviation	0.74

For a better comparison of the data, the series means based on four samples of each test series are displayed as vertical bars in Fig. 99, grouped together according to test material. A variation of one standard deviation (also based on four samples) around the mean of each test series is also shown as vertical bars centred on the mean value of each series.

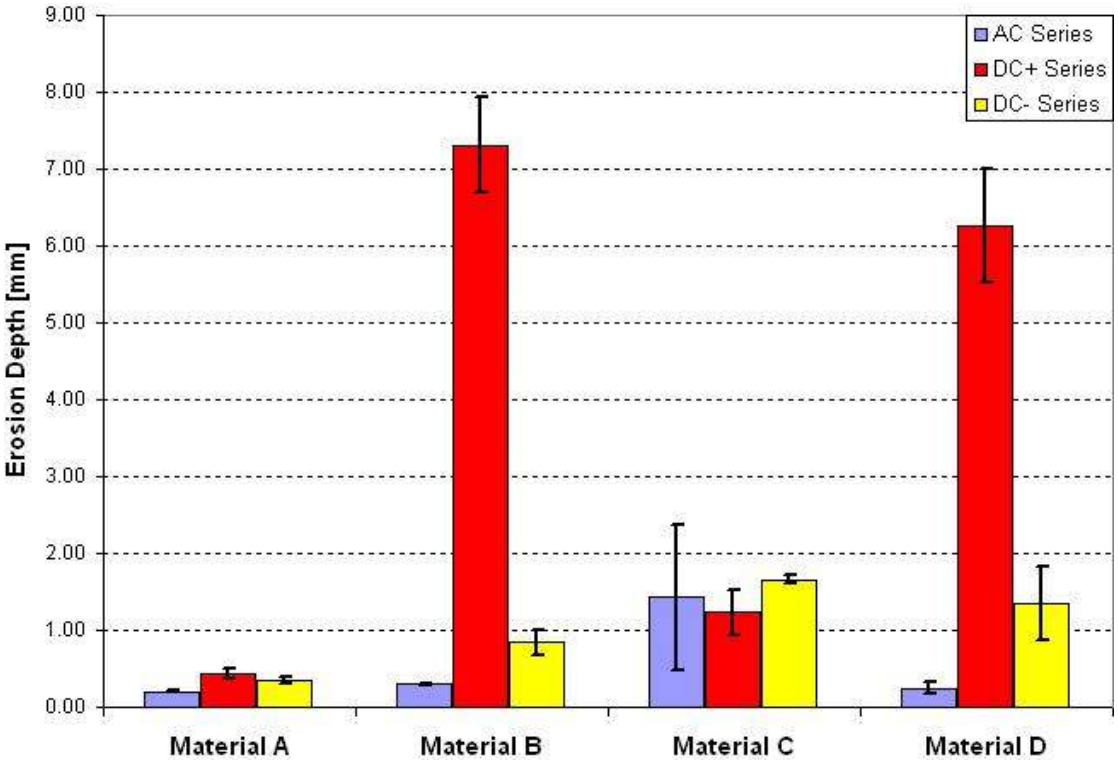

Fig. 99: Erosion depth measurements for four different insulation materials and three different voltage types.

The results show an even greater correlation between the three silicone rubber based materials (A, B and D) than was observed for the mass loss criterion in terms of the effect of a change in voltage type. All three materials show an increase in average erosion depth moving from an AC to a negative DC and finally to a positive DC voltage type. The materials also show an increasing standard deviation for this order of voltage types, which indicates a decreasing stability in the performance of these materials.

Material A shows only small variations in the average erosion depths for the various voltage types. This is to be expected, since the erosion mainly occurs in the RTV silicone rubber coating, which has a thickness of ± 0.3 mm. The erosion depth was thus expected to vary around this value. Series AC4-A shows the smallest erosion depth, since not every sample of this series showed a complete consumption of the coating material. The visual observations for DN4-A showed a complete erosion of the RTV silicone rubber coating across large areas of the samples, exposing the ceramic tile underneath. This is confirmed by an average erosion depth for this series that equals the coating thickness of 0.3 mm. Finally, series DP4-A shows an erosion depth slightly higher than the coating thickness. This was made possible by the

intense arcing observed in these samples, which caused minor damage to the surface of the ceramic tile underneath the coating, thus increasing the erosion depth beyond the coating thickness.

Materials B and D again showed very similar results for this evaluation criterion. Both materials revealed erosion of only minimal depth when exposed to AC voltage conditions. This corresponds to both visual observations and the results of the mass loss criterion, which showed only very small loss of material for AC voltage conditions in both materials. The small standard deviations further indicate a very stable performance of these materials for this voltage type. Both materials showed an increase in erosion depth for the negative voltage series, with material D revealing slightly deeper erosion than material B. The opposite was true for the mass loss criterion, indicating that material D can show deep erosion even for relatively small erosion areas.

Finally, both materials showed extremely deep erosion for the test series conducted under positive DC. This corroborates with the results of both the visual observation and the mass loss criterion, which indicate severe erosion and loss of material for this voltage type. Material B shows a greater average erosion depth than material D. However, an inspection of the results for series DP4-D reveals that the series mean equals the total sample thickness. The samples of material D were thus prevented from achieving a larger erosion depth simply due to a 'lack' of sample material. This would also explain the higher occurrences of failure due to the appearance of a hole in the samples in this material. It is thus impossible to say which material shows a weaker performance for this evaluation criterion.

Once again, the results of material C (EPDM) show marked differences to those of the silicone rubber based materials. This material shows the smallest erosion depth for its positive DC series. At first glance, the negative DC series seems to result in the deepest erosion in this material. However, the sum of the series mean and one (positive) standard deviation is greater for the AC series than for the negative DC series. This suggests the presence of samples within the AC series which incurred deeper erosion than the samples of the negative DC series, which is confirmed by the individual data shown in Table C 1 of Appendix C. The largest erosion depth in this

material is thus observed under AC voltage conditions. Subsequently, the order of severity in erosion depth in this material is, in ascending order: series DP4-C, DN4-C and AC4-C. This order is the exact reverse of that observed in the silicone rubber based materials.

In terms of this evaluation criterion, it can be stated that materials B and D show a better performance than material C for both AC and negative DC voltage conditions, while material C shows a markedly better performance under positive DC voltage conditions. In addition, material C shows the smallest variation between the results for different voltage types, indicating that this material has the most stable overall performance. Material A cannot be considered for this specific type of comparison, since the coating thickness of 0.3 mm severely limits the erosion depth.

5.3.4 Sample erosion area

An inspection of the data for sample mass loss and erosion depth (see Appendices B and C) revealed that the severities of the two criteria are not necessarily equal in a given sample. In other words, some samples experienced a relatively large loss of material while showing a shallow erosion depth, and vice versa. As mentioned already in section 4.3.3, the reason for this is the dependency of the mass loss on the volume of material removed from the sample, which in turn depends on both erosion depth and the area occupied by the erosion. Equation 4.3 states the volume of eroded material being equal to the product of the erosion depth and area (see section 4.3.3). A sample can thus attain similar mass loss either by shallow erosion covering a large portion of the surface area or through deep but localized erosion. The erosion area criterion was thus added to the evaluation of the samples in order to investigate the sizes of the eroded areas formed by the various materials when exposed to the different voltage types.

The erosion area was calculated from the data accumulated during the erosion depth measurements described in section 5.3.3. The measurements were taken along equally spaced contour lines orientated along the longitudinal axis of the samples. The measurement points taken along the contour lines were also taken at a constant pitch, creating a fixed number of measurement points per contour line. The accumulated

data thus forms a matrix of size **n** x **m**, where **n** is the number of data points taken along each contour line and **m** is the total number of contour lines measured across the sample surface. This matrix directly translates into a grid of data points spanning the measured area on the sample surface. Each data point $\mathbf{P}_{i,j}$ of this matrix consists of a X, Y and Z coordinate, with X being orientated along the contour lines, Y along the width of the sample and Z being the measured depth of point $\mathbf{P}_{i,j}$. The variables **i** and **j** indicate the position of point **P** within the matrix or, alternately, within the grid, as shown in Fig. 100.

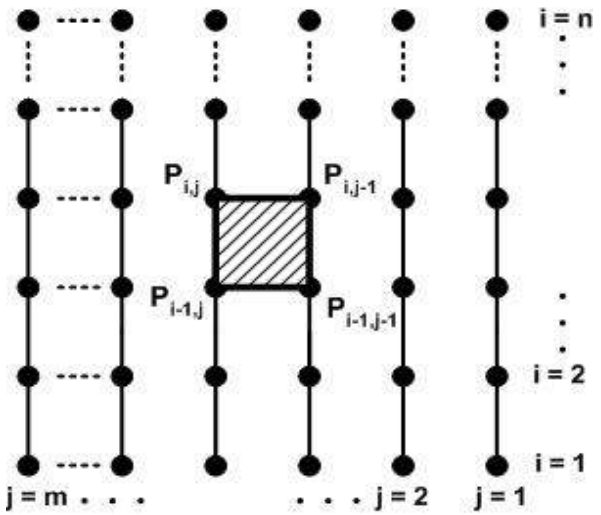

Fig. 100: Small area used for erosion area calculation.

The erosion area was calculated by dividing the grid into small rectangular areas, with four data points forming the corner points of these small areas as shown in Fig. 100. The area of the small rectangles is easily calculated by multiplying the distance between two contour lines with the constant pitch between the data points. If erosion is observed to occur within the rectangle, its area is then added to a running total, whose final value yields the overall erosion area for the sample. The occurrence of erosion within a given rectangle is evaluated according to the depth measured at its corner points. Erosion is considered to have occurred if the measured depth at any corner point of the rectangle exceeds a value of 0.1 mm. Since the samples of material A sometimes developed a permanent deposit within the eroded areas, a positive displacement in the Z-direction of more than 0.1 mm was also considered as erosion due to a destruction of original insulation material. With reference to Fig. 100, erosion is thus considered to have occurred within a rectangular area with base point $\mathbf{P}_{i,j}$:

- If $Z < -0.1$ mm or $Z > 0.1$ mm for point $\mathbf{P}_{i,j}$.

- If -0.1 mm < Z > 0.1 mm for point $\mathbf{P}_{i,j}$ but Z < -0.1 mm or Z > 0.1 mm for point $\mathbf{P}_{i-1,j}$.
- If -0.1 mm < Z > 0.1 mm for point $\mathbf{P}_{i,j}$ but Z < -0.1 mm or Z > 0.1 mm for point $\mathbf{P}_{i,j-1}$.
- If -0.1 mm < Z > 0.1 mm for point $\mathbf{P}_{i,j}$ but Z < -0.1 mm or Z > 0.1 mm for point $\mathbf{P}_{i-1,j-1}$.

If one (or more) of these four conditions is fulfilled, the known area of the small rectangle is added to the running total until this comparison was completed for the whole **n** x **m** matrix, at which point the running total becomes the final eroded area for the sample. The error introduced into these measurements due to erosion not covering the entire surface of a small rectangle was judged to be sufficiently small due to the relatively small size of the rectangles used to calculate the total area.

As an accuracy check of the collected data, the erosion measurements were further used to create 3D surface plots of the measured areas of the samples using Matlab. These plots were then visually compared to the actual sample to see if the detail of the erosion area was accurately captured. A surface plot of a typical sample of each test series is given in Appendix D.

The results for the measured erosion area of each individual test sample are given in Table D 1 in Appendix D. As with the previous evaluation criteria, the series mean and standard deviation were calculated for each test series. Since the area measurements are based on the erosion depth data, the samples selected for chemical testing are once again not included in this criterion and the mean and standard deviation are based on five samples per series. The samples showing the greatest deviation from the series mean were once again omitted and the calculations for series mean and standard deviation were redone for the remaining four samples in order to reduce the effect of extreme data points. Tables containing summaries of the sample data for each test series as well as the values for series mean and standard deviation based on both five and four samples are given in Appendix D. The test series were once again grouped together for the three different voltage types. For example, Table 23 shows the processed data for the test series conducted under negative DC voltage conditions.

Table 23: Processed erosion area for negative DC voltage conditions.

Material A		Material B		Material C		Material D	
Sample	Erosion Area [mm^2]	Sample	Erosion Area [mm^2]	Sample	Erosion Area [mm^2]	Sample	Erosion Area [mm^2]
DN4-A1	1224	DN4-B1	88	DN4-C1	118	DN4-D1	77
DN4-A2	935	DN4-B2	81	DN4-C2	144	DN4-D2	98
DN4-A3	1254	DN4-B3	56	DN4-C3	190	DN4-D3	78
DN4-A5	1357	DN4-B5	58	DN4-C5	226	DN4-D4	76
DN4-A6	1532	DN4-B6	50	DN4-C6	119	DN4-D6	73
5 sample series mean	1261	5 sample series mean	66	5 sample series mean	159	5 sample series mean	80
5 sample standard deviation	218	5 sample standard deviation	17	5 sample standard deviation	47	5 sample standard deviation	10
4 sample series mean	1342	4 sample series mean	71	4 sample series mean	143	4 sample series mean	76
4 sample standard deviation	139	4 sample standard deviation	16	4 sample standard deviation	34	4 sample standard deviation	2

Fig. 101 shows the series mean calculated from four samples for each test series. The series are grouped together according to their test materials. A variation of one standard deviation (also based on four samples) around the mean value is indicated by vertical black lines.

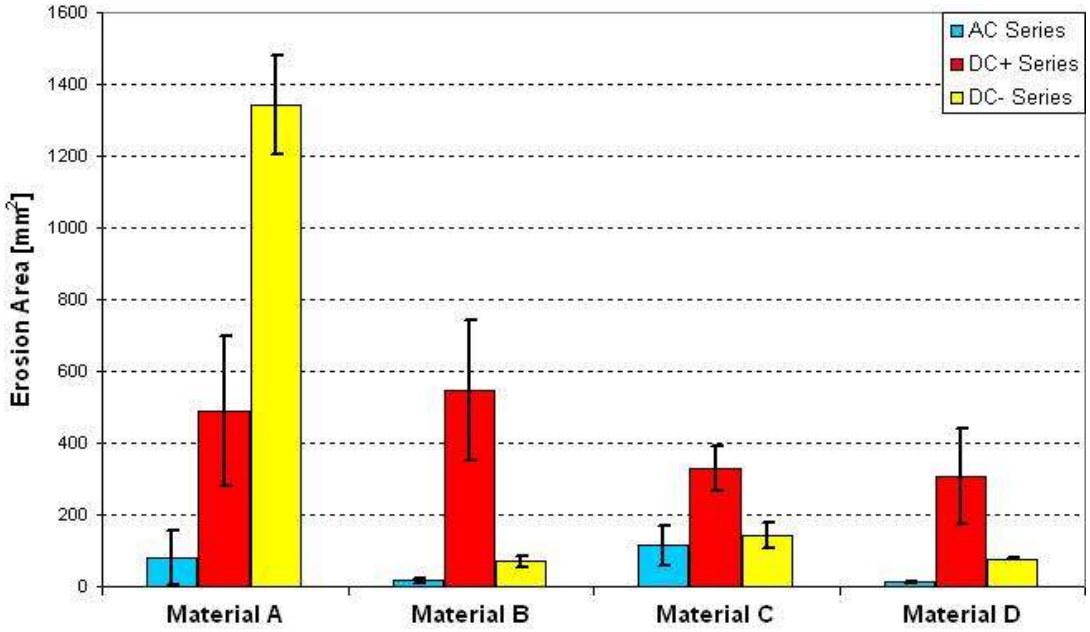

Fig. 101: Erosion area measurements for four different insulation materials and three different voltage types.

The plotted results reveal similar trends for the three different voltage conditions for materials B, C and D, with only material A showing a different trend. This material (RTV silicone rubber coating) showed the smallest average erosion area for the AC

voltage. A relatively large magnitude in the standard deviation further suggested a tendency for unstable results for this combination of material and voltage, with the erosion area being either minimally small or of substantial size. The series conducted under a positive DC voltage shows a large increase in the erosion area, with the biggest erosion being observed during the negative DC test series. This was confirmed by the visual observations described in section 5.3.1.3, which showed large areas of the coating material being consumed during the negative voltage.

Since the erosion depth for this material was limited by the thickness of the coating material, a larger erosion area is expected to cause a greater mass loss in the samples. The mass loss measurements confirm this, showing an increase in mass loss in the samples when moving from an AC to positive to negative DC voltage. The small increase in mass loss between the AC and the positive DC voltage series was already attributed to the large areas of permanent deposits formed on the samples during the positive DC series, which could have influenced the results.

Material B and D, both being HTV silicone rubber materials, once again show very similar trends for this criterion, with almost identical magnitudes for the erosion area of both the AC and the negative DC test series. The test series for both materials can be ranked with regards to the size in average erosion area, in ascending order: AC voltage series, negative DC voltage series and positive DC voltage series. Materials B and D are thus the only materials which show the same trends for their test series for the different voltage types throughout the criteria of mass loss, erosion depth and erosion area. It can thus be safely said that erosion occurring in HTV silicone rubbers progresses proportionally in both depth and area for all different voltage types, but with varying magnitude for each specific type, thus creating different mass losses.

Both materials show small standard deviations for both the AC and the negative DC series, indicating a stable behaviour in terms of erosion area under these conditions. The standard deviation for the positive DC series was large for both materials, which suggests a larger variation in the individual results for this criterion. This can be related to the visual observations, which showed that the high-intensity hotspots and glowing paths responsible for the heavy erosion occurred with varying frequency in the individual samples, which caused the final erosion on the samples to differ as

well. The relatively large standard deviation observed in both the mass loss and the erosion depth criterion for these materials when exposed to positive DC voltage conditions also seem to confirm this. Material B shows a higher average erosion area than material D for the positive DC series. However, this could stem from the fact that three test runs of series DP4-D were interrupted prematurely due to failure occurring in the samples, as opposed to the single failure observed in series DP4-B. The samples of series DP4-B were thus exposed longer to the test conditions, which increased the chance of further erosion occurring in the samples. This might also explain why series DP4-B has a higher average mass loss than series DP4-D.

Material C is a good example of the importance of the combination of erosion depth and area in the formation of erosion of an insulator material. Fig. 101 shows the erosion area measured for series AC4-C to be slightly less than that of series DN4-C, with series DP4-C showing a significantly larger average erosion area than either. The standard deviations show similar magnitudes for all three series. However, series AC4-A showed the highest erosion depth as well as the largest mass loss of all three test series for material C. Series DP4-C, on the other hand, displayed the smallest erosion depth of the three series, but revealed a higher mass loss than series DN4-C, which showed the smallest loss in sample material. This material thus shows that large erosion in a sample can consist either of deep but localized erosion or of shallow erosion areas covering a large portion of the sample surface. However, deep localized erosion seems to result in the most severe loss of insulation material, at least in this type of material.

In general, material C once again shows the smallest variation between the results for this criterion for the three different voltage types, indicating that a change of voltage type has a less significant effect on this material than it does on the other tested materials. In contrast, the erosion area for material A is affected severely by a change in voltage type, showing large variations in its results.

It should be noted at this point that although large erosion areas of even shallow depth are undesirable for any insulator type, the occurrence of deep erosion is highly undesirable, especially for composite insulators. Deep erosion can cause punctures in the sheds of insulators, which severely reduces the creepage distance of the insulator

and increases the risk of a flashover. This type of erosion can also expose the inner core of the insulators by penetrating the housing material, allowing erosion (and possibly tracking) to weaken the core material until mechanical failure of the insulator occurs [7]. The occurrence of deep erosion on insulator materials must thus be taken very seriously.

When combining the results of this criterion with those of the mass loss and erosion depth, a comparison between the two HTV silicone rubber materials shows that material B incurs erosion of a larger severity than material D during both the AC and the positive DC series. This judgement was made according to which material showed higher results for the majority of the three evaluation criteria. A possible explanation for this is the slightly lower filler content in the samples of material B, since fillers like ATH are added to silicone rubber materials to increase their tracking and erosion resistance [19]. Similar results have been observed on field studies on insulator materials under the effects of both AC and DC voltages [55]. However, the negative test series showed a higher erosion severity for the samples of material D than for those of material B, which contradicts the findings of these field studies. A closer inspection of the results where D shows a higher measurement than B in the AC and negative DC series reveals only a slight difference between the series averages, while the large erosion observed in the positive DC series shows a clear tendency for material B to erode stronger than material D. It is thus possible that due to the small difference in filler content between the materials, the effect of filler content on erosion severity only becomes clearly visible for extensive erosion in the materials.

Failures due to severe erosion in the two materials were only observed during the positive DC test series, with material D incurring a larger number of failures than material B. With the samples of material D having a lesser thickness than those of material B, these results correspond well to those of other studies, which state that silicone rubber samples tested using the IPT method have an increased failure rate with decreasing thickness down to 3.0 mm thickness [33]. This observation is attributed to the increased material volume of the thicker samples, allowing them to better conduct and disperse the heat energy of the arcing process. However, the results of this project show that it is only the failure rate that decreases with increasing

sample thickness, while the erosion severity was still observed to be higher for material B during the positive DC series than for material D.

5.3.5 Rms leakage current

The leakage current flowing over the sample surface was measured using the OLCA data logger with a sampling rate of 2 kHz. The OLCA calculates the rms leakage current value and other measurement parameters over a user-defined time interval set at the beginning of the experiment. These intervals were set for a duration of one minute, this being the minimum interval length available for this device, so as to gather a maximum number of data points during each six hour test run.

Due to the large amount of data available for each sample, it was decided to calculate the hourly averages for the rms current for each sample and then perform an analysis based on these results. In order to perform the calculations, the OLCA data files were exported into a Microsoft Excel environment, which allowed for easy manipulation and processing of the data. Since the current measurements were performed during the test runs, no treatment or other manipulation of the samples was necessary after the completion of the test runs for this evaluation criterion. Consequently, all six samples within each test series were considered for this analysis, including the samples selected for chemical testing.

The hourly mean for each test series was then calculated from the hourly averages obtained for each of the six samples within a series, using equation 4.1. The same procedure was followed for the calculation of the hourly standard deviation per series using equation 4.2. An inspection of the hourly averages of the individual samples, however, once again revealed relatively large variations in their magnitudes, indicating the presence of extreme data points. In a process similar to that followed in the previous evaluation criteria, the samples showing the largest deviation from the calculated hourly series means over the entire six hour test period were omitted. The calculations for the hourly series means and standard deviations were then redone based on the data of the remaining five samples within each series. Table E 1 in Appendix E shows the hourly average series means and standard deviations based both on six and five samples for all materials and for each different voltage type.

Fig. 102 shows the hourly series means for the rms currents measured for each material when exposed to the AC voltage. A variation of one standard deviation around each mean is indicated by vertical black lines. The different materials are colour coded as indicated in the legend. Material A shows the highest average currents as well as the largest magnitudes for the standard deviations. The measurements also reveal a rising trend in the data over the entire test duration, causing an increase of the hourly average current by more than 1 mA from the first to the sixth test hour. Materials B and D show similar magnitudes for the first two test hours. At this point, material B develops a continuous declining trend in its leakage currents which continues up to the end of the test period. The current levels in material D, on the other hand, remain fairly constant throughout the experiment, varying around a rms current of ± 11.2 mA (see Appendix E.1). Both materials show relatively small standard deviations, except during the first test hour. Finally, material C shows the lowest current values for the first four test hours, only exceeding the average currents for material B during the last two test hours. The standard deviations for this material remain relatively small throughout the test period, with the biggest variation observed in the first test hour.

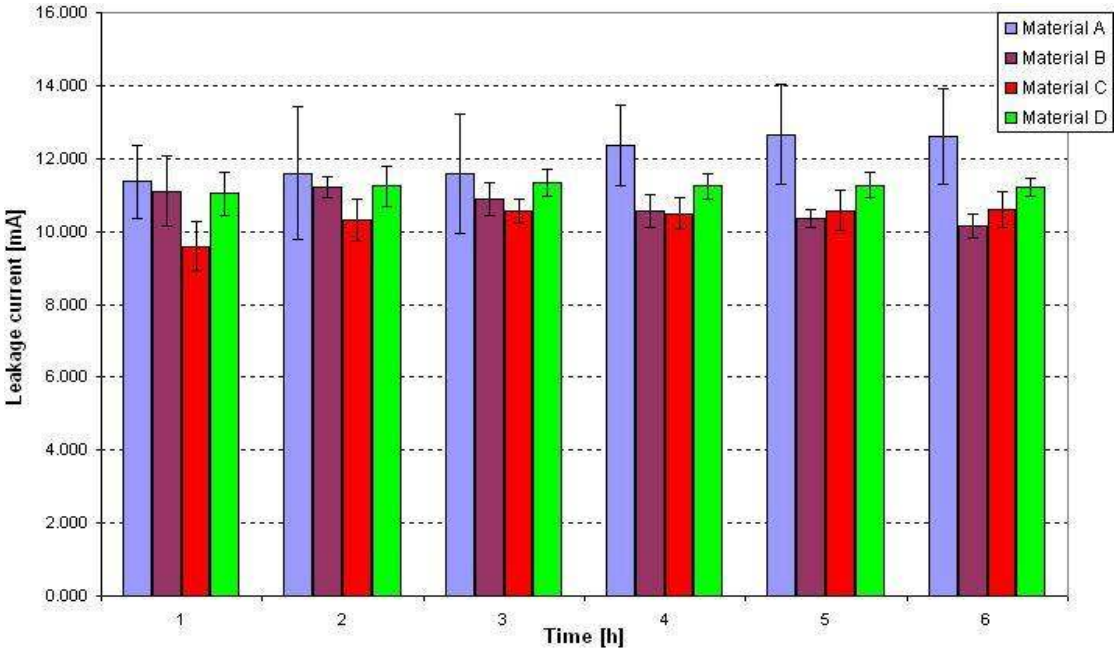

Fig. 102: Hourly average rms currents for four different materials tested under AC conditions.

The leakage current measurements seem to correspond well to the results of the mass loss criterion for the silicone rubber based materials (A, B and D). Material A measured the highest currents of all the materials as well as showing a higher average

mass loss than materials B and D. Material B on the other hand showed the smallest average mass loss between the three silicone rubber materials, as well as measuring the lowest average rms currents for the final four test hours. Furthermore, the relatively large hourly standard deviations observed in material A bear a resemblance to the large variation in the individual mass loss results for the AC test series of this material. There thus seems to be a direct correlation between the magnitude of the rms leakage current and the mass loss experienced by the samples for the silicone rubber based materials. However, material C (EPDM) reveals no such correlation. This material measured the smallest average rms currents for the majority of the test runs while showing the largest recorded mass loss due to severe erosion on the sample surface.

The results for both erosion depth and area also show only weak correlation to the leakage current results for the AC series. Material B shows both a larger depth and surface area for its erosion than material D, while the reverse is true for the leakage currents. Material C again shows the largest averages for both erosion depth and area of all materials for the AC series, while showing the lowest average leakage current. As mentioned previously, care must be taken when comparing the erosion depth of material A to that of the other materials due to the limitation imposed by the coating thickness. However, material A does show a greater erosion area than the other material silicone rubber materials, which again corresponds to the results of the leakage current measurements.

It should also be noted that the increased standard deviation values for the rms leakage currents observed for material B, C and D during the first test hour can be explained by referring back to the visual observations. These materials usually required a certain time period (30 - 90 minutes) to establish constant arcing behaviour at the ground potential electrode, which is required for a continuous flow of leakage current. Since the actual time varied for each individual sample, it is no surprise the rms leakage current values also show a large variation during this time period. Material B shows the largest standard deviation of these three materials during the first test hour, since the samples of this material took the longest time to establish constant arcing behaviour.

Fig. 103 shows the average hourly leakage currents for each test series of the four different materials conducted for the positive DC test voltage. Vertical black lines once again indicate a variation of one standard deviation around the mean value. A special mention must be made of the positive DC test series of material B and D, since these were the only test series where test runs were interrupted prematurely due to the occurrence of sample failure through severe erosion. The hourly average currents of failed samples were not included in the calculation of series mean and standard deviation for those test hours in which the failure occurred, and for all subsequent test hours. The process of choosing the sample to be omitted for the recalculation of series mean and standard deviation was thus also only applied to the test hours during which all samples were active for the full duration. After this time, the failed samples were considered as the extreme data points and were thus already omitted from the calculations. This also explains why the series means and standard deviations based on six and five samples show identical values for the test hours in Table E 1 of Appendix E from the point in time when sample failure occurred.

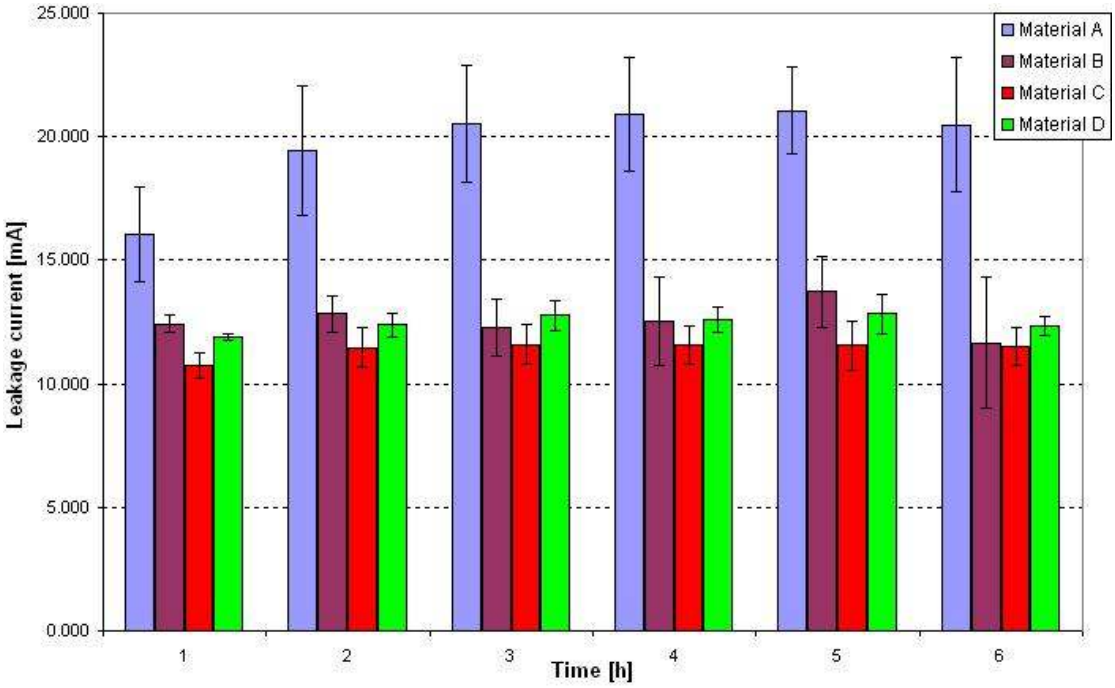

Fig. 103: Hourly average rms currents for four different materials tested under positive DC conditions.

All materials showed an increase in their hourly average positive DC leakage currents compared to the AC test series. This increase in current levels was greatest for material A, whose current levels increased by 5 to 8 mA. Large magnitudes for the hourly standard deviations were also observed for this material, indicating large

variations in the individual results of the samples. The visual observations showed a large increase in the severity of the arcing process. The series averages for mass loss, erosion depth and area were also observed to be larger for this voltage type than for an AC voltage. A good correlation can thus be observed between the rms leakage currents erosion severity for material A. Furthermore, the leakage current for this material displays a rising trend for the first three test hours. During this time, the intensity of the arcing process was also observed to increase. There thus seems to be a direct connection between leakage current levels and arcing intensity.

Apart from showing an increase in the hourly current levels for this voltage type, materials B and D also reveal similar current levels for the majority of the test duration. However, while the current levels stay relatively constant for material D, material B showed a large variation in current levels, especially from the third test hour onwards. This was accompanied by an increase in the magnitude of the hourly standard deviations. A possible explanation for this might be that the samples of material B developed a larger number of interruptions due to the contaminant dropping past the ground potential electrode (see Table 17 and section 5.3.1.5). The resulting absence of current flow in the short period before the application of the cleaning procedure and the re-establishing of the arcing process afterwards had a great influence on the magnitudes of the rms currents measured during these periods. Material D, on the other hand, showed a smaller number of occurrences for interruptions to the test procedure, thus decreasing the possibility of variation within the results. This is further confirmed by the smaller magnitudes for the standard deviations for material D when compared to those of material B.

The increase in leakage current levels is accompanied by an increase in mass loss, erosion area and depth for both materials when tested under positive DC voltage conditions. The intensity of the arcing process was also observed to increase significantly, with a frequent development of hotspots and glowing paths being observed on the samples. These materials thus also show a correlation between leakage current levels and erosion severity. However, the increase in erosion on both materials was extremely high, while the average current levels only increased by 1 to 3 mA. It is thus suspected that the erosion process also depends on other factors besides the leakage current magnitude.

The hourly current levels for material C were also observed to increase by ± 1 mA when moving from an AC to a positive DC voltage. The current levels were observed to remain relatively constant throughout the test period, with the exception of a slightly lower value for the first test hour. This is to be expected, since the visual observations showed that the arcing process required some time (± 30 minutes) to fully establish itself along the ground potential electrode. However, although an increase was observed in the leakage current levels during this test series, the mass loss and erosion depth were less than those measured for the AC test series of this material. Only the erosion area was observed to increase, showing a slight correlation for this criterion to the leakage current measurements. The erosion severity thus seems to rely on other factors than the rms leakage current magnitude for this material.

Finally, the results for the hourly average rms leakage currents of the test series conducted under negative DC voltage conditions are shown in Fig. 104, with vertical black lines again showing a variation of one standard deviation around the mean value.

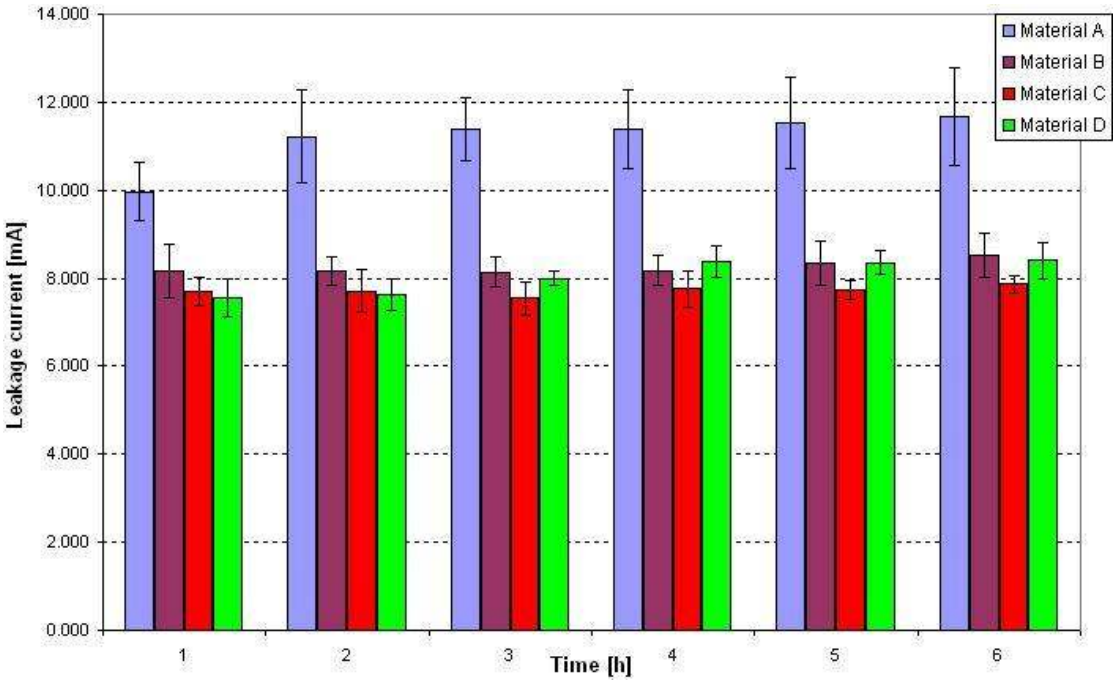

Fig. 104: Hourly average rms currents for four different materials tested under negative DC conditions.

The current values measured during the test series for this voltage type are observed to be lower than those measured for the other voltage types for all four test materials. Material A once again measures the highest average currents as well as the greatest

variation in the hourly results. The current displays a rising trend similar to those observed in the AC and positive DC series of this material. However, the relative current magnitudes remain lower than those measured during the other two test series. These measurements stand in stark contrast to the results for the mass loss and the erosion area criterion, which showed extensive erosion to have occurred on the samples of this test series, far more so than for any other voltage type. The erosion depth measured for test series DN4-A was also slightly larger than that for series AC4-A, despite the latter series measuring larger leakage currents than the former. The extensive erosion observed in this material-voltage combination thus must have been triggered by a factor other than the leakage current magnitude.

Materials B and D once again show comparable results for the leakage current magnitudes for the majority of the test runs. However, material D does show slightly lower average rms currents during the first two test hours than material B. The visual observations revealed that the growth in erosion area for material D only stabilized towards the end of the second test hour, while a stable erosion area was achieved in material within the first 30 minutes of testing. This prolonged time period needed by material D to achieve a stable condition at the ground potential electrode could explain the lower values for the leakage current for that time period. Both materials reveal a rising trend in their hourly averages, with the standard deviations remaining of similar size for both materials.

However, the leakage current levels for this voltage type do not correspond well with the erosion severity observed in the samples of the negative DC test series for both materials. The leakage current levels were observed to be the lowest of the three test series conducted for each material B and D. On the other hand, the materials showed higher values for mass loss, erosion depth and area during this series than for the AC series, where larger leakage current averages were measured.

Material C once again measured the lowest average rms currents of all the materials for the majority of the testing period, only showing slightly higher average currents than material D during test hour one and two. The hourly averages remained fairly constant throughout the test period, with no general trend visible. The magnitude of the hourly rms currents is lower than those measured during the test series for AC and

positive DC voltages. This corresponds with the results for the mass loss criterion, which also revealed the smallest mass loss for this material being obtained during the negative DC voltage test series. However, the results for erosion depth and area do not correspond to this observation, with series DP4-C yielding a smaller average erosion depth and series AC4-C a smaller erosion area than this test series.

Overall, all test materials show a similar behaviour in terms of rms leakage current magnitude for the different voltage types, with an increase in the hourly averages occurring when moving from a negative DC to AC to a positive DC voltage. However, there seems to be little conformity between the erosion severity and the leakage current magnitudes, with the erosion being more severe during DC voltages than for an AC voltage in the silicone rubber materials while the opposite seems to be true for material C (EPDM). The individual erosion parameters (mass loss, erosion depth or erosion area) are observed to vary in intensity for any given material-voltage type combination, with no parameter being equally severe for all materials for any given voltage.

An attempt was also made to investigate the individual data series for the presence of any underlying trends in the rms leakage current data. The rms current data was smoothed before any observations were done in order to remove any large variations which would encumber any analysis of the data. The smoothing technique chosen for this project was adapted from literature describing studies performed on insulator materials using the IPT method [32]. This method is based on the moving average technique, in which each smoothened data point is calculated as the average of a fixed number of data points, which are called the window. The number of data points used is also referred to as the window width. The method used in this project places the smoothened data point at the centre of the window width, according to the equation [32]

$$Y_{sm} = \frac{Av_1 + Av_2}{2}, \tag{5.2}$$

where Y_{sm} represents the smoothened data point and Av_1 and Av_2 donate the average value of the first and second half of the window width, respectively. This process is further illustrated in Fig. 105.

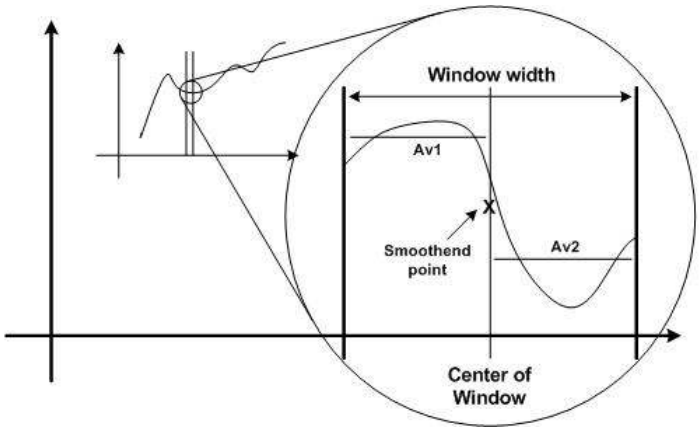

Fig. 105: Smoothing technique employed for rms leakage current data [32].

The advantage of this modification of the conventional moving average technique is that this method takes both past and future data into account when calculating the smoothened data point at a given point in time. The window width was kept at ten data points whenever enough data was available. At the beginning and end of each data series, where sizes of either the first or the second half of the window were limited, the size of the window was reduced to fit the available data. Finally, the first and the last data points of each series were taken at their original value. The plots of the smoothed rms leakage currents for all samples of each individual test series can be found in Appendix E. Fig. 106 shows the smoothened plots for test series DP4-B as an example.

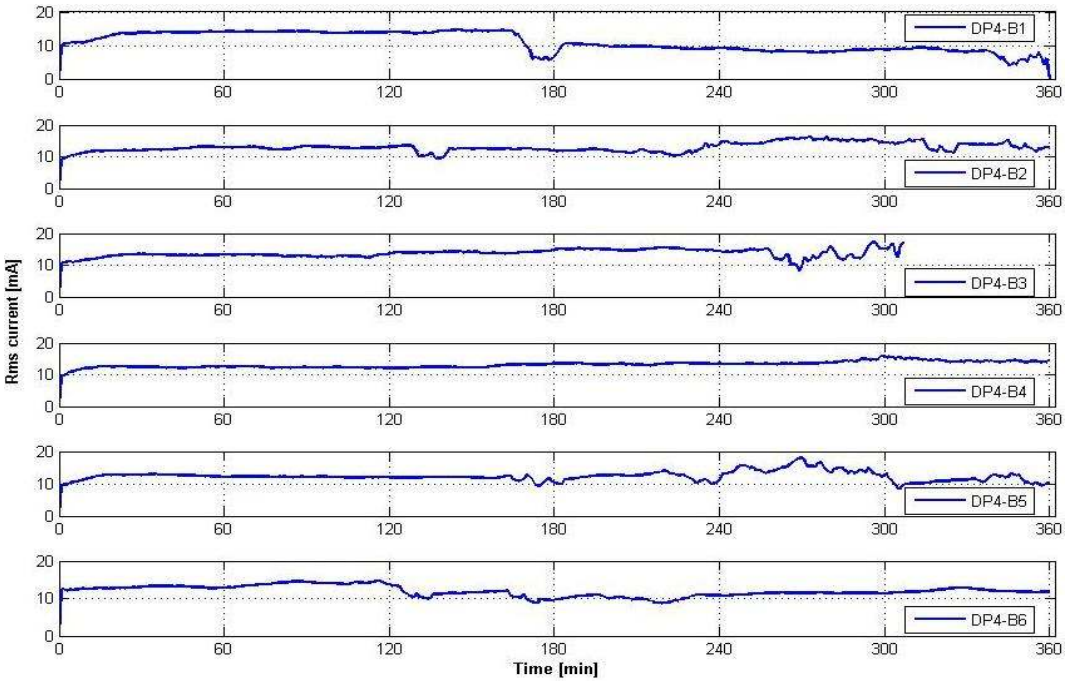

Fig. 106: Smoothened rms current plots for test series DP4-B.

The plots for this particular test series were shown in this text for a specific reason, since a number of highly irregular current flows were observed in most of the sample plots, disturbing the otherwise very smooth plots. Upon inspection of the test reports, it was found that these periods coincide exactly with the time periods where the tests were interrupted to apply the cleaning procedure described in section 5.1.3.5, to prevent the contaminant from dripping past the ground potential electrode. Since the current flow was zero for a short time before the test was interrupted to clean the sample surface, and arcing had to re-establish itself after the test was resumed, irregular leakage current values can be expected during these periods. The numbers of irregular periods displayed in each sample in Fig. 106 correspond well to the number of interruptions recorded in Table 17. For example, sample DP4-B5 incurred the largest number of interruptions and thus also shows a larger occurrence of irregular periods of current flow. Sample DP4-B4, on the other hand, never had to be interrupted and thus maintains a smooth current flow throughout the entire test period. Similar observations were also made for test series DP4-D, where interruptions to the test procedure occurred as well.

Fig. 106 also shows that failed samples are plotted until the time of occurrence of the failure, after which the plot is discontinued since no further leakage current measurements were taken. An exception was made for samples DP4-B1 and DP4-D4 (see Appendix E.2), where the current is shown to return drop to zero before the test was concluded. The reason for this behaviour in sample DP4-B1 was that the contaminant started to drip past the electrode in the final two minutes of the test. Since the test was nearly completed, it was decided not to interrupt the test procedure, which results in the last measured current values to be zero. A similar situation was observed in sample DP4-D4, where the interruption to the contaminant flow occurred in the interval just before the sample was classified as failed. The last valid measurement (during which the sample was classified) was allowed to run to completion before the test was stopped, resulting in a zero value for the rms current for that period. The current plot thus drops down to zero for the final data point.

In order to determine if the individual test series did indeed show trends in the rms leakage current measurements of their respective samples, a cross correlation analysis was performed between all the samples within each series. The analysis was

performed on the data of two samples at a time, with the correlation coefficient r being calculated by [58]

$$r = \frac{\sum_{i=1}^{N}\left[\left(x_i - \bar{x}\right)\times\left(y_i - \bar{y}\right)\right]}{\sqrt{\sum_{i=1}^{N}\left(x_i - \bar{x}\right)^2 \times \sum_{i=1}^{N}\left(y_i - \bar{y}\right)^2}}, \tag{5.3}$$

where x_i and y_i donate the values of data series x and y at position i and N represents the total number of data points within each series. The series averages $\bar{x}$ and $\bar{y}$ are calculated by

$$\bar{x} = \frac{\sum_{i=1}^{N} x_i}{N} \tag{5.4}$$

and

$$\bar{y} = \frac{\sum_{i=1}^{N} y_i}{N}. \tag{5.5}$$

The value of the correlation coefficient falls into a range of $-1 < r > 1$, with -1 indicating a perfect but inverse relationship and 1 a perfect and direct relationship between the data series. A value of 0 suggests that no correlation exists between the data sets. Although it is customary to calculate the square of the correlation coefficient to gain a measure of the magnitude of the correlation, this was not done in this analysis. The reason for this is to gain an appreciation of the nature (inverse or direct) of the correlation between to data sets. A negative value for r was qualified similarly undesirable as a value close to zero, since one would expect samples of the same material and tested using voltages of the same type and magnitude to show similar behaviour in their measured leakage currents, i.e. a positive value of r close to the maximum value of 1.

The correlation analysis was performed for each test series for three different time periods: the first half hour, the first full test hour and the entire test period. The first two periods were used to check the behaviour of the samples during the initial phase of testing, to see if the arcing behaviour established itself similarly for all samples of a specific test series. The results of the cross correlation analysis for the three time periods of each series can be found in Appendix E.3. It should be noted that for test

series DP4-B and DP4-D, the 'full' test period only covers the time until the earliest failure was observed in any of the six samples. This was necessary, since the number of data points N must be equal for every data series in order to perform a correlation analysis between all the samples of a test series. To check the overall correlation of the each series, the average of all the correlation coefficients between the different samples was calculated for each time period and for each series. These averages are displayed in Table 24.

Table 24: Average values for correlation analysis for rms leakage currents of test series.

Material	AC Series			DC+ Series			DC- Series		
	30 min	60 min	Full period	30 min	60 min	Full period	30 min	60 min	Full period
A	0.310	0.273	0.029	0.922	0.945	0.628	0.899	0.911	0.802
B	0.339	0.242	0.314	0.873	0.796	-0.021	0.448	0.141	0.084
C	0.007	-0.047	0.144	0.178	0.485	0.540	0.875	0.788	0.318
D	0.506	0.355	0.160	0.287	0.383	0.267	0.003	0.153	0.388

However, a close inspection of the correlation coefficient tables in Appendix E.3 showed that some samples continuously displayed negative values when compared to all other samples for a given time period and test series. Since these negative values strongly influence the average value for the correlation coefficient, the calculations were redone while omitting these specific samples in order to observe if the remaining samples showed a better correlation. Table 25 shows the average values for the correlation coefficients after these samples were omitted. Coloured fields indicate a change in the coefficient value due to sample omission. The omitted samples are all indicated in the tables of Appendix E.3.

Table 25: Recalculated correlation coefficient averages for rms leakage currents for test series.

Material	AC Series			DC+ Series			DC- Series		
	30 min	60 min	Full period	30 min	60 min	Full period	30 min	60 min	Full period
A	0.912	0.808	0.029	0.922	0.945	0.628	0.899	0.911	0.802
B	0.339	0.242	0.314	0.873	0.796	-0.021	0.788	0.141	0.084
C	0.007	-0.047	0.528	0.521	0.485	0.540	0.875	0.788	0.318
D	0.506	0.355	0.160	0.842	0.812	0.267	0.003	0.153	0.388

In series AC4-A, sample AC4-A6 showed an inverse relationship to all other samples in the series during the first 30 and 60 minutes of the test duration. The other five samples showed very good correlation between them during this specific period. Sample AC4-A6 was already mentioned in section 5.3.1.1 to be a special case, since

its surface was not abraded prior to test begin. On inspection of the plots in Appendix E.2, it can be seen that the leakage current rose swiftly during the first couple of minutes, after which the current started to decrease steadily until reaching a more or less constant value at the end of the first test hour. All other samples showed an increasing trend in the rms currents during the first 30 minutes, after which the current level also remained at relatively constant level from the end of the first test hour onwards. The visual observations confirmed that sample AC4-A6 initially showed an increased arcing performance, but showed a similar performance to the other samples for the majority of the test duration. No general correlation can be observed between the samples for the full test duration. Still, the initial difference in arcing behaviour of sample AC4-A6 once again raises questions about the validity of the initial abrading of the test samples.

The other test series for the AC voltage type showed no significant correlations between the samples. A small increase was observed in the average value for the full test period series AC4-C after omitting sample AC4-C3, but the correlation between the remaining samples still remained relatively weak. The plot of AC4-C3 shows a decrease in current level at the end of the first test hour, after which the current then stabilizes at a much lower value than for all other samples of the series. However, visual observations revealed no explanation for this behaviour. It should also be noted that sample AC4-C3 showed slightly larger values for mass loss, erosion area and depth than sample AC4-C2, which measured higher rms currents for almost the entire test duration.

For the test series for the positive DC voltage, material A showed a very strong correlation for the rms currents during the first test hour. The samples showed a rising continuous rising trend in this time, which coincided with the stabilization of the arcing behaviour during this period. The currents tended to stabilize after the first test hour. However, the samples showed a largely reduced degree of correlation over the entire test time due to differences in the current behaviour. This was especially true for sample DP4-A3, which showed large interruptions in its arcing behaviour during the final test hour due to a puncture in the ceramic tile caused by excessive arcing. However, a greater correlation between the samples was observed for this material-voltage combination then for the AC series.

Series DP4-B and DP4-D showed similarly strong correlations for the fist 30 and 60 minutes. Both materials revealed a rising trend in the leakage current during this time, since the arcing process was observed to stabilize itself during this time period, developing into constant arcing at the ground potential electrode. The plots further show that the currents remained fairly constant after the first test hour. The weak correlation between the samples of each material over the full test period can be explained by the interruptions to the contaminant flow, which occurred during both test series and which resulted in irregular current flows, as described previously. Series DP4-B showed a larger number of interruptions than series DP4-D, which can be seen in the very low average correlation coefficient for the former series. From Table 24 and Table 25, it can be seen that series DP4-D only showed a strong average for the coefficients after sample DP4-D1 was omitted. This sample showed increased arcing during the first couple of minutes, which resulted in the current rising to a higher value than that observed for the other samples. The arcing then started to diminish slightly, resulting in a decreasing trend until the current level reached a relatively constant level by the end of the first test hour.

Material C showed only moderate levels of correlation between the currents measured for its samples. A general tendency for the currents to remain more or less constant for the entire test duration can be seen. However, this behaviour was not observed equally strong for every sample. The average coefficient during the first 30 minutes for this series was improved after omitting sample DP4-D1. This sample showed a slight drop in its current level during this period, since its arcing process was somewhat more interrupted than that of the other samples during this time.

Finally, material A revealed a very strong correlation between its samples for the negative DC test series for all three periods. The leakage current plots show a rising trend in the currents for the first test hour, during which arcing behaviour stabilized and the majority of the erosion occurred. After this, the current levels remain largely constant throughout the remainder of the test period.

Material B, on the other hand, only showed a strong correlation for the first 30 minutes of the test, and only after sample DN4-B3 was omitted. The samples showed an increasing trend in their current levels during this period. Sample DN4-B3, on the

other hand, displayed a fairly constant current level during this time. No explanation can be found for this behaviour due to a lack of recorded visual information during these early minutes. Test series DN4-B showed no further discernable trends during the rest of the test period, which is indicated by the low average values for the correlation coefficient. This behaviour was also observed for series DN4-D, which additionally showed no general trends during the first 30 minutes.

Material C showed a relatively strong correlation between its samples for both the first 30 and 60 minutes of the test. The currents tended to rise in magnitude until the 30^{th} minute, at which point a slight decrease could be observed until a relatively constant level was reached at the end of the first test hour. However, the currents showed some variation for the different samples after the first test hour. As a result, the samples showed very little correlation between them over the full test period, which is discernable in the low average for the correlation coefficients.

Overall, both the positive and the negative DC test series resulted in greater correlation between the leakage currents of the samples of the different materials. This was to be expected, since the arcing behaviour of most of the samples was observed to be much more stable under these voltage types then for the AC voltage. However, the results differ from material to material as well for the different time periods. The samples of material A showed the best correlation between its samples for all three voltage types.

5.3.6 Average dissipated power

During each measurement interval, the OLCA logger multiplies the voltage and the current measured at each sampling instance to obtain a true power measurement. It then calculates the average power dissipated over the entire measurement interval, which for this experiment was kept at a length of one minute, and logs the resulting value. The user can configure the device manually in order to select which of the three existing voltage channels is paired with which one of nine possible current channels for the power measurements. During this experiment, the voltage measured directly across the test sample was combined with the leakage current measurements in order to obtain an accurate reading of the electrical power dissipated in the sample, without

the inclusion of other power dissipating elements in the circuit (e.g. the current limiting resistance).

In order to reduce the large amount of data measured for each sample, it was decided to again calculate the hourly averages of the dissipated power for each sample within a test series. Once this was completed, the mean value and the standard deviation of the test series for each full test hour were calculated using the hourly averages of all six samples within the series. Equations 4.1 and 4.2 were once again used to calculate the series mean and standard deviation, respectively. The samples showing the largest accumulative deviation from the hourly series means for the entire testing period within each test series were omitted. The values of the series mean and standard deviation were then recalculated based on the hourly averages of the remaining five samples of each series. This procedure was once again done with the intent to reduce the variation in the sample measurements caused by the presence of extreme data points. Table F 1 in Appendix F shows the hourly averages of each test series for the average power dissipated per measurement interval, also indicating the series mean and standard deviation for both five and six samples per series.

Fig. 107 shows the plots for the hourly averages of the dissipated power based on five samples per test series for all four materials and each voltage type. A variation of one standard deviation around the hourly mean is indicated by black vertical lines.

It should be noted that the process of choosing the sample to be omitted for the five-sample based calculation of series mean and standard deviation was once again only applied to test hours survived by all samples without failure. For the periods during and after which a failure was observed in any sample of the series, the failed samples were considered to be the extreme data points. Since these samples were not included in the calculations for the hourly series average for these periods, they were already considered to be omitted from the calculations.

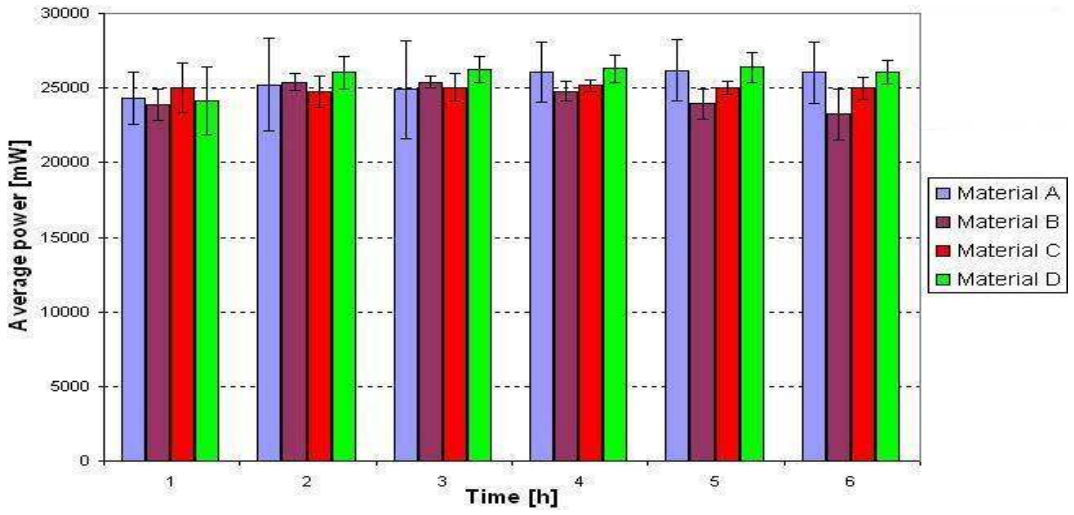

(a)

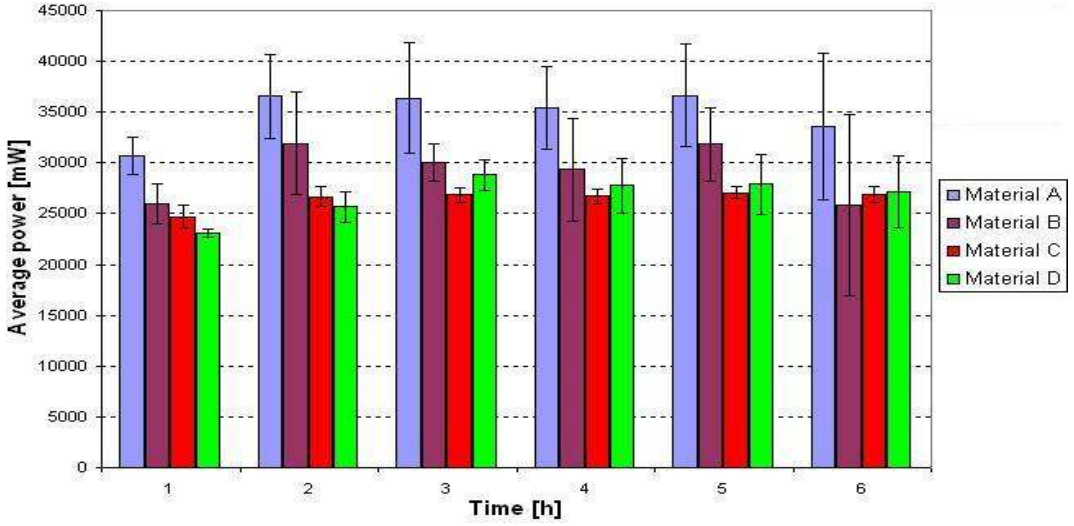

(b)

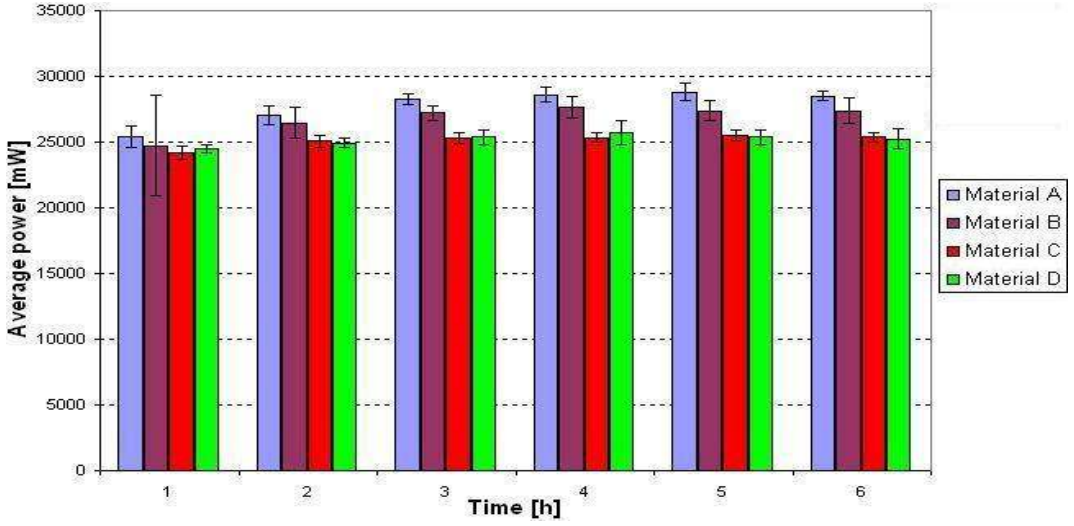

(c)

Fig. 107: Average power dissipated per measurement interval during each full test hour: (a) AC voltage, (b) Positive DC voltage and (c) Negative DC voltage.

Material A showed the highest hourly averages for dissipated electrical power during its positive DC series, which corresponds well to the results of the leakage current criterion. However, the hourly power averages measured during the AC test series displayed the lowest values for this material, whereas the lowest hourly currents were observed during the negative DC test series. A better correlation was observed between the relative standard deviations for the two evaluation criteria. The smallest deviations in both average power and rms leakage current were observed during the negative DC series, the highest during the positive DC series. The two evaluation criteria thus show good correlation between them in terms of data stability for this material.

A larger amount of power dissipated over the samples should be expected to result in a larger erosion severity, since a larger amount of electrical energy is converted into heat and other forms of energy and thus made available to cause erosion or chemical changes along the sample surface. However, such a relationship was not observed in this material, since the negative DC series showed the highest measurements for mass loss and erosion area, but not for the hourly dissipated power for this material. On the other hand, the highest power losses and erosion depths were observed during the positive DC series. However, since the differences between the series averages are far more severe for the mass loss and erosion area criteria than for the measured erosion depth, there seems to be no correlation between erosion severity and electrical power for this material. This provides further basis for the assumption that another process is responsible for the large erosion observed in the samples of series DN4-A.

Materials B and D showed the largest hourly averages for both dissipated power and rms leakage current during the positive DC test series, indicating a good correlation between these two criteria. However, only material D showed a similar correlation between the criteria for the AC and negative DC series. For material B, the hourly averages for the dissipated power were higher for the negative DC than the AC series, with the reverse being true for the leakage currents. While material D thus shows a good correlation between leakage current and dissipated power during all its test series, no such overall correlation can be observed for material B.

In addition, materials B and D show different strengths of correlation between erosion severity and dissipated power. Both materials showed increasing measurements for mass loss, erosion depth and area when moving from AC through negative DC to the positive DC series. As described earlier, only material B showed a similar trend in its power measurements, whereas for material D, the hourly averages for dissipated power were higher for the AC series than the negative DC series. However, both materials showed maximum values for both dissipated power and erosion severity during the positive DC series. These results indicate that, for HTV silicone rubber materials, major erosion can be caused by large leakage currents with an accordingly high dissipation of electrical power. However, erosion seems to rely on other process as well in order to determine its severity.

Finally, material C also showed only weak correlation between the measurements for leakage current and dissipated power. The measurements for the dissipated power showed an increase in the values for the hourly averages when moving from the AC to the negative DC series, while the reverse was true for the leakage current measurements. The highest values were recorded for both criteria during the positive DC series. A weak correlation was again observed between the power measurements and those for erosion severity in material C. The AC series showed larger mass loss and erosion depth in its samples than either of the DC series, while hourly averages for dissipated power reached the lowest values under AC conditions. Furthermore, the erosion depth results revealed larger values for the negative than the positive DC series, which further contradicts the results for the dissipated power for this material.

In terms of erosion severity, a correlation was only observed between erosion area and dissipated power, where both criteria increased in the values of their results for the same sequence of test series, indicated here in an ascending order in terms of magnitude of their results: AC, negative DC and positive DC. The weak correlation between dissipated electrical power and erosion severity thus suggests that a release of electrical power is not the primary factor for the cause of erosion in this material.

Table 26 shows the four test materials arranged in sequences of descending order in terms of their results for the criteria of erosion severity, rms leakage current and average dissipated power for each of the three different voltage types.

Table 26: Order of materials according to results for the evaluation criteria.

Voltage type	Evaluation criterion				
	Rms leakage current	Average dissipated power	Erosion severity		
			Mass loss	Erosion depth	Erosion area
AC	A > D > B >C	D > A > C > B	C > A > D > B	C > B > D > A	C > A > B > D
DC+	A > B > D > C	A > B > D > C	B > D > C > A	B > D > C > A	B > A > C > D
DC-	A > B > D > C	A > B > D > C	A > C > B > D	C > D > B > A	A > C > D > B

This overall comparison seems to suggest that a correlation exists between the results for the leakage currents and dissipated electrical power for the negative and positive DC series, but not for the AC series. However, the comparisons of the results for each voltage type and each individual material have shown that a correlation only exists between these two criteria for the positive DC series, which showed the highest results for both criteria for all materials. The results for the other series varied in the order of their magnitudes for each material.

Table 26 shows a very weak correlation between the relative magnitudes of rms leakage current and average dissipated power for all materials during the AC test series. It was already stated that the OLCA measures the true power by multiplying each voltage measurement with each corresponding current measurement during the sampling process. It was suggested by Vosloo et al. that the equivalent circuits of the dry band arcing process on polluted insulator surfaces can be modelled as shown in Fig. 108 [58].

The circuit models indicate that, during the inception of the arcing process, the impedance presented by the dry band posses large capacitive as well as a small resistive component (see Fig. 108 (a)). The same is observed for the circuit model representing the extinguishing phase of dry band arcing, which occurs when the dry band has grown to a sufficient width so that the electric field strength is too low to maintain full arcing (see Fig. 108 (b)).

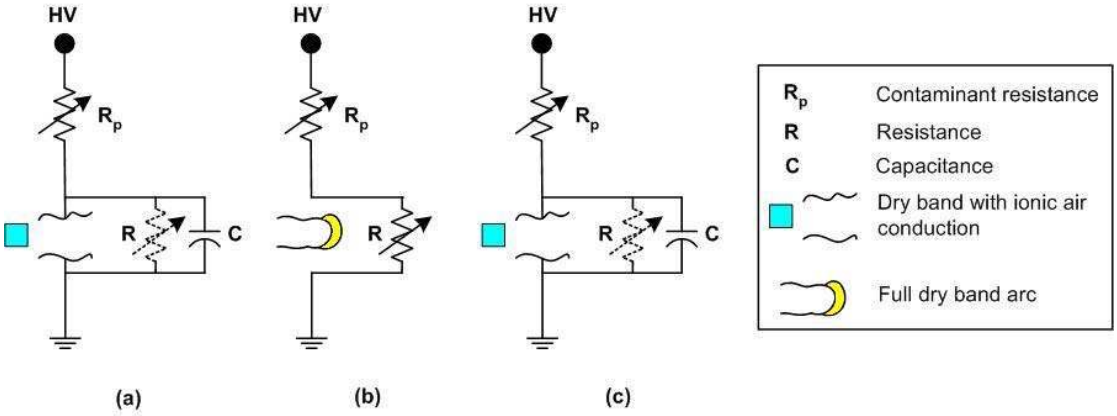

Fig. 108: Equivalent circuits of dry band arcing process on polluted insulator surfaces: (a) Arcing inception due to ionisation of air, (b) Full dry band arcing and (c) Extinguishing of arc with ionic by-product remaining [58].

Since the visual observations revealed the arcing process to be frequently interrupted during the AC test series for the different materials, circuit models (a) and (c) in Fig. 108 also occurred frequently. The capacitance in these circuit models will result in the formation of a reactive power component, which is not picked up by the OLCA since it only measures real (true) power. This would explain the lack of correlation between the rms leakage current and the dissipated power observed in Table 26. However, this effect was not observed during the DC measurements, since capacitors have no effect on the waveforms of a DC voltage. Accordingly, the two DC test series showed good correlations between the relative magnitudes of leakage current and dissipated power measured for the different materials (see Table 26).

Table 26 also shows a weak correlation between the materials according to their results for average power and erosion severity for each voltage type. There thus seems to be no concrete relationship between measured dissipated electrical power and the erosion severity for the different materials for a specific voltage type. However, if one discards material A for this comparison, since these samples are limited in terms of mass loss and erosion depth due to the material being a coating, a correlation can be observed for the positive DC test series between the criteria of dissipated power, rms leakage current, mass loss and erosion depth. This relationship indicates a larger erosion severity for increased values of power and rms current, and materials B, C and D seem to conform to this relationship. However, such a correlation does not exist for the criteria of leakage current, dissipated power and erosion area for this test series and these materials. In general terms, the dissipated power results thus show only

weak or no correlation to the erosion severity for the different materials of a given test voltage type.

The weak correlation between erosion severity and dissipated power in the silicone rubber based materials (A, B and D) for the AC test series is also reported in other works. Studies performed by Meyer et al. [32] suggest that the temperature of the hotspots formed during the arcing process on silicone rubbers does not correspond to the fundamental but rather the 3rd harmonic of the power measurements. These studies also show the existence of a good correlation between the arcing temperature and the resulting mass loss. However, Meyer et al. also reported that irregularities were observed in the comparison of the 3rd power harmonic and the resulting mass loss. These were ascribed to isolated high temperature spots caused not by the dissipation of electrical energy but rather by exothermic chemical reactions, causing erosion above that resulting from dry band arcing [32]

5.3.7 Sample hydrophobicity

As described in the sections of the literature review, insulator materials made from polymer compounds exhibit a strong surface hydrophobicity. These materials also have the ability of transferring their hydrophobicity to pollution layers covering their surfaces. Hydrophobicity can also be lost by various processes, such as electrical surface discharges or leaching of LMW molecules through excess water accumulating on the material surface. However, it can also be regained after a sufficiently long resting time. Since the test materials used in this project are all made from polymeric compounds, it was decided to test the surfaces of the samples after completion of the test runs in order to evaluate the surface hydrophobicity of each individual material.

All tests for hydrophobicity during this project were done using the spray method described in the International IEC Standard 62073 [59]. During this method, the sample surfaces were sprayed with a fine mist of deionised water. The mist was produced using a handheld spray bottle, with the distance between nozzle and sample surface being kept at 15 to 35 cm. The spraying of the surface was continued for a total duration of 20 to 30 seconds. After the spraying procedure was completed, the appearance of the sample surface was then compared to guidelines given in the

standard in order to ascertain the hydrophobicity or wettability class (WC) of the sample surface [59]. A total of seven wettability classes exist, with WC 1 being the most strongly hydrophobic, while WC 7 represents a surface that has formed an uninterrupted fluid film across its entire area, indicating an entirely hydrophilic surface. Photographs of each wettability class as well as a table containing more detailed descriptions of their individual appearances are given in Appendix G.

The judging of the surfaces was done in a period of 10 seconds after the completion of the spraying. Photographs were taken at this point in order to obtain visual records of the hydrophobicity of the sample surfaces. Both during classification and photographing, the samples were placed on a stand elevated at an angle of 30° from the horizontal. Although this is not mentioned in the standard, it was done to allow the water to flow along the surface more easily so as to allow a better distinction between the formation of individual water droplets (hydrophobic behaviour) or water runnels, possibly even a continuous water film (hydrophilic behaviour). Additionally, it should be kept in mind that surfaces on insulators used in the field are seldom orientated at a perfect zero elevation. Since the spray method is commonly used for insulators in active applications, elevating the samples allows for a better correlation between the results of the IPT method and field observations.

However, it was already mentioned that the surface of each test sample was abraded before testing commenced in order to allow for an unhindered flow of the contaminant along the sample surface. This procedure is described in the IEC 60587 standard in conjunction with the testing of samples displaying a high level of surface hydrophobicity. By abrading the samples, their surface hydrophobicity was thus already decreased before the actual tests began. In order to make an accurate observation about possible changes in the sample hydrophobicity during the tests, it was necessary to first establish if the materials were able to recover from the loss of hydrophobicity caused by abrasion even if not subjected to the IPT method, i.e. when in a virgin state.

A virgin test sample of each material was thus taken and its surface cleaned using distilled water and propanol alcohol only, after which the hydrophobicity of the surfaces was tested and recorded. The sample surfaces were then abraded and rinsed

with distilled water to remove any excess material from the surfaces. The surfaces were then tested again in order to determine the difference in surface hydrophobicity brought about by the abrasion process. The samples were then tested for their surface hydrophobicity at hourly intervals for a period of six hours in order to observe the change in hydrophobicity over a time period equal in length to the test runs of the IPT method. Additionally, two measurements were done at 12 and 24 hours after the abrasion of the virgin samples to check if any changes occurred over a longer period of time. The results of the hydrophobicity measurements for these untested samples are shown in Table 27.

Table 27: Results for hydrophobicity tests of virgin samples before and after abrasion.

Material	Instance of hydrophobicity testing									
	Before abrasion	After abrasion	Hour 1	Hour 2	Hour 3	Hour 4	Hour 5	Hour 6	Hour 12	Hour 24
A	1	2	1	2	2	1	2	2	1	2
B	2	5	4	4	4	4	4	4	3	4
C	1	6	5	5	5	5	5	5	5	5
D	1	5	4	4	4	4	4	3	3	3

For a better visual comparison, these results are also plotted in Fig. 109, using vertical bars to indicate the wettability class for each sample at different test instants. The bars are colour coded to indicate the different materials. A dashed vertical line indicates the instant of surface abrasion.

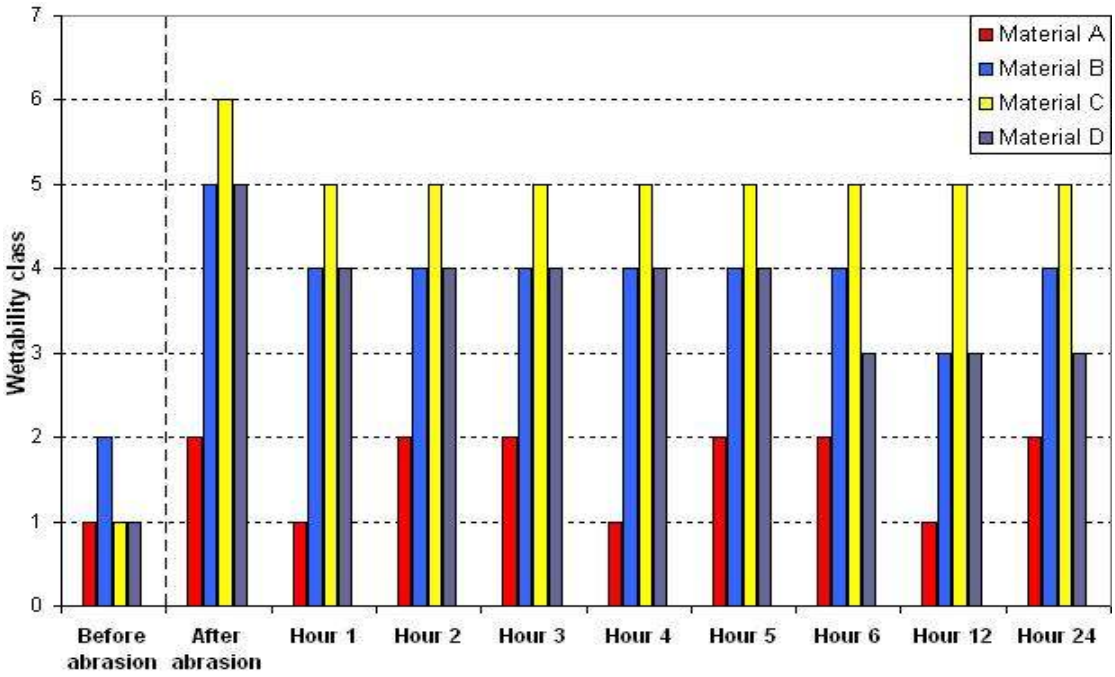

Fig. 109: Plotted results for hydrophobicity tests on virgin samples before and after abrasion.

All materials showed a very high degree of hydrophobicity before surface abrasion, as was expected due to all materials being of a polymeric nature. Material B revealed a slightly higher wettability class than the other materials, but was still observed to be highly hydrophobic. However, the abrasion process resulted in a severe loss of hydrophobicity in most of the samples.

The sample of material C showed the highest loss of surface hydrophobicity directly after surface abrasion, with a large amount of its surface area covered by a continuous water film. A slight recovery of hydrophobicity was observed after the first hour. From this point onwards, however, the wettability class of this material remained at a relatively high level of five for the remaining test procedure, showing no improvement even after 24 hours. It can thus be concluded that the initial abrasion of the samples of material C cause a permanent loss of the majority of their surface hydrophobicity.

A large loss of surface hydrophobicity was also observed for the samples of materials B and D directly after the abrasion process, but to a lesser extend than what was observed for material C. Both materials showed a slight recovery in surface hydrophobicity after the first hour, which then remained constant for the following four hours. After six hours, material D showed another recovery of one wettability class, after which it remained constant at a class of WC 3 even after 24 hours. Material B, on the other hand, showed a decrease in the wettability class only after 12 hours, followed by a slight increase after 24 hours. Material D thus showed a slightly faster and stronger recovery of surface hydrophobicity than material B, with both materials yielding a stronger response than material C. However, a slight permanent loss of hydrophobicity still occurred, since none of the two materials fully recovered its surface hydrophobicity initially shown before the abrasion process.

Finally, the sample of material A yielded the smallest loss of hydrophobicity through abrasion of the sample surface, with a rise of only one wettability class. Furthermore, the sample showed frequent oscillations between the classes WC 1 and WC 2 throughout the measurement period, but never rising above a class of WC 2. These two classes indicate the highest levels of surface hydrophobicity and are very similar in appearance (see Appendix G). A clear-cut distinction between the two classes is

thus very difficult, which could be the reason for the large variation in the results for this material. However, it can be safely stated that the abrasion process causes no large permanent loss of surface hydrophobicity in this material. In fact, it does not even seem to induce a great temporary change in the samples.

Judging by these results, the validity of the abrasion process when testing polymer insulator samples must once again be called into question. The large degree of surface hydrophobicity as well as the ability to recover it when lost is one of the greatest advantages of these materials when used for practical applications. Reducing this effect might create test conditions that are more severe and harsh than any conditions found within the field, since surfaces of insulators newly installed in the field are not abraded in any way. Abrading the samples might thus yield exaggerated results for this kind of laboratory test. Moreover, since not every material is equally affected by the abrasion process, it can also influence the results of a comparison between the various materials, leading to erroneous results. Careful consideration should thus be given concerning the usefulness of the abrading process and its possible influence on the test results.

After having established the influence of the abrasion process on the surface hydrophobicity of the materials, the tested samples were investigated concerning this criterion. Again, the spray method was used for these tests and was executed in the manner as previously indicated. Since the tested samples showed varying amounts of waste deposits on their surfaces, it was decided to check the surface hydrophobicity of each sample twice: once directly prior to the cleaning of the samples (i.e. with the surfaces still covered by deposits) and once immediately afterwards. The first test was done to see if the samples were still able to turn a pollution layer hydrophobic after the completion of the test runs, while the second test was done to evaluate the hydrophobicity in the remaining insulator material. In order to give the samples enough time to recover (if still possible), the samples were only tested regarding their surface hydrophobicity after a minimum period of 24 hours.

Each test sample was further divided into three separate areas according to the distance measured along the longitudinal axis of the samples from the ground potential electrode upwards. These areas were nominated as the lower 17 mm, the

middle 17 mm and the upper 16 mm region, to make up a total distance of 50 mm between the electrodes. The width of each specific area was taken as the width of the sample. Finally, a distinction was made between affected and unaffected regions within each area on a test sample. The affected area covered those locations where a continuous contaminant stream or frequent dry band arcing was observed, which usually coincided with the central region of each area. The unaffected area encompassed those regions which were largely untouched by either the contaminant fluid or electrical discharges. Such regions were usually located along both sides of the sample. The typical locations of the different areas are indicated in Fig. 110, but exact positions were observed to vary occasionally between samples. Photographs were taken of each sample immediately after the spraying procedure so as to accurately classify each separate region.

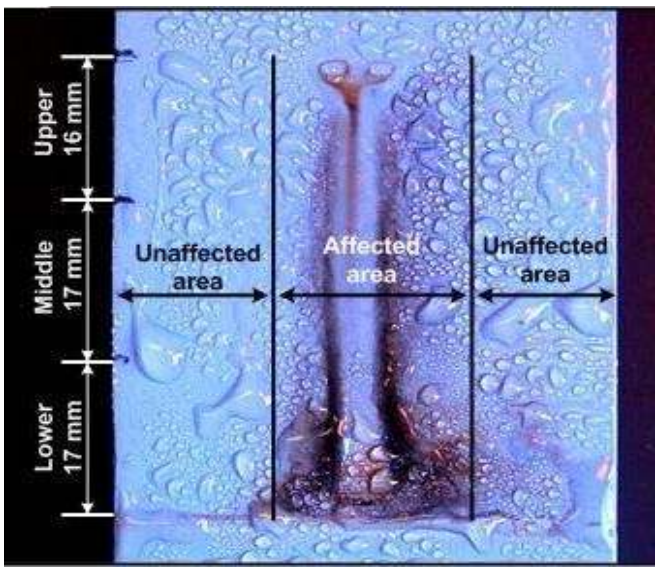

Fig. 110: Allocation of regions investigated for surface hydrophobicity.

The results for each specific region within a test area of the individual samples were then used to calculate the series mean as well as the standard deviation for each region. The samples selected for chemical testing are not considered for this evaluation criterion, since the surfaces of the samples had to be cleaned during the proceedings. This once again leaves a total of five samples per test series. The usual procedure of finding and omitting the sample with the largest deviation from the series mean was not followed for this criterion, since the standard deviations revealed very little or no variation in most results. The analysis was thus done using only the values for series mean and standard deviation based on five samples per series. Table 28 shows the series mean values for every specific area of the samples in a test series.

A complete table showing both the series mean and standard deviation for the different areas of each test series can be found in Appendix G.

Table 28: Series means for wettability class of specific areas on test samples.

Voltage type	Material	Data type	Hydrophobicity classification for area:											
			Lower 17 mm				Middle 17 mm				Upper 16 mm			
			Affected		Unaffected		Affected		Unaffected		Affected		Unaffected	
			Before	After	Before	After	Before	After	Before	After	Before	After	Before	After
AC	A	Series mean	6	2	3	1	6	2	2	1	6	2	2	1
	B	Series mean	5	3	4	2	6	3	4	3	6	3	3	2
	C	Series mean	7	4	7	5	6	4	6	5	6	4	5	5
	D	Series mean	6	4	5	3	7	4	5	2	6	3	4	3
DC+	A	Series mean	7	6	5	2	7	5	5	3	7	4	3	2
	B	Series mean	1	2	2	3	5	4	2	3	6	4	2	3
	C	Series mean	6	5	6	6	5	6	6	6	5	5	6	6
	D	Series mean	2	1	3	5	6	5	3	5	6	5	3	5
DC-	A	Series mean	7	6			7	6	5	3	6	4	4	4
	B	Series mean	5	2	5	4	6	4	5	4	5	4	5	4
	C	Series mean	7	7	7	6	7	7	7	6	7	7	6	6
	D	Series mean	5	4	7	4	7	5	7	4	6	5	6	5

The series means for the various evaluated regions of each test series were also plotted for a better visual comparison of the data, using vertical bars to indicate the average wettability class for each specific location. Different colours and filling patterns were used to distinguish between the affected and unaffected areas as well as between the readings taken before and after the washing of the samples. The plots for the different test series of each material are displayed in Appendix G. As an example, Fig. 111 shows the plots of the results for series AC4-A.

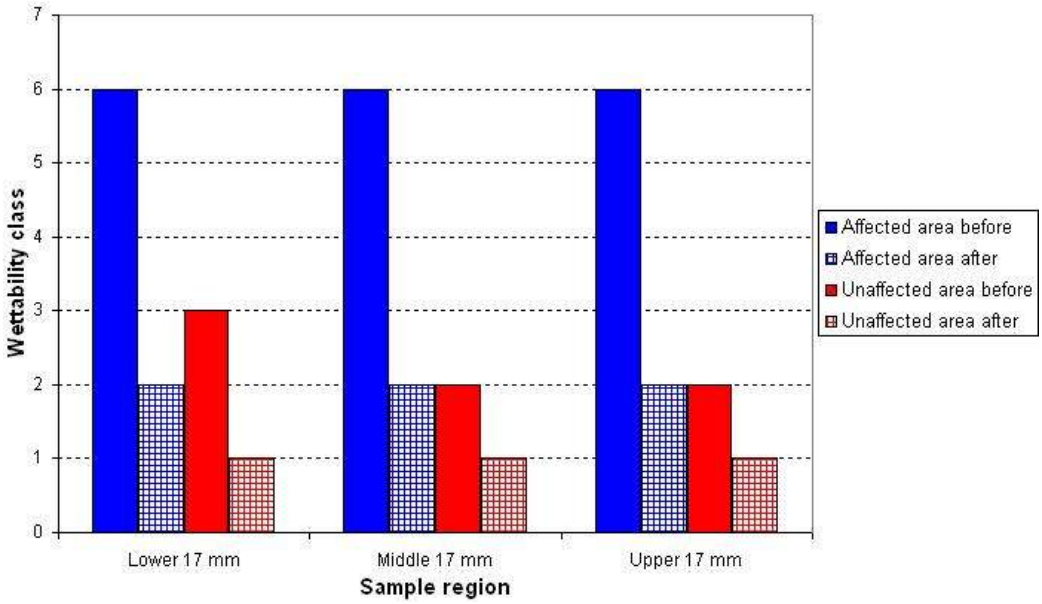

Fig. 111: Hydrophobicity results for series AC4-A, both before and after sample washing.

For material A, the AC series revealed similar results for all of its three different regions, both for the affected and unaffected areas. The affected areas showed a high loss of hydrophobicity while still covered with the deposits of the test runs. However, the cleaned surfaces revealed a strong recovery by four wettability classes, with almost no permanent loss recorded. Those areas largely untouched by either a continuous contaminant flow or frequent dry band discharges showed only a slight loss in hydrophobicity, which was fully recovered after the cleaning procedure so that the samples revealed a wettability class in these regions similar to that found in the virgin material.

A slightly stronger loss was observed in the unaffected areas of the lower 17 mm region. This is to be expected, since these locations were closest to the region where arcing took place almost continuously during the test runs. Since electrical discharges are a major cause for the loss of hydrophobicity, a greater loss of hydrophobicity can be expected in areas closer to the ground potential electrode [19]. However, these losses also fully recovered after the samples were cleaned. Although the samples of this insulator material showed a very strong recovery of hydrophobicity, a transfer of that hydrophobicity to the pollution layer was not observed.

The results of the positive DC series for material A showed a stronger loss of hydrophobicity than that recorded for the samples of the AC series, with the surface in the affected areas having turned completely hydrophilic while still covered in a pollution layer. The washing of the samples resulted in a slight recovery, which grew stronger with an increasing distance to the ground potential electrode (and thus the area of constant arcing). The unaffected areas of this series also showed a higher wettability class before washing, with the upper 16 mm region measuring the strongest hydrophobicity. These regions showed a better recovery than the affected areas after the washing process, but the final wettability classes still remained at higher levels than those observed for the AC series. A larger permanent loss of hydrophobicity was expected for this series, since the arcing processes were also observed to be stronger and of greater intensity than for the AC series. In fact, the high permanent loss observed in the lower 17 mm region is a result of the coating having been completely destroyed in this region, making a recovery of hydrophobicity impossible.

Similar results were observed for the negative DC test series, where the affected areas showed completely hydrophilic surfaces before the samples were washed and only a slight recovery afterwards. The erosion was observed to cover the entire area of the lower 17 mm as well as large parts of the middle 17 mm region, effectively destroying the RTV silicone rubber coating. A recovery in surface hydrophobicity was thus impossible in these areas, which explains the lack of recovery observed in these regions. It also explains the lack of measurements for the unaffected areas in the lower 17 mm region, as almost all of the samples experienced erosion across the entire area of this region, leaving no untouched surfaces. The unaffected areas of the upper regions again showed a stronger recovery than the affected areas, but still attained a higher wettability class than the samples of either the AC or the positive DC series. A possible reason for this can also be found in the large erosion observed in these samples, which decreases the diffusion of LMW molecules as well as causing a reduction in the available amount of these molecules. Since the diffusion of LMW molecules is vital to the recovery of surface hydrophobicity [21], a decrease in the diffusion process can result in a lower recovery and greater permanent loss.

The samples of the AC series for material B showed a strong decrease in the surface hydrophobicity of the affected areas, similar to those of material A. After the samples were cleaned, these areas revealed a good recovery, but showed slightly higher values for the final wettability class than the samples of material A. A similar pattern was observed in the unaffected regions, where the surface hydrophobicity was also observed to be stronger than for the affected areas, both before and after the washing of the samples. Again, little variation was observed between the classifications for the different regions of the sample surface, which suggests that LMW leaching had an equally strong effect on the surface hydrophobicity as the arcing process. This assumption is further confirmed by the relatively weak arcing observed on these samples, suggesting the presence of another strong process causing the loss of hydrophobicity. The recovery process was observed to be weaker in this test series than series AC4-A, which corresponds to the results of the test done on the virgin samples, where material A showed a stronger recovery than material B.

A large variation was observed in the results for the affected areas of series DP4-B. While the middle 17 mm and the upper 16 mm regions revealed a large loss of

hydrophobicity, which was only slightly recovered during sample cleaning, the lower 17 mm region showed an extremely hydrophobic surface which increased in its wettability class during the washing process. A similar observation was made for the results of the unaffected areas of the three regions, where the unwashed surfaces also showed a lower wettability class than the washed surfaces.

A possible explanation for this behaviour can be found in the observation that large areas of the sample surfaces were covered with a white deposit as a result of large and deep erosion areas forming at the ground potential electrode. This deposit was observed to be highly hydrophobic, often obstructing the flow of contaminant to such a degree that the liquid started to drop past the electrode, as was described in section 5.3.1.5. It was already assumed that the deposit must consist largely of filler material due to a similar colouring observed in the eroded areas. The high degree of hydrophobicity could be caused by the formation of large amounts of LMW molecules and polymer chain fragments due to the intense arcing process observed during this series [29]. It is quite possible that these small particles adhere to the filler material scattered across the sample surface, creating a highly hydrophobic surface. Since the deposits were also found in large amounts within the eroded areas, this also explains the low values for wettability class observed in these areas. During the cleaning process, the deposits were largely removed from the sample surface and the eroded areas, thus reducing the hydrophobicity in these areas. The stronger arcing processes observed in this series might also be the cause for the stronger permanent loss of surface hydrophobicity in the regions of this sample when compared to the results of the AC series.

The results for series DN4-B showed a strong loss of hydrophobicity for both affected and unaffected areas of the different regions, with only a slight recovery being observed after the samples were cleaned. An exception was formed by the results for the lower 17 mm region, which showed a very strong recovery. An explanation for this can be found in that while the erosion was not severe enough to form deposits on the entire sample surface, the arcing was strong enough to form localized erosion areas at the ground potential electrode where the deeper material layers were exposed. The large initial values for wettability class in this region are a result of other waste materials covering these small areas, causing a reduction of hydrophobicity. Cleaning

the samples exposes these surfaces, resulting in the formation of highly hydrophobic areas.

This series showed the weakest recovery of hydrophobicity for samples of material B. Since the electrical discharges of this series were weaker than those observed for series DP4-B, another possible reason for this weak recovery is that the negative DC voltage results in a stronger reorientation of the methyl groups, causing a greater loss in hydrophobicity [29]. However, this remains merely speculation, especially since the loss of hydrophobicity due to methyl reorientation is usually classified as a temporary loss, which is recovered as the methyl groups realign themselves once more.

For material C, the samples showed a very large loss of surface hydrophobicity for both affected and unaffected areas during the AC test series. The lower 17 mm region measured the highest wettability classes, which is to be expected due to the majority of the dry band arcing occurring in this region. The recovery of surface hydrophobicity remained weak for all observed regions, with some regions like the unaffected area of the upper 16 mm region showing no recovery at all. The large loss of hydrophobicity and a weak recovery process correspond well to the results obtained for the virgin material, which showed a large permanent loss of surface hydrophobicity after surface abrasion. An extraordinary observation made for this series was that the affected areas showed a slightly stronger recovery than the unaffected areas for all three measurement regions. No plausible explanation could be found for this observation.

Series DP4-C also showed high losses of hydrophobicity throughout the regions, both for the affected and unaffected areas. Moreover, the samples of this series experienced little or no recovery during the washing procedure, indicating that the loss of surface hydrophobicity is permanent. Since no large differences were observed between the values of wettability class for the different regions or between the affected and unaffected areas, it is reasonable to assume that the majority of the permanent loss was caused by the abrasion of the samples. This observation was confirmed by the large permanent losses observed for this material during the tests of the virgin samples. Two peculiar results in this series were the apparent further loss of

hydrophobicity for the affected area of the middle 17 mm region during the washing procedure, as well as the higher wettability classes observed for the unaffected than for the affected areas of the upper 16 mm region. No processes were observed that could give rise to an explanation for these observations. However, it is possible that due to the large discolouration (which was also difficult to remove) observed on these samples, too much pressure was applied when using the soft toothbrush during the cleaning procedure. This might have caused further slight abrasion of the surface, thus interfering with the results for the hydrophobicity tests.

The strongest losses in surface hydrophobicity were observed in the negative DC test series of this material. The affected areas revealed completely hydrophilic surfaces, forming an uninterrupted liquid film. No significant recovery was observed at these locations, indicating a permanent loss of hydrophobicity. Some recovery was observed in the unaffected areas, but only of slight magnitude. For all three different regions, the affected areas showed a higher value for the wettability class after cleaning than the unaffected areas, as was expected. As was observed in the other materials, the negative DC test series showed the highest permanent loss in surface hydrophobicity for material C.

For material D, the samples of the AC test series showed high losses in surface hydrophobicity for all different areas in their unclean state. However, a good recovery was observed in the insulation material underneath the pollution layer, which was shown by the low values for wettability class of the areas after the cleaning procedure was applied. Unaffected areas showed a stronger recovery than the affected areas, since they were less exposed to electrical discharges and/or a continuous flow of liquid contaminant.

Series DP4-D showed results similar to those observed for series DP4-B, with high hydrophobic surfaces formed in the affected areas of the lower 17 mm regions and large losses in surface hydrophobicity observed for the affected areas of the other regions. Additionally, the unaffected areas across the samples showed a loss in surface hydrophobicity after cleaning instead of a recovery. The reasons for these results are similar to those described for series DP4-B, since the samples of the series DP4-D also showed severe erosion along the ground potential electrode with the

subsequent formation of a white deposit of highly hydrophobic nature on the unaffected surfaces. The reasons for the high hydrophobicity of the deposits were already described for series DP4-B. The removal of these deposits during the cleaning of the samples explains the increase in wettability class for the unaffected surfaces, while the severe erosion in the lower region still exposes some of these deposits even after cleaning, leading to a high surface hydrophobicity in this area. All other regions showed a large permanent loss in hydrophobicity, which was expected due to the high-intensity arcing observed during this test series.

Finally, the negative DC series of material D showed very high losses in surface hydrophobicity for all regions and types of areas before the cleaning of the samples. The cleaning procedure resulted in a slight recovery in all regions, but the final values measured after cleaning still showed a large permanent loss surface hydrophobicity. The final values for wettability class were equally high for both affected and unaffected areas in the different sample regions, which seems to indicate the presence of a process other than electrical discharges or excessive fluid flow producing the large hydrophobicity loss. Again, the samples of the negative DC test series showed the highest overall losses for material D, since even the lower 17 mm regions now registered high wettability class values, which was not the case for series DP4-D.

A comparison between the results for the three voltage types revealed a tendency in all the materials to produce the highest permanent losses of surface hydrophobicity during the test series for the negative DC voltage. However, the arcing severity and intensity were observed to be less for this voltage type than for the positive DC voltage, while the contaminant flow rate was kept constant for all test series. Severe electrical discharges or increased leaching by excess liquid on the sample surfaces could thus not be the cause for this large permanent loss. It was already speculated previously that a negative DC voltage could cause a greater reorientation of the methyl groups in the polymeric materials, which would explain the greater loss in hydrophobicity. However, sources state that such a loss is only of a temporary nature [19], so this explanation remains speculation.

Both the results for the hydrophobicity tests of the virgin and the eroded samples revealed a stronger permanent loss in surface hydrophobicity for material C than for

any other material. Material C is an ethylene propylene diene monomer (EPDM), while the other materials are all silicone rubber materials. A possible explanation for the greater hydrophobicity loss in the EPDM material lies in the lower number of methyl groups in the molecule chains of this material. Silicone rubber materials consist of long polymer chains of silicone and oxygen, with two methyl groups (or other reactive groups) bonded to the silicone. Each EPDM molecule, on the other hand, has only one methyl group attached to the propylene monomer in the chains [60]. These methyl groups create a highly hydrophobic surface, since the polar water molecules do not bond with the non-polar methyl groups. Processes like electrical arcing or surface erosion cause a reorientation or even loss of these methyl groups, resulting in the surface turning more hydrophilic [19]. Recovery of the surface can occur through the methyl groups returning to their original position. However, since EPDM has fewer methyl groups than the silicone rubber materials, the process takes longer for EPDM or might even be hindered to such an extend that full recovery does not occur. Even the slight surface erosion introduced by the abrasion process is enough to result in a large change within the surface hydrophobicity of the EPDM material, with electrical discharges increasing this effect.

As described previously, all the tests for hydrophobicity were done using the spray method, with the classification of the results being accomplished by comparing them to visual guides. This rather subjective method of evaluation does tend to introduce a slight inaccuracy to the results, especially since the exact boundaries between different wettability classes were sometimes hard to define. The standard does contain two other evaluation techniques based on the measurements of contact angle or surface tension. However, these methods require relatively flat and clean surfaces to be done with sufficient accuracy, and were thus not suitable for the degree of pollution and erosion observed in the samples of this project. In order to improve the evaluation technique of the spray method, it might be worthwhile to investigate the use of computer software to calculate the exact amount of wetted surface area for each sample and comparing these results to those obtained for the photographs of the different classes shown in the standard.

5.3.8 Chemical analysis of selected samples

One of the six samples of each test series was selected to undergo chemical testing so as to investigate the materials on possible chemical changes. The chosen method for this analysis was the attenuated total reflection (ATR) Fourier transform infrared (FTIR) spectroscopy, which has been described in detail in section 4.3.6. Only one sample per test series was submitted for chemical testing. The reason for this small number of selected samples is that it was decided to keep the surfaces of the selected samples as undisturbed as possible, so as not to interfere with the results for the chemical analysis. This prevents these samples from undergoing the cleaning procedure after testing, which also automatically excludes them from the results for several evaluation criteria, such as mass loss, erosion depth and area and hydrophobicity testing. In order to keep the number of samples for these criteria as big as possible, and since the testing conditions were kept equal for all samples within a test series, only one sample per series was selected for chemical testing.

Accordingly, the chemical analysis results for the selected samples are representative for the entire test series, which means that care had to be taken with the selection of the samples. Sample selection for this part of the project was based on the same criteria used for the method comparison in Chapter 4, which were:

- *Visual appearance:* The surface erosion/discolouration of the selected sample should be comparable to the samples of each series, i.e. no unusually excessive erosion damage/discolouration or lack of it.
- *RMS leakage current:* The rms current of the sample measured by the OLCA over the test period of six hours should be comparable to other samples in the series, both in magnitude and trend.
- *Maximum peak leakage current:* The maximum peak current values measured per one minute interval of the sample should be comparable to those of the other samples within the series over the test period of six hours, both in magnitude and trend.

The comparisons for the rms and maximum peak leakage currents between the samples were done by generating plots using the OLCA DataManager software. The selected sample had to be comparable to at least two other samples in the series for

each of the selection criteria in order to qualify for chemical testing. Table 29 shows the samples selected for each material/voltage combination.

Table 29: Samples selected for chemical testing.

Voltage type	Material type			
	A	B	C	D
AC	AC4-A1	AC4-B5	AC4-C5	AC4-D3
DC +	DP4-A6	DP4-B2	DP4-C4	DP4-D1
DC -	DN4-A4	DN4-B4	DN4-C4	DN4-D5

Three separate test specimens were cut from each of the selected samples, one from the lower 17 mm, the middle 17 mm and the upper 16 mm region. This was done in order to observe any possible differences in the chemical analysis related to a specific location on the sample surface. The cut specimens had a diameter of ± 10 mm and a thickness of ± 1 mm each. The specimens were cut from regions directly adjacent to the eroded areas and the contaminant path, as the surfaces within these two areas were considered to have undergone too large a change to allow for a meaningful comparison between the tested samples and the virgin material.

A spectrum was then generated for each specimen of the various samples, which was then compared to the spectrum obtained from a virgin sample for the corresponding material. The spectra were obtained using the same Smart Golden Gate ATR lens used in the analysis of the method comparison. This lens allows the user to manually adjust the pressure exerted by the lens on the specimen, which was kept constant for all tested specimens. During each measurement, a spectrum of the background was obtained first, after which a scan was performed with the specimen in place. A subtraction of the results for the two scans severely reduces the influence of background noise on the actual spectra. The number of scans for both background and specimen were kept at 16 runs each, with the spectra covering wavenumber range of 4000 – 600 cm^{-1}. All spectra were done in absorbance mode due to the small filtering effect introduced by the conversion from transmittance to absorbance described in section 4.3.6.1.

As was described previously on numerous occasions, materials A, B and D are all based on silicone rubber or, to use a more scientific term, polydimethylsiloxane (PDMS) materials. Material C, on the other hand, is an EPDM type material. Due to

this difference, the spectra of the samples of material C will differ greatly from those obtained for materials A, B and D. The analysis will also focus on different areas of the spectra for these two material groups. It was thus decided to give the results for the chemical analysis of the two material groups separately in the following sections.

5.3.8.1 Results for PDMS materials

Fig. 112 shows spectra obtained for the specimens taken from the lower 17 mm regions of the samples of the AC test series for materials A, B and D to show the quality of the spectra obtained during the analysis of these materials. Due to the large number of spectra obtained for the different regions, materials and voltage types, it was considered impractical to present each of the measured spectra in this report. Instead, only the results of the spectra analysis will be given, while all the different spectra are stored on a DVD appended to this report.

Since the insulator material used during the method comparison in Chapter 4 was also a PDMS type material, the analysis for materials A, B and D again focused on three different areas of the spectra, which are:

- Loss of alumina trihydrate filler (ATH, or Al_2O_3-$3H_2O$) shown by a reduction in the peak height at 3522 cm^{-1}.
- Loss of methyl (CH_3) groups from the PDMS structure, which can be detected by a decrease in the spectra peak height as well as in the area under the peak at 2963 cm^{-1}.
- Oxidation of the PDMS and formation of carbonyl (C=O) groups, revealed as an increase in the area under the curve in the range of 1550 to 1800 cm^{-1}.

As previously described, this analysis method was adapted from reports for tests on polymer insulator materials frequently performed at the Department of Chemistry and Polymer Science of Stellenbosch University.

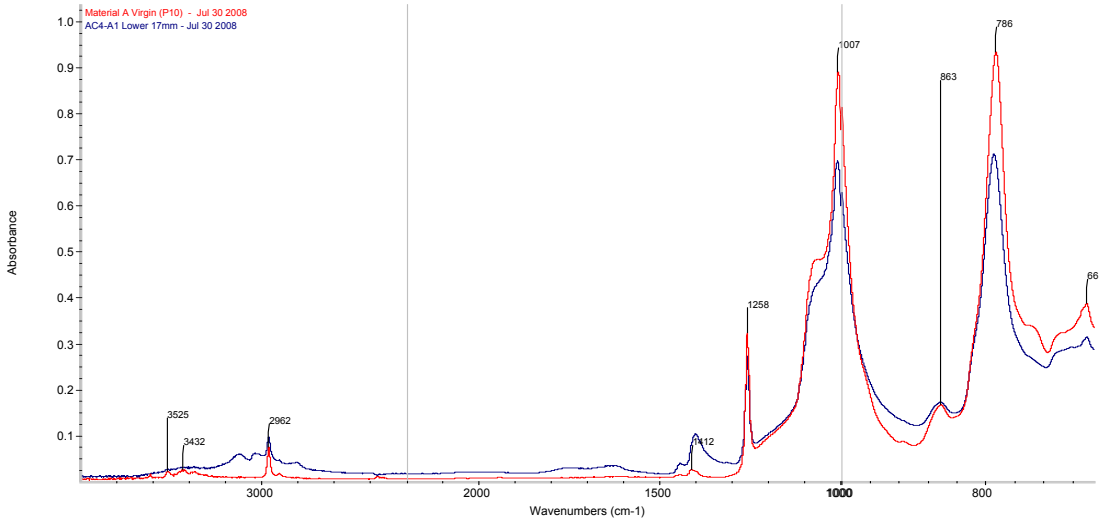

(a)

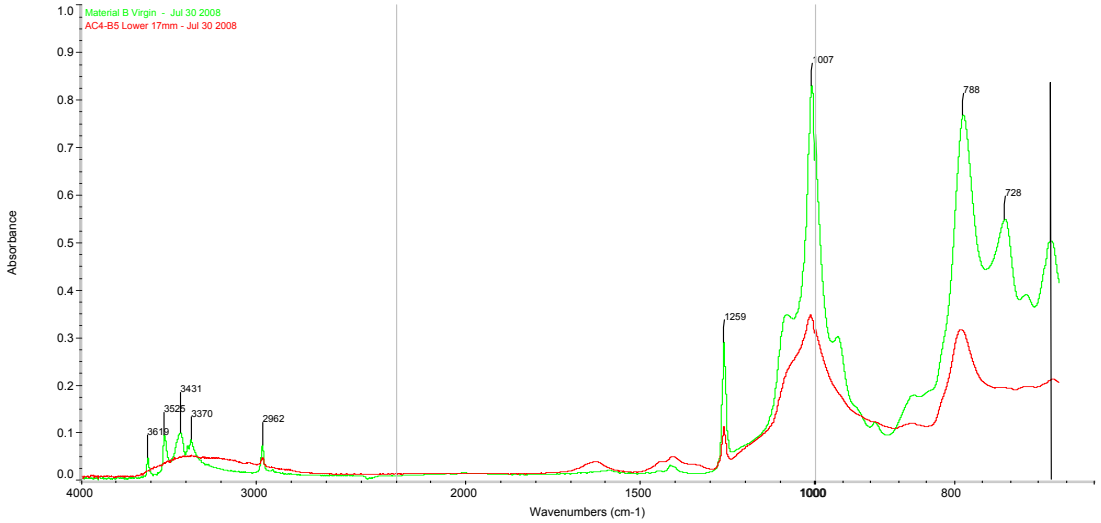

(b)

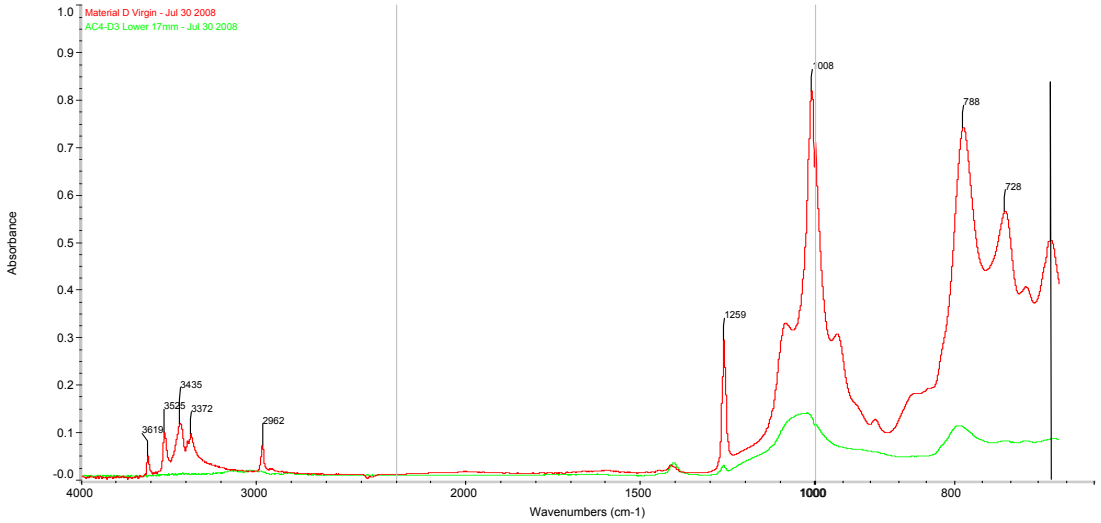

(c)

Fig. 112: ATR FTIR spectra of tested vs. virgin specimen for lower 17 mm region of samples: (a) AC4-A1, (b) AC4-B5 and (c) AC4-D3.

A comparison between peaks measured in the spectra of the tested and the virgin specimen was done by calculating the peak height ratio, where the peak height of the tested specimen is divided by that of the virgin specimen. The peak height at a specific location is taken as the distance of the peak to a baseline drawn between two base wavenumbers to either side of the peak. The comparison of areas underneath the peaks at a certain location is done in the same manner, with the peak area ratio calculated by dividing the peak area of the tested specimen by the peak area for the virgin sample. The peak area is defined as the area between the spectrum curve between two set wavenumber limits and a baseline drawn between the same limits. For the criterion of loss of methyl groups, the degree of conversion β was once again calculated by the relationship

$$\beta = \frac{(H_0 - H)}{H_0}, \tag{5.6}$$

where H_0 and H are the areas underneath the peaks of the virgin and tested samples, respectively.

The locations of the peaks, area limits and base values for the baselines for each analysis criterion are as follows:

- *Loss of ATH filler:* Peak location: 3522 cm^{-1}; baseline values: Base 1 = 3690 cm^{-1}, Base 2 = 3036 cm^{-1}.
- *Loss of methyl groups:* Peak location: 2963 cm^{-1}; peak area limits: Limit 1 = 3010 cm^{-1}, Limit 2 = 2930 cm^{-1}; baseline values: Base 1 = 3010 cm^{-1}, Base 2 = 2930 cm^{-1}.
- *Oxidation by carbonyl formation:* Peak area limits: Limit 1 = 1800 cm^{-1}, Limit 2 = 1550 cm^{-1}; baseline values: Base 1 = 1800 cm^{-1}, Base 2 = 1550 cm^{-1}.

Table 30 shows the analysis results of the specimens for the individual regions on all the selected samples for materials A, B and D for each analysis criterion.

Table 30: Results for chemical analysis on PDMS samples.

Region	Analysis		AC Series			DC + Series			DC - Series		
			AC4-A1	AC4-B5	AC4-D3	DP4-A6	DP4-B2	DP4-D1	DN4-A4	DN4-B4	DN4-D5
Lower 17mm	Loss of ATH filler - peak height ratio		0.234	0.241	NPO	0.851	0.296	NPO	0.993	0.513	0.372
	Loss of methyl groups	Peak height ratio	0.731	0.313	0.037	0.762	0.500	0.172	0.726	0.591	0.258
		Degree of conversion β	0.240	0.665	0.950	0.272	0.544	0.820	0.286	0.417	0.756
	Oxidation by carbonyl formation - peak area		6.713	5.036	0.941	3.240	6.139	2.811	2.387	9.349	16.501
Middle 17mm	Loss of ATH filler - peak height ratio		0.546	NPO	NPO	0.915	0.088	0.244	0.830	0.537	0.053
	Loss of methyl groups	Peak height ratio	0.726	0.356	0.194	0.824	0.356	0.106	0.786	0.489	0.085
		Degree of conversion β	0.283	0.628	0.757	0.186	0.660	0.897	0.264	0.524	0.943
	Oxidation by carbonyl formation - peak area		2.039	2.175	5.113	3.173	2.053	16.385	2.249	9.531	9.213
Upper 16mm	Loss of ATH filler - peak height ratio		0.404	0.110	NPO	0.504	0.115	0.280	0.986	0.566	0.394
	Loss of methyl groups	Peak height ratio	0.815	0.211	0.217	0.812	0.260	0.287	0.845	0.645	0.528
		Degree of conversion β	0.191	0.801	0.773	0.198	0.757	0.716	0.195	0.352	0.488
	Oxidation by carbonyl formation - peak area		1.950	2.936	3.852	2.115	1.566	11.595	1.663	5.314	3.917

*NPO: No Peak Observed

The results for each individual criterion were plotted for each voltage type, with vertical bars representing the individual results. Different colour schemes were used to distinguish between the individual materials. Fig. 113 shows the plot for the loss of ATH filler for the samples tested using a positive DC voltage. All other plots can be found in Appendix H.

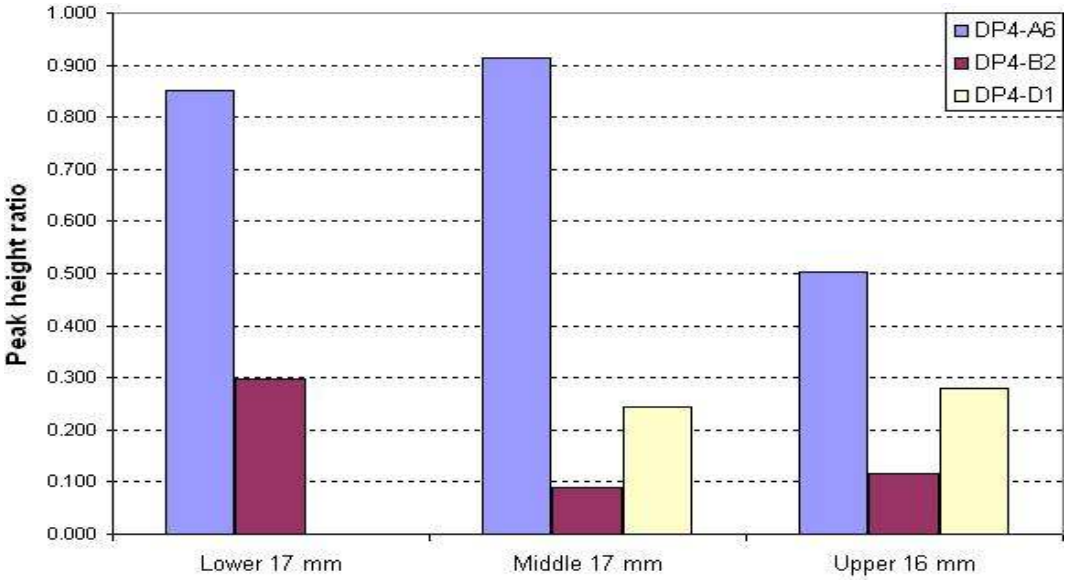

Fig. 113: Loss of ATH filler for samples tested using a positive DC voltage.

For some spectra, it was observed that the peaks for certain locations investigated during the analysis were reduced to such an extent that they fell underneath the baseline, causing a negative result. These results were then replaced with the abbreviation NPO (No Peak Observed) and were omitted in the plots, as is shown for the lower 17 mm region of sample DP4-D1 in Fig. 113. However, rather than discarding such a result, such an occurrence was viewed as a severe chemical change.

For the criteria of loss of ATH, a low peak height ratio indicated a strong change within the specimen when compared to the virgin sample. It was also expected that the samples would show an increased loss of ATH in the regions closer to the ground potential electrode, since this was the region where the highest electrical discharge activity was observed. In effect, this means that a decrease in the peak height ratios was expected when moving from the upper 16 mm through the middle 17 mm to the lower 17 mm region on the samples. However, only samples DP4-D1 and DN4-B4 showed this expected trend, while all other samples measured higher losses of ATH filler in either the middle 17 mm or upper 16 mm regions than in those closest to the ground potential electrode. While it was already stated in the chemical analysis in section 4.3.6.2 that the heating effect of the top electrode might be responsible for a high loss of ATH filler in the insulation material surrounding the electrode, several samples of the three different materials also measured the highest ATH losses in the middle 17 mm region.

Furthermore, the ATH loss was higher for the AC than for both the positive and negative DC test series for all three materials, while the latter two series experienced arcing of stronger intensity and stability than the AC series. It thus follows that there seems to exist no good correlation between the results of this chemical analysis criterion and the observed arcing processes. A similar observation can be made between the results for ATH loss and the erosion severity observed in the different test series. The results for the criteria of mass loss, erosion depth and erosion area displayed higher series means for both the positive and negative DC than for the AC test series, which once again contradicts the results for this chemical analysis criterion. Additionally, the samples of material D showed the highest ATH filler losses for all three voltage types, with the samples of material B revealing the second highest and material A showing the smallest loss. However, the results for erosion

severity frequently revealed material D to have the lowest values for a given voltage type within a criteria, thus showing less severe erosion than either material A or B. A correlation between the results of ATH filler loss and erosion severity was thus not observed for the PDMS materials.

The results for the peak height ratio and the degree of conversion show good correlation between them for the criteria of loss of methyl groups, indicating that both the peak height and the area underneath the peak decrease proportionally in the tested samples when compared to the virgin material specimen. Either of the two criteria can thus be used to describe the conversion of the PDMS material to the bare silicone-oxygen backbone through a loss of methyl groups. The degree of conversion β was chosen for further comparison, since an increase in β simultaneously means a greater loss of methyl groups.

Since energy is needed to break the bond between the silicone and the carbon atom of the methyl group, one would expect that an increased electrical discharge activity as well as the formation of high-intensity hotspots would result in a greater loss of methyl groups from the PDMS material. The values for β where thus expected to be greater for the lower regions of the samples than for those closer to the top electrode. However, only sample DN4-A4 revealed such a tendency. All other samples showed varying results, with the highest degree of conversion frequently occurring in the upper or even in the middle regions. Additionally, materials B and D registered higher values for β in the samples of the AC series than for those of the positive and negative DC series. Material A did show a higher degree of conversion for its negative DC test series than for the AC test series, but also showed the lowest values in the samples of the positive DC series. Since the results of the visual observations reported the arcing intensity and hotspot formation to be much higher for the two DC series than for the AC series, there seems to be little correlation between the results of the chemical analysis and the arcing behaviour.

Sources state that the methyl groups in the PDMS structure contribute strongly to the good surface hydrophobicity commonly observed within these materials [19]. A loss of these methyl groups should then consequently lead to a loss of hydrophobicity. Upon comparing the results of these two criteria, it was indeed seen that both the loss

of hydrophobicity and the degree of conversion increased when moving from material A through material B up to material D, with D showing the highest values for both criteria. There thus seemingly exists a correlation between the two criteria and the type of insulation material. However, no such correlation was observed between the two criteria and test voltage type. While the loss of hydrophobicity decreased when moving from the negative DC through the positive DC to the AC test voltage, materials B and D showed higher values for β during the AC test series than for both the positive and negative DC test series. Material A did measure the highest degree of conversion values for the negative DC series, but the values obtained for the sample from the AC series were higher than those of the positive DC series. The results for this analysis criterion thus do show a small correlation to the observed loss of hydrophobicity for each material type, but show no relation to the discharge activity and type of test voltage used.

Finally, the results for the oxidation of the PDMS through carbonyl formation also showed large variations for the three materials. It was again expected that the samples would show greater changes for the regions closer to the ground potential electrode and thus the region of highest electrical discharge activity, since energy is needed to break the hydro-carbon bonds of the methyl groups and form a carbonyl group (C=O). However, only material A displayed such a trend, while the other materials showed a large variation as to which region displayed the largest oxidation.

A higher arcing stability and intensity should also result in greater oxidation of the material, which is why greater changes were also expected for the samples of the two DC series than for those of the AC series. However, only material D showed a correlation between the severity of the arcing process of the different voltage types and the resulting oxidation, showing the strongest carbonyl formation for the sample of the positive DC test series, followed by that of the negative DC series and with the lowest values recorded in the sample of the AC series. This sequence corresponds to the relative intensity of the arcing process observed for the individual test series. Neither material A nor B showed an adherence to this sequence, with material A showing larger oxidation results for the AC voltage and material B for the negative DC series.

The increased oxygen bonding occurring during the carbonyl formation should also result in a decrease in the hydrophobicity of the material, due to a formation of hydrogen bonds between the PDMS and water molecules [47]. An increase in carbonyl formation at a specific location should thus result in an increasingly hydrophilic surface at that location. However, a comparison between the results for surface hydrophobicity and the chemical analysis for carbonyl formation for materials A, B and D for each specific region and test series revealed little or no correlation for the two criteria. The comparison focused on the results for the unaffected regions for the hydrophobicity criterion, since the specimens for the chemical analysis were also not taken directly from an eroded or heavily discoloured area.

Overall, it can be stated that, although smaller correlations were revealed within a specific material or for a given test series, no general relationship could be observed between electrical discharge activity and the results for the chemical analysis for the PDMS based materials. It was noted, however, that material D consistently showed the greatest changes for each analysis criterion, irrespective of the type of test voltage. This type of HTV silicone rubber thus seems more susceptible to chemical change than either the HTV silicone rubber of material B or the RTV silicone rubber coating of material A. However, no direct correlation could be drawn between this observation and the results for erosion severity, as the erosion (mass loss, depth or area) was frequently observed to be more severe for the samples of material A or B than for D. A correlation could be found between the results of hydrophobicity loss and loss of methyl groups for the different material types, but this relationship remained independent of the voltage type applied to the samples.

5.3.8.2 Results for EPDM material

Fig. 114 shows the spectrum obtained for the specimen of the lower 17 mm region for the sample AC4-C5 as well as the spectrum for the virgin sample. As was already described for the PDMS materials, it was considered impractical to display all the obtained spectra in this thesis due to their large number. Instead, only the analysis results will be given in this text and the appendices, while all the spectra for the EPDM samples can be found on the same DVD as the PDMS spectra, which will be appended to this document.

Although it is obvious from Fig. 114 that changes have occurred along the entire spectrum, the analysis focused mainly on two specific criteria:

- Loss of alumina trihydrate filler (ATH, or Al_2O_3-$3H_2O$) shown by a reduction in the peak height at 3522 cm^{-1}.
- Oxidation of polymer through carbonyl (C=O) formation, shown by an increase in peak height at 1730 cm^{-1}.

Again, these criteria were adapted from analysis reports for tests on polymer insulator materials frequently performed at the Department of Chemistry and Polymer Science of Stellenbosch University.

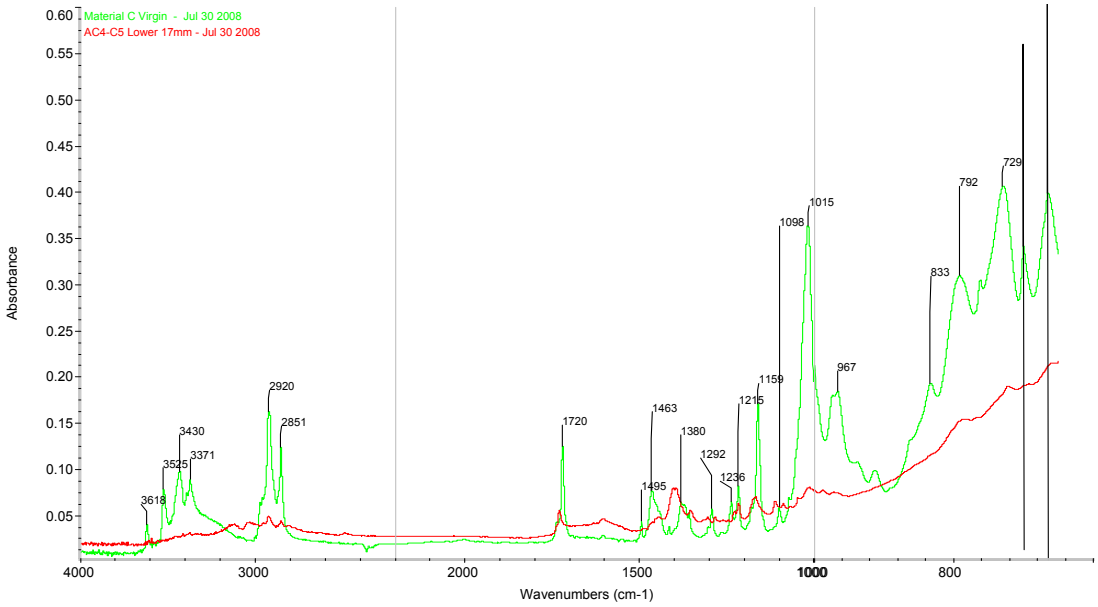

Fig. 114: ATR FTIR spectra for tested vs. virgin specimen of lower 17 mm region of sample AC4-C5.

The two criteria were evaluated using the peak height ratio, which was calculated by dividing the peak height of the tested samples by that of the virgin samples. The peak heights were again measured between the apex and a baseline, as was described for the results of the PDMS based samples. The locations of the peaks and the base values for the baselines for the two criteria are as follows:

- *Loss of ATH filler*: Peak location: 3522 cm^{-1}; baseline values: Base 1 = 3690 cm^{-1}, Base 2 = 3036 cm^{-1}.
- *Oxidation by carbonyl absorption*: Peak location: 1730 cm^{-1}; baseline values: Base 1 = 1810 cm^{-1}, Base 2 = 1690 cm^{-1}.

The results for these two criteria for each of the regions of the three different samples of material C are shown in Table 31.

Table 31: Results for chemical analysis on EPDM samples.

Region	Analysis	AC series, sample AC4-C5	DC+ series, sample DP4-C4	DC- series, sample DN4-C4
Lower 17mm	Loss of ATH	NPO	NPO	0.100
	Oxidation by carbonyl formation - peak height ratio	1.229	0.231	1.282
Middle 17mm	Loss of ATH	0.462	0.362	0.138
	Oxidation by carbonyl formation - peak height ratio	3.053	3.035	1.100
Upper 16mm	Loss of ATH	NPO	0.083	0.342
	Oxidation by carbonyl formation - peak height ratio	2.294	2.865	1.371

*NPO: No Peak Observed

The results were also plotted as bar diagrams, with different colour schemes indicating the samples tested using different voltage types. These plots are shown in Fig. 115 and are also included in Appendix H. Some peaks were again observed to have decreased to such an extent as to fall beneath the baseline, resulting in a negative measurement. The abbreviation NPO was again substituted in these cases, and such measurements were omitted in the plots. However, it must once again be stressed that these results were not ignored, but were rather viewed as a severe chemical change in the samples.

As was described during the analysis for the PDMS materials, it was expected that the chemical changes on the samples would be more severe for regions closer to the ground potential electrode, since this was observed to be the area where the majority of the electrical discharge activity occurred. For the criteria of loss of ATH filler, the samples of the different test series for material C fulfilled this expectation in the sense that the highest losses of ATH filler were recorded for the lower 17 mm region. However, samples AC4-C5 and DP4-C4 showed a higher loss for the upper 16 mm than the middle 17 mm regions. Moreover, the ATH filler losses were observed to be highest for the sample taken from the AC test series, followed by that of the positive DC series. The lowest filler loss was recorded in the sample from the negative DC series. The arcing intensity, however, was observed to increase when moving from the AC series through the positive DC series, with the highest intensity observed during

the negative DC series. There thus seemingly exists only weak correlation between arcing intensity and loss of ATH filler for this material.

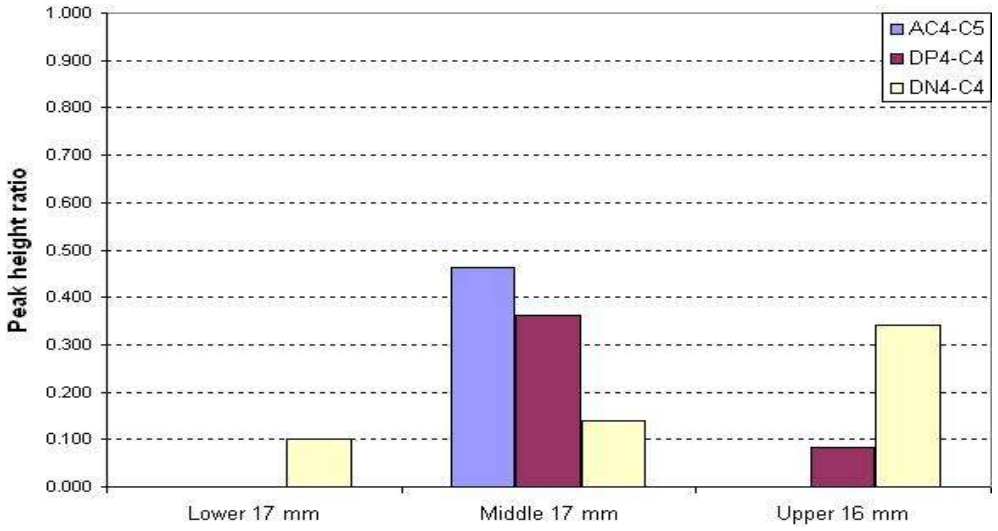

(a)

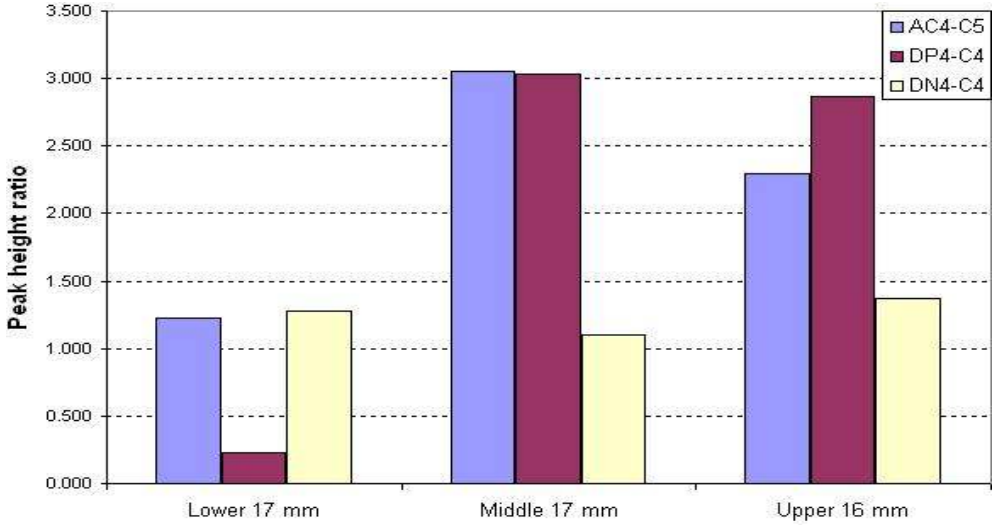

(b)

Fig. 115: Plots for the chemical analysis for the EPDM sample: (a) Loss of ATH filler and (b) Oxidation by carbonyl formation

However, after evaluating the erosion intensity for the different test series for this material according to the three criteria of mass loss, erosion depth and area, the overall erosion was observed to be highest for the AC series, followed by the positive DC series and finally the negative DC series. This sequence for the results of the different test series is identical to that observed for the results of ATH filler loss. There thus seems to be a direct correlation for erosion severity to the loss of ATH filler for material C. This is to be expected, since a loss of the filler material will result in a degradation of the structural strength of the material, making it easier for electrical erosion to develop.

For the criteria of oxidation through carbonyl formation, the samples of all three test series measured higher values for either the middle 17 mm or upper 16 mm regions than for the lower 17 mm region, thus showing higher oxidation in areas removed from the ground potential electrode. Additionally, the highest values for oxidation were recorded for the sample of the AC series, followed by the sample of the positive DC series and with the lowest oxidation values shown by the sample of the negative DC series. Once again, these results show little correlation to the arcing severity observed for the different test series, but do correlate well to the ranking of the test series according to erosion severity. It thus appears that an EPDM material undergoes increasing carbonyl formation with an increase in erosion severity.

Looking at the chemical analysis results for both the PDMS based materials and the EPDM, it is shown that both material types show little or no correlation between the magnitude of the chemical changes and the severity of the electrical discharge processes. However, the EPDM material showed a strong correlation between erosion severity and the chemical analysis results for the different test series, while no such correlation was observed for the PDMS materials. Other studies report using the ATR FTIR method yielded satisfactory results for PDMS materials [47]. The weak correlations observed in this project might have been influenced by the relatively large samples sizes and the fact that the samples were kept untreated. Previous research work in this field suggests using smaller sample sizes (5 x 5 x 0.5 mm^3) as well as a pre-treatment of the samples surface with acetic acid [47, 55].

In order to check the repeatability of the ATR FTIR tests, the virgin samples of all four materials were scanned again after all the sample specimens had been analyzed. The resulting spectra were then compared to the spectra obtained for the virgin materials at the beginning of the analysis process, since the virgin materials were scanned first in order to compare all other specimen spectra to them. The results showed that the spectra obtained for each virgin specimen both at the beginning and at the end of the analysis process were almost identical, indicating that the experiments have a good level of repeatability and that the results were not influenced by a possible bias in the apparatus. The compared spectra for the virgin specimen for each material are given in Appendix H.

Chapter 6: Conclusions & Recommendations

The main objective of this project was to compare four different polymer based insulator materials according to their performance for tracking and erosion resistance when exposed to surface discharges of three different voltage types, namely AC, positive DC and negative DC. Other important aspects were the development of a bipolar DC voltage source and the comparison of the different test procedures, namely the constant tracking voltage method and the stepwise tracking voltage method, for the IPT method described in the International Standard IEC 60587 [34], so as to select the most suitable test method to be used for the material comparison.

6.1 Design & implementation of a bipolar DC source

A bipolar DC source was successfully developed for this project utilizing a combination of single phase half-wave rectification and smoothing capacitor. Rectification was achieved through a series connection of individual circuits, each combining a rectification diode with a parallel connected resistor and capacitor for even voltage distribution during the steady and transient states of the diode, respectively. The number of required diodes was calculated to withstand the proposed test voltage of 4 kV (bipolar DC), with a safety factor of 2 and a minimum current rating of 0.1 A. The rectifier circuits were implemented on PCB's, with two circuits mounted on each PCB, thus forming a basic building block rated for 1.6 kV. Fifteen PCB's were then connected in series to form diode stacks, resulting in a modular design that can be easily adapted for any number of test voltages and source arrangements. The switching of test voltage polarity can be obtained by reversing the conducting direction of the rectification stacks.

The bipolar DC source used in this project was specifically designed to keep the supply voltage ripple below 5%, as was specified by the IEC Standard 60587 [34]. Computer models were developed using HSpice and simulated in order to select the smoothing capacitor value needed to meet this requirement. Although practical tests done at the maximum allowed test leakage current of 60 mA (rms) showed a higher voltage ripple than forecasted by the virtual models, the obtained ripple of 2.73% still

adequately fulfilled the requirement. The rectifier design is currently being adapted for implementation in the construction of a bipolar 18 kV DC source for insulator field tests at KIPTS.

6.2 Comparison of IPT test methods

The comparison of the two test methodologies for the IPT was done by using the results for a number of evaluation criteria obtained from a complete test series of each method performed on the same polymer material. The comparison for these criteria was based on the series mean values after the elimination of extreme data points. An exception was made for the chemical analysis criterion, since only one sample per series was submitted for the ATR FTIR analysis.

Visual observations revealed no significant difference between the two methods in terms of arcing behaviour during the periods where contaminant flow rate and series resistance were the same for both methods. In terms of mass loss, the constant tracking voltage method produced a higher average mass loss, whereas the results for the stepwise tracking voltage method showed a smaller standard deviation and thus a higher degree of repeatability. Both methods show almost identical results for the maximum erosion depth criterion.

In the criteria for rms leakage current and peak current counts, the comparison focused on those time periods where the two methods displayed similar test conditions in terms of contaminant flow rate and series resistance. The samples of the stepwise tracking voltage method measured slightly higher hourly averages for the rms leakage current, but the difference between the results of the two methods remained small. A similar observation was made for the peak current counts, with the stepwise tracking voltage method showing higher counts for the medium (20 – 60 mA) and the high (60 – 100 mA) peak current bins.

The chemical analysis of the selected samples from each test method was performed using an ATR FTIR analysis, with the analysis focussing on chemical changes through the following:

- Loss of ATH filler.

- Loss of methyl groups.
- Oxidisation through formation of carbonyl groups.

Three different specimens were cut from each sample and tested, one from each of the lower, middle and upper regions of the samples as measured along the longitudinal axis of the samples. Some smaller differences were mainly observed in the lower regions where constant arcing took place. The stepwise tracking voltage method showed a slightly higher loss in ATH filler in this region, while the sample of the constant tracking voltage method measured a greater loss of methyl groups as well as an increased formation of carbonyl groups. However, the samples showed similar results and trends for each analysis criterion.

The overall conclusion was that the two methods were comparable in terms of their results obtained for the described evaluation criteria and that it is up to the user to determine which method is preferable. The choice of using the constant tracking voltage method for any further tests during this project was based on problems associated with the test procedure of the stepwise tracking voltage method, most notably of which is the difficulties arising for a comparison between different materials while constantly changing the test parameters of test voltage, contaminant flow rate and series resistance.

6.3 Material comparison under AC & bipolar DC conditions

A total of four different insulator materials were tested:

- *Material A*: A RTV silicone rubber coated ceramic (supplier W).
- *Material B*: A HTV silicone rubbers (supplier X).
- *Material C*: An EPDM rubber (supplier Y).
- *Material D*: A HTV silicone rubber (supplier Z).

Six samples of every material were tested for three different test voltage types, namely AC, positive DC and negative DC. The test voltage magnitude was kept at 4.0 kV (rms) for all three test voltage types. The comparison of the materials was based on the results obtained for the following evaluation criteria:

- Visual observation of electrical discharges and sample appearance.
- Mass loss of samples due to electrical erosion.
- Maximum erosion depth.

- Total erosion area.
- Hourly average rms leakage currents.
- Average dissipated electrical power.
- Loss of surface hydrophobicity.
- Chemical analysis by means of an ATR FTIR spectroscopy.

The following results were obtained for the visual observations:

- The intensity of the electrical surface discharges increased when moving from the AC through the negative DC to the positive DC voltage for all materials.
- During the AC test series, materials B and D (HTV silicone rubber) developed only minor erosion along the ground potential electrode. For the RTV silicone rubber coating (material A), the erosion alternated between small, localized areas and between significant erosion. The samples of material C (EPDM) showed the worst performance, developing severe erosion of large depth and area in the majority of its samples for this voltage type.
- For the positive DC series, material C showed a visible decrease in erosion compared to the results for the AC test series. Material A, on the other hand, showed a significant increase in erosion. The worst performance was observed for materials B and D, which revealed extensive erosion and also frequently developed failures due to holes appearing in the samples.
- In the case of the negative DC series, materials B and D showed the least erosion of all the materials, although the developed erosion still exceeded that observed during the AC test series. Material C showed slightly stronger erosion than the HTV silicone rubbers, but less than what was observed for its AC and positive DC series. Material A showed the strongest erosion for this voltage type, with large areas of the sample coatings destroyed.

The erosion severity was quantified by measuring the mass loss, erosion depth and erosion area of the samples. Combining the results of these three criteria led to the following results:

- The HTV silicone rubber materials (B and D) showed an increase in the measurements for each of these criteria when moving from the AC through the negative DC to the positive DC voltage. Individual results varied in terms

of which of the two materials showed larger magnitudes for the criteria. The positive DC series, however, consistently showed larger results for material B than for D for all three criteria.

- Material A also showed greater mass loss, erosion depth and area for the DC voltages than for the AC series. However, the greatest mass loss and erosion area were measured for the negative DC voltage, while the positive DC series showed a slightly higher erosion depth. Since the erosion depth was limited by the coating thickness, it can be deduced that the overall erosion severity was greatest for the negative DC voltage in this material.
- Material C showed a large variation in the results of the individual criteria for all three voltage types. Since the negative DC series displayed the lowest results for two of the three criteria, this voltage type was considered to produce the least severe erosion for this material, with similar reasoning revealing the positive DC voltage to produce less material erosion than the AC test voltage, which yielded the greatest erosion severity for this material.

The measurements for the rms leakage currents showed that:

- The hourly averages for all materials increased when moving from the AC to the positive DC voltage. However, the application of the negative DC voltage resulted in the lowest rms leakage current measurements for all four materials.
- Material A showed the highest currents during all three test voltages, while material C consistently measured the lowest currents.
- These results revealed no real correlation to the criteria of erosion severity, which indicated that the rms leakage current cannot be used to forecast erosion severity for polymer samples tested using the IPT method.

A correlation analysis was performed between the rms current measurements for individual samples within each test series in order to check their consistency. The results of the analysis revealed a large variation in the result of the individual test series. Only material A showed strong correlations in the current measurements of its samples, which also further increased when moving from the AC through the positive DC to the negative DC voltage.

Measuring the average dissipated electrical power during the test runs yielded the following results:

- No direct correlation was observed between the hourly averages of the dissipated electrical power and the erosion severity measured in the different materials for each voltage type.
- A slightly better correlation was observed between the results for leakage current and dissipated power for the DC voltages. However, the AC series showed only weak correlation between the two criteria. This was attributed to the reactive power dissipated by the capacitive component of the equivalent circuit model for the dry band arcing process, which causes a distortion in the power measurement.
- The comparison between rms leakage current and dissipated power for each individual material across the different test voltages also showed only weak correlation.

Tests were also performed to determine the loss of hydrophobicity in the material samples. The results indicated that:

- All materials showed the lowest hydrophobicity losses for the AC series, followed by the positive DC series. The application of the negative DC voltage resulted in the greatest loss of surface hydrophobicity for all four materials.
- Material C showed the highest permanent loss of hydrophobicity, followed by materials D and B, respectively. The highest degree of hydrophobic recovery was revealed by Material A.
- Since these results do not show strong correlation to those of the erosion severity, rms leakage current or dissipated power criterion, it was concluded that the loss of surface hydrophobicity must be caused depend on other factors.

Finally, the chemical analysis by means of an ATR FTIR analysis was done separately for the PDMS based samples (materials A, B and D) and the EPDM material (material C). The analysis for the PDMS focused on the loss of ATH filler, loss of methyl groups and oxidisation through the formation of carbonyl groups, while the EPDM was investigated on loss of ATH filler and formation of carbonyl groups only. The obtained results were as follows:

- The chemical results for both material types showed little correlation to the intensity of the arcing processes of the different voltage types.
- The PDMS materials showed no significant correlation between the chemical analysis results and those for erosion severity. The only correlation observed was between the results for methyl group loss and the loss for hydrophobicity, in a sense that materials with a greater loss of methyl groups also showed an increased loss of surface hydrophobicity.
- The chemical analysis results for the EPDM corresponded well to the results for the criteria of erosion severity, indicating that the erosion in EPDM can be directly related to the formation of carbonyl groups and the loss of ATH filler material.

From the results obtained in this project, it is gathered that HTV silicone rubbers are most severely eroded by surface discharges under a positive DC voltage, while the same is true for RTV coatings under negative DC voltage conditions. The EPDM material showed the greatest erosion when exposed to an AC voltage. Furthermore, the PDMS based materials showed a greater variation in their results for the different voltage types, indicating a strong dependence of the electrical erosion on the type of voltage applied. The EPDM, on the other hand, revealed smaller differences in its erosion severity results for the three different voltages, indicating a large degree of independence between the voltage type and the expected electrical erosion.

These results also show that the IPT method can be applied and used to compare the tracking and erosion resistance of different polymeric insulator materials when exposed to surface discharges of both AC and bipolar DC.

It should be noted, however, that insulator samples are exposed to extremely harsh pollution and discharge conditions when tested using the IPT method. For example, silicone rubber materials are given no opportunity to recover any lost hydrophobicity during the tests, whereas silicone rubber insulators in field conditions usually have enough time to do so and suppress any electrical discharges, thus decreasing the electrical erosion. The results obtained during the IPT test runs thus might be more severe than those obtained during field conditions. Furthermore, the IPT method is an

isolated laboratory test method focusing on the tracking and erosion resistance of a given insulation material and not a full in-service insulator design. These factors must be kept in mind when drawing parallels between laboratory and field results.

6.4 Recommendations and further work

The following recommendations are given for further research work:

- One should consider omitting the abrasion process from the sample preparation procedure. Although this procedure was done in accordance with the IEC 60587 standard, a test run with an untreated sample during test series AC4-A (sample AC4-A6) showed strong deviations from the results of the abraded samples of the series for several evaluation criteria, including mass loss and the correlation analysis of the rms leakage current. Furthermore, a test for loss of hydrophobicity in virgin samples of the four different materials showed a considerable permanent loss in the EPDM and even the HTV silicone rubber materials caused by the abrasion process. The abrasion process could thus interfere with the results of the IPT.
- Future studies should also be performed to study the effects of varying sample thickness on the results for tracking and erosion resistance of samples tested using the IPT method, especially when the samples are exposed to different voltage types. It was postulated in this thesis that a lower sample thickness can result in an increased occurrence of sample failure, but further work is needed to confirm this.
- The use of computer software should be investigated in evaluating the results of hydrophobicity tests when using the spray method of the IEC 62073 standard. Such measures could aid in making the evaluation of insulator samples more objective, increasing the accuracy of the obtained results.

Having established the relative performance of four typical polymeric insulator materials in terms of their erosion and tracking resistance in a laboratory environment, this study can and should now be adapted for field tests at KIPTS (and other possible tests sites) once the bipolar DC source has been implemented and commissioned at this test site. This is necessary in order to evaluate the performance of actual

insulators under the different voltage types in an in-service environment, since the performance of insulators not only depends on the material it is made of, but also on several other different factors, most notably its shape.

References

[1] http://www.nampower.com.na/pages/caprivi.asp, [12 June 2008]

[2] http://www.rmst.co.il/HVDC_Proven_Technology.pdf, [4 September 2007]

[3] http://www.answers.com/topic/high-voltage-direct-current, [4 September 2007]

[4] J Arrillaga, 1998, *High Voltage Direct Current Transmission*, 2nd Edition, The Institution of Electrical Engineers, London

[5] http://www.answers.com/topic/cascading-failure, [4 September 2007]

[6] L Weimers, *Bulk power transmission at extra high voltages, a comparison between transmission lines for HVDC at voltages above 600 kV DC and 800 kV AC,* ABB Power Technologies AB, Ludvika, Sweden

[7] WL Vosloo, RE Macey, C de Tourreil, 2004, *The Practical Guide to Outdoor High Voltage Insulators*, Crown Publications CC., Johannesburg

[8] RS Gorur, EA Cherney, JT Burnham, 1999, *Outdoor Insulators*, Ravi S. Gorur Inc., Phoenix, USA

[9] International Standard IEC 62217, *Polymeric insulators for indoor and outdoor use with a nominal voltage > 1000 V – General definitions, test methods and acceptance criteria*, First Edition 2005

[10] N van der Merwe, 2000, *An Investigation into the Qualities of New and Field Aged Cycloaliphatic Epoxide Insulation in the Republic of South Africa*, Masters Degree in Engineering Sciences, Stellenbosch University, December 2000

[11] JT Burnham, 1995, *Bird streamer flashovers on FPL transmission lines*, IEEE Transactions on Power Delivery, Vol. 10, No. 2

[12] M Amin, M Salman, 2006, *Ageing of Polymeric Insulators (An Overview)*, Reviews on Advanced Material Science, Vol. 13

[13] R Gorur, 2000, *Ageing*, Arizona State University, INMR quarterly review, February 2000

[14] Electra No.143, *Guide for the identification of brittle fracture of composite insulator FRP rod*, August 1992

[15] F Schmuck, C de Tourreil, 2001, *Brittle fracture of composite insulators: an investigation of their occurrence and failure mechanisms and a risk assessment*, Cigre 4th Southern Africa Regional Conference, Cape Town

[16] C de Tourreil, L Pargamin, G Thevenet, S. Prat, N. Siampiringue, 2001, *Brittle fracture of composite insulators: the new explanation and a field case study*, ISH 2001 Bangalore, India, paper 5-25

[17] http://en.wikipedia.org/wiki/Hydrophobe, [20 December 2007]

[18] http://en.wikipedia.org/wiki/Hygroscopy, [20 December 2007]

[19] JP Reynders, IR Jandrell, SM Reynders, 1999, *Review of Ageing and Recovery of Silicone Rubber Insulation for Outdoor Use*, IEEE Transactions on Dielectrics and Electrical Insulation, Vol. 6, No. 5, page 620 – 631

[20] RS Gorur, GG Karady, A Jagota, M Shah, AM Yates, 1992, *Ageing of Silicone Rubber used for Outdoor Insulation*, IEEE Transactions on Power Delivery, Vol. 7, No. 2, page 525 – 538

[21] RJ Hill, 1994, *Laboratory Analysis of Naturally Aged Silicone Rubber Polymer Insulators from Contaminated Environments, 138 to 765 kV*, Presented at IEEE Power Engineering Society Transmission and Distribution Conference, April 1994

[22] J Kindersberger, M Kuhl, 1989, *Effect of Hydrophobicity on Insulator Performance*, 6th ISH Conference, 1989, New Orleans

[23] A Toth, I Bertoti, M Blazso, G Banhegyi, A Bognar, P Szaplonczay, 1994, *Oxidative Damage and Recovery of Silicone Rubber Surfaces: I. X-ray Photoelectron Spectroscopic Study*, Journal of Applied Polymer Science, Vol. 52, page 1293 – 1307

[24] J Kindersberger, A Schultz, HC Kärner, R van de Huir, 1996, *Service Performance, Material Design and Applications of Composite Insulators with Silicone Rubber Housings*, Cigré Session 1996, page 33 – 303

[25] SH Kim, EA Cherney, R Hackman, 1990, *The Loss and Recovery of Hydrophobicity of RTV Silicone Rubber Insulator Coatings*, IEEE Transactions on Power Delivery, Vol. 5, No. 3, page 1491 – 1499

[26] RS Gorur, LA Johnson, HC Hervig, 1991, *Contamination performance of Silicone Rubber Cable Terminations*, IEEE Transactions on Power Delivery, Vol. 6, No. 4, page 1366 – 1370

[27] H Janssen, A Herden, HC Kärner, 1997, *The Loss and Recovery of Hydrophobicity on Silicone Rubber Surfaces*, ISH Conference, 1997, Montreal, page 145 – 148

[28] J Hofman, R Barsch, 1995, *Effects of Electrohydrodynamic Processes in Droplet Layers to Partial Discharges and Leakage Current and their use for a sensitive Diagnostic on Polymeric Insulating Surfaces*, 9th ISH Conference, 1995, Graz, page 5605-1 to 5605-4

[29] R Barsch, J Lambrecht, H-J Winter, 1997, *On the Evaluation of Influences on the Hydrophobicity of Silicone Rubber Surfaces*, ISH Conference, 1997, Montréal, page 13 – 16

[30] AJ Phillips, DJ Childs, HM Schneider, 1998, *Ageing of Non-Ceramic Insulators due to Corona from Water Drops*, IEEE Power Engineering Society Transactions, WM236

[31] A Tomanek, 1991, *Silicones & Industry: A compendium for practical use, instruction and reference*, Wacker-Chemie GmbH, Munich

[32] LH Meyer, SH Jayaram, EA Cherney, 2004, *Correlation of Damage, Dry Band Arcing Energy, and Temperature in Inclined Plane Testing of Silicone Rubber for Outdoor Insulation*, IEEE Transactions on Dielectrics and Electrical Insulation, Vol. 11, No.3, page 424 – 432

[33] S Kumagai, N Yoshimura, 2001, *Tracking and Erosion of HTV Silicone Rubbers of Different Thickness*, IEEE Transactions on Dielectrics and Electrical Insulation, Vol. 8, No. 4, page 673 - 678

[34] International Standard IEC 60587, *Electrical insulating materials used under severe ambient conditions – Test methods for evaluating resistance to tracking and erosion*, Third edition 2007

[35] International Standard ASTM D2303, *Standard Test Methods for Liquid-Contaminant, Incline-Plane Tracking and Erosion of Insulating Materials*, 1997

[36] V Rajini, K Udaya Kumar, 2007, *Quantification of Damage due to Surface Tracking*, IEEE Transaction on Dielectrics and Electrical Insulation, Vol. 14, No. 5

[37] P Rakeketsi, 2000, *Construction of an Inclined-Plane Tracking and Erosion Tester for High Voltage Polymeric Insulating Materials*, Btech Degree thesis, Cape Technikon, December 2000

[38] CL Sias, 2002, *Comparative Study of Different Insulator types under the effect of Artificial Pollution by means of a Inclined Plane Tester*, B.Eng (Electrical & Electronic) thesis, Stellenbosch University, November 2002

[39] JD Glover, MS Sarma, 2002, *Power System Analysis and Design*, Third edition, Brooks/Cole, Pacific Grove, USA

[40] CB Engelbrecht, 2004, *Skuinsvlaktoetse op Isolatormonsters*, B.Eng (Electrical & Electronic) thesis, Stellenbosch University, December 2004

[41] CT Crowe, DF Elger, JA Roberson, 2001, *Engineering Fluid Mechanics*, Seventh edition, John Wiley & Sons, Hoboken, New Jersey

[42] http://www.coleparmer.com/techinfo/techinfo.asp?htmlfile=Conductivity.htm&ID=78, [4 September 2007]

[43] International Standard IEC 60507, *Artificial pollution tests on high-voltage insulators to be used on a.c. systems*, Second edition 1991

[44] RS Figliola, DE Beasley, 2000, *Theory and Design for Mechanical Measurements*, Third edition, John Wiley & Sons, Hoboken, New Jersey

[45] PR Griffiths, JA de Haseth, 1986, *Fourier Transform Infrared Spectroscopy*, John Wiley & Sons, Hoboken, New Jersey

[46] HF Mark, 2003, *Encyclopaedia of Polymer Science and Technology*, Volume 8, John Wiley & Sons, Hoboken, New Jersey

[47] S Kim, EA Cherney, R Hackam, KG Rutherford, 1994, *Chemical Changes at the Surface of RTV Silicone Rubber Coatings on Insulators During Dry-Band Arcing*, IEEE Transaction on Dielectrics and Electrical Insulation, Vol.1, No. 1, page 106 - 123

[48] DK Thomas, 1966, *Network Scission Processes in Peroxide Cured Methylvinyl Silicone Rubber*, Polymer, Vol.7, page 99 - 105

[49] J Economy, JH Mason, 1970, *Degradation of Inorganic Polymers*, Thermal Stability of Polymers, Vol. 1, page 577 - 615

[50] DC Atkins, CM Murphy, CE Saunders, 1947, *Polymethylsiloxanes: Thermal and Oxidation Stabilities*, Industrial & Engineering Chemistry, Vol. 39, page 1395 - 1401

[51] RC Osthoff, AM Bueche, WT Grubb, 1954, *Chemical Stress Relaxation of Polydimethylsiloxane Elastomers*, Journal of the American Chemical Society, Vol. 76, page 4659 - 4663

[52] P Paloniemi, 1981, *Theory of Equalization of Thermal Ageing Process of Electrical Insulating Materials in Thermal Endurance Tests. I: Review of Theoretical Basis of Test Methods and Chemical and Physical Aspects of Ageing*, IEEE Transaction on Electrical Insulation, Vol. 16, page 1 - 6

[53] C Burgess, A Knowles, 1981, S*tandards in Absorption Spectrometry*, Chapman and Hall, New York

[54] RH Petrucci, WS Harwood, FG Herring, 2002, *General Chemistry: Principles and Modern Applications*, Eighth edition, Prentice Hall, Upper Saddle River, New Jersey

[55] TG Gustavsson, SM Gubanski, H Hillborg, S Karlsson, UW Gedde, 2001, *Ageing of Silicone Rubber under ac or dc Voltages in a Coastal Environment*, IEEE Transactions on Dielectrics and Electrical Insulation, Vol. 8, No. 6, page 1029 - 1039

[56] JM Seifert, R Bärsch, 2007, *Design Evaluation of Silicone Rubber Composite Insulators under the Aspect of Surface Pollution Stress*, ISH 15th International Symposium on High Voltage Engineering, August 2007, Ljubljana, Slovenia

[57] International Standard IEC 61109, *Composite insulators for a.c. overhead lines with a nominal voltage greater than 1000 V- Definitions, test methods and acceptance criteria*, First edition 1992

[58] WL Vosloo, 2002, *A Comparison of the Performance of High-Voltage Insulator Materials in a Severely Polluted Coastal Environment*, PhD dissertation, Department of Electrical and Electronic Engineering, Stellenbosch University, March 2002

[59] International Standard IEC 62073, *Guidance on the measurement of wettability of insulator surfaces*, First edition 2003

[60] WD Callister Jr., 2003, *Materials Science and Engineering: An Introduction*, Sixth Edition, John Wiley & Sons, Hoboken, New Jersey

[61] E Kuffel, WS Zaengl, J Kuffel, 2000, *High Voltage Engineering: Fundamentals*, Second Edition, Newnes, Oxford

[62] S Kumagai, N Yoshimura, 2001, *Tracking and Erosion of HTV Silicone Rubber and Suppression Mechanism of ATH*, IEEE Transaction on Dielectrics and Electrical Insulation, Vol.8, No. 2, page 203 – 211

Appendix A: Waveforms Recorded during Material Comparison

This appendix contains typical leakage current waveforms of all test materials tested under the three different voltage types: AC, positive and negative DC. The waveforms displayed were taken at a test time of 3 h 00 min, halfway through the test runs. This was done to allow the test samples to develop a stable arcing behaviour typical for each insulation material in question.

Additionally, the oscilloscope time scale for these particular waveforms was increased in order to observe the arcing behaviour of the test samples over a longer period. This effect is shown in Fig. A 1 using waveforms recorded during a test run of series AC4-A.

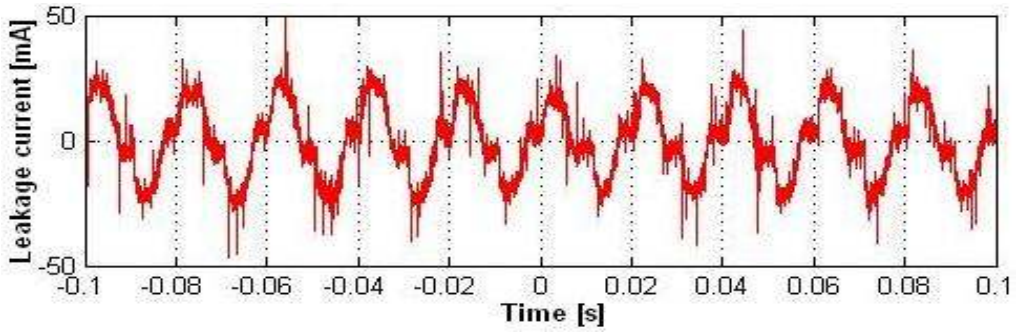

(a)

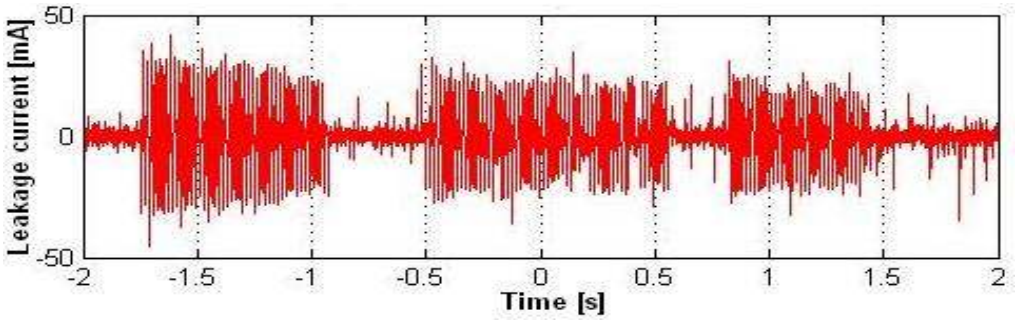

(b)

Fig. A 1: Leakage current waveforms: (a) Normal time scale and (b) Enlarged time scale.

By trial and error, the enlarged time scales used best suited for these observations were 400 ms per major division for the AC test voltage and 1.0 s per major division for both the positive and negative DC voltages.

A.1 Waveforms of AC test series

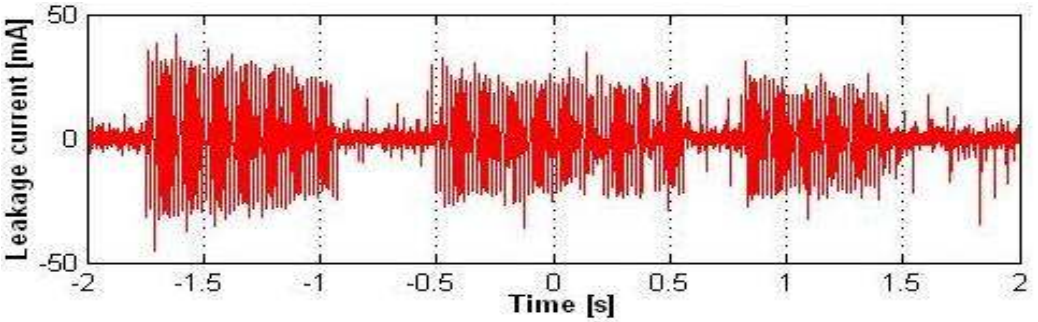

(a)

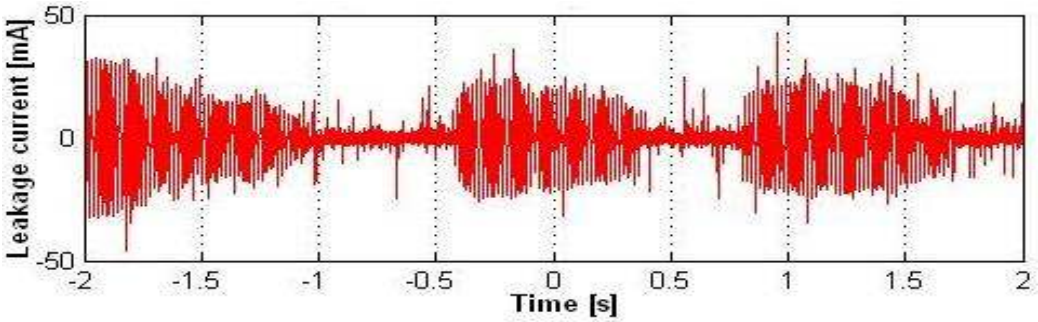

(b)

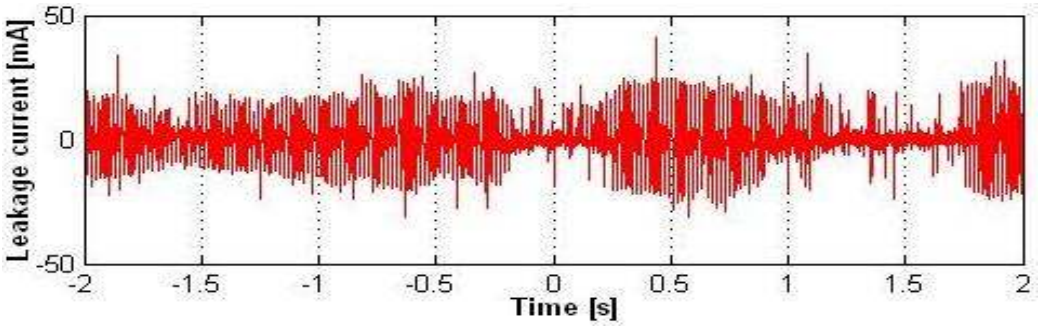

(c)

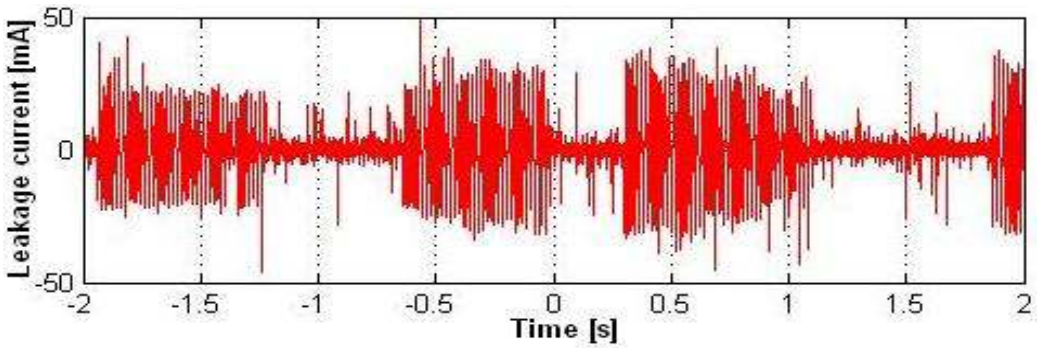

(d)

Fig. A 2: Leakage current waveforms showing amplitude envelope, recorded at time 3 h 00 min of AC4 test series: (a) Material A, (b) Material B, (c) Material C and (d) Material D.

A.2 Graphs of positive DC test series

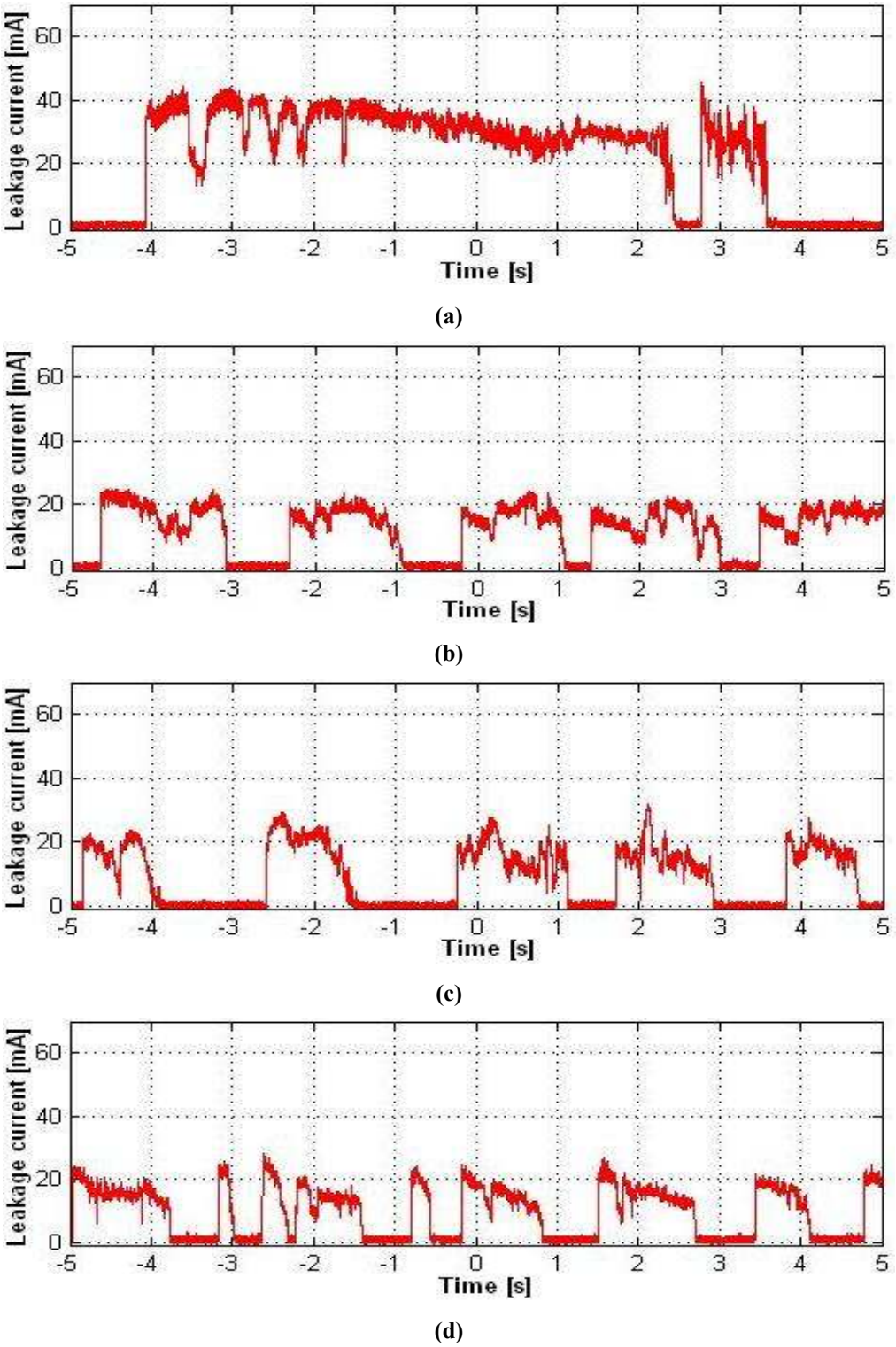

Fig. A 3: Leakage current graphs showing amplitude envelope, recorded at time 3 h 00 min of DP4 test series: (a) Material A, (b) Material B, (c) Material C and (d) Material D.

A.3 Graphs of negative DC series

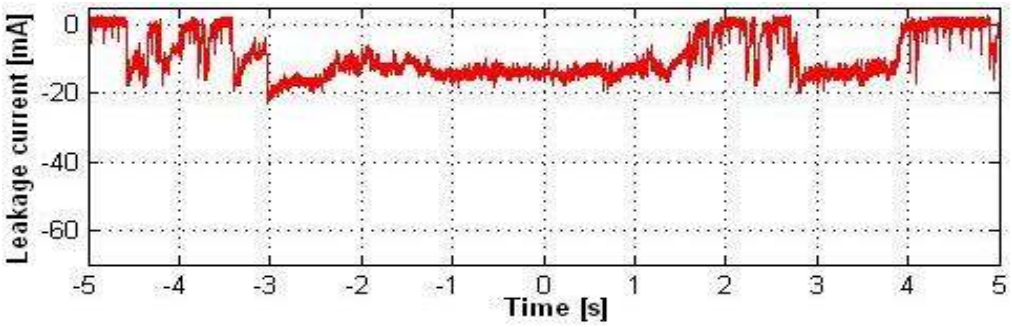

(a)

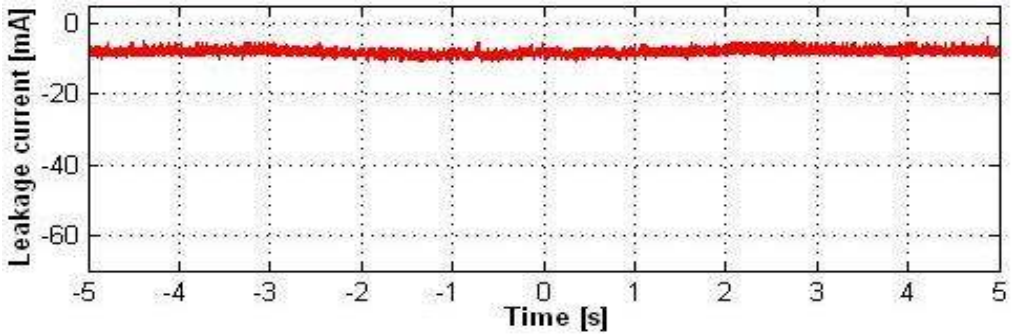

(b)

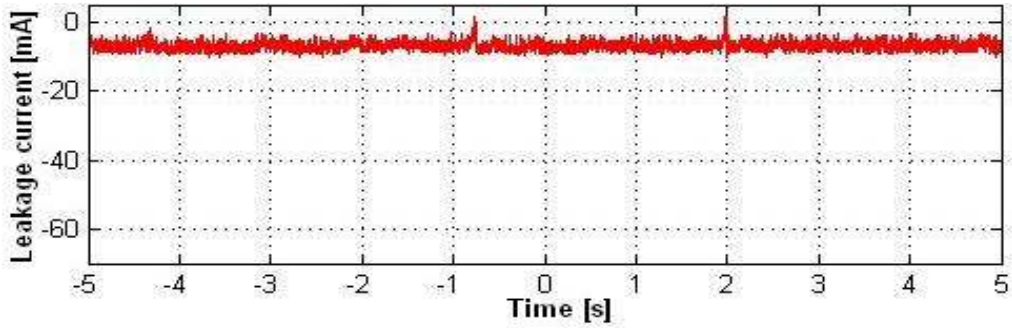

(c)

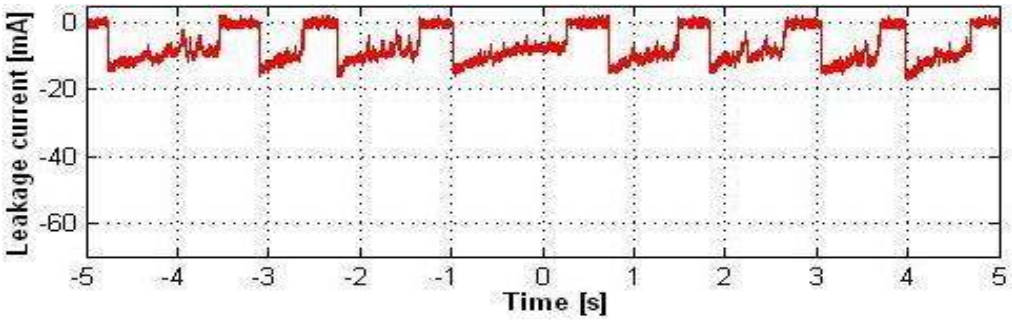

(d)

Fig. A 4: Leakage current graphs showing amplitude envelope, recorded at time 3 h 00 min of DN4 test series: (a) Material A, (b) Material B, (c) Material C and (d) Material D.

Appendix B: Summary of Sample Mass Loss

The material mass losses for each individual sample of the various test series are shown in Table B 1.

Table B 1: Summary of mass loss results.

Material	AC Series		DC + Series		DC - Series	
	Sample	Mass loss [mg]	Sample	Mass loss [mg]	Sample	Mass loss [mg]
A	AC4-A2	209	DP4-A1	126	DN4-A1	956
	AC4-A3	198	DP4-A2	151	DN4-A2	519
	AC4-A4	91	DP4-A3	247	DN4-A3	838
	AC4-A5	136	DP4-A4	184	DN4-A5	458
	AC4-A6	627	DP4-A5	327	DN4-A6	930
B	AC4-B1	119	DP4-B1	2285	DN4-B1	358
	AC4-B2	126	DP4-B3	6861	DN4-B2	238
	AC4-B3	120	DP4-B4	1697	DN4-B3	125
	AC4-B4	116	DP4-B5	7478	DN4-B5	193
	AC4-B6	124	DP4-B6	2724	DN4-B6	131
C	AC4-C1	605	DP4-C1	277	DN4-C1	198
	AC4-C2	115	DP4-C2	296	DN4-C2	203
	AC4-C3	163	DP4-C3	267	DN4-C3	203
	AC4-C4	312	DP4-C5	200	DN4-C5	168
	AC4-C6	394	DP4-C6	179	DN4-C6	174
D	AC4-D1	137	DP4-D2	422	DN4-D1	173
	AC4-D2	134	DP4-D3	735	DN4-D2	217
	AC4-D4	152	DP4-D4	2450	DN4-D3	155
	AC4-D5	140	DP4-D5	2425	DN4-D4	190
	AC4-D6	148	DP4-D6	3294	DN4-D6	161

The average mass loss as well as the standard deviation was calculated for each test series based on the results of the five samples of each series. The samples showing the greatest deviation from the relevant series average were then eliminated and the calculations for series mean and standard deviation were redone based on the four remaining samples. The following pages show tables summarizing the results for the test series of each individual voltage and material type, as well as the calculations for the series mean and standard deviation based on both five and four samples.

B.1 Mass loss summary for AC voltage

Table B 2: Mass loss summary for AC voltage.

Material A		Material B		Material C		Material D	
Sample	Mass loss [mg]	Sample	Mass loss [mg]	Sample	Mass loss [mg]	Sample	Mass loss [mg]
AC4-A2	209	AC4-B1	119	AC4-C1	605	AC4-D1	137
AC4-A3	198	AC4-B2	126	AC4-C2	115	AC4-D2	134
AC4-A4	91	AC4-B3	120	AC4-C3	163	AC4-D4	152
AC4-A5	136	AC4-B4	116	AC4-C4	312	AC4-D5	140
AC4-A6	627	AC4-B6	124	AC4-C6	394	AC4-D6	148
5 sample series mean	252	5 sample series mean	121	5 sample series mean	318	5 sample series mean	142
5 sample standard deviation	215	5 sample standard deviation	4	5 sample standard deviation	196	5 sample standard deviation	8
4 sample series mean	159	4 sample series mean	120	4 sample series mean	246	4 sample series mean	139
4 sample standard deviation	55	4 sample standard deviation	3	4 sample standard deviation	130	4 sample standard deviation	6

B.2 Mass loss summary for positive DC voltage

Table B 3: Mass loss summary for positive DC voltage.

Material A		Material B		Material C		Material D	
Sample	Mass loss [mg]	Sample	Mass loss [mg]	Sample	Mass loss [mg]	Sample	Mass loss [mg]
DP4-A1	126	DP4-B1	2285	DP4-C1	277	DP4-D2	422
DP4-A2	151	DP4-B3	6861	DP4-C2	296	DP4-D3	735
DP4-A3	247	DP4-B4	1697	DP4-C3	267	DP4-D4	2450
DP4-A4	184	DP4-B5	7478	DP4-C5	200	DP4-D5	2425
DP4-A5	327	DP4-B6	2724	DP4-C6	179	DP4-D6	3294
5 sample series mean	207	5 sample series mean	4209	5 sample series mean	244	5 sample series mean	1865
5 sample standard deviation	81	5 sample standard deviation	2736	5 sample standard deviation	51	5 sample standard deviation	1231
4 sample series mean	177	4 sample series mean	3392	4 sample series mean	260	4 sample series mean	2226
4 sample standard deviation	53	4 sample standard deviation	2351	4 sample standard deviation	42	4 sample standard deviation	1073

B.3 Mass loss summary for negative DC voltage

Table B 4: Mass loss summary for negative DC voltage.

Material A		Material B		Material C		Material D	
Sample	**Mass loss [mg]**	**Sample**	**Mass loss [mg]**	**Sample**	**Mass loss [mg]**	**Sample**	**Mass loss [mg]**
DN4-A1	956	DN4-B1	358	DN4-C1	198	DN4-D1	173
DN4-A2	519	DN4-B2	238	DN4-C2	203	DN4-D2	217
DN4-A3	838	DN4-B3	125	DN4-C3	203	DN4-D3	155
DN4-A5	458	DN4-B5	193	DN4-C5	168	DN4-D4	190
DN4-A6	930	DN4-B6	131	DN4-C6	174	DN4-D6	161
5 sample series mean	740	5 sample series mean	209	5 sample series mean	189	5 sample series mean	179
5 sample standard deviation	235	5 sample standard deviation	95	5 sample standard deviation	17	5 sample standard deviation	25
4 sample series mean	811	4 sample series mean	172	4 sample series mean	195	4 sample series mean	170
4 sample standard deviation	201	4 sample standard deviation	53	4 sample standard deviation	14	4 sample standard deviation	16

Appendix C: Summary of Sample Erosion Depth

The maximum erosion depth measured on each sample for the various test series is shown in Table C 1.

Table C 1: Summary of erosion depth results.

Material	AC Series		DC + Series		DC - Series	
	Sample	Erosion depth [mm]	Sample	Erosion depth [mm]	Sample	Erosion depth [mm]
A	AC4-A2	0.21	DP4-A1	0.39	DN4-A1	0.31
	AC4-A3	0.19	DP4-A2	0.48	DN4-A2	0.23
	AC4-A4	0.17	DP4-A3	0.37	DN4-A3	0.37
	AC4-A5	0.19	DP4-A4	0.50	DN4-A5	0.38
	AC4-A6	0.21	DP4-A5	0.29	DN4-A6	0.31
B	AC4-B1	0.28	DP4-B1	6.71	DN4-B1	3.47
	AC4-B2	0.31	DP4-B3	10.37	DN4-B2	0.72
	AC4-B3	0.29	DP4-B4	6.88	DN4-B3	0.80
	AC4-B4	0.31	DP4-B5	8.00	DN4-B5	1.06
	AC4-B6	0.50	DP4-B6	7.66	DN4-B6	0.77
C	AC4-C1	3.41	DP4-C1	1.19	DN4-C1	1.61
	AC4-C2	0.60	DP4-C2	1.46	DN4-C2	1.62
	AC4-C3	0.68	DP4-C3	1.45	DN4-C3	1.73
	AC4-C4	1.87	DP4-C5	0.78	DN4-C5	1.53
	AC4-C6	2.55	DP4-C6	0.83	DN4-C6	1.68
D	AC4-D1	0.33	DP4-D2	2.60	DN4-D1	0.37
	AC4-D2	0.39	DP4-D3	5.14	DN4-D2	1.55
	AC4-D4	0.17	DP4-D4	6.68	DN4-D3	0.98
	AC4-D5	0.24	DP4-D5	6.65	DN4-D4	1.92
	AC4-D6	0.25	DP4-D6	6.55	DN4-D6	0.91

The series mean and standard deviation were calculated for each test series based on the data of the five samples contained in each series. For each series, the sample measurements were the compared with the series mean in order to locate the sample with the greatest deviation from the mean. This sample was then omitted and the calculations for series mean and standard deviation were repeated based on the four remaining samples. The following tables summarize the erosion depth measurements for the test series of each of the three voltage types. They also contain the values for series mean and standard deviation based on both five and four samples per series.

C.1 Erosion depth summary for AC voltage

Table C 2: Erosion depth summary for AC voltage.

Material A		Material B		Material C		Material D	
Sample	Erosion depth [mm]	Sample	Erosion depth [mm]	Sample	Erosion depth [mm]	Sample	Erosion depth [mm]
AC4-A2	0.21	AC4-B1	0.28	AC4-C1	3.41	AC4-D1	0.33
AC4-A3	0.19	AC4-B2	0.31	AC4-C2	0.60	AC4-D2	0.39
AC4-A4	0.17	AC4-B3	0.29	AC4-C3	0.68	AC4-D4	0.17
AC4-A5	0.19	AC4-B4	0.31	AC4-C4	1.87	AC4-D5	0.24
AC4-A6	0.21	AC4-B6	0.50	AC4-C6	2.55	AC4-D6	0.25
5 sample series mean	0.19	5 sample series mean	0.34	5 sample series mean	1.82	5 sample series mean	0.28
5 sample standard deviation	0.02	5 sample standard deviation	0.09	5 sample standard deviation	1.21	5 sample standard deviation	0.09
4 sample series mean	0.20	4 sample series mean	0.30	4 sample series mean	1.43	4 sample series mean	0.25
4 sample standard deviation	0.01	4 sample standard deviation	0.02	4 sample standard deviation	0.95	4 sample standard deviation	0.07

C.2 Erosion depth summary for positive DC series

Table C 3: Erosion depth summary for positive DC voltage.

Material A		Material B		Material C		Material D	
Sample	Erosion depth [mm]	Sample	Erosion depth [mm]	Sample	Erosion depth [mm]	Sample	Erosion depth [mm]
DP4-A1	0.39	DP4-B1	6.71	DP4-C1	1.19	DP4-D2	2.60
DP4-A2	0.48	DP4-B3	10.37	DP4-C2	1.46	DP4-D3	5.14
DP4-A3	0.37	DP4-B4	6.88	DP4-C3	1.45	DP4-D4	6.68
DP4-A4	0.50	DP4-B5	8.00	DP4-C5	0.78	DP4-D5	6.65
DP4-A5	0.29	DP4-B6	7.66	DP4-C6	0.83	DP4-D6	6.55
5 sample series mean	0.41	5 sample series mean	7.93	5 sample series mean	1.14	5 sample series mean	5.52
5 sample standard deviation	0.09	5 sample standard deviation	1.47	5 sample standard deviation	0.33	5 sample standard deviation	1.76
4 sample series mean	0.44	4 sample series mean	7.31	4 sample series mean	1.23	4 sample series mean	6.25
4 sample standard deviation	0.07	4 sample standard deviation	0.62	4 sample standard deviation	0.30	4 sample standard deviation	0.74

C.3 Erosion depth summary for negative DC voltage

Table C 4: Erosion depth summary for negative DC voltage.

Material A		Material B		Material C		Material D	
Sample	**Erosion depth [mm]**	**Sample**	**Erosion depth [mm]**	**Sample**	**Erosion depth [mm]**	**Sample**	**Erosion depth [mm]**
DN4-A1	0.31	DN4-B1	3.47	DN4-C1	1.61	DN4-D1	0.37
DN4-A2	0.23	DN4-B2	0.72	DN4-C2	1.62	DN4-D2	1.55
DN4-A3	0.37	DN4-B3	0.80	DN4-C3	1.73	DN4-D3	0.98
DN4-A5	0.38	DN4-B5	1.06	DN4-C5	1.53	DN4-D4	1.92
DN4-A6	0.31	DN4-B6	0.77	DN4-C6	1.68	DN4-D6	0.91
5 sample series mean	0.32	5 sample series mean	1.36	5 sample series mean	1.63	5 sample series mean	1.15
5 sample standard deviation	0.06	5 sample standard deviation	1.18	5 sample standard deviation	0.07	5 sample standard deviation	0.60
4 sample series mean	0.34	4 sample series mean	0.84	4 sample series mean	1.66	4 sample series mean	1.34
4 sample standard deviation	0.04	4 sample standard deviation	0.15	4 sample standard deviation	0.06	4 sample standard deviation	0.48

Appendix D: Summary of Sample Erosion Area

A summary of the erosion area measurements for each individual sample, obtained from the erosion depth data using the method described in section 5.3.4, is given in Table D 1.

Table D 1: Summary of erosion area measurements.

Material	AC Series		DC + Series		DC - Series	
	Sample	Erosion area [mm^2]	Sample	Erosion area [mm^2]	Sample	Erosion area [mm^2]
A	AC4-A2	157.6	DP4-A1	280.7	DN4-A1	1224.4
	AC4-A3	225.8	DP4-A2	445.2	DN4-A2	935.1
	AC4-A4	15.5	DP4-A3	777.9	DN4-A3	1254.4
	AC4-A5	13.8	DP4-A4	454.1	DN4-A5	1356.8
	AC4-A6	134.2	DP4-A5	878.9	DN4-A6	1531.9
B	AC4-B1	29.7	DP4-B1	501.6	DN4-B1	87.5
	AC4-B2	14.6	DP4-B3	803.8	DN4-B2	80.6
	AC4-B3	10.9	DP4-B4	329.1	DN4-B3	56.1
	AC4-B4	16.8	DP4-B5	1077.5	DN4-B5	58.3
	AC4-B6	26.2	DP4-B6	555.4	DN4-B6	49.5
C	AC4-C1	261.4	DP4-C1	301.0	DN4-C1	117.6
	AC4-C2	71.3	DP4-C2	463.7	DN4-C2	144.4
	AC4-C3	72.6	DP4-C3	421.9	DN4-C3	190.4
	AC4-C4	118.2	DP4-C5	299.0	DN4-C5	225.9
	AC4-C6	193.2	DP4-C6	294.0	DN4-C6	118.6
D	AC4-D1	11.6	DP4-D2	149.0	DN4-D1	77.3
	AC4-D2	14.8	DP4-D3	252.1	DN4-D2	98.0
	AC4-D4	4.7	DP4-D4	388.8	DN4-D3	77.6
	AC4-D5	12.0	DP4-D5	439.7	DN4-D4	75.5
	AC4-D6	10.6	DP4-D6	641.3	DN4-D6	72.8

The series mean and standard deviation were then calculated for every individual test series, both for the original five samples per series and then again for the four samples of each series showing the smallest deviation from the series mean. The results for each test series were grouped into tables according to voltage type, as displayed in the following sections.

D.1 Erosion area summary for AC voltage

Table D 2: Erosion area summary for AC voltage.

Material A		Material B		Material C		Material D	
Sample	Erosion area [mm^2]	Sample	Erosion area [mm^2]	Sample	Erosion area [mm^2]	Sample	Erosion area [mm^2]
AC4-A2	158	AC4-B1	30	AC4-C1	261	AC4-D1	12
AC4-A3	226	AC4-B2	15	AC4-C2	71	AC4-D2	15
AC4-A4	16	AC4-B3	11	AC4-C3	73	AC4-D4	5
AC4-A5	14	AC4-B4	17	AC4-C4	118	AC4-D5	12
AC4-A6	134	AC4-B6	26	AC4-C6	193	AC4-D6	11
5 sample series mean	109	5 sample series mean	20	5 sample series mean	143	5 sample series mean	11
5 sample standard deviation	93	5 sample standard deviation	8	5 sample standard deviation	83	5 sample standard deviation	4
4 sample series mean	80	4 sample series mean	17	4 sample series mean	114	4 sample series mean	12
4 sample standard deviation	76	4 sample standard deviation	7	4 sample standard deviation	57	4 sample standard deviation	2

D.2 Erosion area summary for positive DC voltage

Table D 3: Erosion area summary for positive DC voltage.

Material A		Material B		Material C		Material D	
Sample	Erosion area [mm^2]	Sample	Erosion area [mm^2]	Sample	Erosion area [mm^2]	Sample	Erosion area [mm^2]
DP4-A1	281	DP4-B1	502	DP4-C1	301	DP4-D2	149
DP4-A2	445	DP4-B3	804	DP4-C2	464	DP4-D3	252
DP4-A3	778	DP4-B4	329	DP4-C3	422	DP4-D4	389
DP4-A4	454	DP4-B5	1078	DP4-C5	299	DP4-D5	440
DP4-A5	879	DP4-B6	555	DP4-C6	294	DP4-D6	641
5 sample series mean	567	5 sample series mean	654	5 sample series mean	356	5 sample series mean	374
5 sample standard deviation	251	5 sample standard deviation	292	5 sample standard deviation	81	5 sample standard deviation	188
4 sample series mean	489	4 sample series mean	547	4 sample series mean	329	4 sample series mean	307
4 sample standard deviation	208	4 sample standard deviation	196	4 sample standard deviation	62	4 sample standard deviation	132

D.3 Erosion area summary for negative DC voltage

Table D 4: Erosion area summary for negative DC voltage.

Material A		Material B		Material C		Material D	
Sample	Erosion area [mm^2]	Sample	Erosion area [mm^2]	Sample	Erosion area [mm^2]	Sample	Erosion area [mm^2]
DN4-A1	1224	DN4-B1	88	DN4-C1	118	DN4-D1	77
DN4-A2	935	DN4-B2	81	DN4-C2	144	DN4-D2	98
DN4-A3	1254	DN4-B3	56	DN4-C3	190	DN4-D3	78
DN4-A5	1357	DN4-B5	58	DN4-C5	226	DN4-D4	76
DN4-A6	1532	DN4-B6	50	DN4-C6	119	DN4-D6	73
5 sample series mean	1261	5 sample series mean	66	5 sample series mean	159	5 sample series mean	80
5 sample standard deviation	218	5 sample standard deviation	17	5 sample standard deviation	47	5 sample standard deviation	10
4 sample series mean	1342	4 sample series mean	71	4 sample series mean	143	4 sample series mean	76
4 sample standard deviation	139	4 sample standard deviation	16	4 sample standard deviation	34	4 sample standard deviation	2

D.4 3D contour plots of measured erosion area

The measurement data used to ascertain the erosion depth and area of each sample was further used to plot the measured area on each sample as a 3D surface plot using Matlab. These virtual models of the erosion area were then compared to the actual sample in order to check the accuracy of the measured data. Due to the large number of samples, only one representative sample per test series is shown in the following sections. The plots are grouped together according to material type.

D.4.1 Surface plots for material A

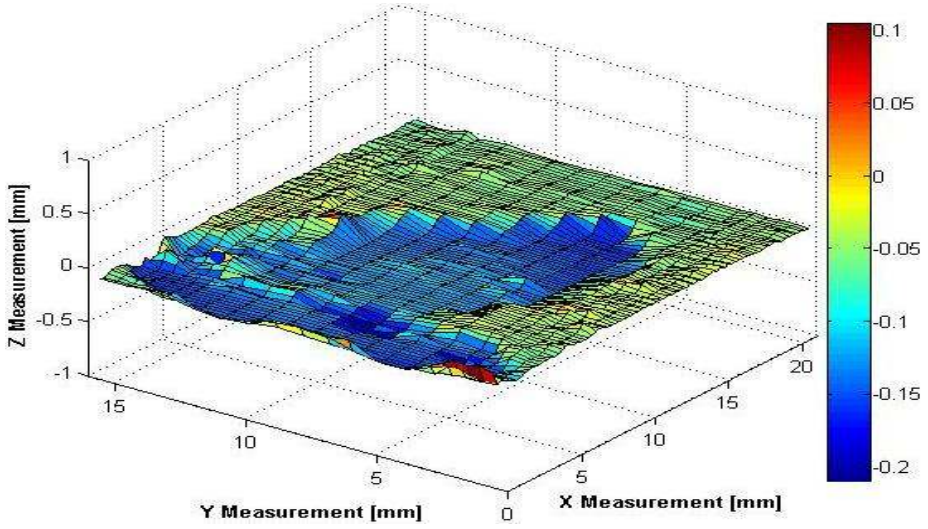

(a)

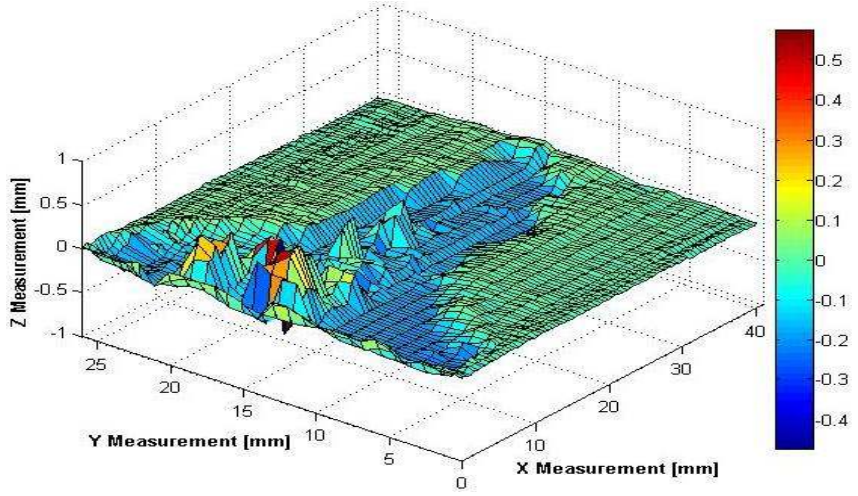

(b)

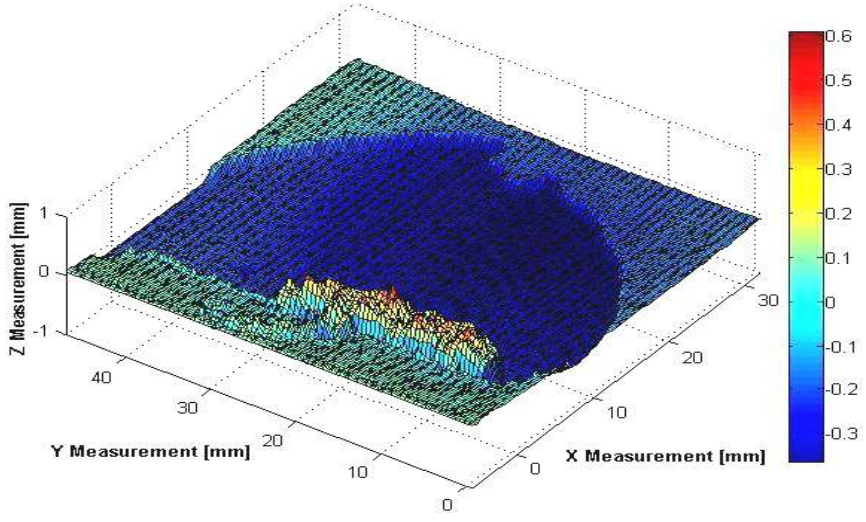

(c)

Fig. D 1: Surface plots of erosion area for material A: (a) AC4-A2, (b) DP4-A2 and (c) DN4-A3.

D.4.2 Surface plots for material B

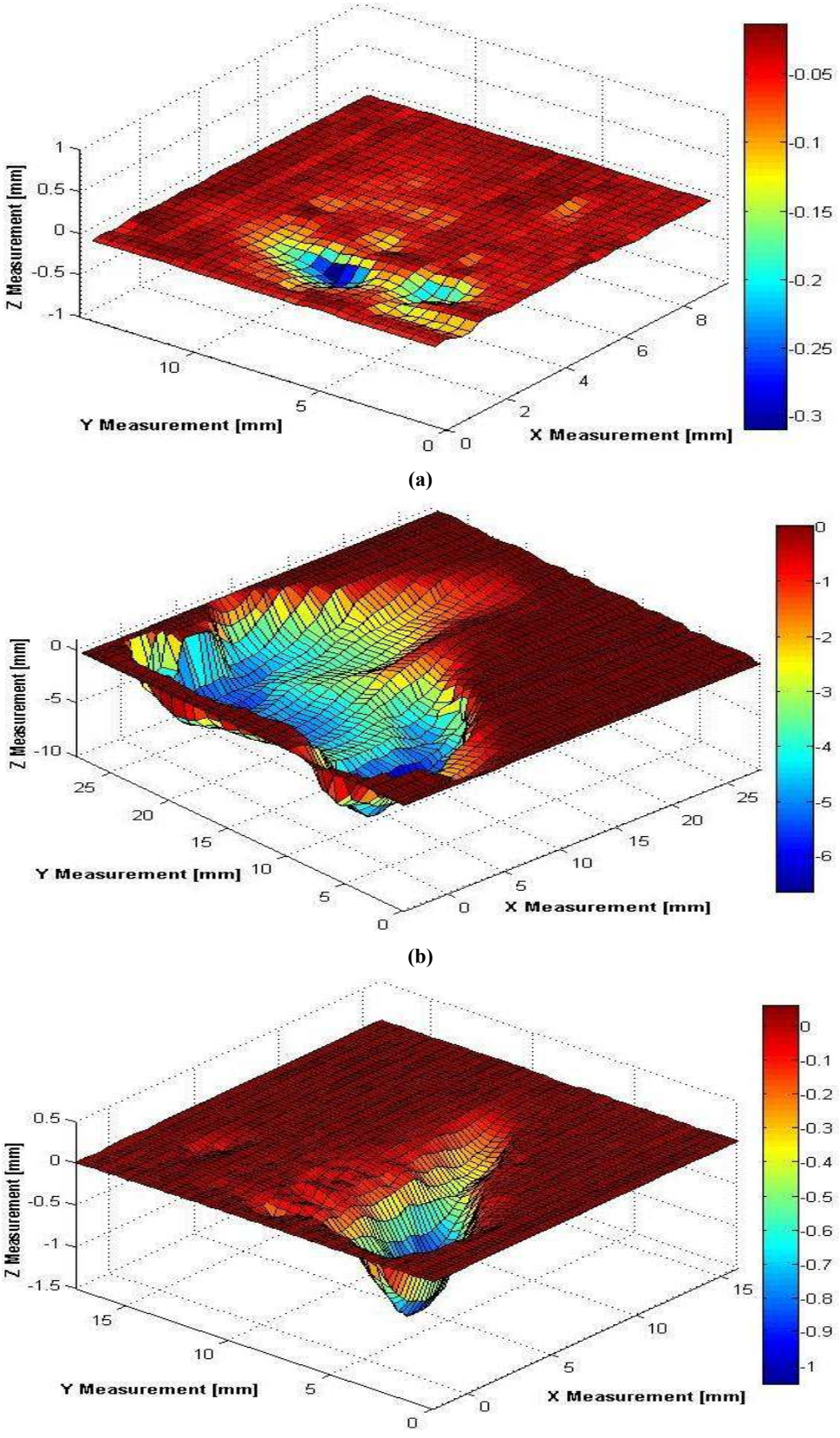

Fig. D 2: Surface plots of erosion area for material B: (a) AC4-B4, (b) DP4-B1 and (c) DN4-B5.

D.4.3 Surface plots for material C

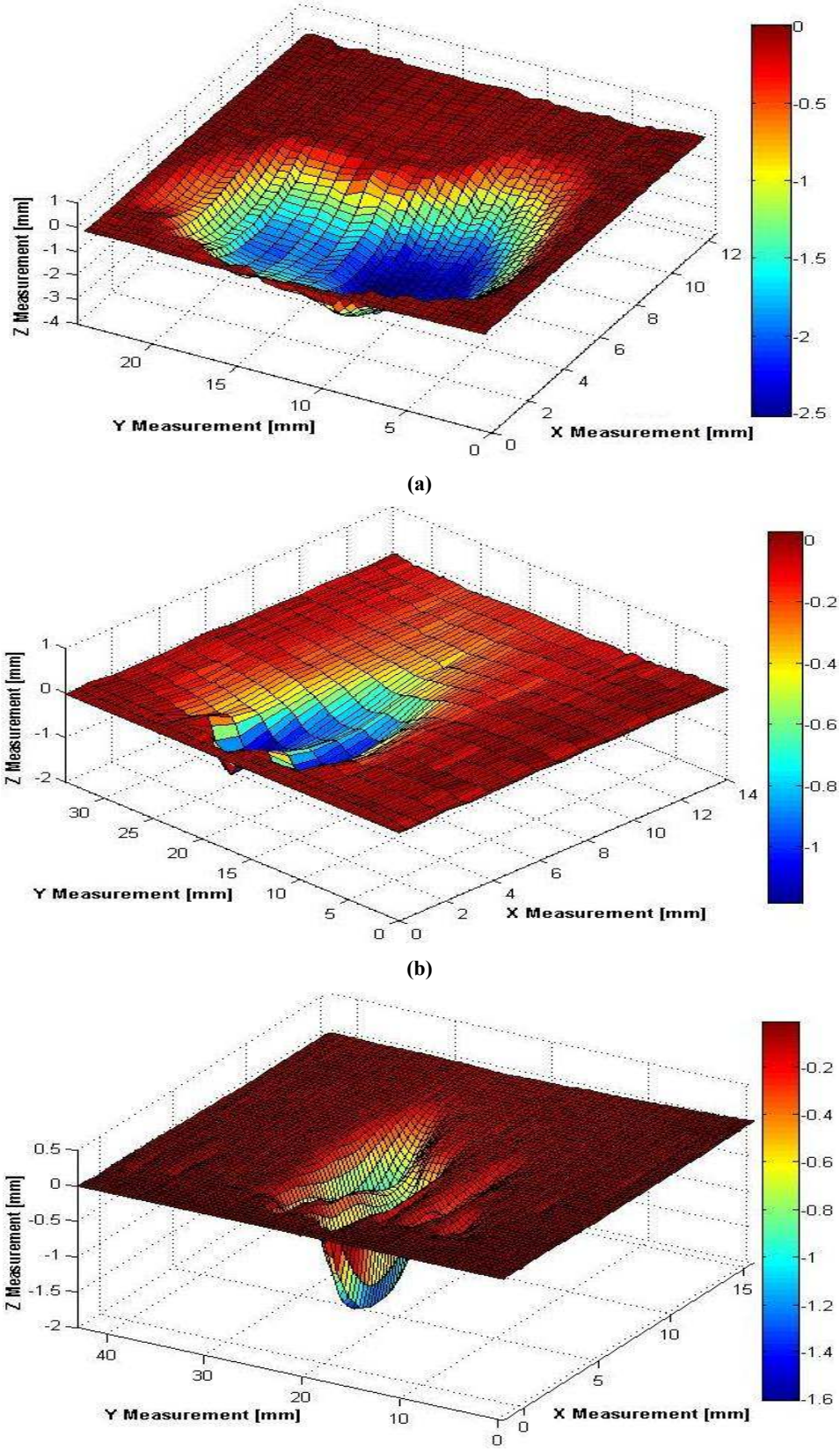

Fig. D 3: Surface plots of erosion area for material C: (a) AC4-C6, (b) DP4-C1 and (c) DN4-C2.

D.4.4 Surface plots for material D

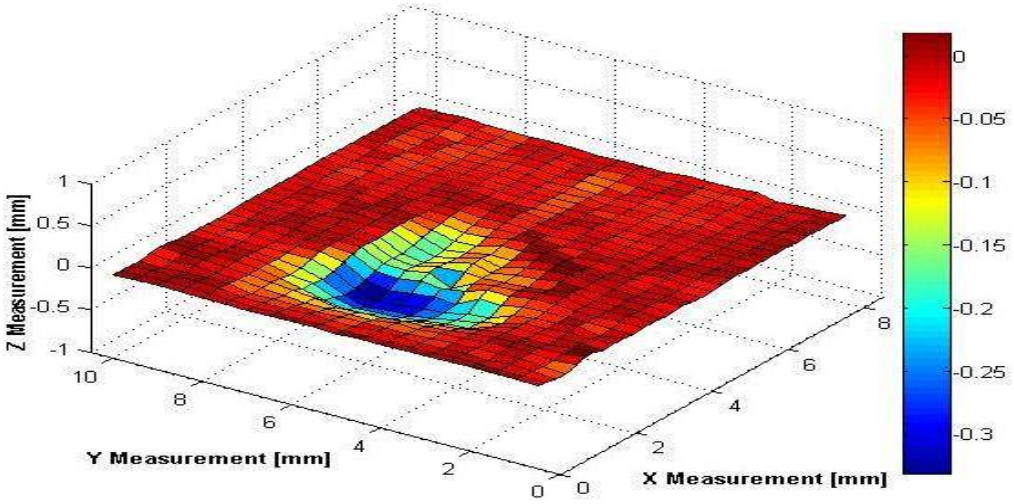

(a)

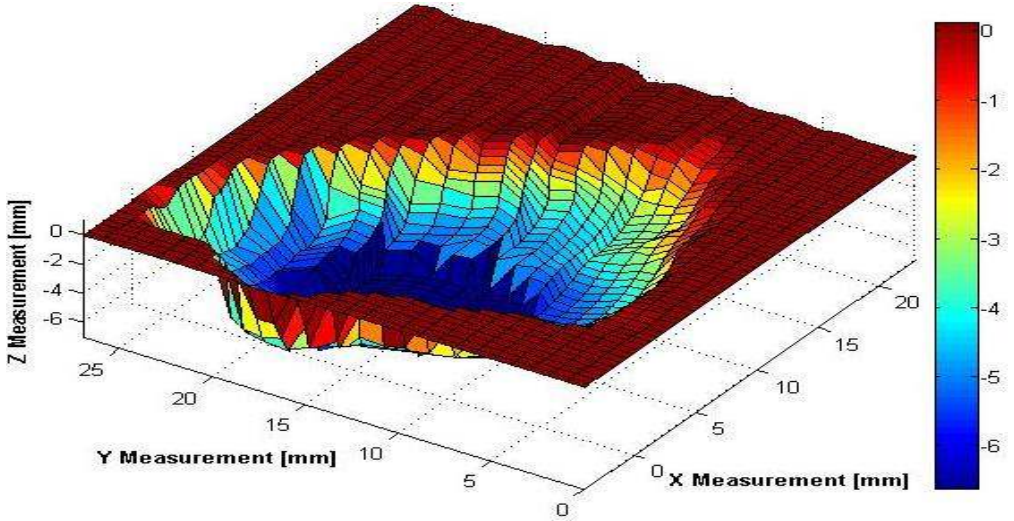

(b)

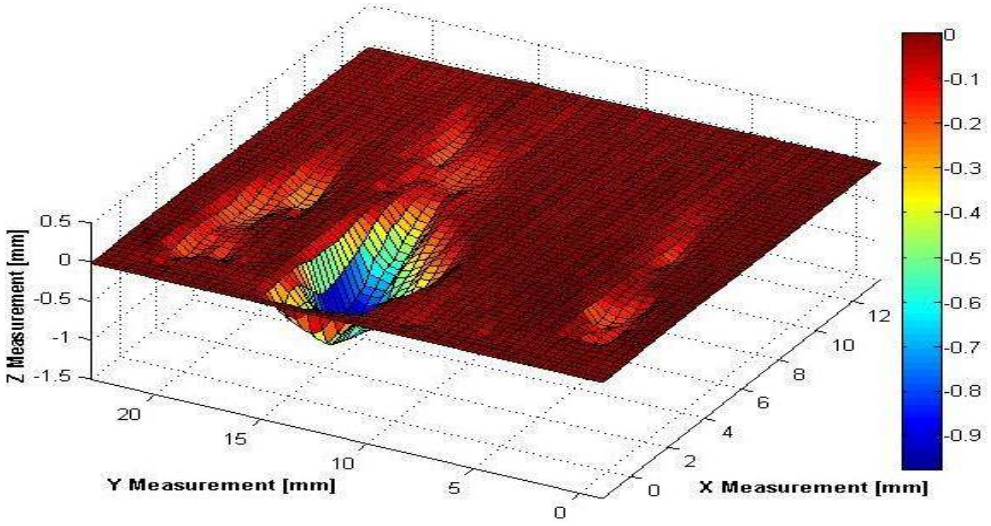

(c)

Fig. D 4: Surface plots of erosion area for material D: (a) AC4-D1, (b) DP4-D4 and (c) DN4-D3.

Appendix E: Rms Leakage Current Data

The rms leakage current values were measured by the OLCA for fixed intervals of one minute each. These measurements were used to calculate the hourly averages for each sample in a test series. The series mean values were then calculated from the hourly averages of the six samples per series, as were the standard deviations. After finding the samples which showed the greatest accumulative deviation from the hourly series means for all six test hours, the series means and standard deviations were recalculated while omitting those samples.

A table showing the hourly series means and standard deviations for both six and five samples for all test series is displayed in Appendix E.1.

E.1 Summary of hourly rms current data

Table E 1: Summary of hourly rms current data for 3 different voltage types.

AC Series

Time [h]	Material A				Material B				Material C				Material D			
	6 Samples		5 Samples		6 Samples		5 Samples		6 Samples		5 Samples		6 Samples		5 Samples	
	Series mean [mA]	Standard deviation [mA]	Series mean [mA]	Standard deviation [mA]	Series mean [mA]	Standard deviation [mA]	Series mean [mA]	Standard deviation [mA]	Series mean [mA]	Standard deviation [mA]	Series mean [mA]	Standard deviation [mA]	Series mean [mA]	Standard deviation [mA]	Series mean [mA]	Standard deviation [mA]
1	11.058	1.178	11.371	1.002	11.188	0.888	11.096	0.960	9.233	1.073	9.593	0.679	11.051	0.535	11.033	0.597
2	11.276	1.808	11.593	1.826	11.299	0.326	11.213	0.276	9.702	1.586	10.314	0.574	11.202	0.497	11.240	0.546
3	11.117	1.864	11.584	1.645	11.045	0.538	10.900	0.452	9.832	1.786	10.550	0.341	11.297	0.338	11.328	0.368
4	11.763	1.772	12.360	1.118	10.754	0.622	10.559	0.446	9.769	1.817	10.494	0.423	11.110	0.451	11.241	0.353
5	11.971	2.077	12.654	1.375	10.556	0.527	10.362	0.253	9.859	1.789	10.561	0.550	11.040	0.655	11.273	0.364
6	11.930	2.029	12.606	1.311	10.400	0.659	10.160	0.333	9.906	1.751	10.597	0.499	10.986	0.597	11.212	0.253

DC+ Series

Time [h]	Material A				Material B				Material C				Material D			
	6 Samples		5 Samples		6 Samples		5 Samples		6 Samples		5 Samples		6 Samples		5 Samples	
	Series mean [mA]	Standard deviation [mA]	Series mean [mA]	Standard deviation [mA]	Series mean [mA]	Standard deviation [mA]	Series mean [mA]	Standard deviation [mA]	Series mean [mA]	Standard deviation [mA]	Series mean [mA]	Standard deviation [mA]	Series mean [mA]	Standard deviation [mA]	Series mean [mA]	Standard deviation [mA]
1	16.521	2.109	16.021	1.921	12.535	0.420	12.423	0.355	10.761	0.455	10.740	0.505	11.839	0.227	11.919	0.127
2	20.284	3.098	19.458	2.624	13.028	0.811	12.836	0.738	11.604	0.774	11.473	0.789	12.203	0.586	12.375	0.455
3	21.225	2.720	20.534	2.381	12.339	1.028	12.288	1.141	11.729	0.798	11.583	0.797	12.820	0.565	12.761	0.611
4	21.541	2.596	20.900	2.311	12.036	1.997	12.507	1.792	11.768	0.821	11.592	0.780	12.601	0.504	12.601	0.504
5	21.737	2.298	21.058	1.773	12.832	2.527	13.715	1.459	11.878	1.196	11.544	0.976	12.840	0.802	12.840	0.802
6	21.079	2.827	20.485	2.709	11.663	2.643	11.663	2.643	11.919	1.226	11.504	0.764	12.329	0.389	12.329	0.389

DC- Series

Time [h]	Material A				Material B				Material C				Material D			
	6 Samples		5 Samples		6 Samples		5 Samples		6 Samples		5 Samples		6 Samples		5 Samples	
	Series mean [mA]	Standard deviation [mA]	Series mean [mA]	Standard deviation [mA]	Series mean [mA]	Standard deviation [mA]	Series mean [mA]	Standard deviation [mA]	Series mean [mA]	Standard deviation [mA]	Series mean [mA]	Standard deviation [mA]	Series mean [mA]	Standard deviation [mA]	Series mean [mA]	Standard deviation [mA]
1	10.032	0.610	9.964	0.656	7.842	0.937	8.152	0.611	7.725	0.307	7.682	0.322	7.440	0.492	7.561	0.439
2	11.455	1.100	11.223	1.053	8.138	0.302	8.158	0.333	7.831	0.525	7.711	0.486	7.517	0.433	7.635	0.360
3	11.726	1.033	11.393	0.708	8.245	0.396	8.141	0.339	7.679	0.489	7.538	0.388	7.824	0.438	7.993	0.160
4	11.714	1.130	11.387	0.891	8.265	0.365	8.182	0.338	7.805	0.389	7.752	0.409	8.409	0.334	8.381	0.366
5	11.852	1.212	11.533	1.035	8.461	0.534	8.344	0.503	7.817	0.269	7.741	0.215	8.497	0.411	8.359	0.262
6	11.993	1.286	11.660	1.112	8.575	0.458	8.525	0.493	7.944	0.260	7.866	0.197	8.402	0.372	8.399	0.416

E.2 Smoothed plots of rms leakage currents

The following sections contain the plots for the rms leakage currents of all samples for each individual test series, using the data measured per one minute interval. Before plotting, the current data was smoothed using a moving average technique with a data window width of 10 samples. The window width was adjusted at the beginning and towards the end of each test series due to the reduced number of data points at these locations. The first and final data points of each series were taken at their original values.

Whenever a test run was aborted prematurely due to failure occurring in the sample, the current data was smoothed and plotted up to the point in time when failure was recorded.

E.2.1 AC voltage

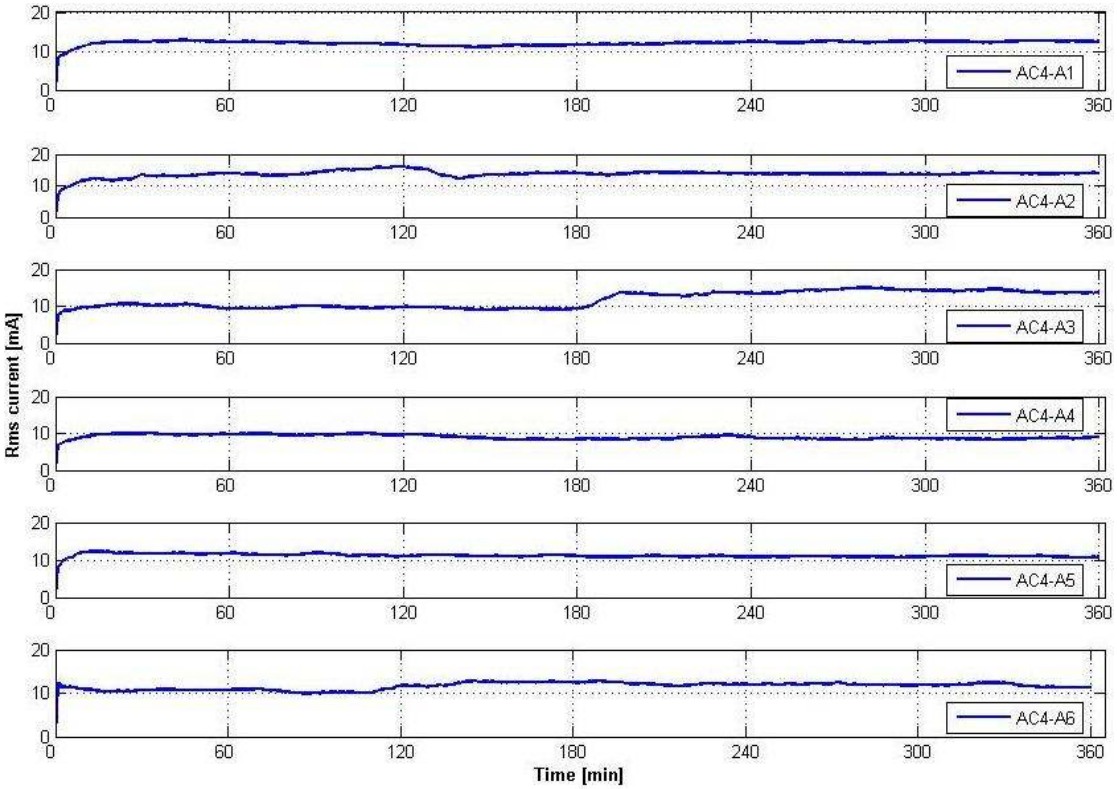

Fig. E 1: Smoothed rms leakage current plots for series AC4-A.

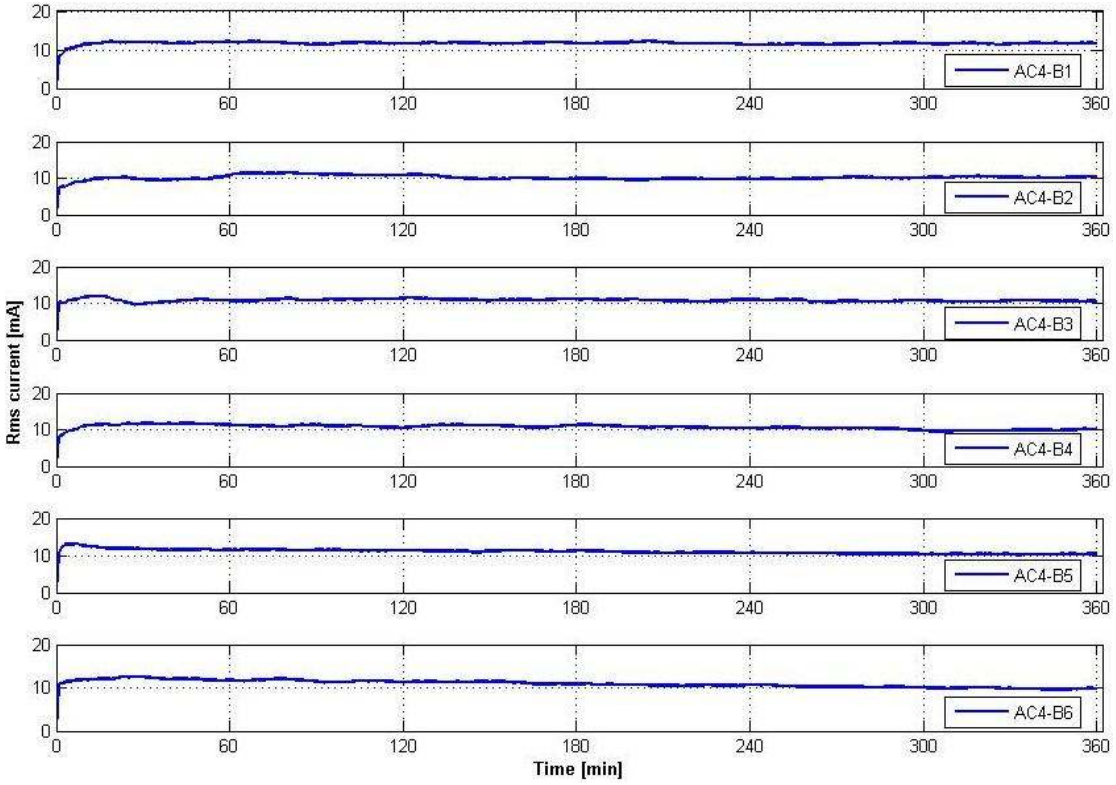

Fig. E 2: Smoothed rms leakage current plots for series AC4-B.

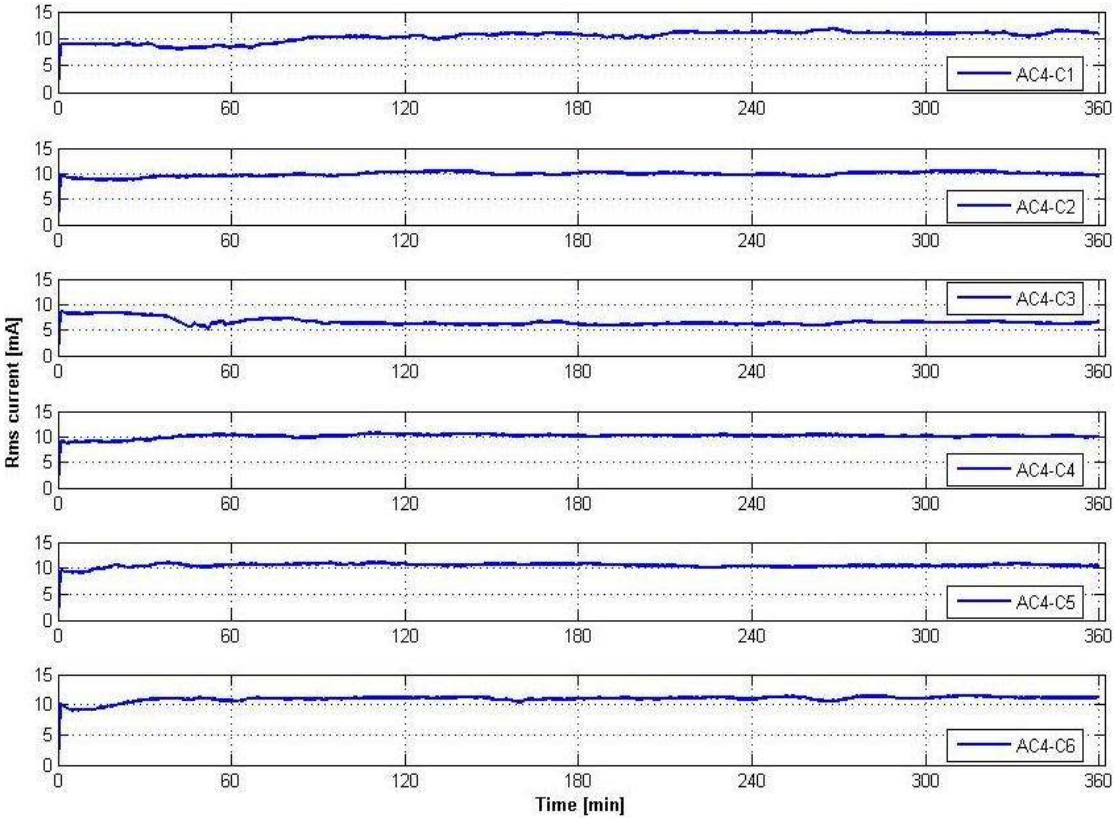

Fig. E 3: Smoothed rms leakage current plots for series AC4-C.

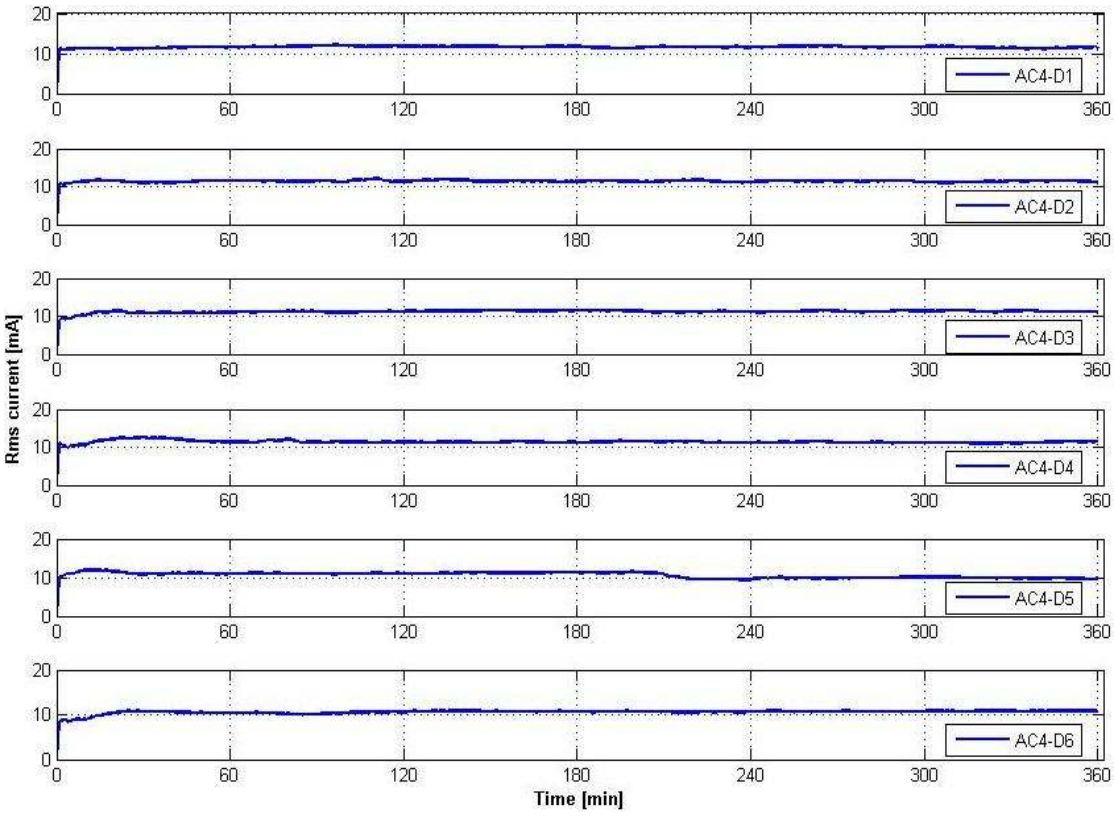

Fig. E 4: Smoothed rms leakage current plots for series AC4-D.

E.2.2 Positive DC voltage

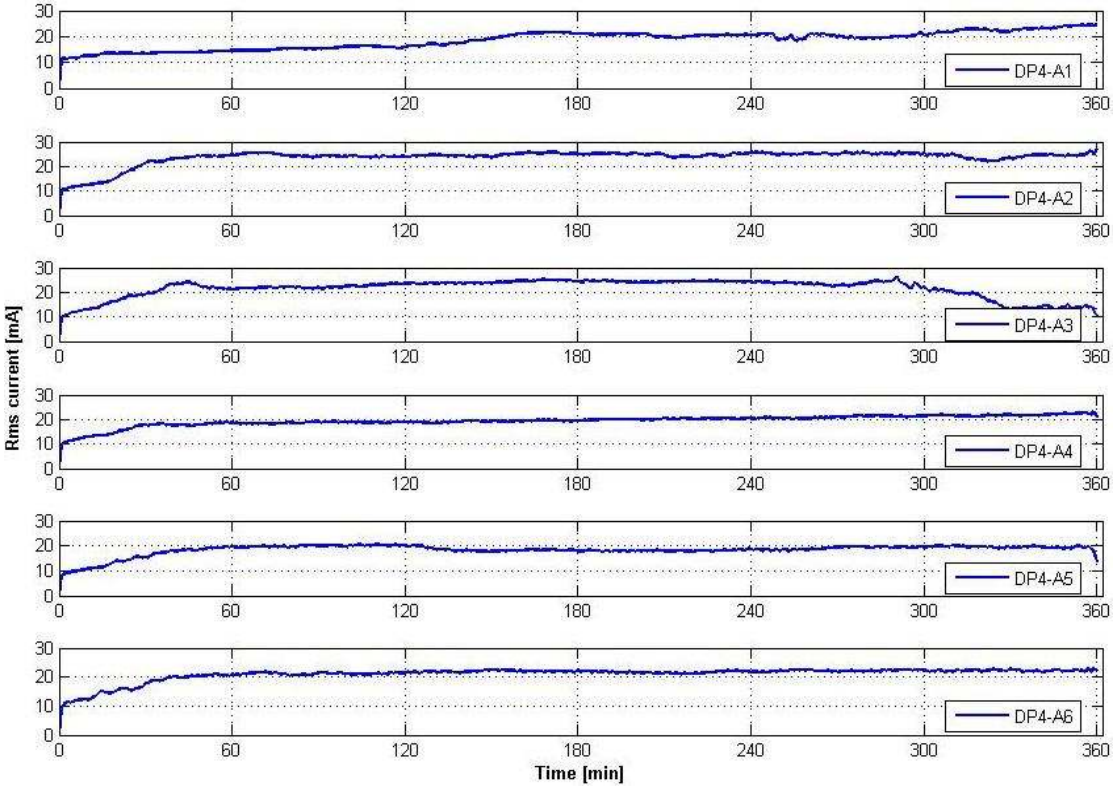

Fig. E 5: Smoothed rms leakage current plots for series DP4-A.

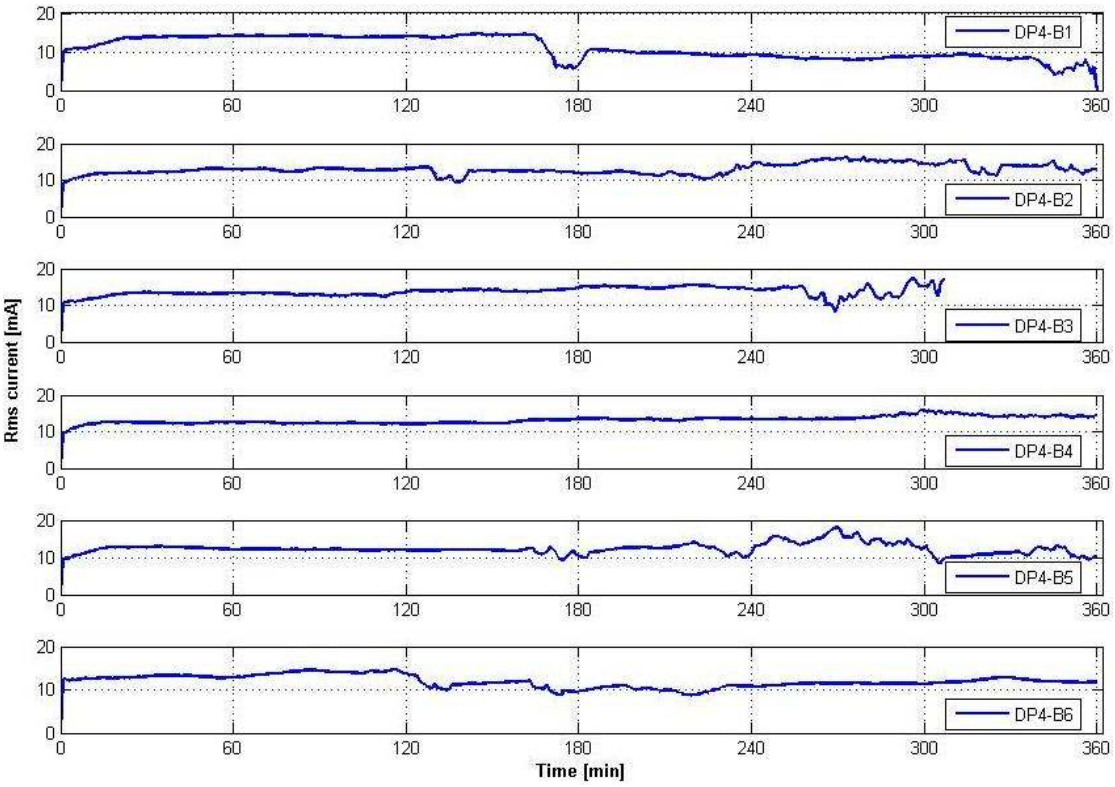

Fig. E 6: Smoothed rms leakage current plots for series DP4-B.

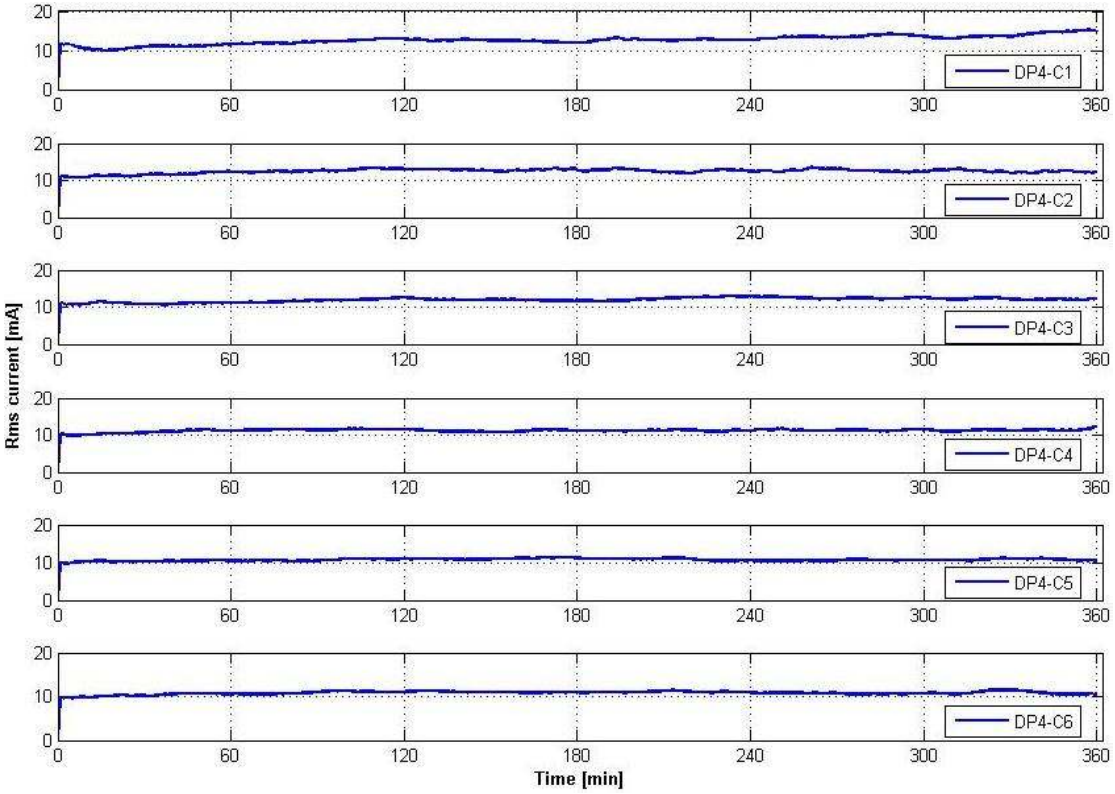

Fig. E 7: Smoothed rms leakage current plots for series DP4-C.

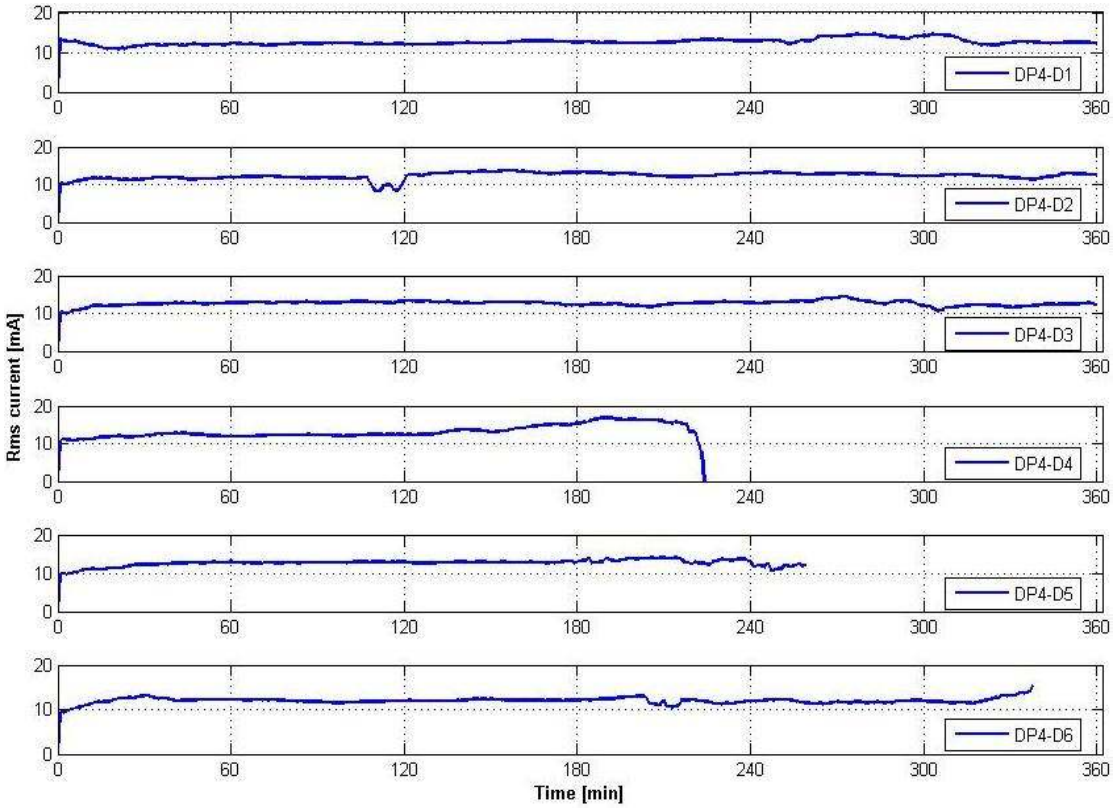

Fig. E 8: Smoothed rms leakage current plots for series DP4-D.

E.2.3 Negative DC voltage

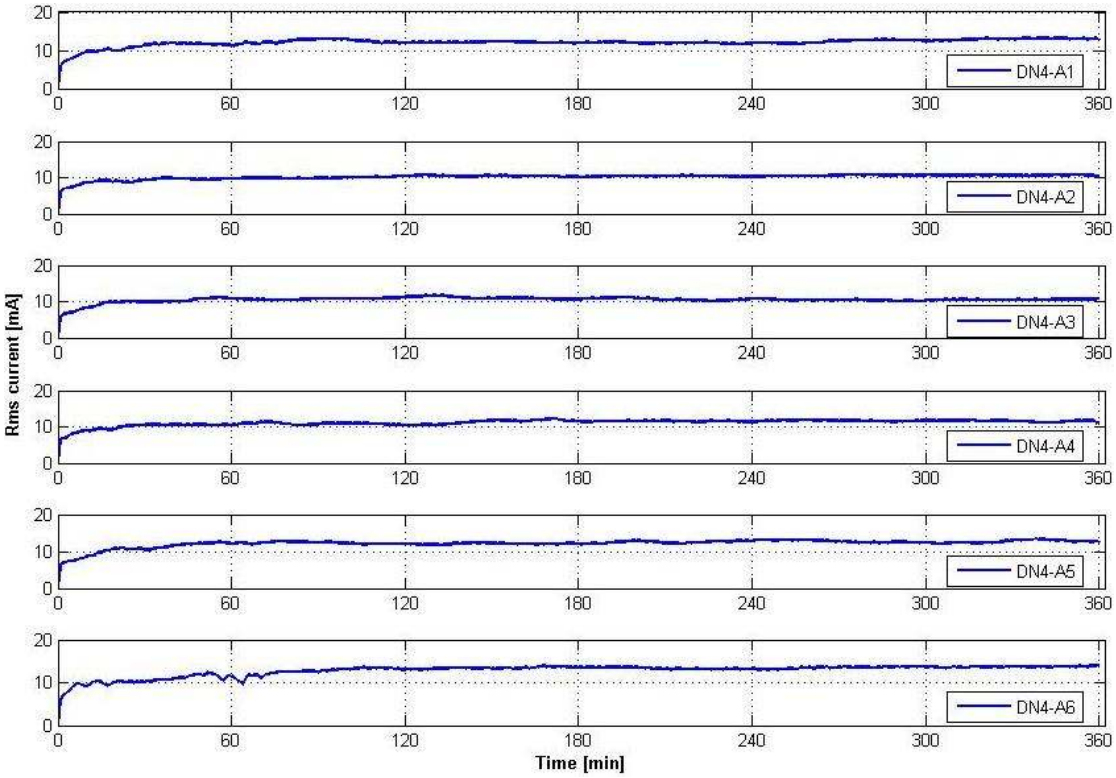

Fig. E 9: Smoothed rms leakage current plots for series DN4-A.

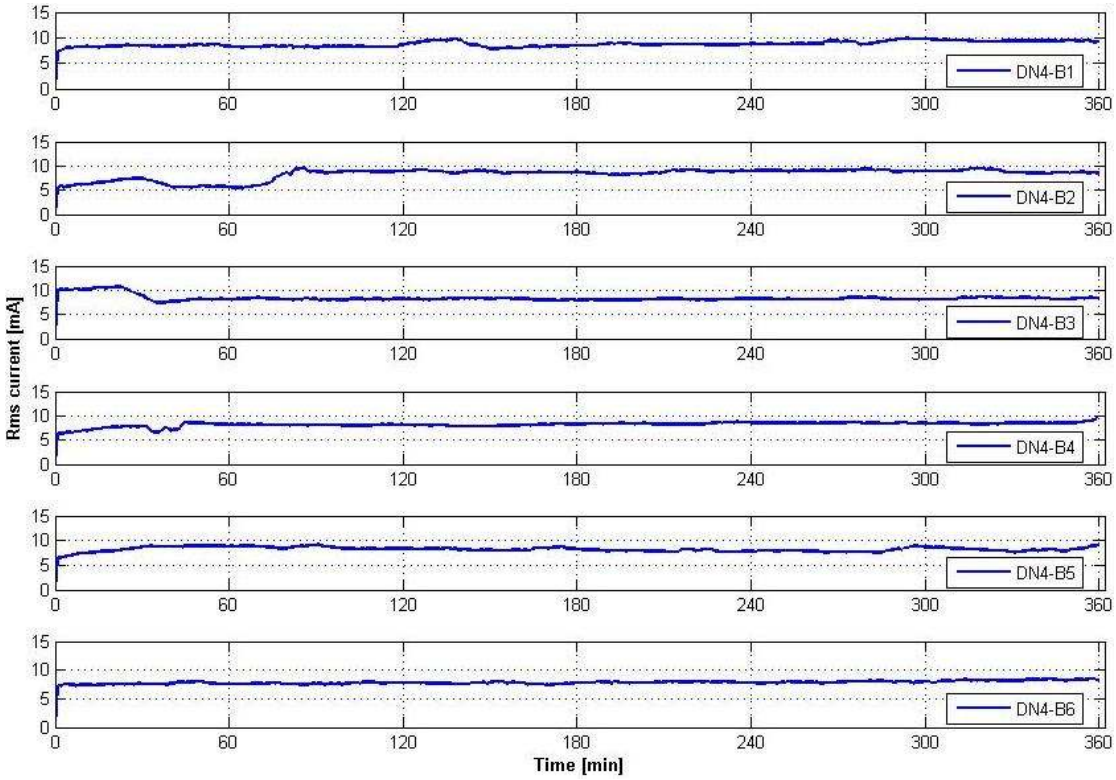

Fig. E 10: Smoothed rms leakage current plots for series DN4-B.

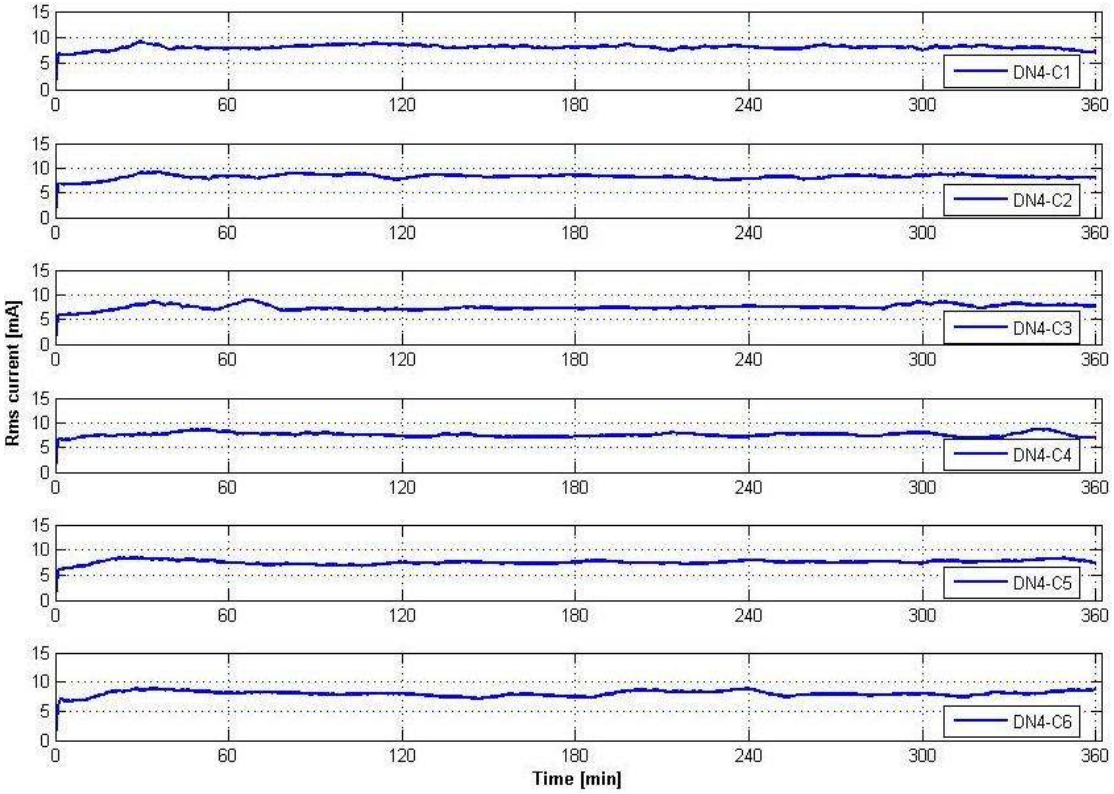

Fig. E 11: Smoothed rms leakage current plots for series DN4-C.

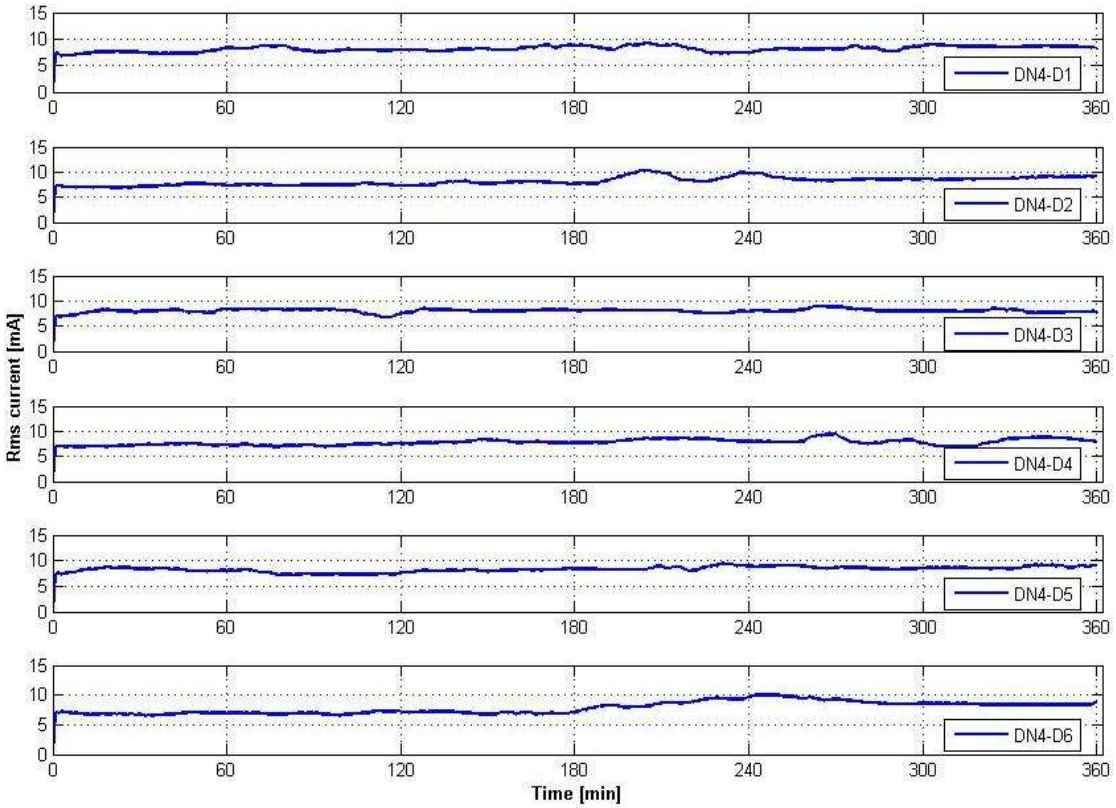

Fig. E 12: Smoothed rms leakage current plots for series DN4-D.

E.3 Correlation tables for rms leakage currents

The following sections display tables containing the correlation coefficients of the correlation analysis performed on the leakage current data of all the samples within each individual test series. The correlation tables were produced using the data analysis toolbox in Microsoft Excel. Since the order of comparison between two samples is of no consequence, Excel only creates the yellow coloured part of the table. The other fields were filled in manually so as to better analyse the correlation of one specific sample to all other samples within the series.

The correlation analysis was done for three separate time periods for each test series, namely the first 30 minute, the first 60 minutes and the full duration of the test runs. Since the number of data points must be equal for any two data series being analysed, the term ‘full duration’ described the time period until the first occurrence of failure in any sample of the series was observed. The first two time periods were included in order to observe if the samples of a specific series showed the same leakage current behaviour during test initiation.

The average of all the correlation coefficients within a series was then calculated for each observed time period in order to gain an impression of the overall correlation of the leakage current data for each test series. The average values are displayed beneath each individual table. Occasionally, a sample showed an inverse relation to all other samples within the series. This sample was then omitted and the average value of the coefficients was recalculated in order to check the correlation of the remaining samples to one another. The improved average values are again displayed beneath the relevant tables, together with the names of the samples omitted. These samples were then further investigated in order to find clues as to the reasons for their behavioural differences.

E.3.1 AC voltage

Table E 2: Correlation tables of rms leakage currents for series AC4-A.

Correlation over full test time:						
	AC4-A1	*AC4-A2*	*AC4-A3*	*AC4-A4*	*AC4-A5*	*AC4-A6*
AC4-A1	1.0000	0.3597	0.5251	0.2907	0.2961	-0.2517
AC4-A2	0.3597	1.0000	0.1392	0.2176	0.0383	0.0062
AC4-A3	0.5251	0.1392	1.0000	-0.4751	-0.4203	0.3908
AC4-A4	0.2907	0.2176	-0.4751	1.0000	0.7042	-0.7938
AC4-A5	0.2961	0.0383	-0.4203	0.7042	1.0000	-0.5867
AC4-A6	-0.2517	0.0062	0.3908	-0.7938	-0.5867	1.0000
Average:	0.0294					
Correlation for 1st full hour:						
	AC4-A1	*AC4-A2*	*AC4-A3*	*AC4-A4*	*AC4-A5*	*AC4-A6*
AC4-A1	1.0000	0.9096	0.8318	0.9638	0.8083	-0.8194
AC4-A2	0.9096	1.0000	0.5947	0.8634	0.7158	-0.6520
AC4-A3	0.8318	0.5947	1.0000	0.8427	0.7192	-0.7962
AC4-A4	0.9638	0.8634	0.8427	1.0000	0.8353	-0.8727
AC4-A5	0.8083	0.7158	0.7192	0.8353	1.0000	-0.8441
AC4-A6	-0.8194	-0.6520	-0.7962	-0.8727	-0.8441	1.0000
Average:	0.2734		0.8085	(without AC4-A6)		
Correlation for 1st half hour:						
	AC4-A1	*AC4-A2*	*AC4-A3*	*AC4-A4*	*AC4-A5*	*AC4-A6*
AC4-A1	1.0000	0.9396	0.9603	0.9951	0.8786	-0.9316
AC4-A2	0.9396	1.0000	0.8860	0.9369	0.9019	-0.8538
AC4-A3	0.9603	0.8860	1.0000	0.9728	0.7860	-0.9041
AC4-A4	0.9951	0.9369	0.9728	1.0000	0.8676	-0.9346
AC4-A5	0.8786	0.9019	0.7860	0.8676	1.0000	-0.8559
AC4-A6	-0.9316	-0.8538	-0.9041	-0.9346	-0.8559	1.0000
Average:	0.3096		0.9125	(without AC4-A6)		

Table E 3: Correlation tables of rms leakage currents for series AC4-B.

Correlation over full test time:						
	AC4-B1	*AC4-B2*	*AC4-B3*	*AC4-B4*	*AC4-B5*	*AC4-B6*
AC4-B1	1.0000	0.4306	0.0924	0.5165	-0.0463	0.2023
AC4-B2	0.4306	1.0000	0.2028	0.1763	-0.0778	0.1282
AC4-B3	0.0924	0.2028	1.0000	0.2457	0.3257	0.2468
AC4-B4	0.5165	0.1763	0.2457	1.0000	0.5888	0.8037
AC4-B5	-0.0463	-0.0778	0.3257	0.5888	1.0000	0.8674
AC4-B6	0.2023	0.1282	0.2468	0.8037	0.8674	1.0000
Average:	0.3135					
Correlation for 1st full test hour:						
	AC4-B1	*AC4-B2*	*AC4-B3*	*AC4-B4*	*AC4-B5*	*AC4-B6*
AC4-B1	1.0000	0.9032	0.0281	0.9486	-0.3719	0.7475
AC4-B2	0.9032	1.0000	0.1469	0.8606	-0.4313	0.6291
AC4-B3	0.0281	0.1469	1.0000	-0.0183	0.3450	-0.2779
AC4-B4	0.9486	0.8606	-0.0183	1.0000	-0.4767	0.7740
AC4-B5	-0.3719	-0.4313	0.3450	-0.4767	1.0000	-0.1831
AC4-B6	0.7475	0.6291	-0.2779	0.7740	-0.1831	1.0000
Average:	0.2416					
Correlation for 1st half test hour:						
	AC4-B1	*AC4-B2*	*AC4-B3*	*AC4-B4*	*AC4-B5*	*AC4-B6*
AC4-B1	1.0000	0.9443	0.1316	0.9729	-0.1841	0.9161
AC4-B2	0.9443	1.0000	0.1743	0.9593	-0.3296	0.8927
AC4-B3	0.1316	0.1743	1.0000	0.1365	0.3194	-0.2043
AC4-B4	0.9729	0.9593	0.1365	1.0000	-0.2652	0.9312
AC4-B5	-0.1841	-0.3296	0.3194	-0.2652	1.0000	-0.3054
AC4-B6	0.9161	0.8927	-0.2043	0.9312	-0.3054	1.0000
Average:	0.3393					

Table E 4: Correlation tables of rms leakage currents for series AC4-C.

Correlation over full test time:						
	AC4-C1	*AC4-C2*	*AC4-C3*	*AC4-C4*	*AC4-C5*	*AC4-C6*
AC4-C1	1.0000	0.5947	-0.5394	0.4418	0.0813	0.4713
AC4-C2	0.5947	1.0000	-0.6316	0.6369	0.4192	0.7276
AC4-C3	-0.5394	-0.6316	1.0000	-0.8618	-0.4148	-0.6688
AC4-C4	0.4418	0.6369	-0.8618	1.0000	0.5795	0.7256
AC4-C5	0.0813	0.4192	-0.4148	0.5795	1.0000	0.6058
AC4-C6	0.4713	0.7276	-0.6688	0.7256	0.6058	1.0000
Average:	0.1445		0.5284	(without AC4-C3)		
Correlation for 1st full hour:						
	AC4-C1	*AC4-C2*	*AC4-C3*	*AC4-C4*	*AC4-C5*	*AC4-C6*
AC4-C1	1.0000	-0.7222	0.7776	-0.8215	-0.6717	-0.7440
AC4-C2	-0.7222	1.0000	-0.7284	0.7918	0.4178	0.6980
AC4-C3	0.7776	-0.7284	1.0000	-0.9140	-0.4103	-0.6637
AC4-C4	-0.8215	0.7918	-0.9140	1.0000	0.6319	0.8027
AC4-C5	-0.6717	0.4178	-0.4103	0.6319	1.0000	0.8496
AC4-C6	-0.7440	0.6980	-0.6637	0.8027	0.8496	1.0000
Average:	-0.0471					
Correlation for 1st half hour:						
	AC4-C1	*AC4-C2*	*AC4-C3*	*AC4-C4*	*AC4-C5*	*AC4-C6*
AC4-C1	1.0000	0.1997	0.2164	-0.5295	-0.4524	-0.2643
AC4-C2	0.1997	1.0000	0.0517	-0.0917	-0.4779	-0.0028
AC4-C3	0.2164	0.0517	1.0000	-0.4206	0.0124	-0.2300
AC4-C4	-0.5295	-0.0917	-0.4206	1.0000	0.6006	0.7047
AC4-C5	-0.4524	-0.4779	0.0124	0.6006	1.0000	0.7833
AC4-C6	-0.2643	-0.0028	-0.2300	0.7047	0.7833	1.0000
Average:	0.0066					

Table E 5: Correlation tables of rms leakage currents for series AC4-D.

Correlation over full test time:						
	AC4-D1	*AC4-D2*	*AC4-D3*	*AC4-D4*	*AC4-D5*	*AC4-D6*
AC4-D1	1.0000	0.2699	0.3962	-0.1651	0.0159	0.2222
AC4-D2	0.2699	1.0000	0.3418	-0.0454	0.1192	0.2063
AC4-D3	0.3962	0.3418	1.0000	0.1338	-0.1025	0.7939
AC4-D4	-0.1651	-0.0454	0.1338	1.0000	0.2780	0.2619
AC4-D5	0.0159	0.1192	-0.1025	0.2780	1.0000	-0.3278
AC4-D6	0.2222	0.2063	0.7939	0.2619	-0.3278	1.0000
Average:	0.1599					
Correlation for 1st full hour:						
	AC4-D1	*AC4-D2*	*AC4-D3*	*AC4-D4*	*AC4-D5*	*AC4-D6*
AC4-D1	1.0000	0.4319	0.4015	0.0831	-0.0772	0.3805
AC4-D2	0.4319	1.0000	0.5980	0.0372	0.6428	0.2019
AC4-D3	0.4015	0.5980	1.0000	0.7750	0.2980	0.8624
AC4-D4	0.0831	0.0372	0.7750	1.0000	-0.0629	0.9004
AC4-D5	-0.0772	0.6428	0.2980	-0.0629	1.0000	-0.1474
AC4-D6	0.3805	0.2019	0.8624	0.9004	-0.1474	1.0000
Average:	0.3550					
Correlation for 1st half hour:						
	AC4-D1	*AC4-D2*	*AC4-D3*	*AC4-D4*	*AC4-D5*	*AC4-D6*
AC4-D1	1.0000	0.6371	0.3542	0.1054	0.6584	0.0481
AC4-D2	0.6371	1.0000	0.7445	0.3691	0.9255	0.3573
AC4-D3	0.3542	0.7445	1.0000	0.8570	0.5322	0.8699
AC4-D4	0.1054	0.3691	0.8570	1.0000	0.0705	0.9707
AC4-D5	0.6584	0.9255	0.5322	0.0705	1.0000	0.0911
AC4-D6	0.0481	0.3573	0.8699	0.9707	0.0911	1.0000
Average:	0.5060					

E.3.2 Positive DC voltage

Table E 6: Correlation tables of rms leakage currents for series DP4-A.

Correlation over full test time:						
	DP4-A1	*DP4-A2*	*DP4-A3*	*DP4-A4*	*DP4-A5*	*DP4-A6*
DP4-A1	1.0000	0.5498	0.0313	0.8357	0.4154	0.6790
DP4-A2	0.5498	1.0000	0.6002	0.8140	0.8714	0.9426
DP4-A3	0.0313	0.6002	1.0000	0.2210	0.4208	0.4918
DP4-A4	0.8357	0.8140	0.2210	1.0000	0.7724	0.8908
DP4-A5	0.4154	0.8714	0.4208	0.7724	1.0000	0.8807
DP4-A6	0.6790	0.9426	0.4918	0.8908	0.8807	1.0000
Average:	0.6278					
Correlation for 1st full hour:						
	DP4-A1	*DP4-A2*	*DP4-A3*	*DP4-A4*	*DP4-A5*	*DP4-A6*
DP4-A1	1.0000	0.8686	0.8845	0.9085	0.9128	0.9140
DP4-A2	0.8686	1.0000	0.9679	0.9703	0.9843	0.9781
DP4-A3	0.8845	0.9679	1.0000	0.9436	0.9651	0.9658
DP4-A4	0.9085	0.9703	0.9436	1.0000	0.9658	0.9565
DP4-A5	0.9128	0.9843	0.9651	0.9658	1.0000	0.9847
DP4-A6	0.9140	0.9781	0.9658	0.9565	0.9847	1.0000
Average:	0.9447					
Correlation for 1st half hour:						
	DP4-A1	*DP4-A2*	*DP4-A3*	*DP4-A4*	*DP4-A5*	*DP4-A6*
DP4-A1	1.0000	0.7495	0.8929	0.8343	0.8594	0.9039
DP4-A2	0.7495	1.0000	0.9561	0.9763	0.9589	0.9027
DP4-A3	0.8929	0.9561	1.0000	0.9783	0.9871	0.9566
DP4-A4	0.8343	0.9763	0.9783	1.0000	0.9827	0.9487
DP4-A5	0.8594	0.9589	0.9871	0.9827	1.0000	0.9404
DP4-A6	0.9039	0.9027	0.9566	0.9487	0.9404	1.0000
Average:	0.9219					

Table E 7: Correlation tables of rms leakage currents for series DP4-B.

Correlation over full test time:						
	DP4-B1	*DP4-B2*	*DP4-B3*	*DP4-B4*	*DP4-B5*	*DP4-B6*
DP4-B1	1.0000	-0.3451	-0.1913	-0.6761	-0.2639	0.6764
DP4-B2	-0.3451	1.0000	-0.1774	0.5148	0.5624	0.1224
DP4-B3	-0.1913	-0.1774	1.0000	0.3261	-0.0710	-0.5051
DP4-B4	-0.6761	0.5148	0.3261	1.0000	0.2723	-0.5116
DP4-B5	-0.2639	0.5624	-0.0710	0.2723	1.0000	-0.0461
DP4-B6	0.6764	0.1224	-0.5051	-0.5116	-0.0461	1.0000
Average:	-0.0209					
Correlation for 1st full hour:						
	DP4-B1	*DP4-B2*	*DP4-B3*	*DP4-B4*	*DP4-B5*	*DP4-B6*
DP4-B1	1.0000	0.8809	0.9695	0.7325	0.8461	0.7910
DP4-B2	0.8809	1.0000	0.8286	0.8010	0.7783	0.6409
DP4-B3	0.9695	0.8286	1.0000	0.8007	0.9152	0.7890
DP4-B4	0.7325	0.8010	0.8007	1.0000	0.8965	0.5015
DP4-B5	0.8461	0.7783	0.9152	0.8965	1.0000	0.7642
DP4-B6	0.7910	0.6409	0.7890	0.5015	0.7642	1.0000
Average:	0.7957					
Correlation for 1st half hour:						
	DP4-B1	*DP4-B2*	*DP4-B3*	*DP4-B4*	*DP4-B5*	*DP4-B6*
DP4-B1	1.0000	0.8291	0.9885	0.7921	0.8999	0.8380
DP4-B2	0.8291	1.0000	0.8653	0.9751	0.9737	0.7979
DP4-B3	0.9885	0.8653	1.0000	0.8210	0.9274	0.8791
DP4-B4	0.7921	0.9751	0.8210	1.0000	0.9548	0.7254
DP4-B5	0.8999	0.9737	0.9274	0.9548	1.0000	0.8289
DP4-B6	0.8380	0.7979	0.8791	0.7254	0.8289	1.0000
Average:	0.8731					

Table E 8: Correlation tables of rms leakage currents for series DP4-C.

Correlation over full test time:						
	DP4-C1	*DP4-C2*	*DP4-C3*	*DP4-C4*	*DP4-C5*	*DP4-C6*
DP4-C1	1.0000	0.5181	0.7136	0.5493	0.3468	0.4017
DP4-C2	0.5181	1.0000	0.5941	0.5755	0.5651	0.6267
DP4-C3	0.7136	0.5941	1.0000	0.5196	0.3541	0.5905
DP4-C4	0.5493	0.5755	0.5196	1.0000	0.4310	0.5958
DP4-C5	0.3468	0.5651	0.3541	0.4310	1.0000	0.7157
DP4-C6	0.4017	0.6267	0.5905	0.5958	0.7157	1.0000
Average:	0.5398					
Correlation for 1st full hour:						
	DP4-C1	*DP4-C2*	*DP4-C3*	*DP4-C4*	*DP4-C5*	*DP4-C6*
DP4-C1	1.0000	0.4883	-0.3054	0.4462	0.0389	0.3635
DP4-C2	0.4883	1.0000	0.3681	0.8779	0.7300	0.8198
DP4-C3	-0.3054	0.3681	1.0000	0.3019	0.4443	0.3060
DP4-C4	0.4462	0.8779	0.3019	1.0000	0.7047	0.9516
DP4-C5	0.0389	0.7300	0.4443	0.7047	1.0000	0.7351
DP4-C6	0.3635	0.8198	0.3060	0.9516	0.7351	1.0000
Average:	0.4847					
Correlation for 1st half hour:						
	DP4-C1	*DP4-C2*	*DP4-C3*	*DP4-C4*	*DP4-C5*	*DP4-C6*
DP4-C1	1.0000	-0.3663	-0.6451	-0.3208	-0.7808	-0.4239
DP4-C2	-0.3663	1.0000	0.5242	0.7507	0.4063	0.6803
DP4-C3	-0.6451	0.5242	1.0000	0.3819	0.5190	0.3846
DP4-C4	-0.3208	0.7507	0.3819	1.0000	0.2834	0.8591
DP4-C5	-0.7808	0.4063	0.5190	0.2834	1.0000	0.4200
DP4-C6	-0.4239	0.6803	0.3846	0.8591	0.4200	1.0000
Average:	0.1782		0.5209	(without DP4-C1)		

Table E 9: Correlation tables of rms leakage currents for series DP4-D.

Correlation over full test time:						
	DP4-D1	*DP4-D2*	*DP4-D3*	*DP4-D4*	*DP4-D5*	*DP4-D6*
DP4-D1	1.0000	0.3188	-0.1004	0.3024	0.2744	-0.3021
DP4-D2	0.3188	1.0000	0.1927	0.4576	0.3621	0.3203
DP4-D3	-0.1004	0.1927	1.0000	-0.0470	0.5373	0.4708
DP4-D4	0.3024	0.4576	-0.0470	1.0000	0.5780	0.2213
DP4-D5	0.2744	0.3621	0.5373	0.5780	1.0000	0.4261
DP4-D6	-0.3021	0.3203	0.4708	0.2213	0.4261	1.0000
Average:	0.2675					
Correlation for 1st full hour:						
	DP4-D1	*DP4-D2*	*DP4-D3*	*DP4-D4*	*DP4-D5*	*DP4-D6*
DP4-D1	1.0000	-0.5439	-0.5375	-0.3618	-0.2736	-0.6636
DP4-D2	-0.5439	1.0000	0.8738	0.6947	0.7345	0.7508
DP4-D3	-0.5375	0.8738	1.0000	0.8466	0.9302	0.8997
DP4-D4	-0.3618	0.6947	0.8466	1.0000	0.8532	0.7339
DP4-D5	-0.2736	0.7345	0.9302	0.8532	1.0000	0.8035
DP4-D6	-0.6636	0.7508	0.8997	0.7339	0.8035	1.0000
Average:	0.3827		0.8121	(without DP4-D1)		
Correlation for 1st half hour:						
	DP4-D1	*DP4-D2*	*DP4-D3*	*DP4-D4*	*DP4-D5*	*DP4-D6*
DP4-D1	1.0000	-0.8082	-0.8636	-0.8869	-0.7124	-0.8445
DP4-D2	-0.8082	1.0000	0.8704	0.6456	0.6830	0.7311
DP4-D3	-0.8636	0.8704	1.0000	0.8779	0.9248	0.9589
DP4-D4	-0.8869	0.6456	0.8779	1.0000	0.8487	0.9279
DP4-D5	-0.7124	0.6830	0.9248	0.8487	1.0000	0.9549
DP4-D6	-0.8445	0.7311	0.9589	0.9279	0.9549	1.0000
Average:	0.2872		0.8423	(without DP4-D1)		

E.3.3 Negative DC voltage

Table E 10: Correlation tables of rms leakage currents for series DN4-A.

Correlation over full test time:						
	DN4-A1	*DN4-A2*	*DN4-A3*	*DN4-A4*	*DN4-A5*	*DN4-A6*
DN4-A1	1.0000	0.8564	0.7332	0.7846	0.8460	0.8171
DN4-A2	0.8564	1.0000	0.7385	0.8881	0.8419	0.9103
DN4-A3	0.7332	0.7385	1.0000	0.6476	0.7681	0.6917
DN4-A4	0.7846	0.8881	0.6476	1.0000	0.8436	0.8516
DN4-A5	0.8460	0.8419	0.7681	0.8436	1.0000	0.8057
DN4-A6	0.8171	0.9103	0.6917	0.8516	0.8057	1.0000
Average:	0.8016					
Correlation for 1st full hour:						
	DN4-A1	*DN4-A2*	*DN4-A3*	*DN4-A4*	*DN4-A5*	*DN4-A6*
DN4-A1	1.0000	0.9598	0.9196	0.9681	0.9155	0.8724
DN4-A2	0.9598	1.0000	0.8999	0.9299	0.8932	0.8586
DN4-A3	0.9196	0.8999	1.0000	0.9244	0.9764	0.8774
DN4-A4	0.9681	0.9299	0.9244	1.0000	0.9116	0.8684
DN4-A5	0.9155	0.8932	0.9764	0.9116	1.0000	0.8893
DN4-A6	0.8724	0.8586	0.8774	0.8684	0.8893	1.0000
Average:	0.9110					
Correlation for 1st half hour:						
	DN4-A1	*DN4-A2*	*DN4-A3*	*DN4-A4*	*DN4-A5*	*DN4-A6*
DN4-A1	1.0000	0.9399	0.9498	0.9549	0.9073	0.8533
DN4-A2	0.9399	1.0000	0.9148	0.8849	0.8735	0.8819
DN4-A3	0.9498	0.9148	1.0000	0.9314	0.9880	0.8173
DN4-A4	0.9549	0.8849	0.9314	1.0000	0.9093	0.8811
DN4-A5	0.9073	0.8735	0.9880	0.9093	1.0000	0.7913
DN4-A6	0.8533	0.8819	0.8173	0.8811	0.7913	1.0000
Average:	0.8986					

Table E 11: Correlation tables of rms leakage currents for series DN4-B.

Correlation over full test time:						
	DN4-B1	*DN4-B2*	*DN4-B3*	*DN4-B4*	*DN4-B5*	*DN4-B6*
DN4-B1	1.0000	0.4316	-0.2029	0.5402	-0.0129	0.6272
DN4-B2	0.4316	1.0000	-0.3445	0.5108	-0.2084	0.4219
DN4-B3	-0.2029	-0.3445	1.0000	-0.4925	-0.4455	-0.2733
DN4-B4	0.5402	0.5108	-0.4925	1.0000	0.1597	0.6260
DN4-B5	-0.0129	-0.2084	-0.4455	0.1597	1.0000	-0.0844
DN4-B6	0.6272	0.4219	-0.2733	0.6260	-0.0844	1.0000
Average:	0.0835					
Correlation for 1st full hour:						
	DN4-B1	*DN4-B2*	*DN4-B3*	*DN4-B4*	*DN4-B5*	*DN4-B6*
DN4-B1	1.0000	0.1242	-0.4307	0.7436	0.7910	0.6242
DN4-B2	0.1242	1.0000	0.3956	-0.0990	-0.0159	-0.3095
DN4-B3	-0.4307	0.3956	1.0000	-0.3635	-0.8094	-0.5926
DN4-B4	0.7436	-0.0990	-0.3635	1.0000	0.6999	0.6697
DN4-B5	0.7910	-0.0159	-0.8094	0.6999	1.0000	0.6846
DN4-B6	0.6242	-0.3095	-0.5926	0.6697	0.6846	1.0000
Average:	0.1408					
Correlation for 1st half hour:						
	DN4-B1	*DN4-B2*	*DN4-B3*	*DN4-B4*	*DN4-B5*	*DN4-B6*
DN4-B1	1.0000	0.8014	-0.1731	0.8131	0.8578	0.6276
DN4-B2	0.8014	1.0000	-0.2908	0.9627	0.9678	0.5974
DN4-B3	-0.1731	-0.2908	1.0000	-0.1383	-0.3339	-0.2207
DN4-B4	0.8131	0.9627	-0.1383	1.0000	0.9611	0.6431
DN4-B5	0.8578	0.9678	-0.3339	0.9611	1.0000	0.6448
DN4-B6	0.6276	0.5974	-0.2207	0.6431	0.6448	1.0000
Average:	0.4480		0.7877	(without DN4-B3)		

Table E 12: Correlation tables of rms leakage currents for series DN4-C.

Correlation over full test time:						
	DN4-C1	*DN4-C2*	*DN4-C3*	*DN4-C4*	*DN4-C5*	*DN4-C6*
DN4-C1	1.0000	0.6119	0.1777	0.0854	0.1421	0.2500
DN4-C2	0.6119	1.0000	0.4135	0.2027	0.2091	0.1886
DN4-C3	0.1777	0.4135	1.0000	0.3524	0.5490	0.4512
DN4-C4	0.0854	0.2027	0.3524	1.0000	0.2858	0.3549
DN4-C5	0.1421	0.2091	0.5490	0.2858	1.0000	0.5021
DN4-C6	0.2500	0.1886	0.4512	0.3549	0.5021	1.0000
Average:	0.3184					
Correlation for 1st full hour:						
	DN4-C1	*DN4-C2*	*DN4-C3*	*DN4-C4*	*DN4-C5*	*DN4-C6*
DN4-C1	1.0000	0.9296	0.8832	0.5520	0.8333	0.8581
DN4-C2	0.9296	1.0000	0.9612	0.5832	0.8052	0.8874
DN4-C3	0.8832	0.9612	1.0000	0.5892	0.8263	0.9115
DN4-C4	0.5520	0.5832	0.5892	1.0000	0.5838	0.6684
DN4-C5	0.8333	0.8052	0.8263	0.5838	1.0000	0.9465
DN4-C6	0.8581	0.8874	0.9115	0.6684	0.9465	1.0000
Average:	0.7879					
Correlation for 1st half hour:						
	DN4-C1	*DN4-C2*	*DN4-C3*	*DN4-C4*	*DN4-C5*	*DN4-C6*
DN4-C1	1.0000	0.9801	0.9670	0.7797	0.8422	0.8501
DN4-C2	0.9801	1.0000	0.9819	0.7309	0.8566	0.8729
DN4-C3	0.9670	0.9819	1.0000	0.7781	0.9134	0.9295
DN4-C4	0.7797	0.7309	0.7781	1.0000	0.8770	0.7916
DN4-C5	0.8422	0.8566	0.9134	0.8770	1.0000	0.9687
DN4-C6	0.8501	0.8729	0.9295	0.7916	0.9687	1.0000
Average:	0.8747					

Table E 13: Correlation tables of rms leakage currents for series DN4-D.

Correlation over full test time:						
	DN4-D1	*DN4-D2*	*DN4-D3*	*DN4-D4*	*DN4-D5*	*DN4-D6*
DN4-D1	1.0000	0.4980	0.3198	0.3228	0.1972	0.2463
DN4-D2	0.4980	1.0000	0.0685	0.6424	0.6239	0.7723
DN4-D3	0.3198	0.0685	1.0000	0.1601	0.1128	0.0700
DN4-D4	0.3228	0.6424	0.1601	1.0000	0.5032	0.5836
DN4-D5	0.1972	0.6239	0.1128	0.5032	1.0000	0.7033
DN4-D6	0.2463	0.7723	0.0700	0.5836	0.7033	1.0000
Average:	0.3883					
Correlation for 1st full hour:						
	DN4-D1	*DN4-D2*	*DN4-D3*	*DN4-D4*	*DN4-D5*	*DN4-D6*
DN4-D1	1.0000	0.1614	0.6050	0.0878	0.3275	-0.0881
DN4-D2	0.1614	1.0000	0.1300	0.7848	-0.3333	0.4930
DN4-D3	0.6050	0.1300	1.0000	0.4170	0.7843	-0.4752
DN4-D4	0.0878	0.7848	0.4170	1.0000	0.0439	0.0799
DN4-D5	0.3275	-0.3333	0.7843	0.0439	1.0000	-0.7246
DN4-D6	-0.0881	0.4930	-0.4752	0.0799	-0.7246	1.0000
Average:	0.1529					
Correlation for 1st half hour:						
	DN4-D1	*DN4-D2*	*DN4-D3*	*DN4-D4*	*DN4-D5*	*DN4-D6*
DN4-D1	1.0000	-0.3863	0.9148	0.3581	0.9063	-0.7433
DN4-D2	-0.3863	1.0000	-0.5576	0.0558	-0.5726	0.5333
DN4-D3	0.9148	-0.5576	1.0000	0.2070	0.9770	-0.7780
DN4-D4	0.3581	0.0558	0.2070	1.0000	0.2337	-0.2774
DN4-D5	0.9063	-0.5726	0.9770	0.2337	1.0000	-0.8291
DN4-D6	-0.7433	0.5333	-0.7780	-0.2774	-0.8291	1.0000
Average:	0.0028					

Appendix F: Average Power Measurements

The OLCA calculates the average electrical power dissipated for each one minute measurement interval during each test run. The averages of these measurements were then calculated for each full test hour for each individual sample. The hourly averages of the six samples within each test series were then used to calculate the values for the hourly series mean and standard deviation for each test hour of each test series.

For each test series, the hourly averages of the individual samples were then compared against the series mean for each test hour in order to find the sample with the largest accumulative deviation from the series means of each test hour. This sample was then omitted and the hourly series mean and standard deviation were recalculated for each series based on the data of the five remaining samples. The comparison of individual sample data to the six-sample series mean was only performed for test hours where no failure in a sample occurred. Since failed samples were automatically excluded from the calculations for the series mean for those hours where failure occurred as well as any following test hours, these samples were considered as the extreme data points during those time periods and were thus already omitted from the calculations.

Table F 1 shows the hourly series means and standard deviations for each test series, both for the calculations based on six and five samples per series. The data is grouped according to insulation material and voltage type.

Table F 1: Summary of average dissipated power during each full test hour for every material and voltage type.

AC Series

Time [h]	Material A				Material B				Material C				Material D			
	6 Samples		5 Samples		6 Samples		5 Samples		6 Samples		5 Samples		6 Samples		5 Samples	
	Series mean [mW]	Standard deviation [mW]	Series mean [mW]	Standard deviation [mW]	Series mean [mW]	Standard deviation [mW]	Series mean [mW]	Standard deviation [mW]	Series mean [mW]	Standard deviation [mW]	Series mean [mW]	Standard deviation [mW]	Series mean [mW]	Standard deviation [mW]	Series mean [mW]	Standard deviation [mW]
1	23468	2631	24329	1759	22978	2364	23861	1071	24131	2572	24987	1664	24291	2061	24173	2281
2	24134	3824	25206	3109	25110	868	25395	575	23458	3269	24738	1029	25914	1046	26032	1113
3	23479	4565	24910	3271	24752	1596	25389	376	23532	3807	25050	909	26126	824	26236	870
4	24409	4387	26041	2016	24106	1768	24786	666	23491	4087	25154	360	25830	1417	26304	908
5	24308	4945	26182	2056	23498	1384	23927	1005	23451	3919	25042	438	25664	1944	26374	969
6	24167	4976	26054	2060	23070	1582	23250	1699	23436	3852	24985	749	25331	1896	26048	801

DC+ Series

Time [h]	Material A				Material B				Material C				Material D			
	6 Samples		5 Samples		6 Samples		5 Samples		6 Samples		5 Samples		6 Samples		5 Samples	
	Series mean [mW]	Standard deviation [mW]	Series mean [mW]	Standard deviation [mW]	Series mean [mW]	Standard deviation [mW]	Series mean [mW]	Standard deviation [mW]	Series mean [mW]	Standard deviation [mW]	Series mean [mW]	Standard deviation [mW]	Series mean [mW]	Standard deviation [mW]	Series mean [mW]	Standard deviation [mW]
1	31337	2196	30729	1805	25572	2025	25965	1992	24468	1177	24717	1125	23170	408	23093	405
2	37438	4275	36564	4134	31870	4615	31903	5053	26471	999	26654	997	25570	1382	25657	1527
3	37671	5815	36364	5427	29831	1698	30032	1816	26641	802	26831	730	28109	2266	28851	1512
4	36466	4378	35455	4035	27669	6131	29364	5043	26536	815	26733	736	27762	2670	27762	2670
5	38660	6623	36664	4996	29076	7501	31833	3646	26865	760	27073	632	27907	2976	27907	2976
6	35479	7912	33582	7161	25854	8916	25854	8916	26694	893	26919	785	27156	3519	27156	3519

DC- Series

Time [h]	Material A				Material B				Material C				Material D			
	6 Samples		5 Samples		6 Samples		5 Samples		6 Samples		5 Samples		6 Samples		5 Samples	
	Series mean [mW]	Standard deviation [mW]	Series mean [mW]	Standard deviation [mW]	Series mean [mW]	Standard deviation [mW]	Series mean [mW]	Standard deviation [mW]	Series mean [mW]	Standard deviation [mW]	Series mean [mW]	Standard deviation [mW]	Series mean [mW]	Standard deviation [mW]	Series mean [mW]	Standard deviation [mW]
1	25685	923	25451	809	24865	3435	24721	3820	24279	543	24189	555	24322	503	24488	334
2	27379	1117	27005	714	26653	1157	26472	1195	25204	506	25069	427	24740	542	24922	348
3	28363	483	28230	397	27547	986	27205	580	25477	553	25303	396	25190	691	25381	569
4	28764	619	28620	569	27784	786	27661	813	25461	485	25315	365	25462	1039	25714	934
5	28992	743	28801	646	27678	1024	27370	774	25579	385	25536	414	25172	727	25385	564
6	28829	816	28520	341	28228	2265	27371	956	25466	362	25395	356	24986	917	25230	776

Appendix G: Hydrophobicity Measurements

The surface hydrophobicity of the samples was measured using the spray method described in the International Standard IEC 62073 [59]. The samples surfaces were sprayed with distilled water from a distance of 15 to 35 cm using a spray bottle. The spraying was continued for a duration of 20 to 30 seconds. The samples were then placed on a stand, angling them at 30° to the horizontal. Surface hydrophobicity was evaluated according to the appearance of the surfaces. The surfaces were then assigned values corresponding to certain wettability classes (WC), which are outlined in the standard by the visual guideline shown in Fig. G 1 and the descriptions given in Table G 1.

Table G 1: Criteria for the determination of wettability class [59].

Wettability Class (WC)	Description
1	Only discrete droplets are formed. Their shape when viewed perpendicular to the surface is practically circular. This corresponds to r θ = 80° or larger for the droplets.
2	Only discrete droplets are formed. The major part of the surface is covered by droplets with a shape, as seen perpendicular to the surface, still regular but deviates from circular form. This corresponds to 50° < r θ < 80° for the majority of droplets.
3	Only discrete droplets are formed. The major part of the surface is covered by droplets with an irregular shape. This corresponds to 20° < r θ < 50° for the majority of droplets.
4	Both discrete droplets and wetted traces from the water runnels or water film are observed (i.e. r θ = 0° for some of the droplets). Less than 10 % of the observed area is covered by water runnels or film.
5	Both discrete droplets and wetted traces from the water runnels or water film are observed (i.e. r θ = 0° for some of the droplets). More than 10 % but less than 90 % of the observed area is covered by water runnels or film.
6	More than 90 % but less than 100 % of the observed area is covered by water runnels or film (i.e. small non-wetted areas/spots/traces are still observed).
7	Continuous water film is formed over the whole-observed area.

Each sample surface was further divided into three different regions (lower 17mm, middle 17 mm and upper 16 mm, measured from the ground potential electrode) as well as affected and unaffected areas, as was described in section 5.3.7. These areas were assessed individually for each sample of a given test series. Furthermore, the

surface hydrophobicity was evaluated twice, once before and once after the cleaning of the samples surfaces. This was done to evaluate the samples with and without the presence of a pollution layer on the surface. The evaluation was done not later than 10 seconds after the completion of the spraying procedure. Photographs were taken during each evaluation for possible re-evaluation of the results at a later date.

For each test series, the series mean and standard deviation were then calculated for both the affected and unaffected areas of each of the three regions. Since no great deviations were observed, the usual procedure of determining and eliminating the sample with the greatest deviation from the sample mean was not applied to these results. The results are given in Table G 2 in section G.2 and were also plotted for better visual comparison, with vertical bars indicating the series mean for each specific area. These plots are also shown in section G.2, grouped together according to test material.

G.1 Guide for judging wettability class

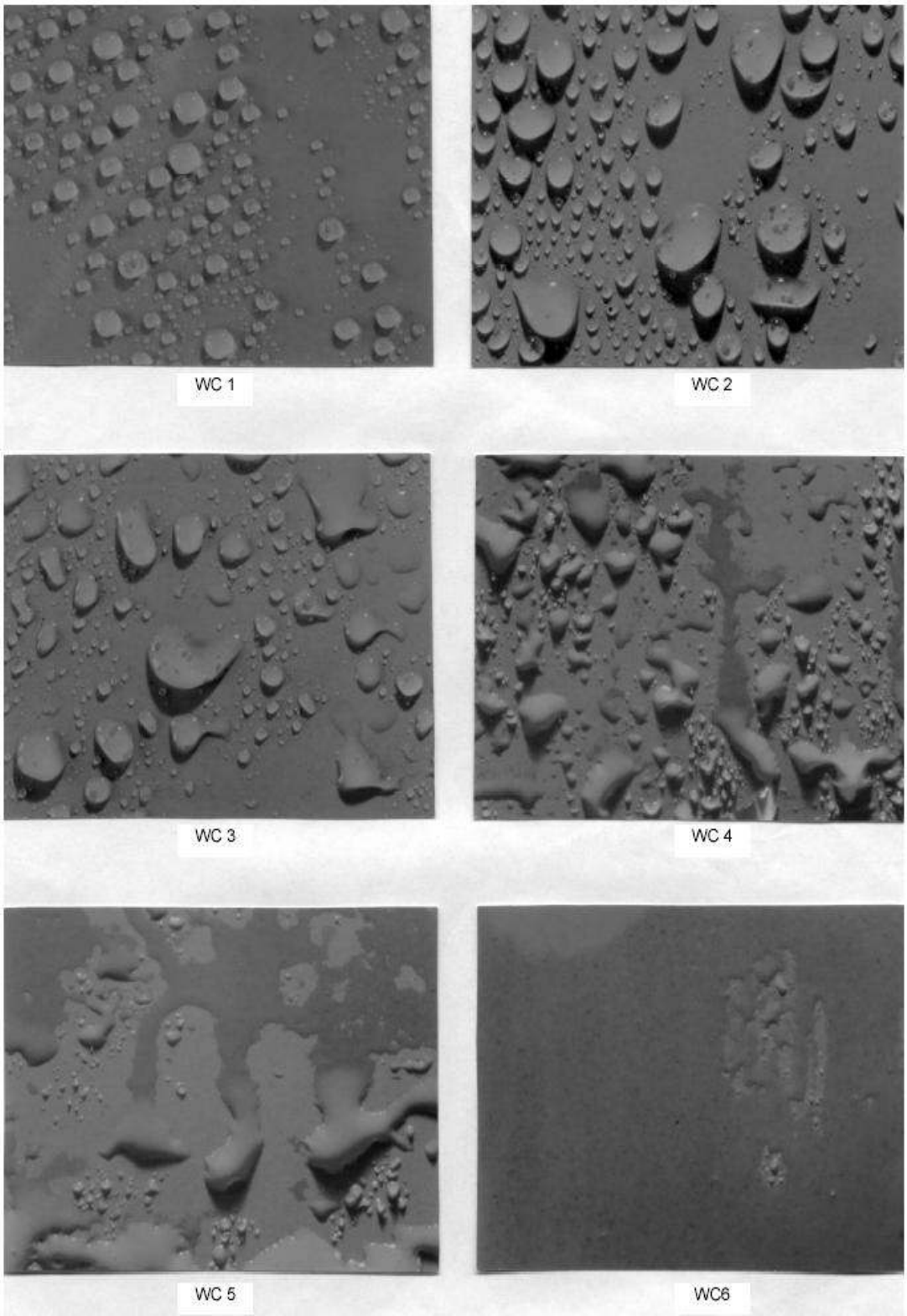

Fig. G 1: Photos indicating the general appearance of each wettability class (WC), with a class of WC 7 indicating a surface that is completely wetted with no observed dry spots [59].

G.2 Results for hydrophobicity measurements

Table G 2: Series mean and standard deviations of wettability classes for specific locations on the samples of each test series, before and after cleaning of the samples.

Voltage type	Material	Data type	Hydrophobicity classification for area:											
			Lower 17 mm				Middle 17 mm				Upper 16 mm			
			Affected		Unaffected		Affected		Unaffected		Affected		Unaffected	
			Before	After	Before	After	Before	After	Before	After	Before	After	Before	After
AC	A	Series mean	6	2	3	1	6	2	2	1	6	2	2	1
		Standard deviation	0	0	0	1	0	0	0	0	0	0	1	0
	B	Series mean	5	3	4	2	6	3	4	3	6	3	3	2
		Standard deviation	1	0	0	1	0	1	0	1	0	1	1	0
	C	Series mean	7	4	7	5	6	4	6	5	6	4	5	5
		Standard deviation	0	1	0	1	0	1	0	1	0	1	0	1
	D	Series mean	6	4	5	3	7	4	5	2	6	3	4	3
		Standard deviation	0	1	0	1	0	1	0	1	0	1	1	1
DC+	A	Series mean	7	6	5	2	7	5	5	3	7	4	3	2
		Standard deviation	0	1	1	1	0	1	1	1	1	0	1	0
	B	Series mean	1	2	2	3	5	4	2	3	6	4	2	3
		Standard deviation	0	1	0	1	2	2	1	1	1	1	1	1
	C	Series mean	6	5	6	6	5	6	6	6	5	5	6	6
		Standard deviation	1	1	1	0	1	1	1	0	1	1	0	0
	D	Series mean	2	1	3	5	6	5	3	5	6	5	3	5
		Standard deviation	1	1	2	1	0	0	2	0	0	1	2	0
DC-	A	Series mean	7	6			7	6	5	3	6	4	4	4
		Standard deviation	0	1			0	1	1	0	0	1	1	1
	B	Series mean	5	2	5	4	6	4	5	4	5	4	5	4
		Standard deviation	2	1	1	0	1	1	0	0	1	1	0	0
	C	Series mean	7	7	7	6	7	7	7	6	7	7	6	6
		Standard deviation	0	1	0	1	1	0	0	1	1	0	0	1
	D	Series mean	5	4	7	4	7	5	7	4	6	5	6	5
		Standard deviation	0	0	1	1	1	1	1	0	1	1	1	0

G.2.1 Material A

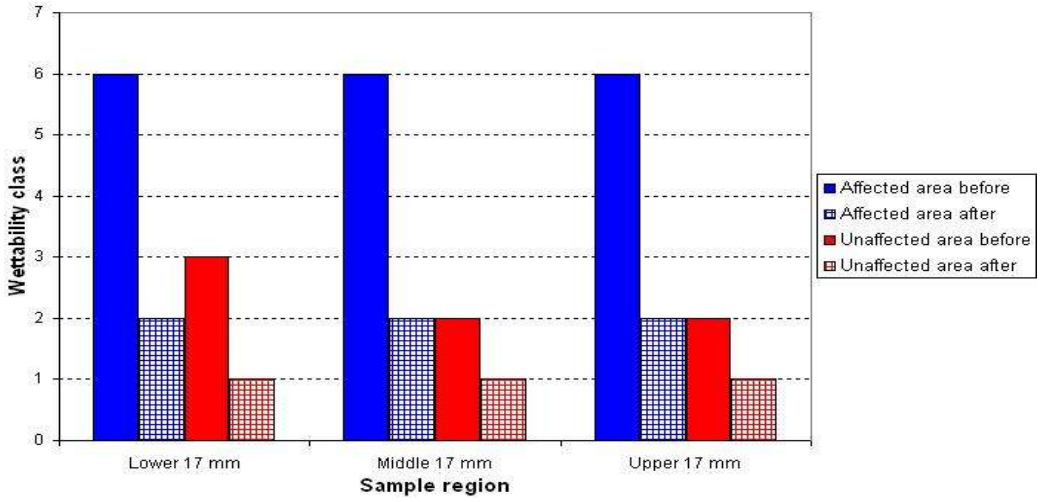

(a)

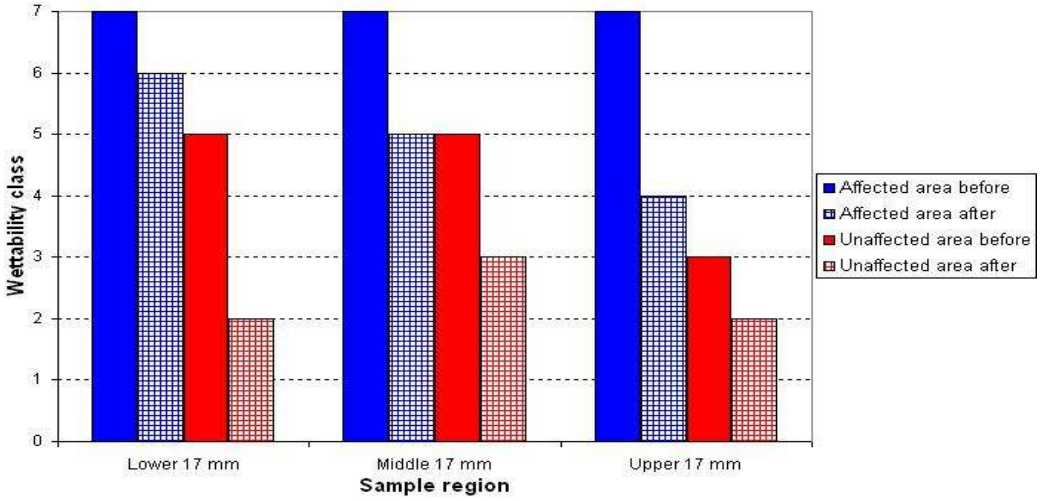

(b)

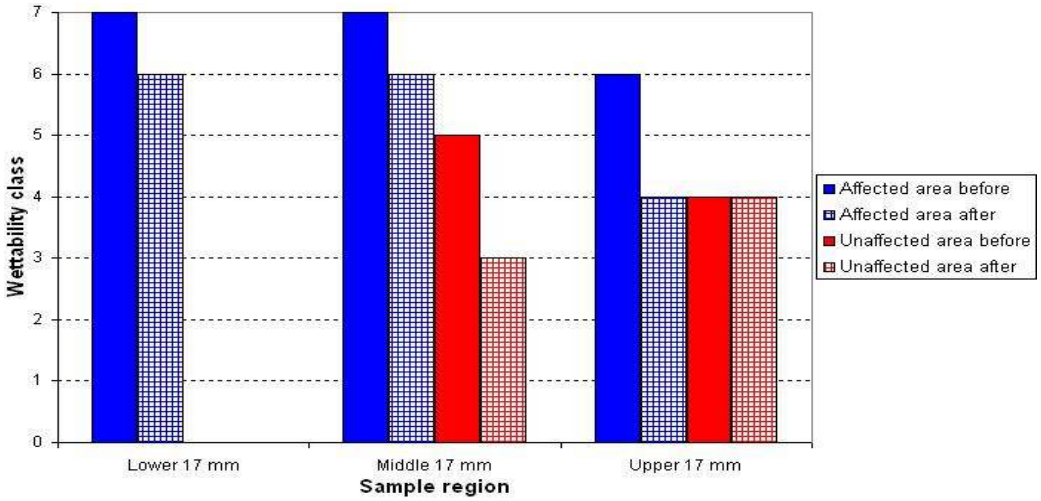

(c)

Fig. G 2: Series means for hydrophobicity results of samples of material A, before and after washing of the sample surface: (a) Series AC4-A, (b) Series DP4-A and (c) Series DN4-A.

G.2.2 Material B

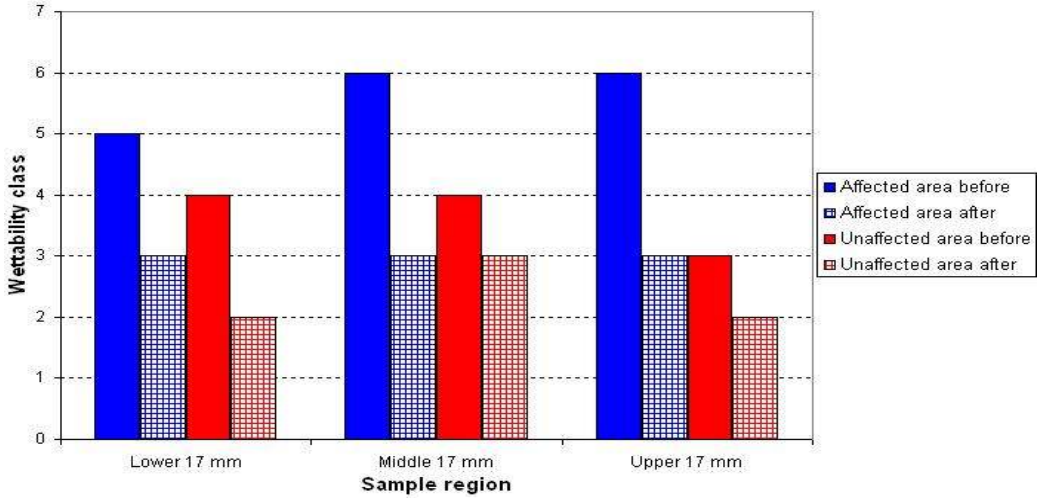

(a)

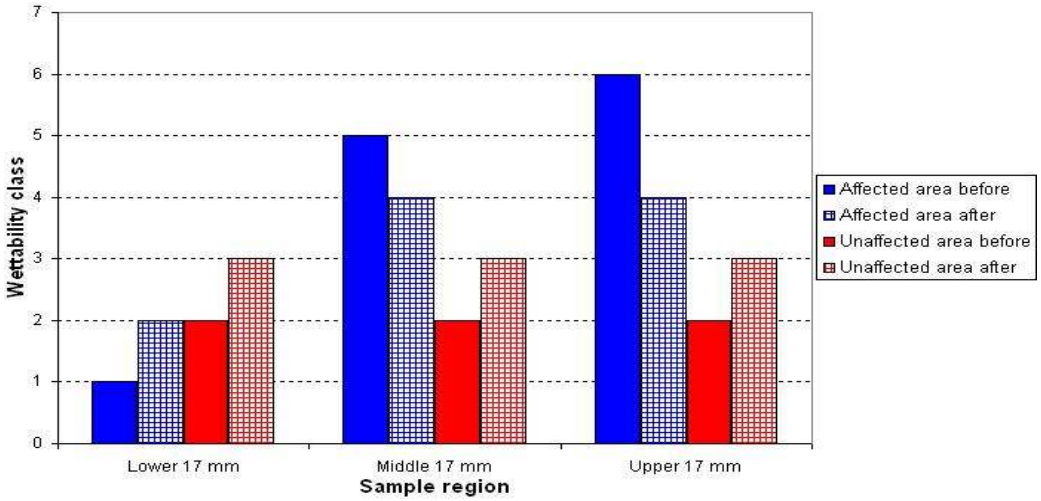

(b)

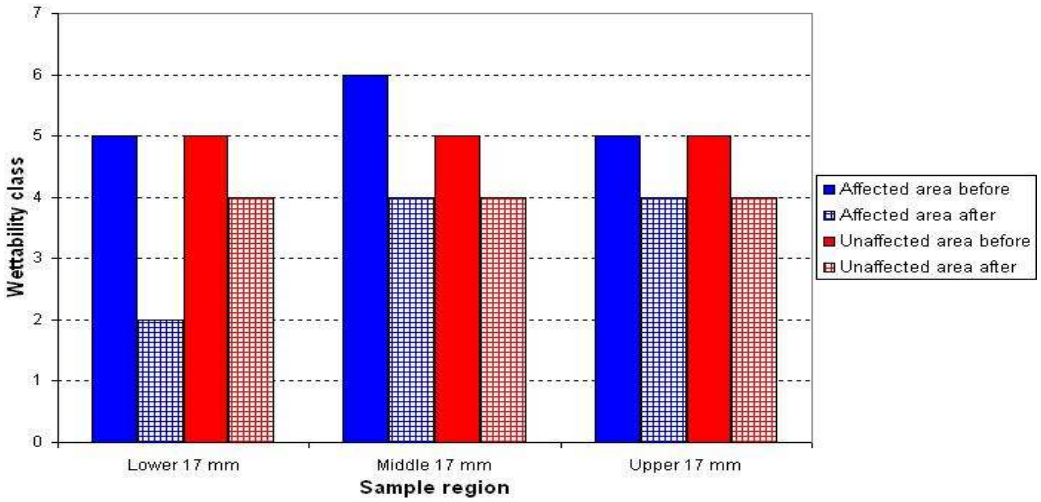

(c)

Fig. G 3: Series means for hydrophobicity results of samples of material B, before and after washing of the sample surface: (a) Series AC4-B, (b) Series DP4-B and (c) Series DN4-B.

G.2.3 Material C

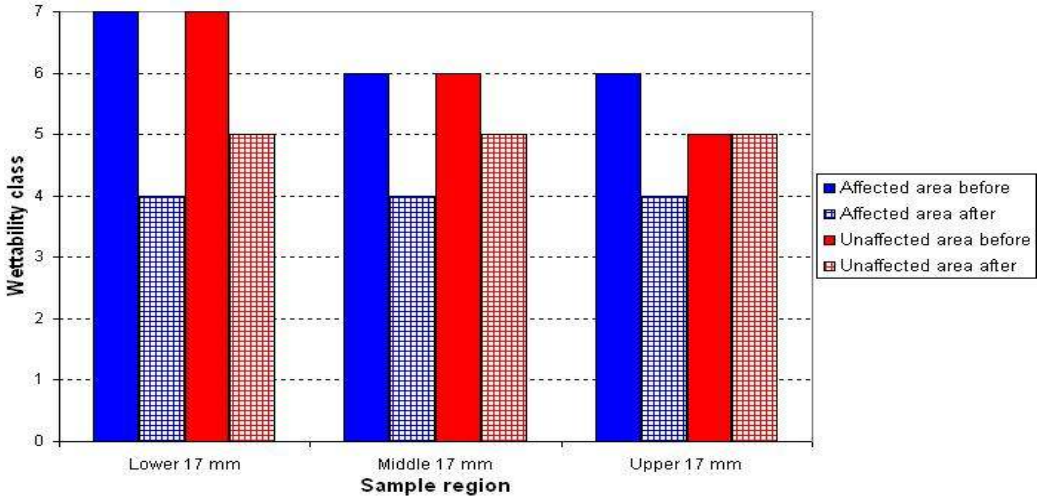

(a)

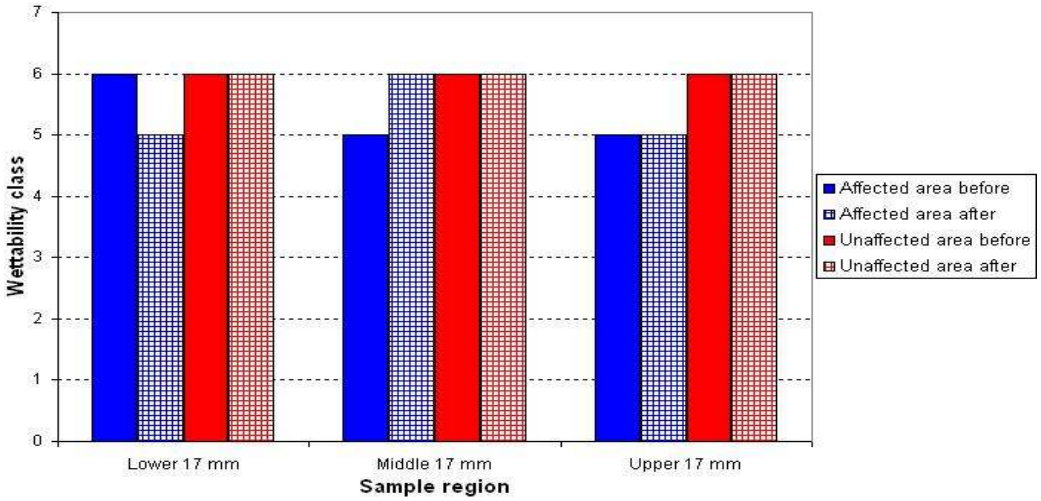

(b)

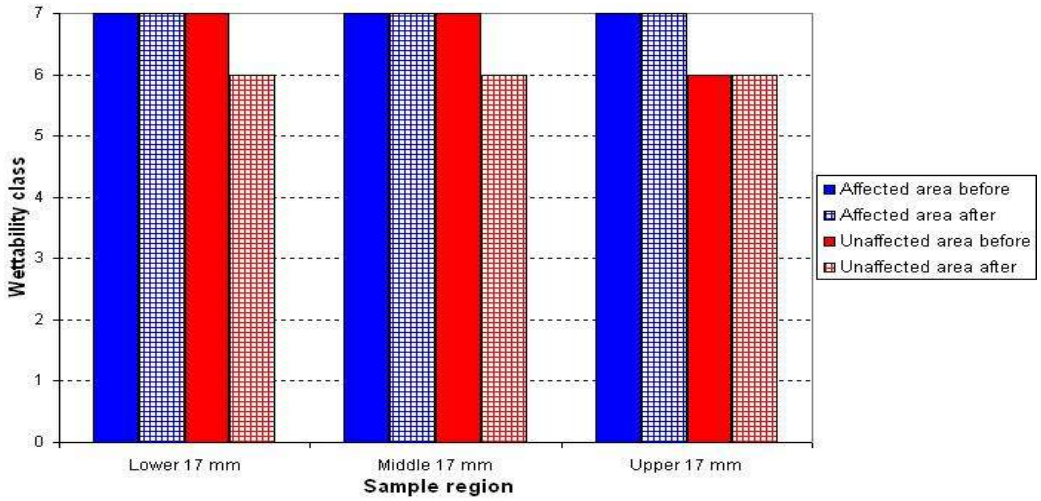

(c)

Fig. G 4: Series means for hydrophobicity results of samples of material C, before and after washing of the sample surface: (a) Series AC4-C, (b) Series DP4-C and (c) Series DN4-C.

G.2.4 Material D

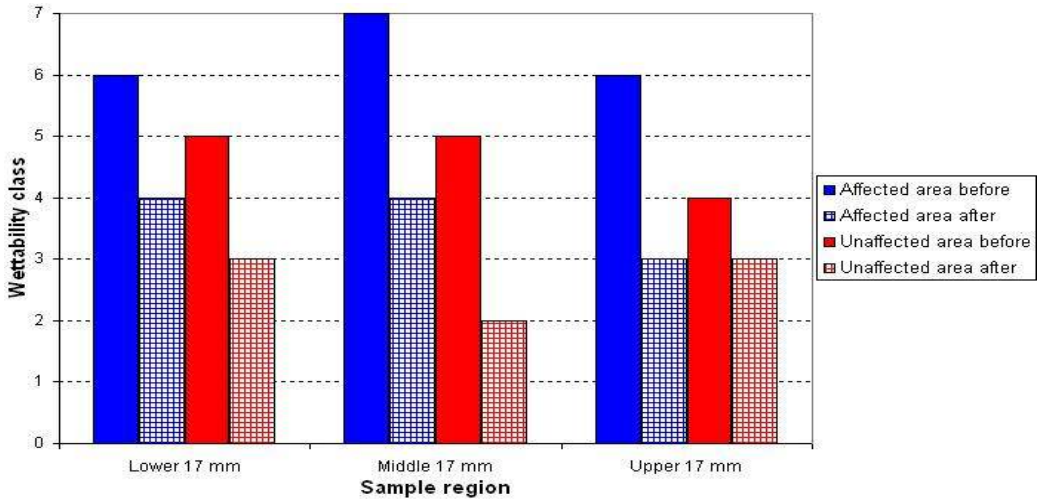

(a)

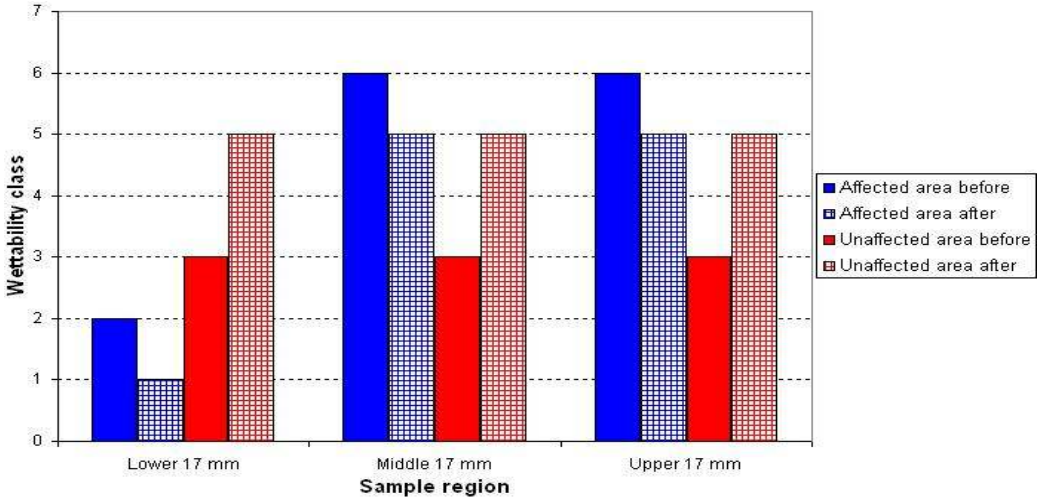

(b)

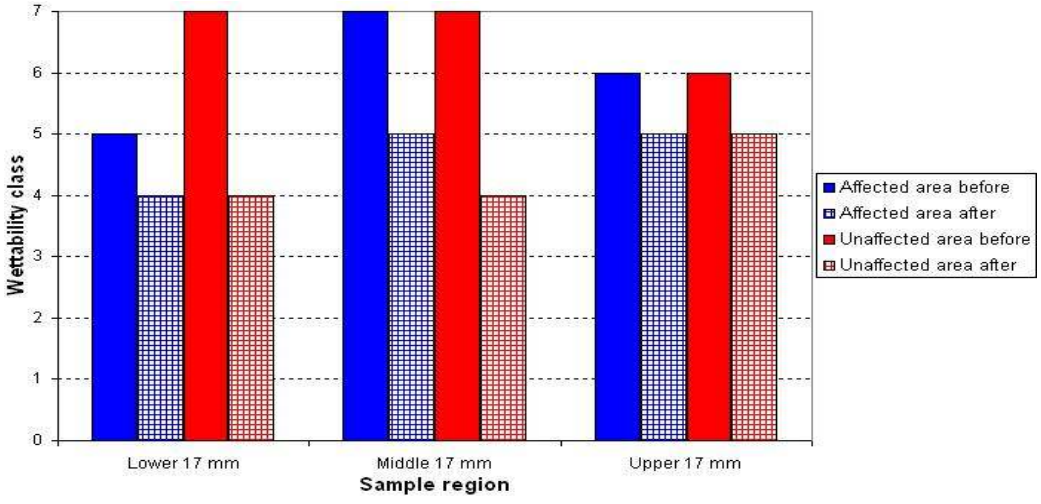

(c)

Fig. G 5: Series means for hydrophobicity results of samples of material D, before and after washing of the sample surface: (a) Series AC4-D, (b) Series DP4-D and (c) Series DN4-D.

Appendix H: Chemical Analysis Results for Chapter 5

The chemical analysis was performed on one chosen sample per test series by means of spectra obtained by ATR FTIR spectroscopy. Three specimens were cut from each sample, one from the lower 17 mm, the middle 17 mm and the upper 16 mm region each. The regions were divided according to the distance from the ground potential electrode measured along the longitudinal axis of the sample. The spectrum of each specimen of the tested sample was compared against a spectrum obtained for a virgin sample of the corresponding material. Each spectrum was obtained by measuring the background spectrum first, which was then subtracted from the spectrum measured for the actual sample to improve the accuracy of the sample. The number of scans for both background and actual sample was kept at 16 scans.

The four different materials were divided into two groups: materials of a polydimethylsiloxane (PDMS) type, which included materials A, B and D, and the EPDM material type (material C). Different analysis procedures were used for the two material groups, which are described in the following sections.

H.1 Results for PDMS materials

The analysis procedure for this general material type focused on three different criteria, which were:

- Loss of alumina trihydrate filler (ATH, or Al_2O_3-$3H_2O$) shown by a reduction in the peak height at 3522 cm^{-1}.
- Loss of methyl (CH_3) groups from the PDMS structure, which can be detected by a decrease in the spectra peak height as well as in the area under the peak at 2963 cm^{-1}.
- Oxidation of the PDMS and the formation of carbonyl (C=O) groups, revealed as an increase in the area under the curve in the range of 1550 to 1800 cm^{-1}.

The peak heights and areas underneath the peaks were measured between the spectrum curve and a baseline drawn between two chosen wavenumber locations. Peak heights measured in the tested specimen were compared to the heights of the virgin sample (peak height ratio), with a similar procedure followed for the peak areas

(peak area ratio). For the criterion of loss of methyl groups, the peak areas were used to calculate the degree of conversion β. The definitions were given in section 5.3.8.1.

The locations of the peaks, area limits and base values for the baselines for each analysis criterion are as follows:

- *Loss of ATH filler:* Peak location: 3522 cm^{-1}; baseline values: Base 1 = 3690 cm^{-1}, Base 2 = 3036 cm^{-1}.
- *Loss of methyl groups:* Peak location: 2963 cm^{-1}; peak area limits: Limit 1 = 3010 cm^{-1}, Limit 2 = 2930 cm^{-1}; baseline values: Base 1 = 3010 cm^{-1}, Base 2 = 2930 cm^{-1}.
- *Oxidation by carbonyl formation:* Peak area limits: Limit 1 = 1800 cm^{-1}, Limit 2 = 1550 cm^{-1}; baseline values: Base 1 = 1800 cm^{-1}, Base 2 = 1550 cm^{-1}.

Table H 1 shows the analysis results of the specimens for the individual region on all the selected samples for materials A, B and D for each analysis criterion, with the subsequent sections showing the plots generated from the results for a better visual comparison.

Table H 1: Chemical analysis results for PDMS type materials.

Region	Analysis		AC Series			DC + Series			DC - Series		
			AC4-A1	AC4-B5	AC4-D3	DP4-A6	DP4-B2	DP4-D1	DN4-A4	DN4-B4	DN4-D5
Lower 17mm	Loss of ATH filler - peak height ratio		0.234	0.241	NPO	0.851	0.296	NPO	0.993	0.513	0.372
	Loss of methyl groups	Peak height ratio	0.731	0.313	0.037	0.762	0.500	0.172	0.726	0.591	0.258
		Degree of conversion β	0.240	0.665	0.950	0.272	0.544	0.820	0.286	0.417	0.756
	Oxidation by carbonyl formation - peak area		6.713	5.036	0.941	3.240	6.139	2.811	2.387	9.349	16.501
Middle 17mm	Loss of ATH filler - peak height ratio		0.546	NPO	NPO	0.915	0.088	0.244	0.830	0.537	0.053
	Loss of methyl groups	Peak height ratio	0.726	0.356	0.194	0.824	0.356	0.106	0.786	0.489	0.085
		Degree of conversion β	0.283	0.628	0.757	0.186	0.660	0.897	0.264	0.524	0.943
	Oxidation by carbonyl formation - peak area		2.039	2.175	5.113	3.173	2.053	16.385	2.249	9.531	9.213
Upper 16mm	Loss of ATH filler - peak height ratio		0.404	0.110	NPO	0.504	0.115	0.280	0.986	0.566	0.394
	Loss of methyl groups	Peak height ratio	0.815	0.211	0.217	0.812	0.260	0.287	0.845	0.645	0.528
		Degree of conversion β	0.191	0.801	0.773	0.198	0.757	0.716	0.195	0.352	0.488
	Oxidation by carbonyl formation - peak area		1.950	2.936	3.852	2.115	1.566	11.595	1.663	5.314	3.917

*NPO: No Peak Observed

Some peaks were observed of having decreased to such a degree that the peak fell beneath the baseline, yielding a negative peak height. In these cases, the values were

substituted by the abbreviation NPO (No Peak Observed). Such occurrences were omitted during the plotting of the results. As a result, the plots for the results of the AC series for the criterion of loss of ATH filler are not shown in the following sections, due to the large number of occurrences of measurements classified as NPO during this series. However, such results were by no means discarded during the analysis, but were rather regarded as a severe chemical change in the sample in terms of the respective criterion.

H.1.1 Loss of ATH filler

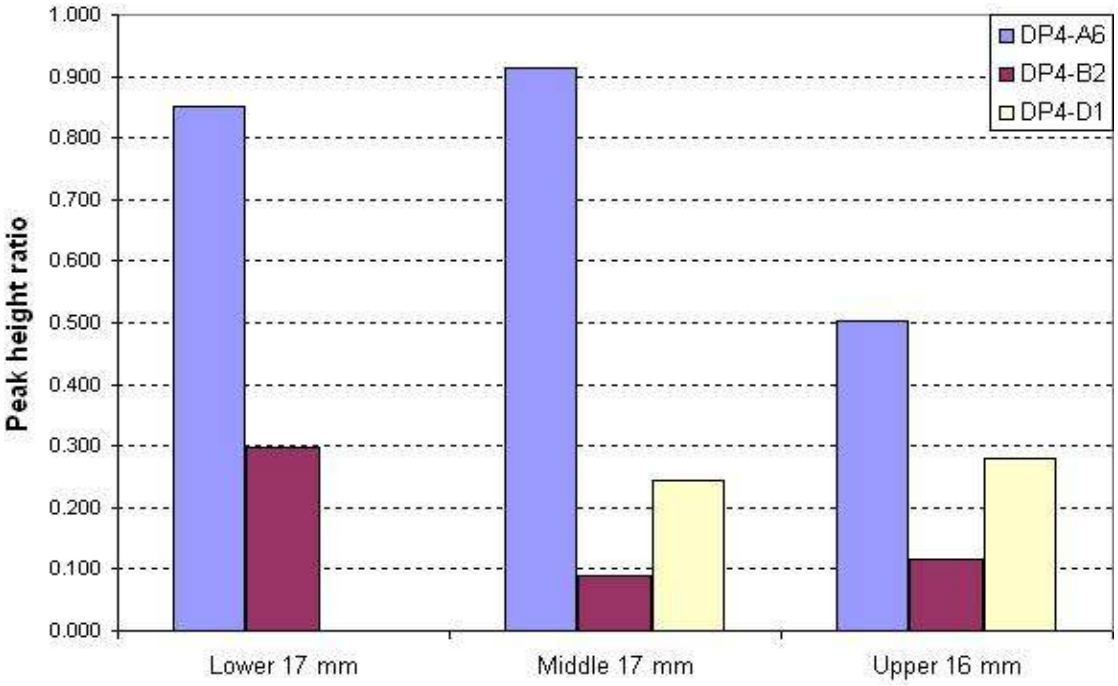

(a)

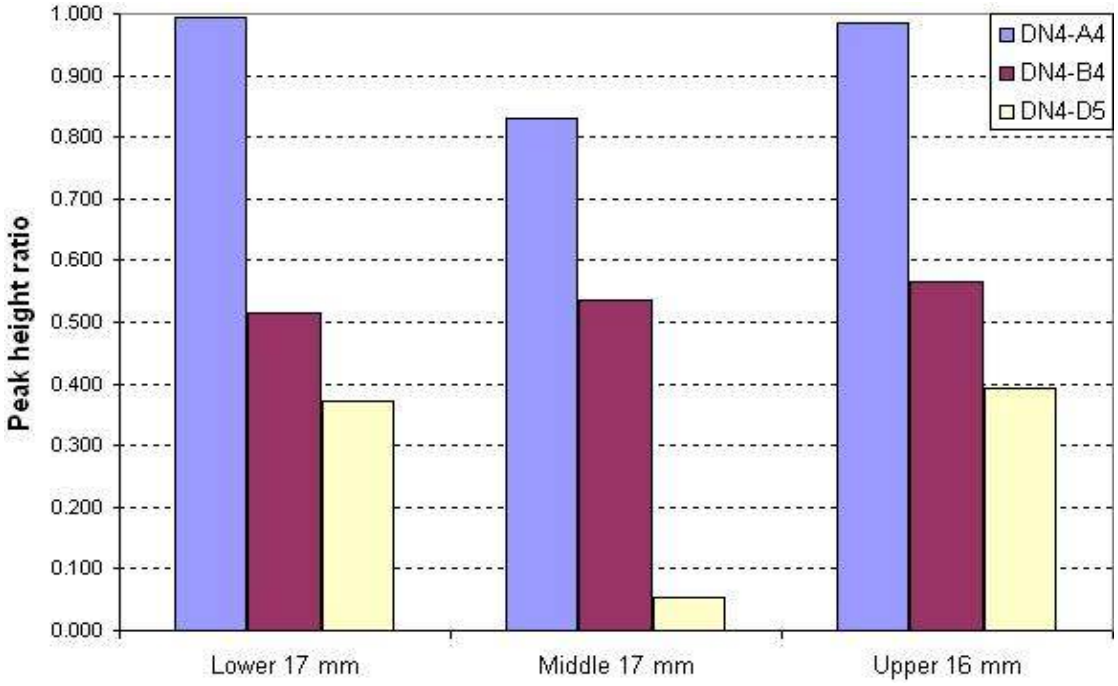

(b)

Fig. H 1: Peak height ratios for loss of ATH filler in PDMS materials for different voltage types: (a) Positive DC voltage and (b) Negative DC voltage.

H.1.2 Loss of methyl groups

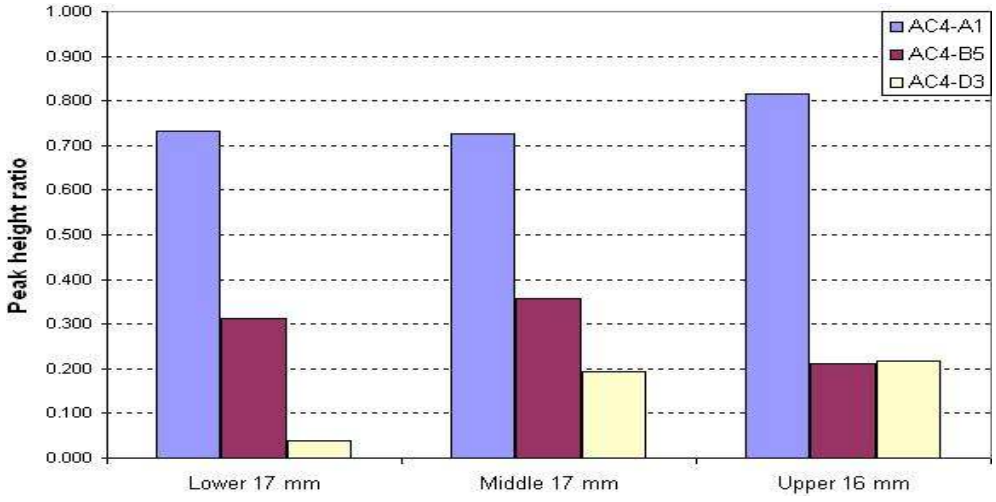

(a)

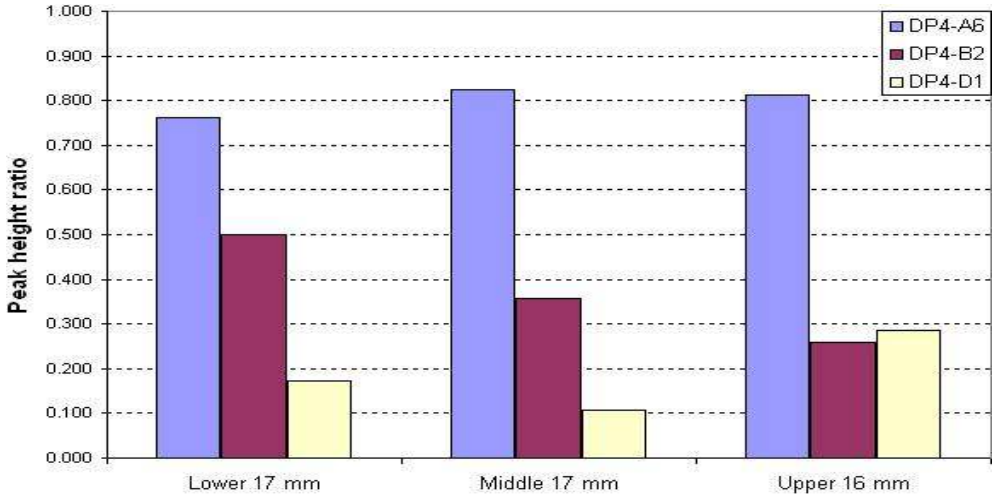

(b)

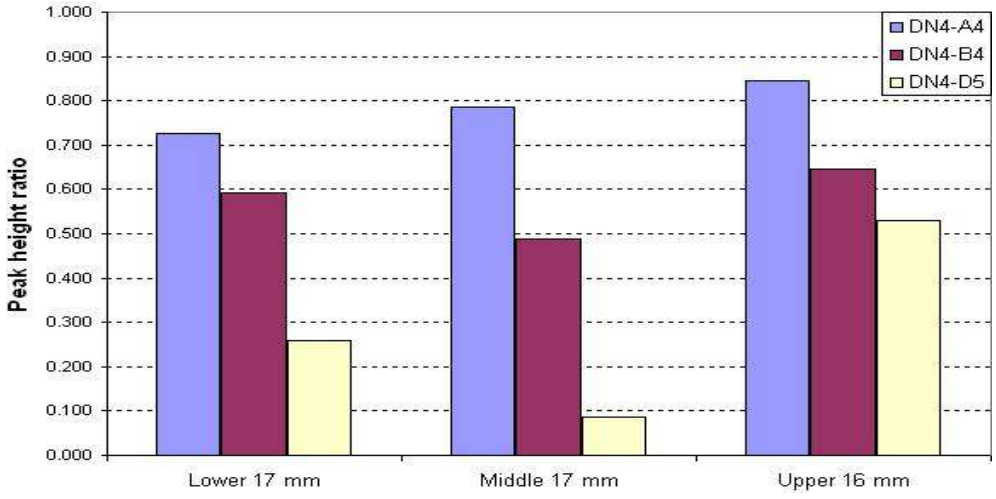

(c)

Fig. H 2: Peak height ratio for loss of methyl groups in PDMS materials for different voltage types: (a) AC voltage, (b) Positive DC voltage and (c) Negative DC voltage.

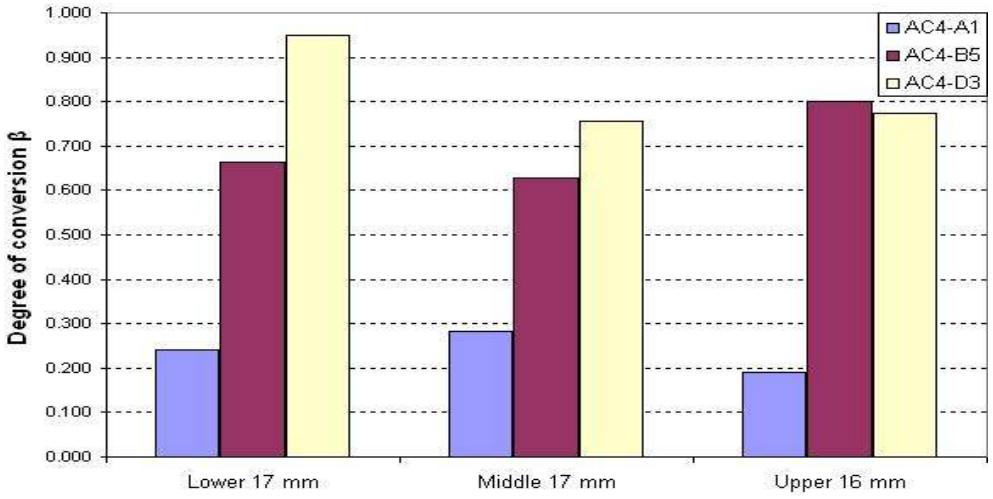

(a)

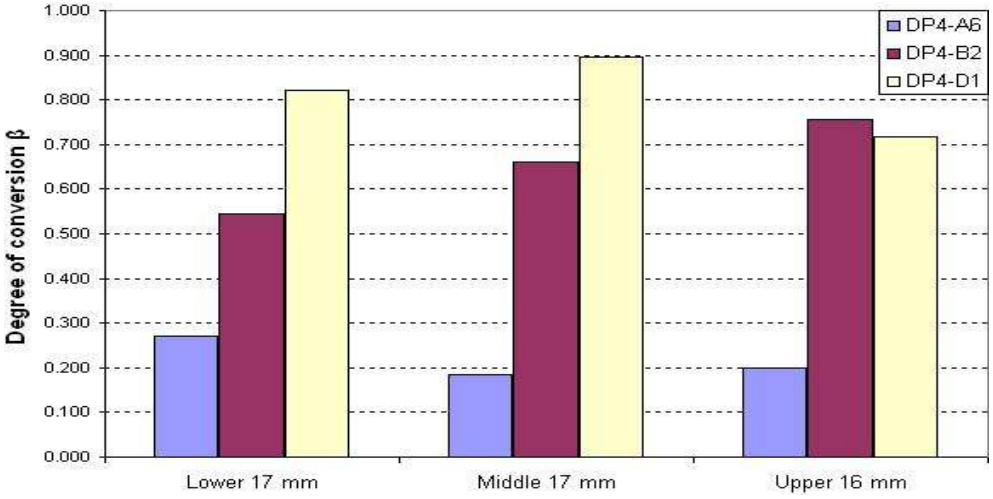

(b)

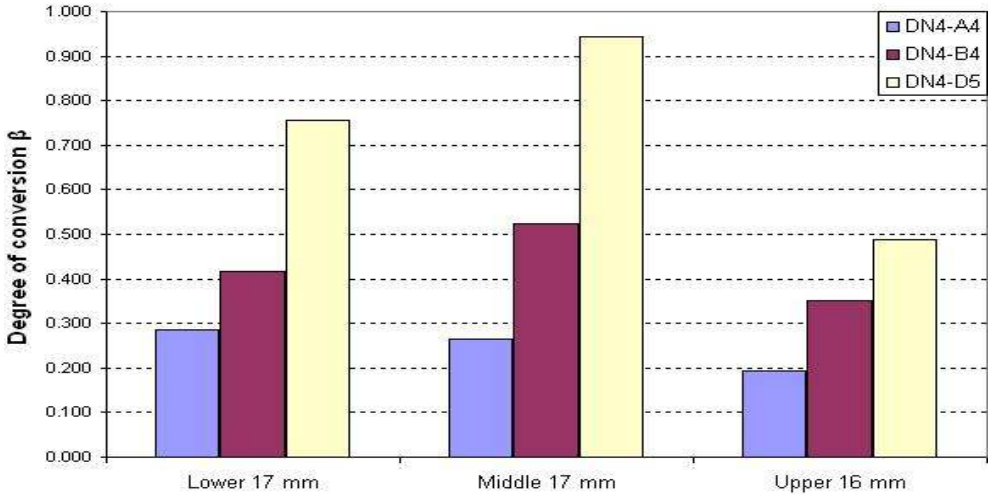

(c)

Fig. H 3: Degree of conversion β for loss of methyl groups in PDMS materials for different test voltages: (a) AC series, (b) Positive DC voltage and (c) Negative DC voltage.

H.1.3 Oxidation by carbonyl formation

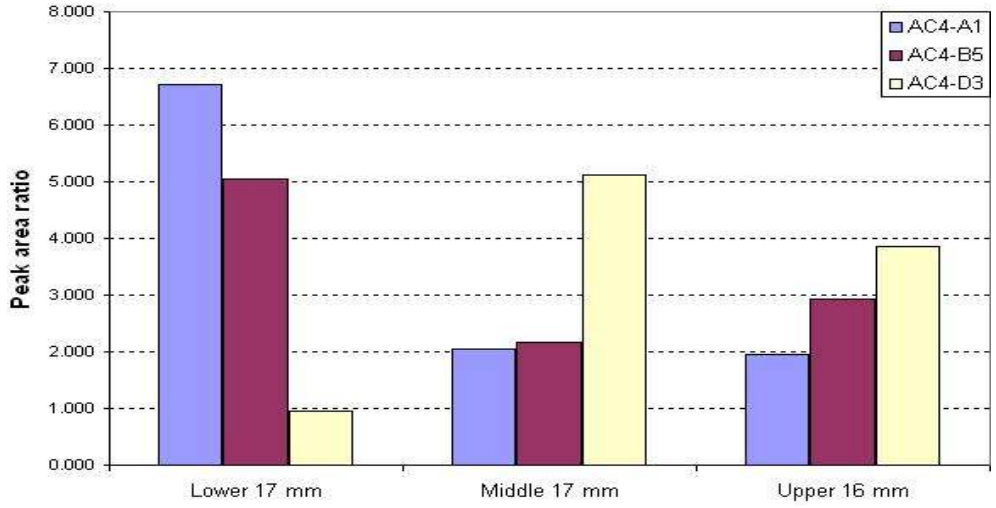

(a)

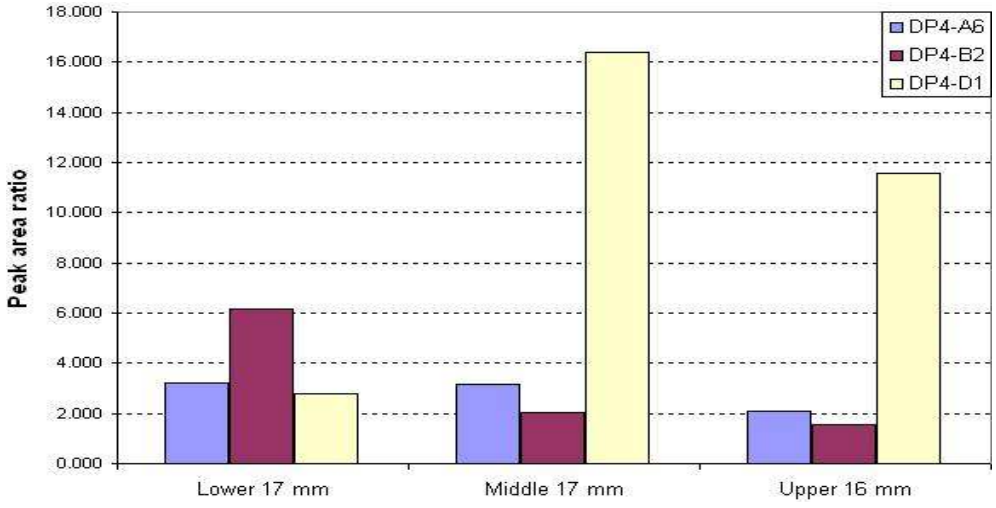

(b)

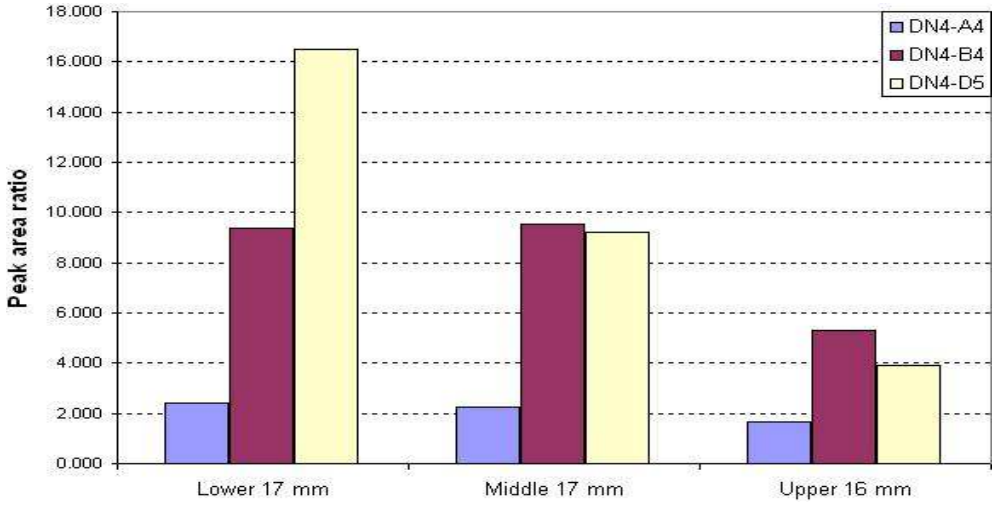

(c)

Fig. H 4: Peak area ratio for oxidation by carbonyl formation in PDMS materials for different voltage types: (a) AC voltage, (b) Positive DC voltage and (c) Negative DC voltage.

H.2 Results for EPDM material

Two main areas of focus were used for the analysis of this material:

- Loss of alumina trihydrate filler (ATH, or Al_2O_3-$3H_2O$) shown by a reduction in the peak height at 3522 cm^{-1}.
- Oxidation of polymer through carbonyl (C=O) formation, shown by an increase in peak height at 1730 cm^{-1}.

The method of measuring the peak heights was identical to that used for the PDMS materials, and the measured peaks were also compared to the peak heights measured for the virgin material. The locations of the peaks and the base values for the baselines for the two criteria are:

- *Loss of ATH filler*: Peak location: 3522 cm^{-1}; baseline values: Base 1 = 3690 cm^{-1}, Base 2 = 3036 cm^{-1}.
- *Oxidation by carbonyl absorption*: Peak location: 1730 cm^{-1}; baseline values: Base 1 = 1810 cm^{-1}, Base 2 = 1690 cm^{-1}.

Table H 2 shows the results for each evaluation criterion obtained for the different samples. The following sections contain plots generated from the results.

Table H 2: Chemical analysis results for EPDM type material.

Region	Analysis		AC series, sample AC4-C5	DC+ series, sample DP4-C4	DC- series, sample DN4-C4
Lower 17mm	Loss of ATH		NPO	NPO	0.100
	Ester carbonyl degradation	Peak height ratio	1.229	0.231	1.282
Middle 17mm	Loss of ATH		0.462	0.362	0.138
	Ester carbonyl degradation	Peak height ratio	3.053	3.035	1.100
Upper 16mm	Loss of ATH		NPO	0.083	0.342
	Ester carbonyl degradation	Peak height ratio	2.294	2.865	1.371

*NPO: No Peak Observed

The abbreviation NPO has the same significance as for the PDMS materials, and regions where such a measurement occurred were again omitted from the plots, but not from the analysis.

H.2.1 Loss of ATH filler

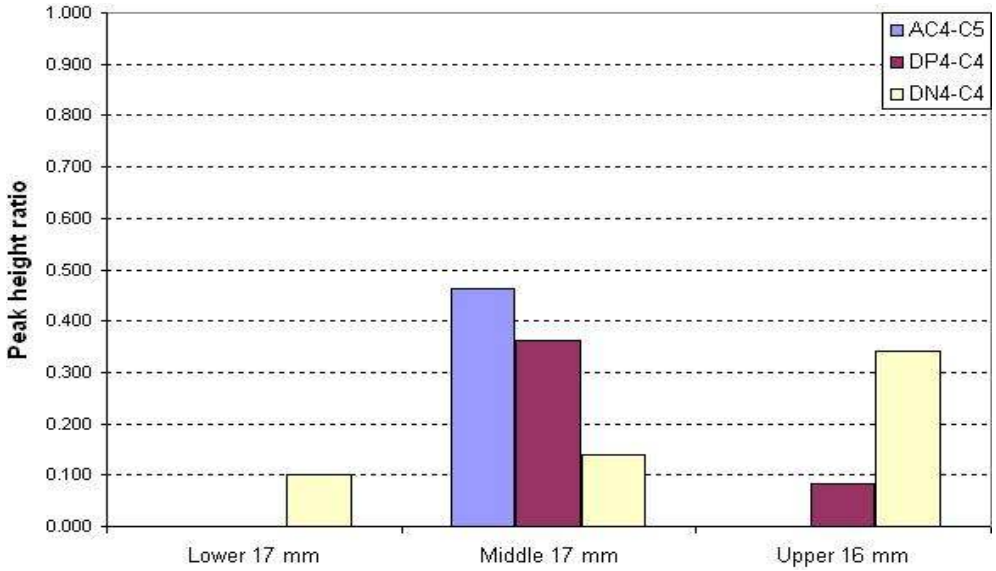

Fig. H 5: Peak height ratios for loss of ATH filler in EPDM material for different voltage types.

H.2.2 Oxidation by carbonyl formation

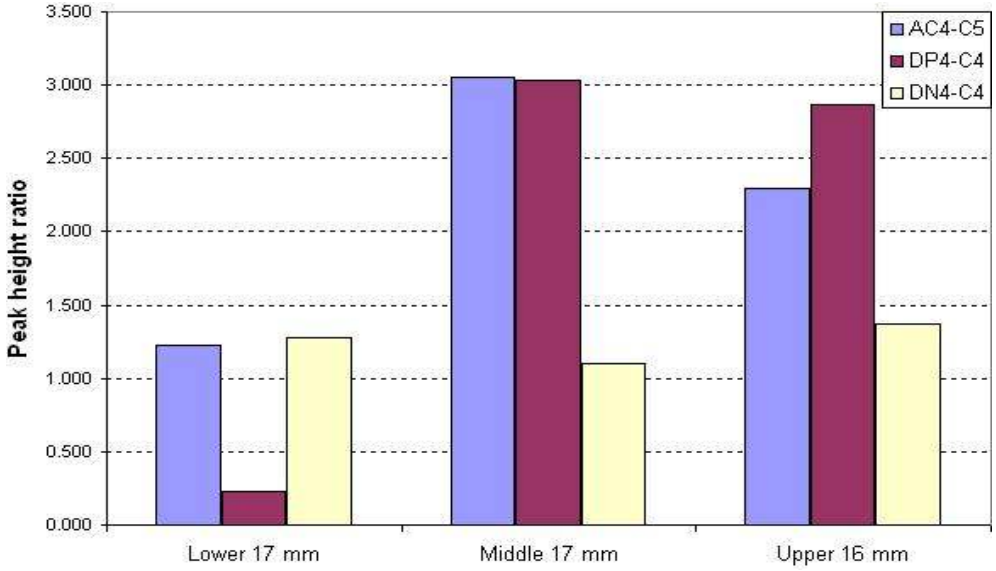

Fig. H 6: Peak height ratio for oxidation by carbonyl formation in EPDM materials for different voltage types.

H.3 Repeatability check for ATR FTIR analysis

In order to check if the results obtained for the chemical analysis from the various spectra generated for each test specimen were not influenced by a possible bias in the apparatus, the samples of all virgin materials were scanned once more at the end of the analysis procedure. These spectra were then compared to those obtained for the virgin samples at the beginning of the chemical analysis process, to see if any deviation existed in the results. The following plots show the spectra obtained at the beginning and at the end of the chemical analysis for the virgin samples of each tested material.

The results show that the different spectra were almost identical for each material, indicating that the ATR FTIR tests can be performed with a high degree of repeatability and accuracy.

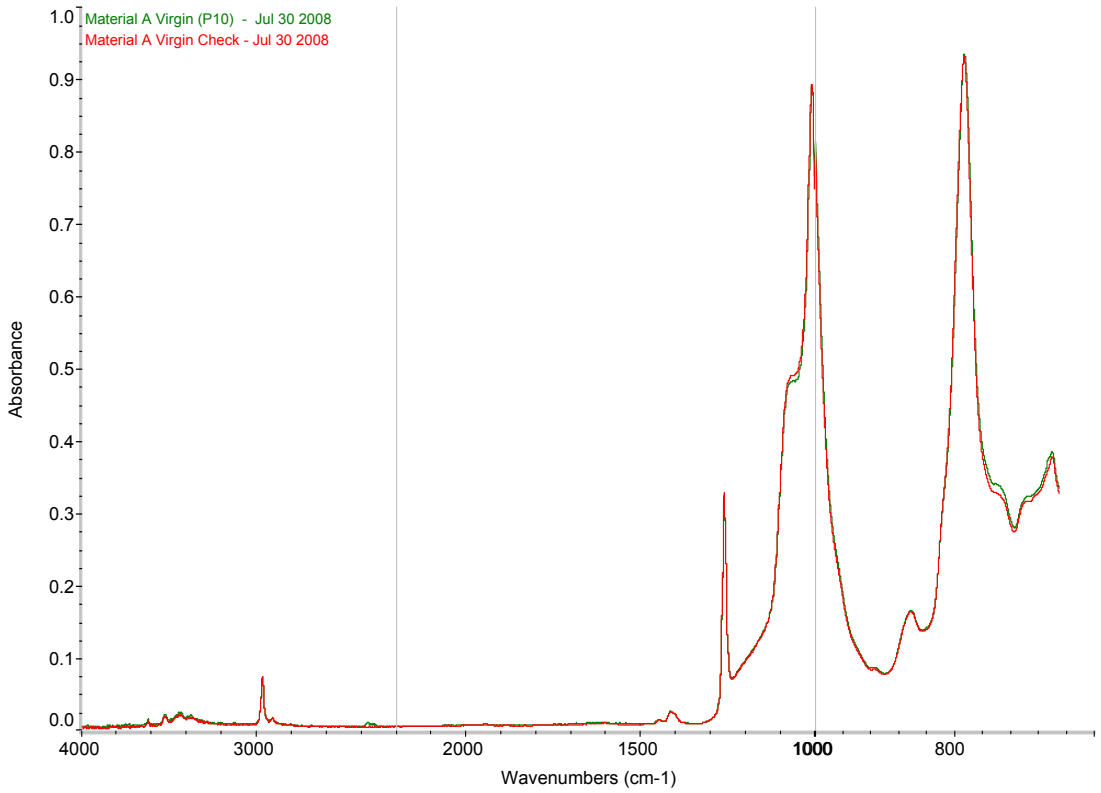

Fig. H 7: Spectra for repeatability check for virgin specimen of material A.

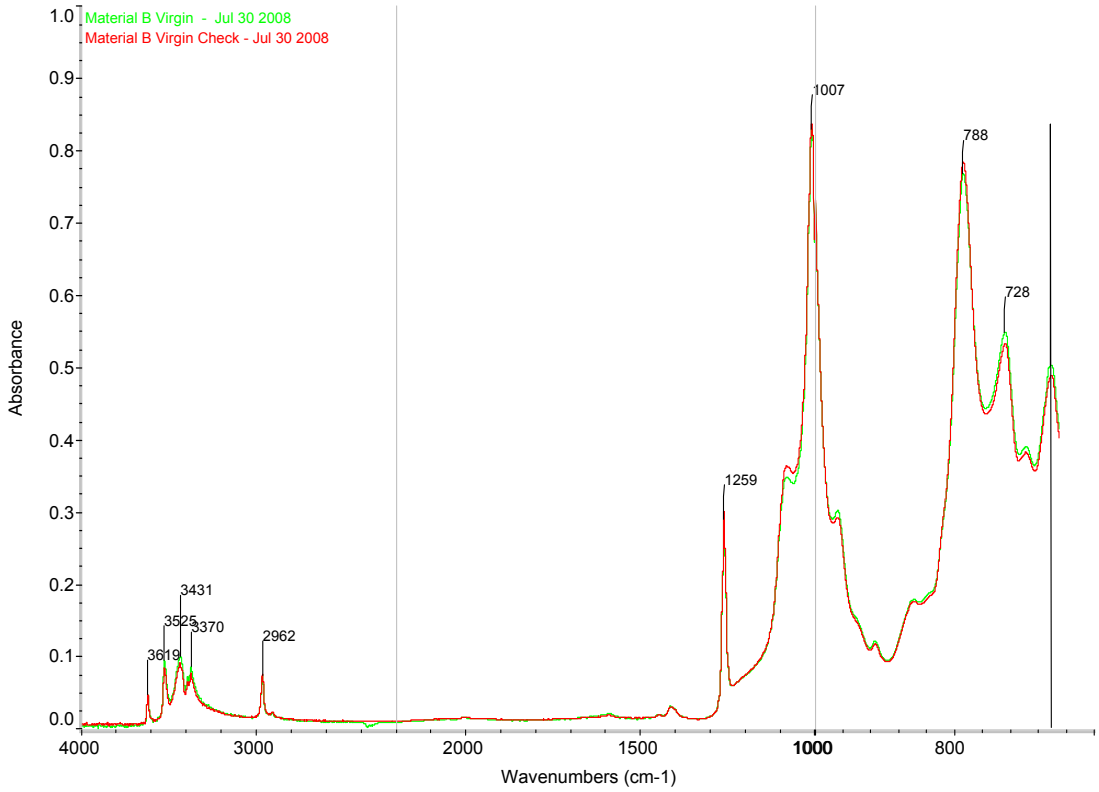

Fig. H 8: Spectra for repeatability check for virgin specimen of material B.

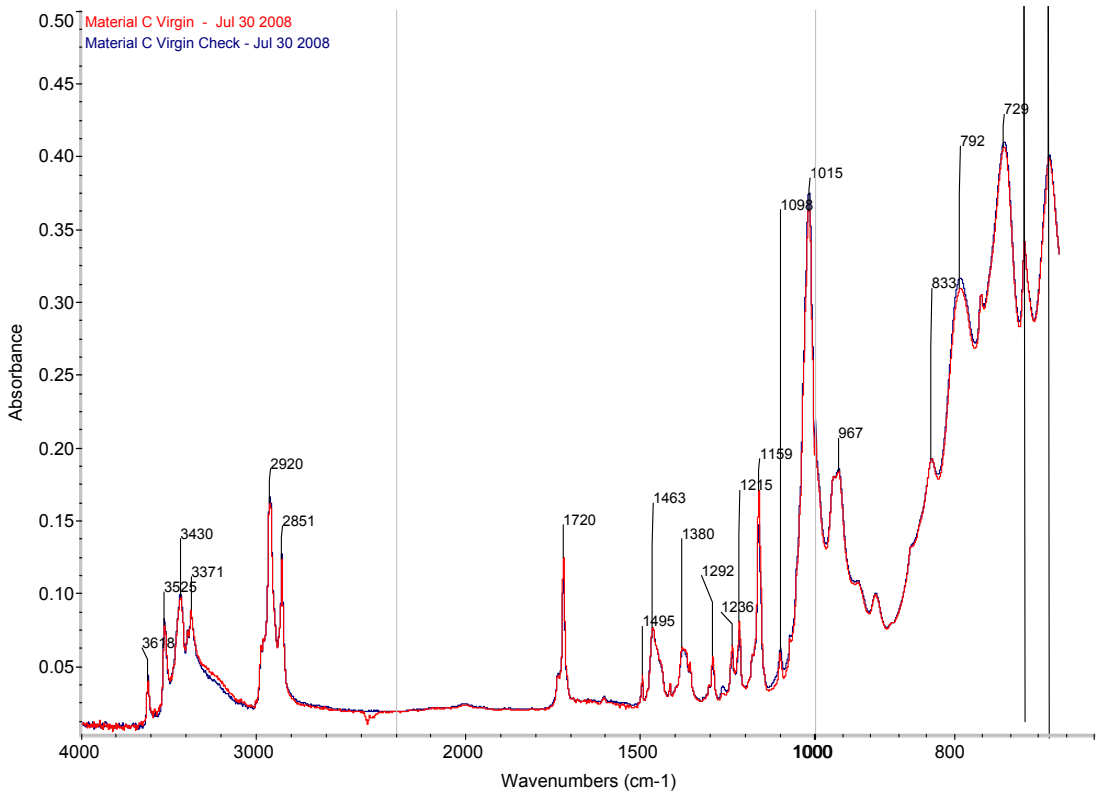

Fig. H 9: Spectra for repeatability check for virgin specimen of material C.

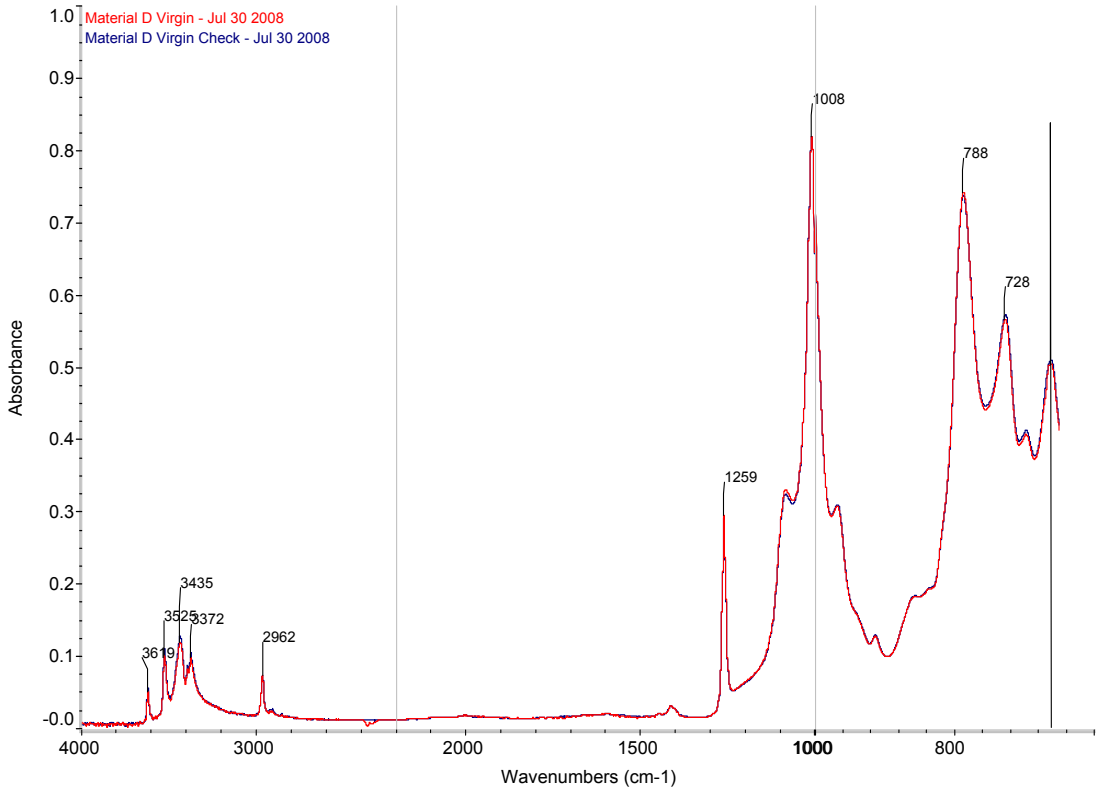

Fig. H 10: Spectra for repeatability check for virgin specimen of material D.

Appendix I: Project DVD

This DVD contains the following:

- Results and spectra for the chemical analysis
- Oscilloscope waveforms
- Processed data for evaluation criteria
- Photos of tested samples
- Thesis document in pdf-format